The Oncogenic Potential of Human Ether-a-go-go-related Gene (hERG) Potassium Channels

Thesis submitted for the Degree of

Doctor of Philosophy

at the University of Leicester

by

David Pier BSc (Edinburgh)

Department of Cell Physiology and Pharmacology

University of Leicester

May 2007

ProQuest LLC
789 East Eisenhower Parkway
P.O. Box 1346
Ann Arbor, MI 48106-1346

The oncogenic potential of hERG potassium channels

Human ether-à-go-go-related gene product (hERG) is a potassium channel found ubiquitously in embryonic tissue, but only in key excitable tissues in the adult. hERG is expressed in many tumours of different histological origin, and is not found in the healthy tissues from which the tumour originates. The related EAG channel has been shown to possess oncogenic potential. Having investigated the effect of stable, recombinant hERG expression in NIH-3T3 and HEK293 cell-lines, it was found that there was no significant difference in the proliferative rate or serum-dependency of growth at physiological hERG expression levels, compared to mock-transfected cells. However, hERG expression increased the ability of confluent cells to overgrow each other resulting in a significant increase in post-confluent cell density compared with wild-type cells. In contrast to the parental cell-line, hERG-expressing NIH-3T3 cells grew in soft agar, and exhibited increased rates of cell migration. hERG-mediated transformation appeared to be cell density-dependent, with effects on cell shape and cytoskeletal organization only being seen in confluent cultures. None of the effects of hERG expression were affected by the presence of hERG channel-blocking compounds, or co-expression of non-conducting, dominant-negative hERG subunits. However, hERG-mediated overgrowth seemed to be dependent on p38 MAPK, protein kinase C, phosphoinositide 3-kinase and Src signalling, and independent of MEK/ERK signalling. In addition, hERG expression permitted Src-independent cell proliferation not seen in control cell-lines.

In summary, stable expression of hERG results in NIH-3T3 and HEK293 cell-lines exhibiting some of the characteristics of a transformed phenotype. Pharmacological and molecular biological evidence suggests that this effect on cell phenotype is not dependent on a functional channel current. Instead, the hERG channel protein may interact with protein components of key cell signalling pathways, in a similar fashion to the protein-protein interactions observed for the EAG channel.

Acknowledgements

Firstly, I would like to express my gratitude to my supervisors Dr. John Mitcheson and Professor John Challiss, whose expertise, understanding, and patience, added considerably to both the quality of my experience as a PhD student and the quality of my thesis.

I would also like to thank everyone in the Department of Cell Physiology and Pharmacology at the University of Leicester for all their support and guidance over the last three and a half years, with special thanks to Lab 447. I must also acknowledge in particular: Sarah for all her help with cell culture and Rachel for her support in molecular biology. I would also like to thank Drs. Jim Norman and Catrin Pritchard for sharing with me their expertise and knowledge on cell transformation.

My appreciation must also go out to my industrial supervisor, Dr. Derek Trezise, and everyone in the assay development and reagent validation department at GlaxoSmithKline for making me feel so welcome, and making my time in Stevenage so productive.

Lastly I would like to thank my fiancée, Katie. She has encouraged me throughout my time in Leicester – sometimes with a carrot, at other times with a stick! Ultimately, without her I don't think I would have got through the last three years.

Finally, I gratefully acknowledge the financial support of the British Biotechnology and Biological Sciences Research Council (BBSRC) and GlaxoSmithKline.

Abbreviations

ATM	Ataxia-telangiectasia-mutated
ATR	Ataxia and rad3-related
CaMKII	Calcium calmodulin kinase II
CDK	Cyclin-dependent kinase
CHO	Chinese hamster ovary
CKI	CDK inhibitor
Co-IP	Co-immunoprecipitation
CMV	Cytomegalovirus
cNBD	Cyclic nucleotide binding domain
DAG	Diacylglycerol
DMSO	Dimethylsulphoxide
EAG	Ether-a-go-go gene
ECG	Electrocardiogram
EMT	Endothelial to mesenchymal transition
ERG	ether-a-go-go related gene
ER	Endoplasmic reticulum
ERK	Extracellular signal-regulated kinase
FAK	Focal adhesion kinase
FAT	Focal adhesion targeting sequence
FN	Fibronectin
FRET	Fluorescence resonance energy transfer
FRNK	FAK-related non-kinase domain
GDP	Guanosine 5'-diphosphate
GEF	Guanine nucleotide-exchange factor
GPCR	G protein-coupled receptor
GRB	Growth factor receptor binding protein
GTP	Guanosine 5'-triphosphate
HEK293	Human embryonic kidney 293
hERG	Human ether-a-go-go-related gene
HIF-1	Hypoxia-inducible factor-1

HRP	Horseradish peroxidase
Hsp70/90	Heat shock protein 70/ 90
IκB	Inhibitor of NF-κB
IKK	IκB kinase
ILK	Integrin-linked kinase
IP_3	inositol 1,4,5-trisphosphate
I-V	Current-voltage
JNK	c-Jun *N*-terminal kinase
LB	Luria-Bertani
LQT	Long QT
MAPK	Mitogen-activated protein kinase
MAPKK	MAPK kinase
MAPKKK	MAPK kinase kinase
MEK	ERK kinase
MinK	Minimum conductance potassium channel
MiRP	MinK-related protein
MMP	Matrix metalloproteinase
NF-κB	Nuclear factor-κB
PAK	p21-activated kinase
PAS	Per-ant-sim
PCR	Polymerase chain reaction
PI3K	Phosphoinositide-3 kinase
PIP_2	Phosphatidylinositol 4,5-bisphosphate
PIP_3	Phosphatidylinositol 3,4,5-trisphosphate
PKB	Protein kinase B
PKC	Protein kinase C
RTK	Receptor tyrosine kinase
ROS	Reactive oxygen species
SDS-PAGE	Sodium dodecyl-sulphate-polyacrylamide gel electrophoresis
SOC	Salt-optimized and carbon
TGFβ	Transforming growth factor β
VEGF	Vascular endothelial growth factor

WT	Wild-type

Contents

Introduction

1.1 Potassium channel gating and structure

Ions and ion channels

Potassium (K^+) is an important cation for normal cell function in both excitable and non-excitable cells. Potassium is maintained at high concentrations within the cell with respect to the extracellular environment, generating a concentration gradient across the plasma membrane. Opening of K^+ channels stabilises the resting membrane potential, and moves membrane potential towards E_K (the equilibrium potential for potassium) and further away from the threshold for firing action potentials in excitable cells. Closure of K^+ channels tends to result in a more depolarised membrane potential. K^+ channels serve many functions. In excitable cells they set the resting membrane potential, repolarise action potentials and regulate refractoriness and action potential firing. They may also have other roles in non-excitable cells such as influencing osmolarity, cell size, and even apoptosis. The modulation of the membrane potential via K^+ channels may also be important in the cell cycle and proliferation (see later). K^+ channels are essential for life and their function cannot be performed by substitution with other ion channels; this is unlike sodium channels which are not found in all organisms and whose function can partially be replaced by calcium channels. The importance of regulation of potassium is reflected by the huge array of genes encoding K^+ channels. In fact, the K^+ channel gene family is the largest and most diverse of all ion channel families, consisting of voltage-gated K^+ channels, inwardly-rectifying K^+ channels, tandem pore-region (also known as 'leak') K^+ channels and Ca^{2+}-dependent K^+ channels.

Structure of the potassium channel pore

All K^+ channels share a similar core structure that is adapted for different functions. The pore is formed by 4 subunits, each with two transmembrane α-helical domains separated by a linker region that forms the K^+ ion selectivity filter. The first K^+ channel crystal structure to become available was the bacterial K^+ channel KcsA (Doyle *et al.*, 1998) (Figure 1.1). The two transmembrane domains from each subunit form anti-parallel α-helices. These pairs of helices

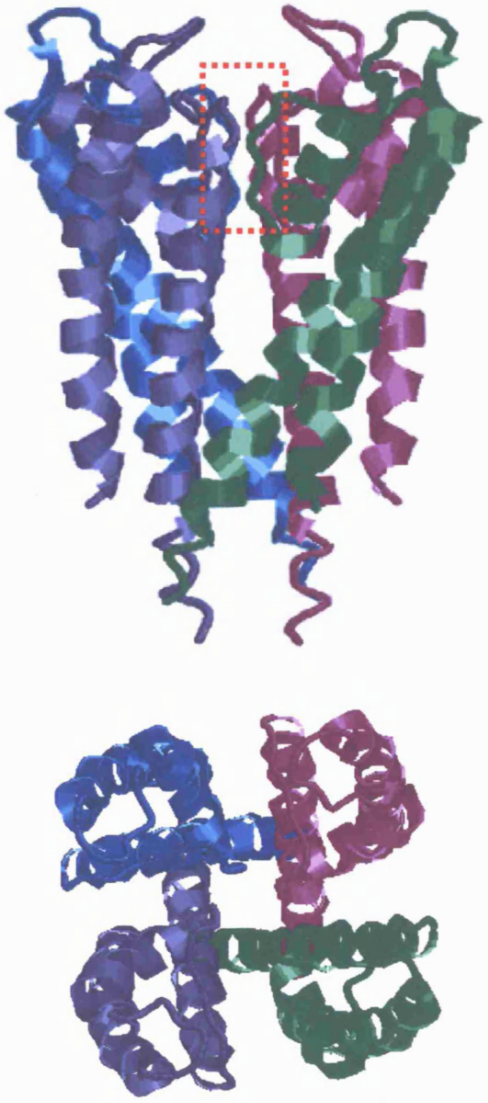

Figure 1.1 Structure of KcsA K^+ channel, which was crystallised in the closed conformation. The upper cartoon shows the crystal structure of KcsA as viewed from the side, with the extracellular side of the channel facing the top of the page. The different subunits are rendered in different colours. The lower figure shows the channel as viewed from the extracellular side of the membrane. Each subunit consists of 2 TM domains. The inner TM helices cross over to for a tee-pee like structure. The re-entrant P-loop can also be seen to form the selectivity filter, highlighted by the red box

from one subunit cross over a neighbouring subunit near the cytoplasmic side of the membrane, forming an inverted tee-pee like structure. In KcsA, the channel is in the closed state and the inner helices cross over to occlude the pore and block conduction. Between the cytoplasmic gate formed by the inner helices and the selectivity filter is a water filled cavity - the inner vestibule. The K^+ ion must then move through the selectivity filter, a process that requires the ion to shed its hydration shell. This process is facilitated by the Gly-X-Gly amino acid motif (where X represents either Phe or Tyr) of the selectivity filter that helps to coordinate the unhydrated ion. The structure and charge of the selectivity filter make it highly selective for K^+ ions; however this is not to say that it is impassable for Na^+, Ca^{2+}, and Cl^- ions (Hille, 2001), and in fact, the selectivity to K^+ varies between channels.

Structure of the voltage-gated potassium channels

K^+ channels are modular and frequently consist of a pore coupled to a variety of regulatory domains that confer sensitivity to voltage, pH or other (usually intracellular) regulatory factors, such as Ca^{2+}, ATP and cyclic nucleotides. Voltage-gated K^+ channels have four additional transmembrane helices per subunit that form the voltage-sensing domains. This gives a total of six transmembrane helices that are named S1 at the N-terminal end through to S6 at the C-terminus. S4 carries a number of positively charged amino acid residues and is thought to have a major role in gating the K^+ channel with to changes of membrane potential, although S1 – S3 are also important (Vandenberg *et al.*, 2004). S4 contains six positive charges that are in part balanced by negative charges spread over S2 and S3. S4 is known to move outward with depolarisation and in doing so moves charged amino acids across the membrane generating 'gating currents'. These small currents can be successfully measured using voltage clamp apparatus when current through the pore is abolished. The precise movements of the voltage sensor remain contentious and are the subject of intense ongoing investigation.

Voltage sensor movement modulates the pore structure. S4 movement may act as a lever that indirectly acts on S6, or the movement of S4 may create space to allow for a tilt in S6 (Bezanilla, 2005). Upon depolarisation of the cell the positive membrane potential acts upon the positive charges in S4 to move S4 towards the extracellular side of the membrane. This movement of S4 causes the S6 domains to splay apart at the intracellular side of the membrane to open the pore

allowing a flow of ions (Vandenberg *et al.*, 2004). This is defined as activation, and the S6 helices that form the barrier to K^+ efflux, defined as the intracellular activation gate. Deactivation, the reverse process to activation, closes the channel pore in response to membrane repolarisation.

Many voltage-gated K^+ channels undergo further conformational changes with depolarisation that renders them non-conducting. This decrease of conduction with depolarisation is referred to as inactivation. Inactivation may be 'N-type' or 'C-type' depending on which structures are involved (Figure 1.2), and both types of inactivation can be present in the same channel. N-type inactivation occurs on the intracellular side of the channel. The *N*-terminus forms a 'ball' of around 20 amino acids, which is tethered to the channel by a 'chain' of amino acids. On depolarisation and following activation of the channel the ball moves into the inner cavity, blocking the pore (Rasmusson *et al.*, 1998). C-type inactivation occurs at the extracellular side of the pore and involves a collapse of the selectivity filter such that the channel cannot pass current. Both N- and C-type inactivation are affected by charge neutralisation of S4 and it is likely that they are linked to movements of the voltage sensor in some way (Rasmusson *et al.*, 1998).

Structure of hERG potassium channel

The *human ether-a-go-go related gene* (*hERG*, also called *KCNH2* or *Kv 11.1*) encodes an important voltage-sensitive, inwardly-rectifying K^+ channel and is the focus of this project. hERG is a member of the EAG (ether-a-go-go) family of K^+ channels that also includes EAG and ELK (EAG-like) channels. Like other voltage-gated K^+ channels, hERG is a tetramer of subunits, each of which has 6 transmembrane segments and an intracellular N- and C-termini. So far it has not been fully determined whether the hERG pore-forming α-subunit associates with an accessory (β-) subunit. hERG expressed alone in *Xenopus* oocytes produces a current that is slightly different from native hERG channel currents (I_{Kr}) in the heart. However, co-expression of the hERG mRNA with that of MiRP1 or mink produces currents with faster deactivation properties similar to the native hERG currents (Weerapura *et al.*, 2002; Sanguinetti & Tristani-Firouzi, 2006). hERG subunits have a large intracellular N-terminus that contains a PAS (PER-ARNT-SIM) domain and a large C-terminus with a cyclic nucleotide binding domain (cNBD) (Morais Cabral *et al.*, 1998). Experiments with *N*-terminally truncated hERG mutants have demonstrated that the PAS domain decreases the deactivation rate of the hERG channel, and causes a +20 mV shift in the voltage-

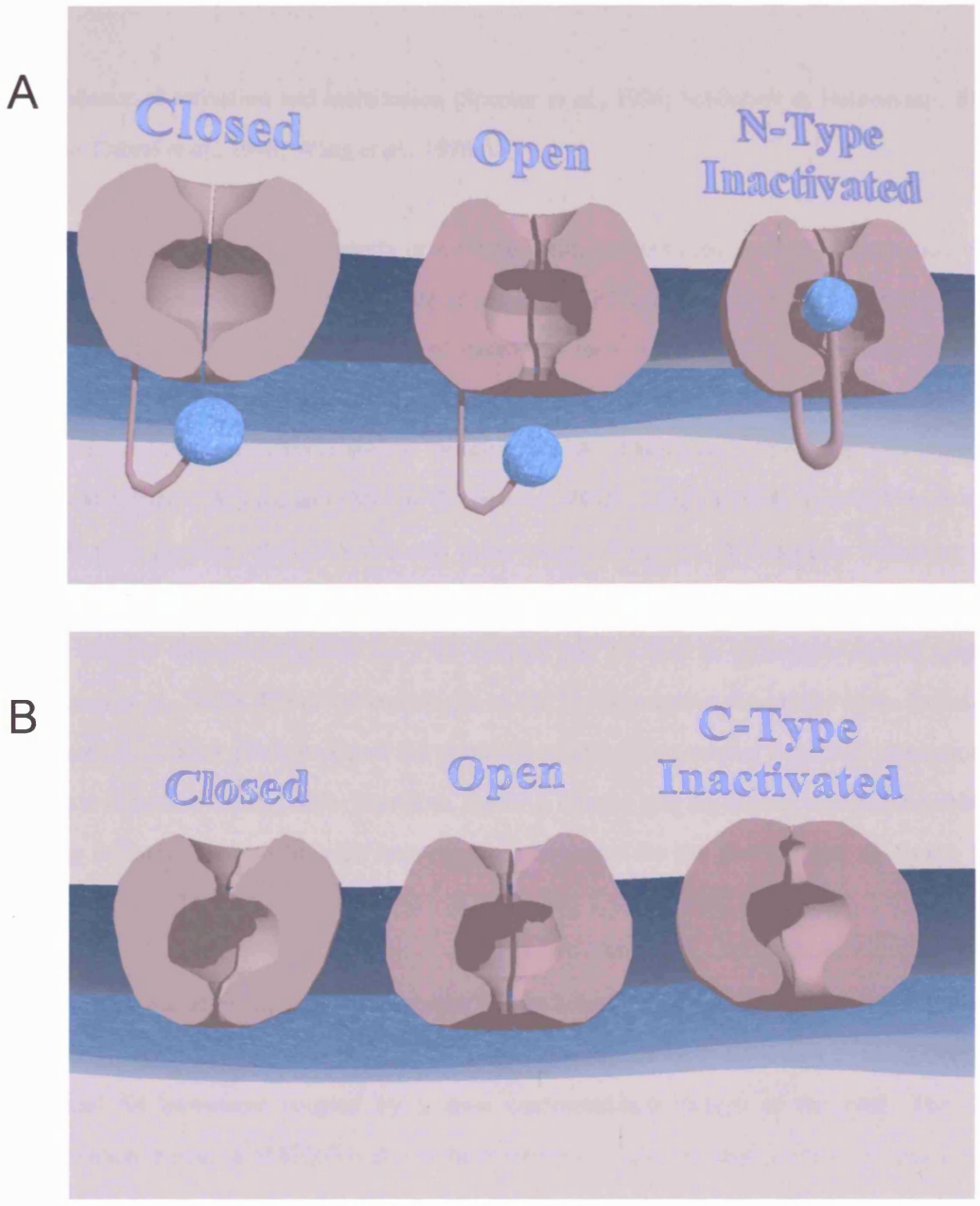

Figure 1.2 Potassium channel gating. A) and B) show the differences between N and C type inactivation, respectively, of voltage gated potassium channels. A) Classical N-type inactivation involves a charged globular domain (ball) tethered to the intracellular mouth of the channel by a flexible linker region (chain). Depolarisation of the membrane causes the ball region to enter the inner cavity of the channel and block conduction. B) C-type inactivation occurs through collapse of the selectivity filter, thus preventing ion flow.

dependence of activation and inactivation (Spector *et al.*, 1996; Schönherr & Heinemann, 1996; Morais Cabral *et al.*, 1998; Wang *et al.*, 1998a).

The PAS domain belongs to a family of sensor domain proteins used in signal transduction via a common conformational change (Vreede *et al.*, 2003). PAS domains in different proteins share little sequence homology; they are related instead by their conserved α/β fold tertiary structure. This domain is able to fold completely independently, and addition of the purified hERG *N*-terminus (residues 1 to 135) is able to reconstitute a WT-like currents in oocytes expressing *N*-terminal deleted hERG mutants (Morais Cabral *et al.*, 1998). Using *in silico* methods Vreede et al. (2003) have proposed that PAS domains have conserved regions of flexibility indicating that although different PAS domains bind different ligands they probably signal this binding in the same way. In the case of hERG the PAS domain may be used as an oxygen-sensing domain (Crociani *et al.*, 2003). The rabbit homologue of ERG is expressed in the carotid sinus. Dofetilide application, to block ERG, produces the same effects on action potential frequency adaptation as hypoxia (Overholt *et al.*, 2000). Therefore, the PAS domain may be used to regulate the channel during hypoxia. This could have important consequences for the development of cancer (see later).

The time-course of hERG channel activation is slow compared to most other K^+ channels, such as Shaker (Wang *et al.*, 1997). This is thought to arise because of slow movement of S4, rather than 'normal' S4 movement coupled by a slow conformational change of the pore. The slow deactivation indicative of hERG is due to the *N*-terminus binding to sites on the pore - possibly on the S4-S5 linker - a region that becomes accessible on channel opening (Wang *et al.*, 1998a). Deactivation may also be slowed due to extra negative charges in hERG relative to other K^+ channels that help to stabilise the open state. hERG inactivates in a voltage-dependent manner that is analogous to C-type inactivation; i.e. collapse of the selectivity filter region (Spector *et al.*, 1996; Schönherr & Heinemann, 1996; Wang *et al.*, 1997). However, hERG inactivation is fast and occurs within milli-seconds compared with seconds for Shaker and other K^+ channels (Figure 1.3).

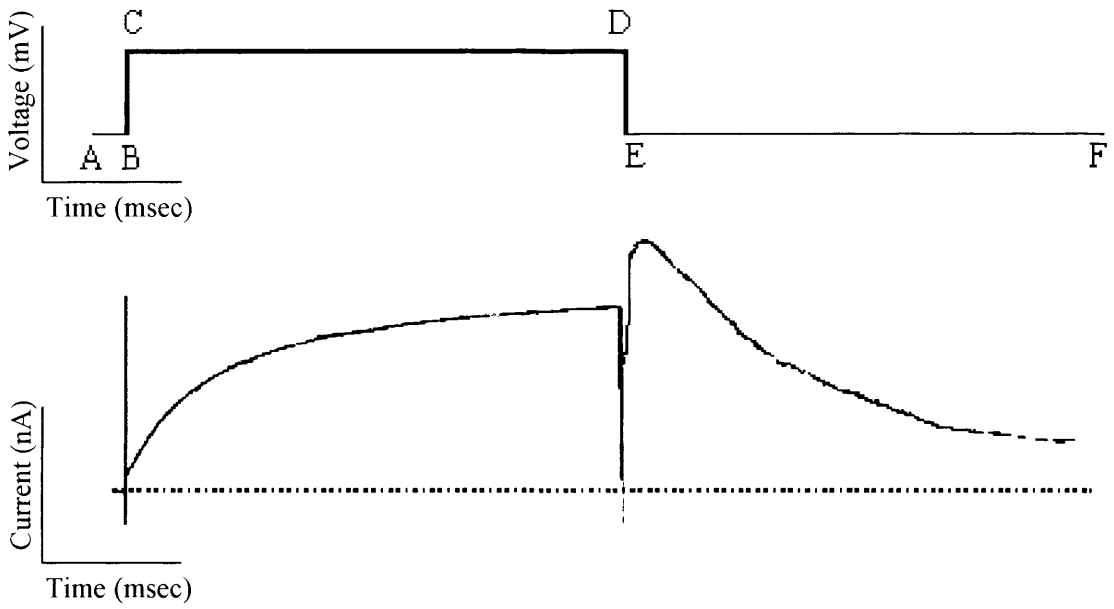

Figure 1.3 Time course of elicited current for hERG. Upper panel: depolarising pulse protocol used in patch-clamp experiments to elicit hERG currents. A-B and E-F represents a holding potential. C-D represents a step depolarisation of membrane potential. Lower panel: hERG current in response to voltage protocol. Dotted line represents 0 nA. Upon depolarisation of the membrane potential (C-D) the hERG channel slowly activates, allowing current flow. However, rapid inactivation of the channel also occurs in response to membrane depolarisation and quickly prevents current flow. If the membrane potential is now repolarised (E-F) the hERG channel rapidly recovers from inactivation and slowly deactivates. The kinetics of these events allows a 'peak-tail' current to flow.

Alternatively spliced variants of hERG

hERG mRNA is alternatively spliced and the various different proteins produced have different properties. The full-length *hERG* gene is termed *hERG*1 and is the default channel referred to in this Thesis. $hERG_{(USO)}$ is a C-terminal splice variant that lacks a full cNBD. Nearly all the C-terminus encoded by exons 9 to 15 has been spliced out and replaced with the small USO exon (Kupershmidt *et al.*, 1998). This protein will only produce a functional current when co-expressed with hERG1. When expressed in a 1:1 ratio $hERG_{(USO)}$ has no effect upon the current generated by hERG1. However, $hERG_{(USO)}$ mRNA is found to be around twice as prevalent in the heart, and when $hERG_{(USO)}$ is expressed at higher levels than hERG1 it can increase the activation rate of I_{hERG1} while having no effect upon deactivation (Kupershmidt *et al.*, 1998).

hERG1b is another alternatively spliced transcript of the hERG1 gene that lacks part of the *N*-terminal sequence, including the PAS domain found in the full-length protein (Crociani *et al.*, 2003). hERG1b can function on its own, and can also form heterotetramers with full-length hERG1 subunits (Crociani *et al.*, 2003). The voltage-dependence of hERG1b is shifted to more depolarised potentials than the full-length hERG1 protein. hERG1b expression, like many K^+ channels, is cell-cycle dependent, and is up-regulated during S-phase. This correlates with the observed depolarisation of the membrane potential in tumour cells during S phase, which is hypothesised to be important for their passage through cell cycle checkpoints (Crociani *et al.*, 2003).

The different transcripts of the hERG gene can form heterotetramers with the full-length hERG1 channel. In doing so the biophysical properties of the hERG channels are altered. By varying expression of the different isoforms cells are able to modulate the gating of the channel, which may, in turn, exert an influence over membrane potential and K^+ homeostasis.

1.2 Physiological roles of hERG

Role of hERG in the heart

Many K^+ channels are used in myocardial tissues to regulate action potentials in cells. In the heart a delayed rectifier K^+ current known as I_K is responsible for modulating the action potential. I_K itself is made up of at least 3 distinct currents (I_{Kur}, I_{Kr}, I_{Ks}) that are named according to their relative rates of activation. The rapid component, I_{Kr}, increases in amplitude during the plateau phase and is important for termination of the plateau phase of the action potential (Mitcheson & Sanguinetti, 1999). The hERG channel is highly expressed in the heart and is the pore-forming subunit of the I_{Kr} channel (Sanguinetti *et al.*, 1995).

As mentioned earlier, hERG has an unusual gating mechanism that makes it important for the termination of the plateau phase of the cardiac action potential. When an action potential is invoked in a ventricular cardiac myocyte it causes a rapid and large influx of sodium ions. This causes a rapid depolarisation, similar to action potentials that occur in the nervous system. However, a major difference is that the cardiac action potential lasts for hundreds of ms rather than just a few ms in nervous tissue (Keating & Sanguinetti, 2001). The period of sustained depolarisation is called the plateau phase and is maintained by a combination of slowly inactivating inward calcium current through L-type calcium channels, and small, slow to activate outward K^+ currents. There is a gradual repolarisation throughout the plateau phase due to the I_{Kur}, current passed by the ultra-rapid delayed rectifier K^+ channels. This current is small and cannot by itself repolarise the cell. However, I_{Kur} current will bring the membrane potential within the voltage range for recovery from inactivation of hERG channels. At the beginning of the action potential the hERG channel activates, but also quickly inactivates such that little current is passed. At the end of the plateau phase the membrane potential reaches a sufficiently repolarised potential to allow recovery from inactivation of the hERG channel. This allows the channel to pass a larger current, repolarising the membrane potential. Once the membrane has been repolarized sufficiently the K_{ir} channels take over and rapidly return the membrane potential to the resting potential (Figure 1.4).

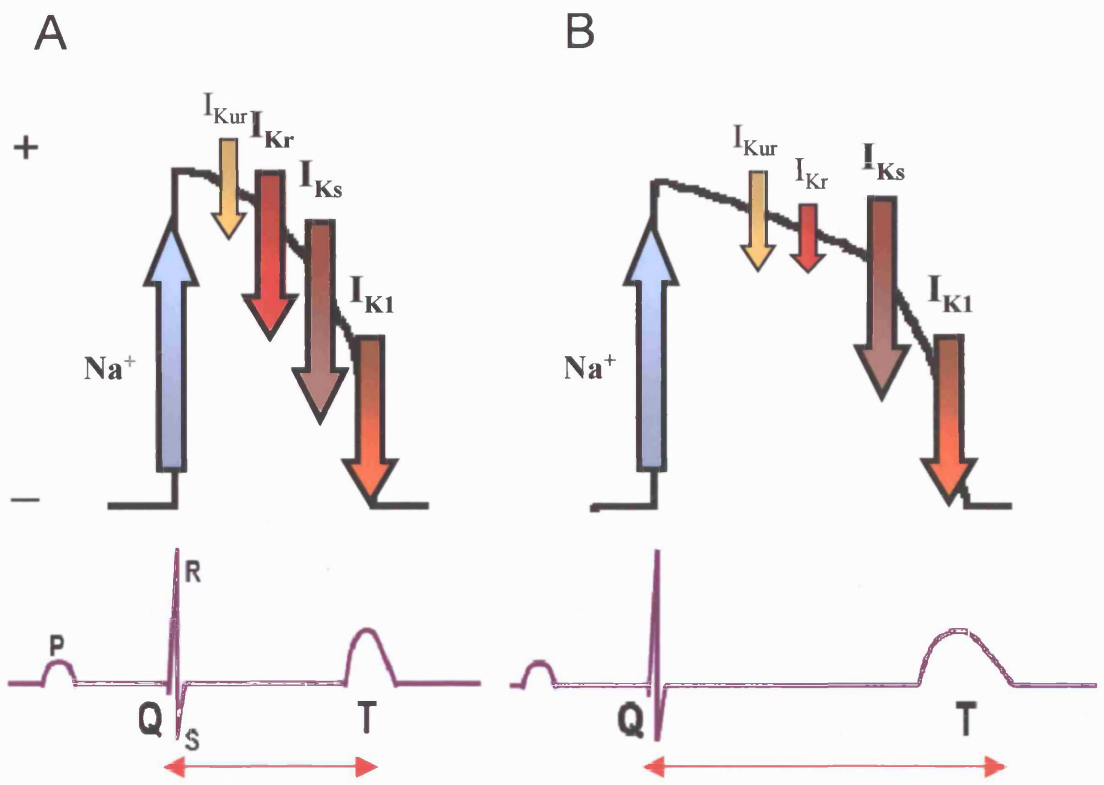

Figure 1.4 Diagram of ventricular action potential and Electrocardiogram (ECG) measurements during normal **(A)** and long QT **(B)** cardiac events. The electrocardiogram measures the size and direction of electrical activity in the heart. The P-wave is generated due to atrial depolarisation. The following QRS complex is caused by ventricular depolarisation. Finally the T-wave is caused by ventricular repolarisation. The ECG measurements correspond to ion channel activity throughout the action potential. The initial depolarisation of the membrane potential is generated via activation of Na^+ channels, and movement of Na^+ ions into the cell. Depolarisation causes activation of I_{Kur}, I_{Kr}, I_{Ks}, and I_{K1} K^+ currents sequentially involved in repolarising the membrane potential (see main text for detail). **A,** A normal heart beat. **B,** If the hERG mediated current I_{Kr} is reduced the membrane potential takes longer to repolarise, and causes prolongation of the QT interval, known as long QT syndrome.

hERG current and long QT syndrome

Long QT syndrome (LQTS) is diagnosed as a lengthening of the QT interval on an electrocardiogram (ECG) caused by a delay in the repolarisation of the action potential. Excessive QT prolongation can predispose the heart to cardiac arrhythmias, particularly torsades de pointes, ventricular tachycardia and ventricular fibrillation, which can lead to sudden death (Keating & Sanguinetti, 2001). LQTS can have a genetic or acquired cause basis. The genetic basis of LQTS is primarily through mutations in cardiac ion channels, including hERG (Keating & Sanguinetti, 2001). Mutations in the hERG protein induce loss of function via different mechanisms including: defective synthesis, inefficient trafficking to the plasma membrane or altered gating properties (Anderson *et al.*, 2006).

Acquired LQTS is more common than the genetic disorder and has a number of causes, particularly block of hERG by medications. Due to the unique structure of hERG many medicinal drugs are able to bind within the inner cavity, and block the channel. This is in part due to the large size of the inner cavity, enabling it to accommodate larger drug molecules (Mitcheson *et al.*, 2000); also the presence of aromatic and polar residues within the pore create a highly appropriate environment for high affinity drug binding (Witchel *et al.*, 2004) (Figure 1.5). Drug block of hERG channels and the resulting LQTS is now of major concern in the pharmaceutical industry. Many drugs, such as terfenadine and cisapride, have had to be withdrawn or their use carefully monitored due to this unwanted side-effect. It has now become common practice to screen all drugs against hERG channel block to try and avoid this possibility. Much work is also concentrating on developing pharmacophore models of hERG blockers and *in silico* models of the hERG channel to try and predict which drugs will block hERG early in the drug development process (Sanguinetti & Mitcheson, 2005).

hERG channels in neuronal tissue

Unlike in non-excitable tissue, hERG is highly expressed in the brain and the nervous system, and has been reported in cells of neural crest origin, such as neuroblastoma (Bianchi *et al.*, 1998), quail neural crest cells (Arcangeli *et al.*, 1997), and glomus cells of the rabbit carotid body (Overholt *et al.*, 2000), where it is thought to regulate the resting membrane potential. hERG channel expression, and the resulting current are also thought to be important for regulating the

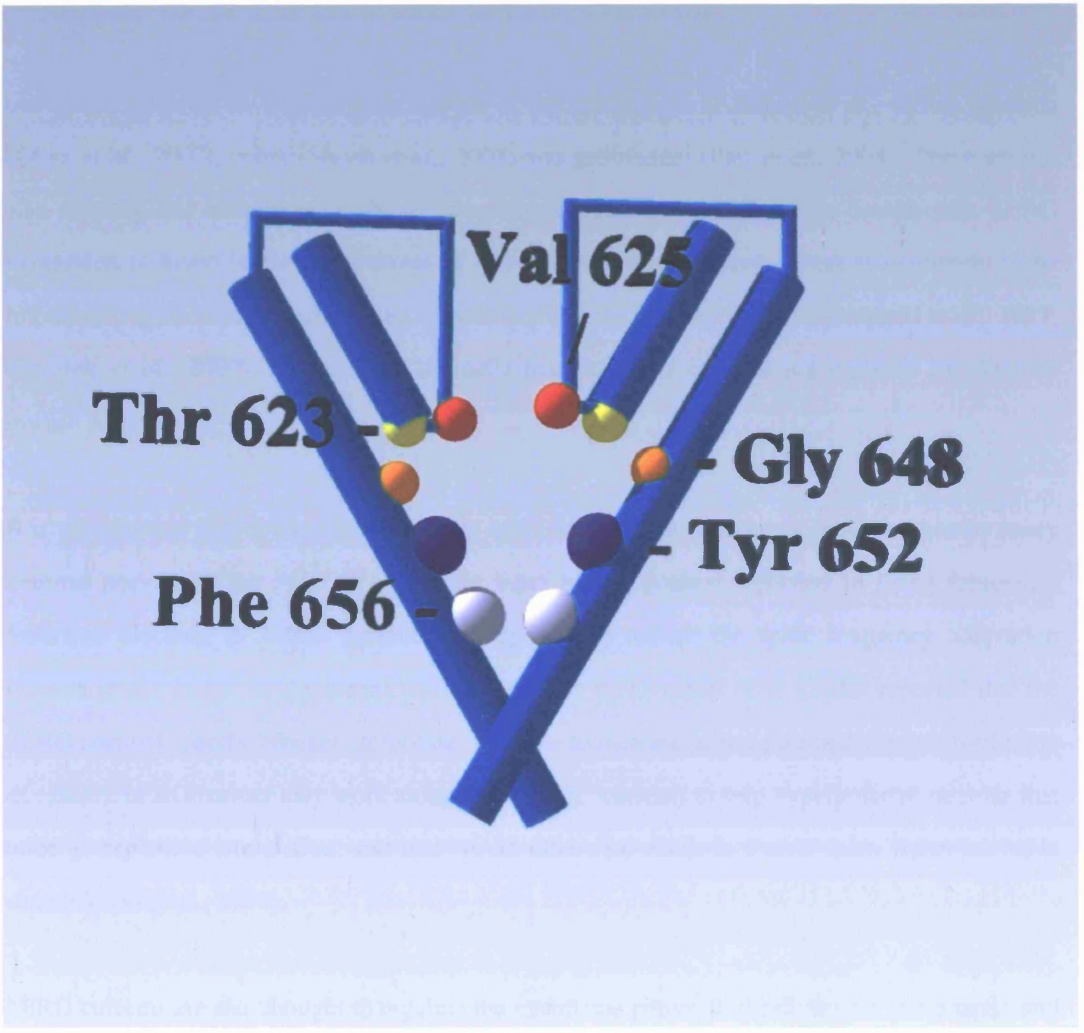

Figure 1.5 Cartoon to show residues important in drug block of hERG channels: The cartoon shows the S6 and re-entrant P-loop (with linker region) of two subunits of the hERG channel. The residues important for high affinify binding are highlighted; including the aromatic residues Y652 and F656, that are important for binding most hERG blockers.

membrane potential in smooth muscle cells of the oesophagus (Akbarali *et al.*, 1999), stomach (Ohya *et al.*, 2002), colon (Shoeb *et al.*, 2003) and gallbladder (Parr *et al.*, 2003). These studies also reported that hERG channel block caused an increase in smooth muscle contractility. hERG expression is found in the early stages of quail embryo development, where it is thought to be important for the development of cell excitability and the nervous system (Arcangeli *et al.*, 1997; Crociani *et al.*, 2000). However, as the cells mature hERG currents are replaced by classical inward rectifiers.

It is thought that hERG may be involved in spike frequency adaptation, a process whereby many neurons respond to the onset of a constant input with a gradual reduction in firing frequency. Selective blocking of hERG current was reported to reduce the spike frequency adaptation (Chiesa *et al.*, 1997). In agreement with this a study by Overholt *et.al.* (2000) reported that the hERG channel-specific blocker, dofetilide, was able to increase action potential firing (Overholt *et al.*, 2000). hERG current may work alongside other K^+ currents to help hyperpolarize neurons that undergo repetitive stimulation, and that would otherwise result in a continuous hyper-excitable state (Chiesa *et al.*, 1997).

hERG currents are also thought to regulate the membrane potential of primary rat lactotrophs, and in turn the release of the hormone prolactin (Bauer, 1998; Schafer *et al.*, 1999). Binding of thyrotrophin-releasing hormone to its G protein-coupled receptor (GPCR), which in turn reduces hERG current by an as yet unknown pathway. The resulting depolarisation of the membrane causes Ca^{2+} influx and stimulates prolatin secretion (Bauer *et al.*, 1999).

Expression of hERG channels in cancer cells

hERG is expressed in early development (before differentiation) in most cells (Crociani *et al.*, 2003). During development most or all the hERG channel expression is downregulated in most tissues. Recent work has shown that many tumour cell-lines express hERG even though the healthy cells from which they originated were devoid of hERG expression (Bianchi *et al.*, 1998; Wang *et al.*, 2002). This may indicate that hERG expression in differentiated non-excitable tissues causes a collapse of the normal regulation of cell division leading to cancerous growth. However, there is also a possibility that hERG gives some sort of selective advantage to tumour

cells and so is a symptom of transformation and not a cause of it, or alternatively that *hERG* is one of many genes that is poorly regulated in cancer cells. In the following sections the role of ion channels in proliferation and cancer will be discussed, with particular emphasis on hERG channels.

1.3 Ion Channels and proliferation

Ion channels are thought to be linked with the cell cycle and proliferation. While the expression profiles of ion channels have been observed to change with the cell cycle and proliferative state, the mechanisms behind this are not well understood. The two most popular ideas are that ion currents produced by ion channels regulate either cell size via osmotic influences or membrane potential.

Changes to membrane potential throughout the cell cycle

Most cells in the adult body are differentiated, have stopped proliferating, and are referred to as quiescent. A small number of cells however are still able to divide and produce daughter cells. These actively dividing cells are referred to as stem cells, and follow a defined growth pattern to ensure that the cell is ready for division before the event. This growth pattern is referred to as the cell cycle. Quiescent cells are outside the cell cycle in G0, but given the correct stimulus may re-enter the cell cycle. The cell cycle is controlled by a complex arrangement of molecules that interact together to induce whole cell changes that ensure that the correct processes occur at specific points in the progression of the cell through its growth and division. The cell cycle has two major phases, known as the S phase (where DNA is replicated) and the M (mitosis) phase (where the cell divides into two daughter cells). These two phases are separated by gap phases, which are called G1 (preceding S phase) and G2 (preceding M phase). In the gap phases the cell grows, and duplicates intracellular organelles such as the Golgi apparatus so that each new daughter cell will have the correct complement of organelles (Figure 1.6).

Entering into the cell cycle and progressing through it necessitates many internal changes such as replication of cell organelles and DNA. The cell cycle must only progress in a single direction - entery into any phase of the cell cycle must be an 'all-or-none' response. This would introduce

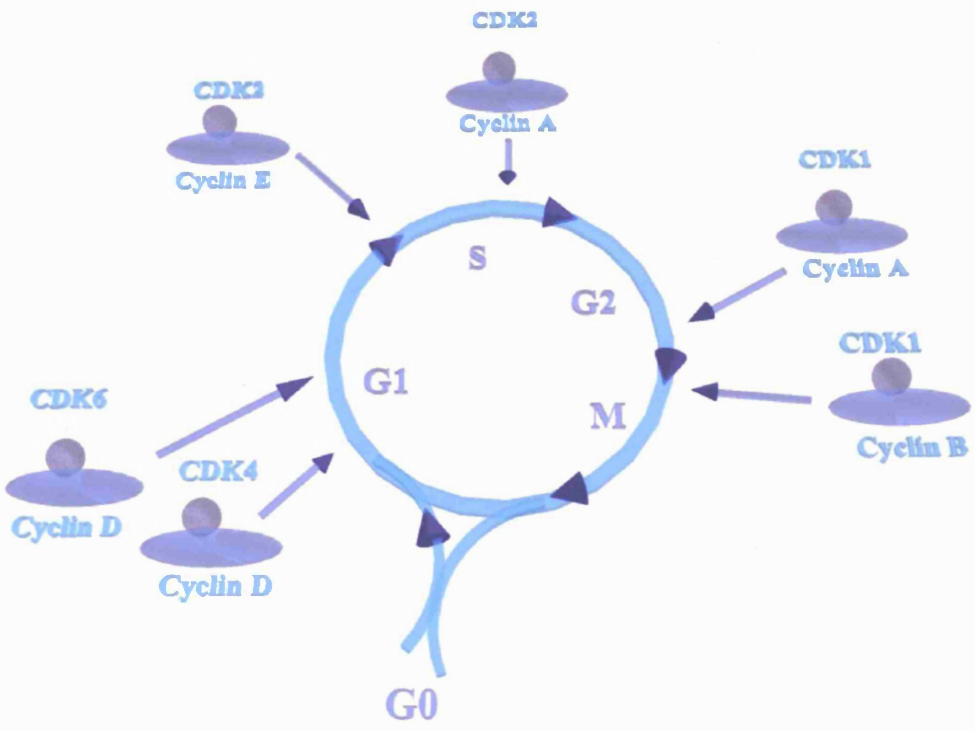

Figure 1.6 Diagram of the cell cycle. The cell cycle consists of S phase and M phase separated by two gap (G) phases (see text). G0 represents quiescent cells not in the cell cycle. Cyclins and cyclin dependant kinases (CDK) regulate each phase of the cell cycle.

problems if a cell were to enter a particular phase before it had the necessary cellular constituents to do so. To overcome this problem cells have set up specific 'checkpoints' at the boundaries of the different phases. In order to pass through checkpoints cells must have the required signalling proteins. This ensures that the cell has performed everything required to enter the next phase. Checkpoints also allow the cell to arrest at critical points in the cell cycle until they are fully prepared to commit to the next phase of the cell cycle (Stewart *et al.*, 2003).

There is a large body of evidence to support the idea that modulation of the membrane potential at cell cycle checkpoints is a key aspect of normal cell proliferation. In order to induce a change in membrane potential at specific time-points the cell can either alter the expression of ion channels or alter the activity/gating of those channels already expressed. For instance, it is documented (LeppleWienhues *et al.*, 1996; Crociani *et al.*, 2000) that there is an increase in K^+ current flow at G1 leading to a relatively hyperpolarised membrane potential in healthy cells. This is thought to be necessary for progression through the G1-S phase checkpoint. Indeed, acute application of the mitogens (prolactin, FBS and EGF) has been reported to generate a transient increase in K^+ currents, via an increase in open channel probability, in LNCaP and RCE cells, presumably generating a hyperpolarisation of the membrane potential (Roderick *et al.*, 2003; Van Coppenolle *et al.*, 2004). In agreement with these data, addition of non-specific K^+ channel blockers was reported to significantly reduce mitogen-induced proliferation, causing arrest at the G1 phase of the cell cycle (Roderick *et al.*, 2003; Van Coppenolle *et al.*, 2004; Guo *et al.*, 2005). LeppleWienhues *et al* (1996) showed that K^+ channel blockers, which depolarise the membrane, inhibit proliferation in the melanoma cell-line SK MEL 28 (LeppleWienhues *et al.*, 1996). The authors also show a similar decrease in proliferation upon application of high external K^+, which will also depolarise the resting membrane potential. A few reports dispute the need for membrane hyperpolarisation at the G1 checkpoint and instead argue that a depolarisation is required (Arcangeli *et al.*, 1995; Smith *et al.*, 2002; Crociani *et al.*, 2003). It has been reported that the resting potential of terminally differentiated cells in G0 is very hyperpolarized, while quiescent cells are moderately hyperpolarized, and cycling cells that do not enter G0 are depolarised (Arcangeli *et al.*, 1995). Arcangeli *et al.* (1995) also suggested that hyperpolarized membrane potentials inhibit DNA synthesis and that cycling cells never produce a sufficiently negative membrane potential to enter G0 (Arcangeli *et al.*, 1995). Whether a cell requires membrane hyperpolarisation or depolarisation to navigate a checkpoint is likely to depend on cell-type and

may account for these conflicting data. Irrespective of the change in membrane polarity, most authors link this change in membrane potential and cell cycle progression with an increase in calcium entry into the cell. Depolarisation may allow entry of Ca^{2+} into the cell through activation of L-type calcium channels (found mainly in excitable cells). Alternatively, hyperpolarisation of the membrane is thought to increase Ca^{2+} entry due to an increased driving force in non-excitable cells (Wonderlin & Strobl, 1996). Ca^{2+} is used as a second messenger in many signalling pathways and Ca^{2+} influx is required for cell proliferation (Means, 1994).

Wonderlin and Strobl (1996) proposed two different models by which the membrane potential might affect the cell cycle. In the first model (the *fixed threshold* model) the membrane potential needs only to reach a specific value for the cell to proceed through the checkpoint. In the second *hyperpolarising transition* model, there must be a change in potential equal or greater than some specified value. The major difference between these two models is their dependence upon the cell cycle. According to the *fixed threshold* model all a cell needs to do is maintain a membrane potential of a given value throughout its cycle and it will continue to divide. This is therefore independent of the cell cycle. The *hyperpolarising transition* model on the other hand requires a change in membrane potential coinciding with the G1 checkpoint. In this case, during the cell cycle the activity and/or expression of ion channels modifies the membrane potential at specific stages. Wonderlin and Strobl (1996) did not provide much in the way of direct experimental evidence for either proposed model. However, there are many studies demonstrating that K^+ currents and/or channel expression levels change during the cell cycle (Arcangeli *et al.*, 1995; Pardo *et al.*, 1998; Wang *et al.*, 1998b; Day *et al.*, 1998; Macfarlane & Sontheimer, 2000; Czarnecki *et al.*, 2000; Ouadid-Ahidouch *et al.*, 2001; Chittajallu *et al.*, 2002; Crociani *et al.*, 2003; Czarnecki *et al.*, 2003). Many of these studies show dramatic changes at the G1 and S-phase checkpoints of the cell cycle, that would seem to support the *hyperpolarising transition* model (see 'Ion channel regulation throughout the cell cycle' section for specific examples).

Cell volume regulates proliferation

Under non-dividing conditions cells maintain a constant volume and carefully control the flow of solutes and ions into and out of the cell. This in turn regulates the osmotic potential of the cell and thus movement of water across the plasma membrane. Progression through the cell cycle has been

observed to correlate with volume changes, with the largest changes seen around the G1/S phase checkpoint and at M phase (Kunzelmann, 2005). Are these volume changes a product of the cell cycle or do they regulate it? In yeast cells it is widely accepted that cell size is critical for progression through the G1 and G2 cell cycle checkpoints (Grewal & Edgar, 2003; Conlon & Raff, 2003). This is based on observations that larger yeast cells proliferate faster than smaller cells. The mean cell volume of a population of yeast cells is constant, arguing for volume-regulated checkpoints, although the mechanisms behind this control are unclear. In studies using mammalian cells, cell growth seems to be independent of cell size. The largest cells will grow at the same rate as the smallest cells (Conlon & Raff, 2003). As Conlon and Raff explained, this universal growth rate will lead to the cells eventually reaching mean population cell size over subsequent divisions without the need for a cell size checkpoint. In the same study, Schwann cells were shown to decrease in cell size (but continue proliferating) when cells were grown to confluency (Conlon & Raff, 2003). This evidence points to a cell cycle that is independent of cell size. While there may not be strict cell size checkpoints in mammalian cells, proliferation is still thought to be influenced by cell volume. Mitogens induce cell swelling, and cell swelling can induce Ca^{2+} entry (Shen *et al.*, 2002), which is known to have many important cell signalling roles, including effects upon cell proliferation. On the other hand, large volume increases can also be deleterious to the cell, whilst significant cell shrinking is sufficient in some cases to induce apoptosis (Maeno *et al.*, 2006).

K^+ channel block has been reported to cause an increase in cell volume (Rouzaire-Dubois & Dubois, 1998). This is expected as channel block will lead to an increase in intracellular K^+ and increased osmotic potential. The increase in cell volume also correlates well with a decrease in cell proliferation due to K^+ channel block. Rouzaire-Dubois and colleagues have published a series of reports that examine the effect of volume on cell proliferation of glioma and retinoblastoma cell-lines. They showed that alterations in cell volume via modulation of osmotic gradients is sufficient to alter proliferation rates (Rouzaire-Dubois & Dubois, 1998; Rouzaire-Dubois *et al.*, 2000; Dubois & Rouzaire-Dubois, 2004). This would suggest that ion channels may not directly affect cell proliferation and it is simply their effect on cell volume that is important. In agreement with this, non-specific K^+ channel block (with inhibitors such as tetraethylammonium) produced a decrease in proliferation. Additionally, these changes in cell proliferation do not correlate well with membrane potential changes (Rouzaire-Dubois *et al.*, 2000). It is unfortunate

that the authors did not investigate further the effects of specific channel blockers to try and narrow the field of possible channels involved, as it is possible that tetraethylammonium had effects on the cell independent of K^+ channel block, e.g. tetraethylammonium can block volume activated chloride currents that may also play a role in volume regulation.

The loss of large amounts of free K^+ ions from the cell will lead to cell shrinkage due to the change in osmolarity. A decrease in cell volume has been shown to be sufficient for activation of apoptotic processes in human lymphoid U937 and epithelial HeLa cells (Maeno *et al.*, 2006). The loss of K^+ may remove inhibitory factors of caspase-3-like proteases (Yu *et al.*, 2001; Wang *et al.*, 2002). Under normal conditions the high K^+ levels inhibit the activation of caspases by preventing cleavage of the pro-enzyme (Bortner *et al.*, 1997). Indeed, if K^+ channels are blocked then apoptosis can be avoided (Yu *et al.*, 2001). It should be noted here that a much larger K^+ flux is needed to induce apoptosis than the ionic currents needed for effects on cell proliferation (Kunzelmann, 2005). This helps to explain why K^+ channels may have dual roles in apoptosis and proliferation. A plot of proliferation versus cell volume reveals a bell-shaped curve indicating that there is an optimal cell volume for growth (Dubois & Rouzaire-Dubois, 2004). Taken together the available evidence suggests that while there may not be a strict volume-regulated cell cycle checkpoint, volume regulation is still critical for optimal cell proliferation.

The high rate of proliferation in cancer cells requires many more reactions to occur in a given time frame, thus solute levels (and osmotic potential) must increase, resulting in cell swelling. For this reason cancer cells must increase their ability to control their volume via regulation of ion channels. It has been observed that volume-regulated anion channels (VRAC) are up-regulated in cervical cancer cells to help reduce swelling of the cell. This expression decreases upon cell cycle arrest (Shen *et al.*, 2002; Kunzelmann, 2005). K^+ channels are also likely to be important in this process (Rouzaire-Dubois & Dubois, 1998). This observation may help to explain some of the changes in ion channel regulation seen in many cancer types. Cell swelling also alters the cytoskeleton, which may act as a mechanosensor and influence cell proliferation (Macfarlane & Sontheimer, 2000). Large volume increases cause the cell to round up (a sphere has the largest volume for a given surface area) reducing cell spreading and focal adhesion contacts with the ECM, and cells become arrested at G1. Whilst the cytoskeleton may play an important role in cell

proliferation via cyclin production it is also important for volume regulation. An intact cytoskeleton may alter cell volume by regulating ion channel activity (Schwab, 2001).

Potassium channels and cell cycle progression

K^+ channels have been shown to be intimately involved in the cell cycle (Arcangeli *et al.*, 1995; Pardo *et al.*, 1999; Smith *et al.*, 2002; Abdul & Hoosein, 2002b; Crociani *et al.*, 2003; Roderick *et al.*, 2003; Van Coppenolle *et al.*, 2004; Pardo *et al.*, 2005; Guo *et al.*, 2005). One of the most important pieces of evidence for this is that drug block of K^+ channels inhibits proliferation of many cell-lines and also primary cancer cells (a few examples are listed below; for a more complete list see (Wonderlin & Strobl, 1996). The K^+ channel blockers Ba^{2+}, quinidine and TEA have been shown to reduce proliferation of the human melanoma cell-line SK MEL 28 (LeppleWienhues *et al.*, 1996). Blockade of the Kv1.3 channel using r-agitoxin (AgTx) and r-margatoxin (MgTx), has been reported to significantly reduce cell proliferation of oligodendrocyte progenitor cells from primary tissue and cultured cells (Chittajallu *et al.*, 2002). However, channel block was not sufficient to prevent cyclin D accumulation in response to platelet derived growth factor (PDGF), suggesting that quiescent (G0) cells remained able to enter the G1-phase of the cell cycle (Chittajallu *et al.*, 2002). In a series of studies Abdul and Hoosein reported a significant effect of Kv1.3 channels on the proliferation of prostate cancer and colon cancer cell lines (Abdul & Hoosein, 2002; Abdul & Hoosein, 2002b). In both cases K^+ channel activators/openers caused a significant increase in cell proliferation, whilst channel blockers, such as glibenclamide, caused dose-dependent decreases in proliferation. Also, as mentioned previously, K^+ channel block has been reported to reduce mitogen-stimulated proliferation in a variety of cell-lines (Roderick *et al.*, 2003; Van Coppenolle *et al.*, 2004; Guo *et al.*, 2005).

Some of the most important work in this field has concentrated on the relationship between expression of the ether a-go-go (EAG) channel and cell proliferation. Using BrdU incorporation and a metabolic dye, rEAG expression was shown to increase the proliferation of Chinese hamster ovary (CHO) cells (Pardo *et al.*, 1999) and Human embryonic kidney (HEK293) cells (Weber *et al.*, 2006). The most obvious way that EAG channels may influence cell proliferation is via ion flux; consequently EAG channel blockers have been used to investigate the role of the EAG current. In breast cancer and melanoma cells, non-specific EAG blockers (imipramine and

astemizole) produce a decrease in cell proliferation not seen in healthy cells (Gavrilova-Ruch *et al.*, 2002). While this study recognised the non-specific actions of the drugs used and performed many controls, there is still a question mark regarding the specific involvement of the EAG current. Unfortunately, the lack of specific EAG channel blockers means that pharmacological approaches are always likely to provide inconclusive data. Recently, researchers have started to use RNAi to knockdown endogenous EAG mRNA levels allowing EAG channel and current reduction to be achieved with greater specificity (Pardo *et al.*, 1999; Pardo *et al.*, 2005). Weber *et. al.* (2006) in particular have produced a complete study providing many of the control experiments needed to validate these types of experiments (Weber *et al.*, 2006). They showed that RNAi can be used to knockdown native EAG causing a decrease in the cell proliferation rate, consistent with that shown using drug block. However, RNAi will not discriminate between the effects of reduction in channel expression or reduction in functional current.

A recent paper has shown evidence that EAG may influence cell proliferation through a K^+-flux independent mechanism (Hegle *et al.*, 2006). The authors used a range of mutant EAG channels expressed in NIH-3T3 cells to show that EAG channel expression increased proliferation in the presence and absence of a functional EAG current. This is the first study to indicate that EAG channels may be bi-functional i.e. that the channel may pass current, but may also be involved in signalling pathways through protein-protein interactions. The study of Hegle *et al.* (2006) used mutant channels (F456A) that have a non-conducting selectivity filter preventing current flow. These mutant channels produced the same increases in rates of cell proliferation as wild type channels indicating that ion flux is unlikely to be required for this effect. However, the channels would only initiate proliferation when the channel was in the closed conformation, suggesting that conformational changes of the channel (due to a change in the membrane potential) were necessary to maintain the effects upon cell proliferation. These data suggest that the effect of EAG on cell proliferation may be through a signalling pathway independent of ion flux. Indeed, p38 MAPK inhibitors (but not p44 or p42 ERK inhibitors) were demonstrated to remove the proliferative effect of EAG expression (Hegle *et al.*, 2006). The authors proposed that a region of EAG is able to interact with downstream signalling molecules and this channel region is likely to be hidden within the protein unless the channel is in the closed state.

Ion channel regulation throughout the cell cycle

The regulation of ion channel expression and modulation is now becoming recognised as a critical determinant of cell cycle control. Many ion channel expression profiles in an array of cell-lines and primary cells have been observed to change in a cell cycle-dependent way. Below are just a few examples of calcium, chloride and sodium channel regulation during the cell cycle.

T-type calcium channels have been shown to be regulated by the state of cell proliferation and differentiation. Kuga *et al.* (1996) showed that expression of calcium channels was cell cycle-specific (Kuga *et al.*, 1996). While the L-type calcium current was unchanged during progression through the cell cycle, T-type calcium currents were only found in G1 and S phases. Unlike many other studies which rely on cell cycle synchronization, this study measured calcium currents in untreated cells. Once the currents had been measured, the stage of the cell cycle was determined by immunocytochemistry for each individual cell; removing the possibility of any potential artifacts resulting from synchronization. The authors attribute this increase in current directly to changes in channel expression rather than modulation of open channel probability (Kuga *et al.*, 1996). This study correlated well with previous observations that neurons, myocytes and skeletal muscle cells express T-type calcium channels at points of increased growth such as early in development. After maturation the expression of these channels is discontinued unless the cells are stimulated to proliferate (Xu & Best, 1990). Since this early study T-type calcium channels have been found to regulate cell proliferation in excitable, non-excitable, healthy and cancerous cells (Panner *et al.*, 2005).

Chloride channel activity has also been observed to be cell cycle-dependent in a range of cell-types including gliomas and lymphocytes (Chen *et al.*, 2002). Chloride channels are also found to be more highly expressed in proliferating than quiescent cells. Chloride channel blockers have been shown to inhibit cell proliferation in many different healthy and cancerous cell-types, including neuroblastoma, Schwann, lymphocytes, liver and cervical cancer cells (Chen *et al.*, 2002). A study using synchronized nasopharyngeal carcinoma cells provided evidence for the cell cycle-dependent regulation of volume-activated chloride current (Chen *et al.*, 2002). It should be noted that this study showed no evidence for a change in channel expression levels. A glioma-specific chloride current has been reported to be regulated by cell cycle, giving an increase in G1 and a decrease in current at S-phase (Ullrich & Sontheimer, 1997). The authors expressed the

view that the regulation of the chloride currents is through cytoskeletal organisation, and provided evidence that chloride currents are increased in response to disruption of the cytoskeleton through hypotonic and cytochalasin D treatments (Ullrich & Sontheimer, 1997). While this study did not present any evidence for the regulation of channel expression, the observed rapid changes in current levels in response to hypotonic and cytochalasin D treatments were too rapid to be due to increased channel synthesis. In a separate study Jiang et.al. (2004) presented convincing evidence that the C1C-5 chloride channel is regulated by the cell cycle at the mRNA level in myeloid cells (Jiang *et al.*, 2004). Interestingly, channel expression was up-regulated in S and G2/M phase and down-regulated in G0/G1 phases, in direct contrast to the glioma channel mentioned above (Jiang *et al.*, 2004).

A study performed in glial cells showed that many ion channels, including sodium channels are modulated throughout the cell cycle (Macfarlane & Sontheimer, 2000). Sodium channel currents appeared to increase through G1, such that the current had doubled by the G1/S phase boundary. This increase in sodium current continued into S phase where a near ten-fold increase in current was observed relative to that at G1 (Macfarlane & Sontheimer, 2000). However, block of the sodium channels with TTX had no effect on cell proliferation and it remains unclear what role(s) the sodium currents might play in cell proliferation.

Potassium channel expression and the cell cycle

Many K^+ channel expression levels and channel activities have been shown to vary through the cell cycle (Arcangeli *et al.*, 1995; Bruggemann *et al.*, 1997; Meyer & Heinemann, 1998; Pardo *et al.*, 1998; Macfarlane & Sontheimer, 2000; Day *et al.*, 2001; Chittajallu *et al.*, 2002; Czarnecki *et al.*, 2003; Crociani *et al.*, 2003). For instance, expression of Kv1.3 and Kv1.5 channel proteins change depending on the proliferative state of microglial cells, and a selective increase in Kv1.3 and Kv1.5 channels is seen at the G0/G1 transition (Chittajallu *et al.*, 2002). Indeed, there seems to be a general trend for K^+ channels to increase current density around G1 (LeppleWienhues *et al.*, 1996; Crociani *et al.*, 2000). Mitogens (such as prolactin and epidermal growth factor) increase the level of K^+ channel activity around G1 (Roderick *et al.*, 2003; Van Coppenolle *et al.*, 2004; Guo *et al.*, 2005). Furthermore, the activity and gating kinetics of the expressed K^+

channels alters with progression through the cell cycle, to produce an increase in current at G1 (Ghiani *et al.*, 1999). This was observed in mouse oocytes where a large-conductance voltage-activated K^+ channel that is active around G1 becomes inactive during the transition into S phase (Czarnecki *et al.*, 2000). Similarly, glial cells show an increase in K_{ir} currents through G1 up to the G1/S phase checkpoint (Macfarlane & Sontheimer, 2000). It has been proposed that this increase in K^+ current keeps the membrane potential at a sufficiently hyperpolarised level for passage through the G1/S phase checkpoint. After passing into S phase K^+ currents are dramatically reduced producing a relatively depolarised membrane potential that may be important for DNA synthesis (Macfarlane & Sontheimer, 2000). It is not yet known how the K^+ channel expression is regulated.

Regulation of EAG during the cell cycle

EAG currents and other inwardly rectifying currents are shown to be similar in size in unsynchronised SH-SY5Y (neuroblastoma) cells. However, upon synchronization at the G1/G0 phase transition of the cell cycle, the inwardly rectifying channel currents increased while the EAG currents dramatically decreased (Meyer & Heinemann, 1998). The regulation of EAG by the cell cycle has also been shown in oocytes. Bruggemann *et al.* (1997) demonstrated that treatment with both progesterone and mitosis promoting factor (MPF) to release the oocytes from their inherent arrest in G2 of the cell cycle, caused a net decrease in EAG current. Cell-cycle sensitivity was shown to be specific to the EAG current, as Shaker and Kv1.4 channels were unaffected (Bruggemann *et al.*, 1997). In a later study, the reduction and rectification of the EAG current seen in oocytes on entering M phase was more closely examined. Unlike the related hERG channel, EAG channels do not inactivate. The inward rectification is produced via Na^+ block of the channel pore (Pardo *et al.*, 1998). This rectification was found to be cell cycle-specific. During M phase of the cell cycle the EAG channel was found to have reduced specificity for ion channel conduction. At this point EAG channels allow the conduction of Na^+ rather than being blocked by this cation (Pardo *et al.*, 1998). This decrease in specificity suggests a change in the conformation of the pore of the channel. Further work by the same lab has shown that the effects upon EAG current rectification in M phase could be due to the loss of interaction of EAG with microtubules/cytoskeleton that are disassembled during cell division. In this study the authors showed that simply excising a patch of membrane, and thus disrupting the microtubule framework

and actin cytoskeleton, produced similar effects on rectification of EAG current as seen in M phase (Camacho *et al.*, 2000). This effect was also recreated by using colchicines or nocodazole to disrupt microtubules. However, the decrease in current amplitudes in M phase was not reproduced with microtubule or actin filament disruption. In fact, actin filament disruption induced an increase in current. The voltage-dependent gating of EAG channels appears to be regulated in a cell cycle-dependent manner. It is thought that this regulation may be mediated via cyclins and cyclin-dependent kinases (CDK), (important signalling molecules involved in the regulation of the cell cycle). However, even though hEAG has 7 consensus sites for phosphorylation there is no direct evidence of phosphorylation by CDKs (Camacho *et al.*, 2000).

Regulation of hERG during the cell cycle

The voltage-dependent properties of hERG varies through the cell cycle (Meyer & Heinemann, 1998). The human neuroblastoma cell-line SH-SY5Y endogenously expresses hERG. Arcangeli *et.al.* (1995) showed that the voltage-dependency for the steady-state inactivation of the hERG current changes during the cell cycle. At G1 phase, inactivation of hERG channels occurs at relatively more hyperpolarised membrane potentials than at S phase (Arcangeli *et al.*, 1995). There appears to be an increase in expression and increased open probability of hERG channels at the G1/S phase boundary (Crociani *et al.*, 2003). As mentioned earlier, hERG is also expressed as the hERG1b isoform, which has a more depolarised activation voltage relative to the full-length hERG1 protein. The ratio of the two co-expressed subunits thus determines the membrane potential at which the heteromeric hERG channel activates. Crociani *et al.* (2003) showed that full-length hERG1 expression dwarfs that of hERG1b at the start of G1 phase; however, at S phase full length hERG is down-regulated and hERG1b is up-regulated (Crociani *et al.*, 2003). The mechanisms behind cell cycle-dependent regulation of ion channel expression are not well understood. Many authors propose the involvement of cell cycle-specific kinases (Day *et al.*, 1998). Overall, there seems to be a general increase in many different ion channels during phases of increased growth; thus aberrant regulation of ion channel expression may be linked with unregulated growth and potentially to play a role in cancer. The evidence for this will be discussed in the following section.

1.4 Ion channels and cancer

Non-potassium channels involvement in cancer

$Ca_v1.2$ is the $\alpha1$ (pore-forming) subunit of an L-type voltage-gated calcium channel expressed in numerous excitable tissues. The channel is not normally found in healthy colon tissue, however, an elevation in $Ca_v1.2$ mRNA and protein levels in colon cancers has been reported (Wang *et al.*, 2000). mRNA levels for $Ca_v1.2$ were elevated in primary colon cancer tissue relative to the surrounding healthy mucosa. $Ca_v1.2$ mRNA was found in all primary cancers tested, with the level of expression being more markedly increased in more developed cancers (Wang *et al.*, 2000). Although the authors suggest that this channel is unlikely to be involved in cell proliferation, as channel agonists were unable to increase [^{3}H]-thymidine incorporation, these studies are not conclusive and further studies are certainly warranted.

TRPM8 is a member of the transient receptor potential (TRP) family of Ca^{2+}-permeable channels. They have a structure similar to that of a K^+ channel with 6 TM domains, and a pore-forming region between the 5th and 6th TM helices (Clapham *et al.*, 2005). TRPM8 is voltage-dependent and relatively non-selective and causing depolarisation of the membrane potential via an influx of Ca^{2+} and Na^+ ions (Clapham *et al.*, 2005). This channel is thought to act as a thermo-sensor in primary sensory neurons. TRPM8 is found in colon cancer, prostate cancer, melanoma and lung cancer. In healthy tissue the channel is only found in significant amounts in prostate cells (Tsavaler *et al.*, 2001; Zhang & Barritt, 2004). Inhibition of TRPM8 activation and siRNA knockdown of the channel were demonstrated to induce apoptosis in LNCaP prostate cancer cell-line, suggesting that TRPM8 is important in cancer cell survival (Zhang & Barritt, 2004). A second TRP channel, TRPV6 (CaT-L), has also been found to be expressed in prostate cancer, and expression levels correlate with tumour grade (Peng *et al.*, 2001). TRPV6 is highly Ca^{2+}-selective and is though to be important in Ca^{2+} uptake in epithelial cells (Clapham *et al.*, 2005).

SCN9A (a voltage-gated sodium channel) expression correlates with metastatic potential in prostate cancer. Blockade of the channel was found to reduce motility in prostate cancer cell line

(MAT-LyLu), whilst channel activation caused a corresponding increase in motility, indicating a possible role in metastasis (Fraser *et al.*, 2003). In a separate study, expression of voltage-gated sodium channels was found to be up-regulated in metastatic human and rat prostate cancer cell-lines, with no expression found in the non-metastatic parental cell-lines (Diss *et al.*, 1998). Sodium channel protein levels correlated with an increased ability to migrate through matrigel, suggesting that the channel may be responsible for this change. In addition, block of the sodium channels with tetrodotoxin (TTx) reduces the invasive potential of the cells (Bennett *et al.*, 2004). This evidence is paralleled by a study of T-lymphocytes. Block of an as yet unidentified Na^+ channel with TTx dramatically reduced invasion (Fraser *et al.*, 2004). Bennett *et al.* (2004) also reported that expression of the human adult skeletal muscle sodium channel, $Na_v1.4$ (hSkM1), was sufficient to generate an invasive phenotype (Bennett *et al.*, 2004). However, the authors failed to demonstrate any functional currents for either the recombinant or native sodium channels. These findings show a direct relationship between sodium channel expression and function and metastasis of prostate cancer *in vitro* that would seem to be dependent upon the functional current of the channel. Sodium channel expression was also reported in strongly metastatic, but not non-metastatic, human breast cancer cells by Fraser *et.al.* (2005). In this study the authors reported that block of the sodium channel $Na_v1.5$ with TTx significantly reduced migration and invasion in human breast cancer cell-lines (Fraser *et al.*, 2005). Expression of the channel also correlated with the metastatic grade of primary human breast cancers (Fraser *et al.*, 2005).

As well as an increase in specific ion channels it has been documented that some channels are downregulated during transformation (for example CLCA1 and CLCA2). In colon and breast cancer both CLCA1 and 2 are down-regulated relative to healthy tissue from which the tumour originates. In breast cancer, stable transfection of CLCA2 has a tumour-suppressing effect and reduces the metastatic potential *in vitro* (Schönherr, 2005; Kunzelmann, 2005).

Potassium channels involved in cancer

As mentioned previously, K^+ channels are known to be essential for normal cell function and proliferation. Therefore it seems reasonable to predict that overexpression or aberrant expression

may lead to abnormalities in the control of cell proliferation. Indeed, there is growing evidence that some K^+ channels possess oncogenic potential.

Calcium-activated potassium channels

The expression of small conductance, calcium-activated K^+ channels (SK1 to SK3) has been characterized in the neuroblastoma cell-line IGR1 and in human primary melanoma human tissue. SK channels are also found in tumours from colon, breast, glial cells, pituitary, prostate (Bloch *et al.*), and pancreas (Jager *et al.*, 2004). Calcium activated K^+ (K_{Ca}) currents (SK2 and IK) are reported to be up-regulated in response to hypoxic conditions via the control of the hypoxia-inducible factor (HIF) protein. The up-regulation of these currents during hypoxia has been shown to hyperpolarise the membrane potential of IGR1 cells and also to increase their proliferation (Tajima *et al.*, 2006). In malignant prostate cancer cells, IK channels were found to be significantly more active than in control cells (Jager *et al.*, 2004). This would seem to suggest that IK channels are advantageous for cancerous growth. In separate studies blockade of the K_{Ca} channels IK and SK2, caused a decrease in growth in IGR1 human melanoma cells (Tajima *et al.*, 2006). While this provides additional evidence for the importance of K_{Ca} channels in cancerous growth, it may also indicate that K_{Ca} channels are involved in normal healthy cell proliferation.

TWIK-related acid-sensitive K^+ channels (TASK3)

The TASK3 (TWIK-related acid-sensitive K^+ channel type 3) channel is a non-voltage-gated K^+ channel that is part of the two-pore domain family of K^+ channels. Native TASK3 expression is only found at significant levels in the brain (Patel & Lazdunski, 2004). The role of TASK3 in healthy tissue has not yet been defined, however, the voltage-independent current is thought to act on membrane potential and the regulation of cell excitability (Pei *et al.*, 2003). In contrast to healthy tissue, TASK3 is over-expressed in many cancers, such as breast, lung, colon, and prostate cancers (Mu *et al.*, 2003). Over-expression of the channel permits serum-independent growth and confers resistance to hypoxic conditions (Mu *et al.*, 2003). The over-expression of TASK3 in a variety of cell-lines (partially transformed mouse embryonic fibroblast, normal murine mammary gland epithelial (NMuMG), and C8 mouse embryonic fibroblast cell-lines) has been reported to increase proliferation and also produce tumours *in vivo* (Pei *et al.*, 2003; Mu *et al.*, 2003). It has also been shown, using a non-conducting, dominant-negative mutant form of

TASK3, that the oncogenic potential and proliferative effects of TASK3 channels are most likely to be mediated by their functional current (Pei *et al.*, 2003). TASK3 also plays an important role in apoptosis (Lauritzen *et al.*, 2003), where its activity is thought to cause excessive K^+ loss from the cell resulting in cell shrinkage and caspase activation (Yu *et al.*, 2001; Wang *et al.*, 2002). Although not well understood the pro-apoptotic and oncogenic effects of this channel may be linked to the cell background in which it is expressed. The amplitude of the K^+ current may also be important with apoptosis requiring a much larger K^+ conductance than proliferation (for review see Patel and Lazdunski, 2004).

G protein-coupled inwardly rectifying potassium channels (GIRK)

G-protein coupled inwardly rectifying K^+ channels (GIRK) are found in both the heart and the brain (Schoots *et al.*, 1996). Activation of G protein-coupled receptors (GPCRs) releases activated $G\beta\gamma$ subunits that bind directly to the GIRK channel increasing its open probability. The channel is also modulated by phosphatidylinositol 4,5-bisphosphate (PIP_2) (Bender *et al.*, 2002). In a study of primary tissue, Takanami *et al.* (2004) showed that GIRK mRNA levels are raised in non-small cell lung carcinoma (NSCLC), where the level of expression correlated with lymph node metastasis and advanced cancer stage, (Takanami *et al.*, 2004). In a similar study GIRK1 mRNA expression levels were also found to correlate with lymph node metastasis in primary breast carcinomas (Stringer *et al.*, 2001).

Kv1.3

As mentioned previously expression of the Kv1.3 channel has been shown to be cell cycle-dependent and important in the regulation of cell proliferation (Abdul & Hoosein, 2002; Chittajallu *et al.*, 2002; Abdul & Hoosein, 2002b). A study of primary human colon cancer tissue showed that the delayed, outwardly-rectifying voltage-gated K^+ channel Kv1.3 is expressed in cancerous tissue while being absent from healthy tissue (Abdul & Hoosein, 2002). Kv1.3 mRNA levels were also reported to be elevated in primary glioblastoma tumours relative to healthy tissue, although there was no observed correlation with the metastatic potential of the tumour (Preussat *et al.*, 2003). On the other hand, a study of primary prostate cancer biopsies reported a decrease in Kv1.3 immunostaining in some (but not all) samples (Abdul & Hoosein, 2002b). Interestingly, this study also reported a link between channel block (with amiodarone) and a reduction in

proliferation (Abdul & Hoosein, 2002b). However, amiodarone is a non-selective blocker and also blocks Na^+ and Ca^{2+} channels, thus further study with specific Kv1.3 channel inhibitors are needed. Unfortunately neither study by Abdul and Hoosein (2002a,b) demonstrated functional Kv1.3 currents.

EAG

Ether a-go-go (EAG) is a voltage-gated K^+ channel that, like hERG, has large intracellular *N*- and *C*-termini that contain PAS and cNBD domains respectively. EAG has two isoforms EAG1 and EAG2. EAG is found most abundantly expressed in the brain, although its function is not well understood. Like hERG, EAG is glycosylated and this glycosylation is important for membrane localisation. The glycosylation is also important for the functional current produced by EAG; de-glycosylation results in reduced current amplitude and slowed activation (Napp *et al.*, 2005). EAG expression is widespread in development, but reduces as cells differentiate. It has been shown that differentiation of neuroblastoma cells leads to loss of EAG expression (LeppleWienhues *et al.*, 1996; Camacho *et al.*, 2000). EAG expression in adult tissues is normally only found in the brain and to a small extent in the placenta. However, EAG is found to be widespread in cancer cell-lines such as HeLa (although no functional currents have been documented in these cells), MCF-7 (breast cancer) and SH-SY5Y (retinoblastoma) cells (Pardo *et al.*, 1999). EAG is also found in a wide range of primary cancer tissues: cervix carcinoma (Farias *et al.*, 2004), neuroblastomas, breast cancer, and melanoma (Camacho, 2006). In similar studies AKT1, a plant homologue of EAG, has been shown to be upregulated in plant tumours, and its deletion reduces tumour size (Deeken *et al.*, 2003). The importance of EAG expression in cancer development was confirmed in a key paper by Pardo *et al.* (1999). This study provided evidence that EAG, expressed in a CHO cell background, was sufficient for an increase in cell proliferation, loss of contact inhibition, growth in soft agar, and *in vivo* tumour formation in severe combined immune deficient (SCID) mice. Expression of the inwardly rectifying K^+ channel Kv1.4 was used in parallel experiments to show that the effects seen with EAG were channel-specific. The oncogenic potential of EAG was further confirmed by showing that antisense knockdown of native EAG expression in cancer cell-lines (such as MCF-7, HeLa and SH-SY5Y) reduced proliferation (Pardo *et al.*, 1999; Weber *et al.*, 2006).

EAG channels activate slowly on depolarisation of the membrane potential and have a threshold for activation of approx -40 mV. The relatively positive activation range of EAG means that if it is expressed in cells where there are no inward rectifier K^+ channels then these cells will have a relatively depolarised resting membrane potential. This was originally proposed to be important to the oncogenic potential of the EAG channel. However, as mentioned earlier, recent studies have showed that the transforming ability of the EAG channel may be independent of ion flux, and may instead involve alterations in p38 MAPK signalling (Hegle *et al.*, 2006).

hERG

In the developing embryo hERG is ubiquitously expressed. However, as cells start to differentiate they lose this expression and in adulthood only excitable cells such as nervous tissue, smooth muscle and the heart express hERG. This expression pattern has similarities to that of EAG. De-differentiated, cycling cells such as tumour cells have been shown to re-express hERG. Indeed, hERG expression is found in many transformed cell lines as well as primary tissues including: neuroblastoma (SHSY-5Y cell line), rhabdomyosarcoma (TE671 cell line), mammory adenocarcinoma (SK-BR3 cell line), lung microcytoma (NCL-N592 cell line), monoblastic leukaemia (FLG29 cell line) (Bianchi *et al.*, 1998), human endometrial cancer (Cherubini *et al.*, 2000), myeloid leukemias (Pillozzi *et al.*, 2002), colon cancer (Lastraioli *et al.*, 2004), breast cancer, immature neoplastic B-CLL cells, glioblastoma multiforme (Masi *et al.*, 2005), CD5-Burkitt's lymphoma cell-line, and a number of haematopoietic cell lines (Smith *et al.*, 2002). However, hERG is not found in any of the healthy tissues from which these cells/cell-lines originate. It is of note that hERG is expressed in every major class of cancer and is not limited to cancers that affect just one type of tissue. hERG protein and current expression levels correlate well with the metastatic phenotype of cancerous tissue. In colon cancer (Lastraioli *et al.*, 2004) and gliomas (Masi *et al.*, 2005) hERG channels are most prevalent in the late stage, more aggressive tumours. These observations implicate hERG expression as important in the generation of a fully transformed phenotype, rather than just a consequential up-regulation within the cancer phenotype.

It has been proposed that during development hERG channel expression allows cells to divide rapidly. After the initial stages of development however, most cells have no need to divide constantly. This correlates with the loss of hERG expression seen in differentiating cells. As cells differentiate hERG expression is replaced by that of other inwardly-rectifying K^+ channels whose currents are able to more fully hyperpolarise the membrane potential. During transformation and de-differentiation cancer cells regain a rapidly proliferating phenotype correlating with re-expression of the hERG channel. Cancer cells also have a relatively depolarised membrane potential compared to differentiated tissue; although whether this can be attributed to the expression of hERG is not yet known. Data produced by Crociani and colleagues indicate that the depolarisation of the resting membrane potential observed in many tumours may be explained by a decrease or removal of the native inwardly-rectifying K^+ current, and replacement with the hERG current (Crociani *et al.*, 2003). Expression of hERG somehow causes a change in the inwardly rectifying K^+ current, such that it can no longer hyperpolarise the cell to the same extent. This has given rise to the concept that it may be the loss of K_{ir} channels, rather than gain of hERG channels that is responsible for the change in membrane potential. hERG undergoes variations in voltage-dependent activation throughout the cell cycle (Meyer & Heinemann, 1998). This indicates that hERG K^+ current (I_{hERG}) may influence the resting membrane potential at critical points in the cell cycle. It is likely that I_{hERG} and the absence of I_{Kir} current are both important in producing the more depolarised membrane potential characteristic of transformed cells, which is thought to allow progression through the cell cycle.

Evidence for the involvement of I_{hERG} in cancer is limited. Many papers (LeppleWienhues *et al.*, 1996; Macfarlane & Sontheimer, 2000; Pillozzi *et al.*, 2002; Crociani *et al.*, 2003) that claim to show a link between I_{hERG} and cancer progression/formation have done so by using very high concentrations of hERG blockers, far in excess of that needed to fully block the channel. In such investigations the hERG channel blockers have been shown to produce decreases in cell growth and proliferation, however, the high concentrations of drug used may have led to non-specific effects on the cell, such as cytotoxicity, which may itself cause the observed change in cell phenotype. For this reason the potential involvement of I_{hERG} needs to be corroborated, preferably using different experimental approaches.

The expression of hERG channels is also regulated by extracellular conditions, such as hypoxia, which may play an important role in the involvement of hERG in cancer. Tumours often develop so rapidly that the vasculature struggles to maintain an adequate blood supply for the growing tissue mass. Thus, overcoming normally growth-limiting hypoxia is a normal step in cancer development. Hypoxia often leads to depolarisation of the membrane, which if left unchecked could prove harmful to the cell. If hERG current is the only hyperpolarising current expressed in a particular cancer cell then its up-regulation would prove beneficial (Fontana *et al.*). The PAS domain has been demonstrated to give oxygen- and redox-sensing capabilities to other unrelated proteins (Taylor & Zhulin, 1999; Kurokawa *et al.*, 2004). The hERG channel PAS domain structure resembles that of the hypoxia-induced factor 1α (HIF-1α). HIF-1α is a transcription factor that regulates the expression of genes important in cell adaptation to hypoxia. HIF-1α protein levels are controlled by the proline hydroxylases that create a binding site on HIF-1α for the tumour suppressor von Hippel-Lindau (VHL) protein. Under oxygenated conditions VHL targets HIF-1α for degradation via the ubiquitin pathway. In hypoxic conditions, HIF-1α is no longer targeted for degradation and thus increases the transcription of "hypoxic" genes (Jaakkola *et al.*, 2001). HIF-1α has been shown to regulate the activation of calcium-activated K^+ channels during hypoxic conditions both in tumour cell lines and in primary human melanoma tissue (Tajima *et al.*, 2006). The presence of the PAS domain in EAG and hERG channels may indicate that these channels can also be regulated during hypoxia (Crociani *et al.*, 2003). Indeed, Heinemann and colleagues have announced on their web site that they have seen VHL-mediated regulation of the EAG channel, although these results have not yet gone through peer review.

hERG expression may also facilitate proliferation caused by tumour necrosis factor (TNF). The TNFα receptor (TNFR) is overexpressed in many malignant cancers (de Miguel *et al.*, 2000). It has been reported that high concentrations of TNFα (1-10 ng ml^{-1}) can induce apoptosis - an effect which was potentiated by hERG channel expression. Addition of the specific hERG channel blocker dofetilide was able to reduce TNFα-induced cell death, but only in hERG-expressing cells (Wang *et al.*, 2002). At low concentrations (0.1ng ml^{-1}) TNFα promotes cell proliferation in tumour cells, and this effect is potentiated by hERG expression in cancer cell-lines and stably transfected HEK293 cells. Interestingly, the increase in proliferation was not affected by channel block with dofetilide, or expression of a non-conducting hERG mutant (Wang *et al.*, 2002). hERG is pulled down with TNFR in co-immunoprecipitation assays and is thought to help

recruit the receptor to the cell surface (Wang *et al.*, 2002). These authors have also presented preliminary immunocytochemical evidence that hERG expression correlates with an increased nuclear localisation, and thus activation, of NF-κB. These initial data are far from conclusive, but may indicate a link between hERG channel expression and cancer development. NF-κB is a downstream target of TNFR activation and has been shown to be upregulated in many cancers such as non-small-cell lung cancer, breast, prostrate, pancreatic, thyroid and melanoma (Richmond, 2002). The activation of NF-κB is believed to have many important oncogenic effects, and in turn reduction in activity of NF-κB (using the PS-341 inhibitor) in tumour cells causes reduction of tumour formation, reduction in vascular endothelial growth factor (VEGF) production, and apoptosis (Sunwoo *et al.*, 2001; Richmond, 2002). Taken together, these results suggest that hERG current may play a role in tumour cell apoptosis, although how this relates to channel expression in tumour cells is presently unclear.

So far I have explained the role of hERG in membrane potential regulation and as a potential cause of cancer. However, hERG expression may in fact be a secondary consequence of the transformation process. hERG channels may play an important role in regulating the membrane potential in conditions that preclude the use of other ion channels. A possible example of this is in conditions of high polyamine production generated during cancer development. Polyamines, such as putrescine, spermidine and spermine are small organic cations. The levels of polyamines are highly regulated by various biosynthetic and catabolic enzymes (Shah *et al.*, 1999). It has long been known that polyamine production is under hormonal control such that growth signals cause an increase in polyamine biosynthesis. In clinical studies it was noticed that in cancer patients there was an increase in polyamines in the urine (Russell, 1973) leading to the discovery that polyamine production is up-regulated in cancer cells. It has been proposed that the up-regulation of polyamine synthesis is necessary for cell proliferation, and the development of a neoplastic phenotype (Shah *et al.*, 1999). The accumulation of polyamines within the cancer cells is akin to what happens to embryonic cells. However, as embryonic cells differentiate the polyamine levels are much reduced, whereas in cancer the high levels of polyamines are constant. Investigations using antibodies to reduce the effective concentration of polyamines showed a decrease in cancer cell growth (Russell, 1973). This has lead to potential anti-cancer treatments that act to block polyamine production or reduce the levels of polyamines in the cell. K^+ channels (such as the K_{ir} and Kv families) have inwardly rectifying gating properties due to block by magnesium ions and

polyamines (Nichols & Lopatin, 1997). It is possible that the high levels of polyamines prevent IRK channels from passing sufficient current to regulate the membrane potential. In the absence of other K^+ channels the membrane potential will become increasingly depolarised, which may become deleterious to the cell. hERG channels are inwardly rectifying through a distinct structural mechanism and are unaffected by polyamines; thus upregulation of the hERG channel may provide a way for cancer cells to regulate membrane potential.

1.5 Cancer cell biology

The process by which a healthy, differentiated cell becomes cancerous and de-differentiates is called transformation. Transformation is a multistep process requiring many different signalling pathways to be modified. The initial steps towards transformation are thankfully rare events. However, once the barrier to initial stages of transformation has been overcome mutations occur with increasing frequency. In general there are six major stages of cancer formation leading to a fully transformed phenotype (Hanahan & Weinberg, 2000), and these are briefly described below.

1.5.1. Self-sufficiency in growth signals

Healthy cells in the body do not divide unless exposed to extracellular stimuli such as mitogens. Without mitotic growth signals, cells stay in G0 and do not enter into the cell cycle. Mitogens are normally produced by cells of a different type to those on which they act (Hanahan & Weinberg, 2000). However, some tumour cells can produce mitogens that they themselves are sensitive to. This creates a positive feedback loop, removing the requirement for an external stimulus. Cancer cells also up-regulate growth factor receptors, and can even modify these receptors so that inhibitory domains are removed therefore making them constitutively active and ligand-independent (Hanahan & Weinberg, 2000). Oncogenes may also allow the cell to traverse the checkpoints imposed by the lack of mitogens/growth factors. For example, a small number of cancers show CDK and cyclin mutations so that these proteins are overexpressed, increase in activity, or become resistant to the binding of CDK inhibitors (CKIs) (Kim *et al.*, 1999).

1.5.2. Insensitivity to anti-growth signals

Just as cells receive growth factors from other cells, they also receive growth-inhibitory signals that act on cell surface receptors such as TGFβ (transforming growth factor-β) receptors (Hanahan & Weinberg, 2000). Some cells contain anti-growth signals in their membranes that provide contact inhibition e.g. contactinhibin (Wieser *et al.*, 1985). Anti-growth signals can either be used to place the cell into G0 (e.g. stem cells that will need to replicate at a later date), or to remove the cells replicative potential and allow differentiation into a specialised cell-type (Hanahan & Weinberg, 2000). TGFβ acts on receptors to induce the phosphorylation of the Smad4 (tumour suppressor gene) protein. Phosphorylated Smad4 proteins then translocate to the nucleus where they induce synthesis of p21 (Peng *et al.*, 2002), a transcription factor that will induce cell-cycle block at G1 (Hanahan & Weinberg, 2000). There are many ways in which this regulatory system can be disrupted in much the same way that the growth signal pathways mentioned above are disrupted. Cancer cells must also avoid differentiation signals to retain their replicative potential.

1.5.3. Evading apoptosis

Cancer cells have damaged DNA that is normally detected at cell cycle checkpoints, which if not able to deal with the abnormality, may activate the apoptosis pathway. Imbalance of cell signalling factors induced by oncogenes can force the cell to implement the apoptotic pathway (Hanahan & Weinberg, 2000). External signals are also important for the continued life of a cell. Cell-cell and cell-matrix adhesions are usually necessary for cell survival and if removed may induce programmed cell death (Hanahan & Weinberg, 2000). There are also external signals that either allow survival (insulin-like growth factor (IGF-1, -2) binding the IFG-1R receptor) or promote death (FAS ligand binding the FAS receptor, a protein that belongs to the TNF superfamily) (Newell & Desbarats, 1999; Hanahan & Weinberg, 2000).

In the early stages of cancerous growth the rate of proliferation is generally high. In these early stages the rate of apoptosis is also high, such that the tumour does not grow at a rapid rate. It is only as the cancer cells acquire the ability to evade apoptosis that the growth of the tumour proceeds at a faster rate. There are many different strategies that the cell can use to avoid pro-apoptosis signals. One example is the production of 'dummy' FAS receptors that will bind the FAS ligand but induce no response.

1.5.4. Limitless replicative potential

Once cancer cells have developed such that they are capable of unregulated growth and division they must find a way to continue replicating indefinitely. In normal eukaryotic cells the replication of DNA involves the shortening of the chromosome ends. Cells are designed to cope with this by having an array of 6bp tandem repeats at the ends of the chromosome called telomeres. The loss of these repeats will not affect any transcribed genes in the normal life span of a cell. The life span of cancer cells however is infinite, therefore the telomere repeats will eventually run out (after 60-70 doublings) and genes will start being lost after chromosome replication. Continued loss of these genes will eventually lead to the death of the cell. This is called the crisis state of a tumour and at this point there is massive cell death. However, from the emerging pool of dead cells there will be a few cells that have found the ability to copy their genome without the loss of important gene information - they have become immortal (Hanahan & Weinberg, 2000). For cancerous cells to divide past crisis point they must somehow obtain the ability to produce telomerase, an enzyme which is able to extend the length of the telomeres after they have been shortened.

1.5.5. Tissue invasion and metastasis

Due to the nature of cancer tissue growth, the cells will eventually proliferate to the point where space or blood supply is limiting. In order for the cancer to spread further it becomes metastatic. Individual cells move away from the original site of cancer and move to other parts of the body to invade new tissues in search of more favourable growth conditions. Metastasis is usually the final stage of cancer development and potentially the most harmful. Normal healthy cells require a substrate on which to grow and have specialised cell surface proteins that bind the cell to other cells and the extracellular matrix. Cell-cell adhesion molecules (CAMs), cadherins and integrins are examples of such proteins (Hanahan & Weinberg, 2000). In metastatic cancer cells these adhesion molecules are down-regulated/deleted or mutated such that they are no longer adhesive and may even become repulsive (Hanahan & Weinberg, 2000). For tissue invasion and metastasis it is important that cancer cells are able to move through the surrounding tissue structures. To do this transformed cells release proteolytic enzymes to digest the surrounding ECM components, allowing the cell to move through the disrupted tissue. Some of these protease molecules are

localised to the leading edge of the cell membrane via interaction with integrins. An example is the matrix metalloproteinase (MMP), involved in the breakdown of collagen (Hood & Cheresh, 2002). As well as interacting with, and being localised by integrins (such as αvβ3), MMPs are also activated by integrins. In fact, the increase in expression of αvβ3 is a common feature of increased invasion potential of transformed cells (Keely *et al.*, 1998). The activation of MMP uses a negative feedback pathway to ensure that there is sufficient ECM structure left after degradation to allow points of adhesion for cell migration (Hood & Cheresh, 2002).

1.5.5.1 Cancer cells may attain the ability to grow in the absence of adhesion

Integrin signalling is essential for normal anchorage-dependent healthy cells. Detachment from the ECM and loss of integrin-ligand interactions will reduce integrin-mediated signalling and will lead to a specialised form of apoptosis known as anoikis. For cancer cells to migrate and invade new areas of the body they must overcome the system that was designed to prevent them from doing so. Substrate-independent growth is a property of many high-grade tumours and allows them to grow and proliferate in the absence of contact with the ECM. Integrin attachment to the ECM activates the MAPK pathway, which is essential for normal cell growth. ERK1/2 activation is a necessary cell survival signal and without this integrin activated signalling the cell will commit to anoikis. On detachment from the ECM cells also lose focal adhesions, and thus stress fibres are unable to form (Pawlak & Helfman, 2001). The re-organisation of the actin cytoskeleton is known to reduce ERK1/2 activation in NIH-3T3 cells (Frisch & Screaton, 2001). Similarly, cytoskeleton disorganisation by cytochalasin D blocks cyclin D production and thus proliferation in NIH-3T3 cells (Roovers & Assoian, 2000). Oncogenic proteins, such as Ras, can bypass the need for integrin-matrix adhesion in order to activate the MAPK signalling pathway. This is possible because Ras acts downstream of the integrin signal. Constitutively active FAK is also able to produce substrate-independent growth (Frisch *et al.*, 1996; Hood & Cheresh, 2002). In agreement with this, expression of dominant-negative forms of FAK can cause anoikis in anchorage independent cells (Hood & Cheresh, 2002).

FAK, Shc and ILK (integrin-linked kinase) are all linked to cell survival signalling (Frisch & Screaton, 2001). These kinases share a common survival pathway that involves the phosphoinositide 3-kinase (PI3K). PI3K is activated by receptor tyrosine kinases (such as growth

factor receptors) and activated integrins. Activation of PI3K causes it to locate to the plasma membrane, where the kinase generates phosphatidylinositol 3,4,5-trisphosphate ($PI(3,4,5)P_3$). $PI(3,4,5)P_3$ and $PI(3,4)P_2$ are important second messengers in the cell and will bind Akt (protein kinase B) locating it to the inner surface of the plasma membrane, and causing a conformational change in Akt to allow optimal phosphorylation by kinases such as ILK (Datta *et al.*, 1999). Akt is critical to the survival pathway and is able to inactivate many downstream targets, such as caspases and transcription factors involved in apoptosis (Datta *et al.*, 1999). Akt is also able to induce the expression of cyclin D1 and thus help induce cell-cycle progression (Gille & Downward, 1999). PI3K may also induce cyclin D1 expression independently of Akt. PI3K and Akt are so important that over-expression of either kinase will prevent apoptosis after stress such as loss of substrate adhesion, UV irradiation or growth factor withdrawal. Also, expression of dominant-negative Akt is sufficient to induce apoptosis (Datta *et al.*, 1999).

PI3K can be directly activated by activated Ras and Shc (Datta *et al.*, 1999). PI3K also activates Rac which in turn activates p21-activated kinase (PAK) (Frisch & Screaton, 2001), which may then go on to induce Raf1 and MEK activation in the MAPK pathway. FAK is also able to interact with the p85 subunit of PI3K and cause its activation. After integrin ligation at focal adhesions, FAK is phosphorylated and activates the MAPK pathway, indirectly activating Akt (although FAK may also directly activate Akt) thus repressing anoikis (Frisch & Screaton, 2001).

ILK associates with the cytoplasmic domains of integrins β1, β2 and β3 and is rapidly activated on integrin ligation (Frisch & Screaton, 2001). ILK is also activated by $PI(3,4,5)P_3$ and in turn is able to activate Akt (Datta *et al.*, 1999). ILK-null fibroblasts show defects in cell attachment, focal adhesion formation and reduced cell proliferation (although the reduction in proliferation was not due to a reduction in PKB/Akt phosphorylation). This phenotype could be rescued by expression of a 'kinase-dead' mutant of ILK (Sakai *et al.*, 2003). In direct contradiction to this study, Troussard et.al. (2003) have reported that ILK knockdown (siRNA and CRE-recombinase techniques) lead to a reduction of Akt phosphorylation at site S473, that was rescued after expression of kinase-active ILK, but not kinase-dead ILK (Troussard *et al.*, 2003). This study also presented evidence that loss of ILK expression lead to apoptosis, presumably through the loss of Akt signalling (Troussard *et al.*, 2003). Using a "floxed" allele, Sakai *et al.* (2003) have also

presented evidence that ILK deletion is embryonic lethal (Sakai *et al.*, 2003). It is possible that cell type-specific effects may help reconcile the results from these studies.

If FAK, Shc or ILK is able to constitutively activate Akt in transformed cells then this will enable cells to survive in the presence of apoptotic stimuli. This is critical in the formation of tumours as the cells at the centre of the mass of rapidly dividing cells will have to endure harsh conditions such as hypoxia. Metastasis will also necessitate the survival of the cell in the absence of matrix adhesion.

1.5.6. Sustained angiogenesis

Cells in the body must be no more than 100 μm away from a capillary in order to obtain the nutrients needed for survival (Hanahan & Weinberg, 2000). This obviously provides problems for rapidly growing cancer cells that may quickly grow to greater sizes than the original vasculature can supply. Therefore, cancer cells must induce the growth of capillaries into the tumour in a process termed angiogenesis, see review (Yancopoulos *et al.*, 2000). In the initial stages of tumour development, the size of the tumour is limited by the blood supply, until the cancer cells gain the ability to induce vessel growth. Limited blood supply leads to hypoxia, and this is thought to trigger the activation of the transcription factor HIF-1α that increases transcription of pro-angiogenic genes (Carmeliet *et al.*, 1998). The transcription factor NF-κB (a downstream target of TNFR) has also been reported to be activated in response to hypoxia (Koong *et al.*, 1994). NF-κB is found in many cancers (Richmond, 2002) and its activation is thought to be important in tumour-mediated angiogenesis (Sunwoo *et al.*, 2001). Angiogenesis is induced by soluble factors released by tumour cells to induce growth of vascular endothelial cells, such as TNF-α, and vascular endothelial growth factor (VEGF) (Ferrara *et al.*, 2003). Indeed, many cancer cells show an increased expression of VEGF (Brown *et al.*, 1995), and TNF-α (de Miguel *et al.*, 2000). VEGF has proved to be particularly important in tumour-mediated angiogenesis, and an array of studies have reported that reduction of VEGF signalling (through a variety of technigues, including expression of dominant-negative receptors) can reduce tumour growth, and newly developed inhibitors are now in clinical trials, see review (Ferrara & Alitalo, 1999). Angiogenesis might also be induced through integrin signalling: αvβ3 has been reported to be

important in this process, and blockade of this integrin inhibits angiogenesis and tumour growth, see review (Keely *et al.*, 1998).

Oncogenes and tumour suppressors

Oncogenes are genes that when overexpressed or constitutively active contribute to a transformed phenotype. Increased activity through mutation may occur through a variety of mechanisms. Mutations that lead to a change in the folding of the protein may promote increased stability and thus increase the effective concentration of the protein. Mutations in the active site of an enzyme may also occur generating a constitutively active oncogene. The protein may simply be upregulated increasing its concentration. Finally, protein sites that facilitate the interaction of negatively regulating (tumour suppressor) genes may be mutated so that the protein can no longer be inactivated. Cell surface growth factor receptors are also proto-oncogenes. These proteins can become mutated such that they bind with greater affinity to growth factors or become active in the absence of growth factor, thus initiating growth in the absence of sufficient growth signals (see above). Each oncogene/tumour suppressor has a different degree of effect on the cell cycle. The transformation of a normal differentiated cell into a cancerous cell is a multi-step process that is not controlled by one gene alone. Therefore, in each tumour lineage there are a variety of different oncogenes that are mutated at different times.

The oncogenic potential of a particular gene is often determined through its ability to transform a well characterised cell line, such as the mouse fibroblast NIH-3T3 cell line. For instance the Ras and Fyn oncogenes have been shown to transform NIH-3T3 cells (Greig *et al.*, 1985; Kawakami *et al.*, 1988; Dartsch *et al.*, 1994). Cells expressing the Ha-Ras oncogene showed were found to have a dramatic changes in cytoskeletal organisation, and cell volume leading to decreased adhesion. Ha-Ras expression also increased proliferation (Dartsch *et al.*, 1994). The oncogenes Src, myc, and Lyn were also found to be transfoming, although in the NIH-3T3 cell background these oncogenes needed to be co-expressed, as their individual expression was not sufficient (Shalloway *et al.*, 1987; Abrams & Zhao, 1995). Co-expression lead to the development of foci formation and substrate independent growth. The observation of co-operating oncogenes again points to the idea that cancer development is a multi-step process.

Tumour suppressor genes have the opposite effect to oncogenes. Tumour suppressors act to negatively regulate the expression of potential oncogenes (proto-oncogenes), and over-expression will lead to cell growth arrest and even apoptosis. Activation of tumour suppressors can be caused following cell stress, such as DNA damage. Upon DNA damage tumour suppressors such as p53 are activated. p53 is the central tumour suppressor for the cell and its mutation is found in ~50 % of cancers. p53 is a transcription factor which promotes the transcription of genes involved in arresting the cell cycle, such as the CDK inhibitor p21. Growth arrest of the cell occurs until the DNA damage is repaired, if this is not possible then the cell commits to apoptosis. When mutated or deleted the absence of the tumour suppressor allows unregulated growth and division.

Contact inhibition

Contact inhibition of growth is a property of nearly all tissues, which prevents tumour formation in healthy cells. Once cell-cell contact is made on all sides of a cell, various signalling pathways are modulated in order to inhibit the proliferation of the cell. This mechanism ensures that cells will not continue dividing once the available space is used up. In transformed cells the contact inhibition of growth can be severely reduced or even absent, such that these cells can grow on top of one another. The process of contact inhibition of growth is far from fully understood at present. Initially experiments were hampered by the loss of contact inhibition in many cultured cell-lines. The development of the NIH-3T3 mouse fibroblast cell-line has proved to be of great importance in this respect. The NIH-3T3 cell-line is one of only a few immortal cell lines that will grow to confluency and then stop dividing. Once resuspended and plated at sub-confluent levels these cells will again divide until a monolayer has been created.

Membrane preparations made from confluent cells are sufficient to induce contact inhibition when applied to sparse sub-confluent cells (Wieser *et al.*, 1985). Thus, extracellular proteins and receptors are responsible for contact inhibition of growth. The membrane glycoprotein contactinhibin and its receptor are thought to be the proteins responsible for the initiation of contact inhibition (Wieser *et al.*, 1990; Wieser *et al.*, 1995; Gradl *et al.*, 1995). Signals generated by the contactinhibin molecules have been associated with the CDK inhibitor $p27^{kip1}$ binding to and inhibiting the Cdk2/cyclin E complex. This in turn will prevent the de-phosphorylation of the retinoblastoma protein (pRB) leading to G1 arrest (Faust *et al.*, 2005). However, there is presently

no mechanistic link between the activation of the receptor and G1 arrest. A few of the potential signalling networks involved in contact inhibition are discussed below.

MAPK pathways are thought to be important in the process of contact inhibition. It has been observed in fibroblasts that at confluency the phosphorylation state of ERK1/2 and its upstream kinase MEK are reduced compared with actively dividing cells (Faust *et al.*, 2005; Wayne *et al.*, 2006). A corresponding increase in MAPK phosphatases is also seen, although this increase is not as dramatic. However, in fibrosarcoma cells, which have reduced contact inhibition of growth, these MAPK phosphatases were shown to remain constant independent of confluency. Thus, the phosphorylation state of ERK1/2 and MEK also remained constant (Wayne *et al.*, 2006). It is clear that activated ERK1/2 is necessary for the continued proliferation of cells.

p38 is a MAPK that is activated, via a separate pathway from ERK1/2, in response to stress stimuli. p38 activates many transcription factors that could potentially inhibit proliferation. p38 activation is up-regulated in confluent cells relative to actively proliferating cells, as is its downstream target ATF-2. This correlates well with the dephosphorylation of pRB (Faust *et al.*, 2005). This was confirmed by data showing that specific p38 inhibitors could release contact-inhibited p38-null fibroblasts from growth arrest (Faust *et al.*, 2005). p38α-/- fibroblasts have also been shown to grow to greater density: these cells have a delayed response in pRB dephosphorylation, $p27^{kip1}$ and associated cdk2 down-regulation compared with wild-type MEF cells (Faust *et al.*, 2005).

Protein kinase C (PKC) isoforms, of which 11 are known, are involved in many cellular responses including growth, differentiation and proliferation through a variety of pathways. PKC isoforms are also thought to be involved in regulation of contact inhibition. Over-expression of PKCε in NIH-3T3 cells has been shown to induce some of the properties of a transformed phenotype, such as growth in soft agar. In contrast, over-expression of the PKCδ isoform induced a slower growth rate and decreased saturation density (Mischak *et al.*, 1993b). PKCδ is thought to act as a tumour suppressor, as inhibition of PKCδ activity allowed a transformed phenotype to develop in v-src-transfected fibroblasts (Heit *et al.*, 2001). PKCδ expression levels are increased in confluent fibroblast cultures promoting the idea that PKCδ expression is somehow linked to cell-cell contact signalling (Heit *et al.*, 2001). The mechanism of action of PKCδ may potentially be through an

action on cyclins D and E and may also involve regulation of p27 (a CDK inhibitor) (Heit *et al.*, 2001).

1.6 Signalling pathways involved in cancer

As I have discussed above, a possible role for ion channels in cancer is via their functional current and its ability to regulate membrane potential/cell volume. However as I will now explain, ion channels (and hERG in particular) may also contribute to a cancerous phenotype via interactions with signalling pathways.

Overview of MAPK pathway

The mitogen-activated protein kinase (MAPK) pathways have a vital role in converting external growth signals into changes in the cell. The MAPK pathways are regulated at many different points by diverse stimuli creating complex signalling networks that can interact with many other signalling systems. Alterations to the MAPK pathways have profound implications for the cell. Indeed, mutation of many of the MAPK signalling molecules is sufficient to produce a cancerous phenotype. hERG may interact with some MAPK proteins (see below), and MAPK signalling may play a role in hERG-mediated transformation.

Receptor tyrosine kinases (RTKs) are transmembrane receptors used by the cell to detect external growth factors such as epidermal growth factor (EGF), nerve growth factor (NGF), and platelet-derived growth factor (PDGF) (Lodish *et al.*, 2003). Upon binding to its ligand the receptor dimerises and autophosphorylates: the activated receptor then activates the MAPK/ERK pathway. Activation of the ERK cascade will give rise to different responses in different cell-types, or when activated by different stimuli in the same cell (Aplin *et al.*, 1998; Lodish *et al.*, 2003). In general the ERK pathway is used to regulate growth and differentiation. The cascade nature of the ERK signalling pathway allows the cell many opportunities to modulate the signal. In turn this makes the pathway flexible and amenable to amplification.

Though activation of the ERK pathway may be initiated in several different ways the signalling cascade is a conserved process. In the following example I will explain the classic Ras/ERK

signalling pathway as a basis for MAPK signalling pathways generally (Figure 1.7). First, the external stimulus activates the receptor, i.e. RTKs or integrin ligation. These receptors then activate membrane bound Ras, through two adaptor proteins, Grb2 and SOS. The SOS protein has GEF (guanine nucleotide-exchange factor) activity and is responsible for the replacing the GDP bound to Ras with GTP. Once activated Ras is able to phosphorylate Raf-1 (here Raf-1 can also be referred, in more general terms, as MAPK kinase kinase, or MAPKKK due to its position in the kinase cascade). Activated Raf-1 is now able to phosphorylate MAP/ERK kinase (MEK, which can also be termed MAPK kinase or MAPKK) and this in turn phosphorylates the MAPK known as ERK (extracellular signal-regulated kinase). ERK can then translocate to the nucleus where it can phosphorylate a range of proteins including transcription factors involved in cell cycle progression and cell differentiation. For example, the expression of the early response genes c-Fos and c-Jun may be regulated in this way (Lodish *et al.*, 2003).

It is important to note that there are a number of different and completely separate MAPK signalling pathways in mammals that activate different MAPKKK/MAPKK/MAPK modules. These include, but are not limited to, the ERK pathway mentioned above and the JNK/SAPK and the p38 MAPK pathways (Krauss, 2003; Lodish *et al.*, 2003). The MAPK molecules can be identified by a TXY motif that represents a dual phosphorylation site for upstream kinases. While the ERK pathway is involved in growth and differentiation the JNK/SAPK and the p38 MAPK pathways are classically associated with stress responses to UV light radiation, heat, and bacterial toxins. The different MAPK signalling molecules are thought to be brought into close contact with one another by scaffolding proteins. This allows fast and efficient signalling between the different kinases, and also reduces unwanted cross-talk. (Lodish *et al.*, 2003).

p38

p38 exists in 4 isoforms α, β, γ, and δ. α and β are expressed in all tissues while γ and δ are tissue specific. γ is found in skeletal muscle and δ is found in the lung, kidney and pancreas among other tissues (Ono & Han, 2000). These isoforms can be independently regulated via the upstream kinases MKK3 and MKK6. Differential activation of isoforms allows p38 to be involved in mediating many different physiological effects such as inflammation, growth, differentiation, cell cycle and cell death (Ono & Han, 2000). The p38 MAPK pathway may be activated by a variety

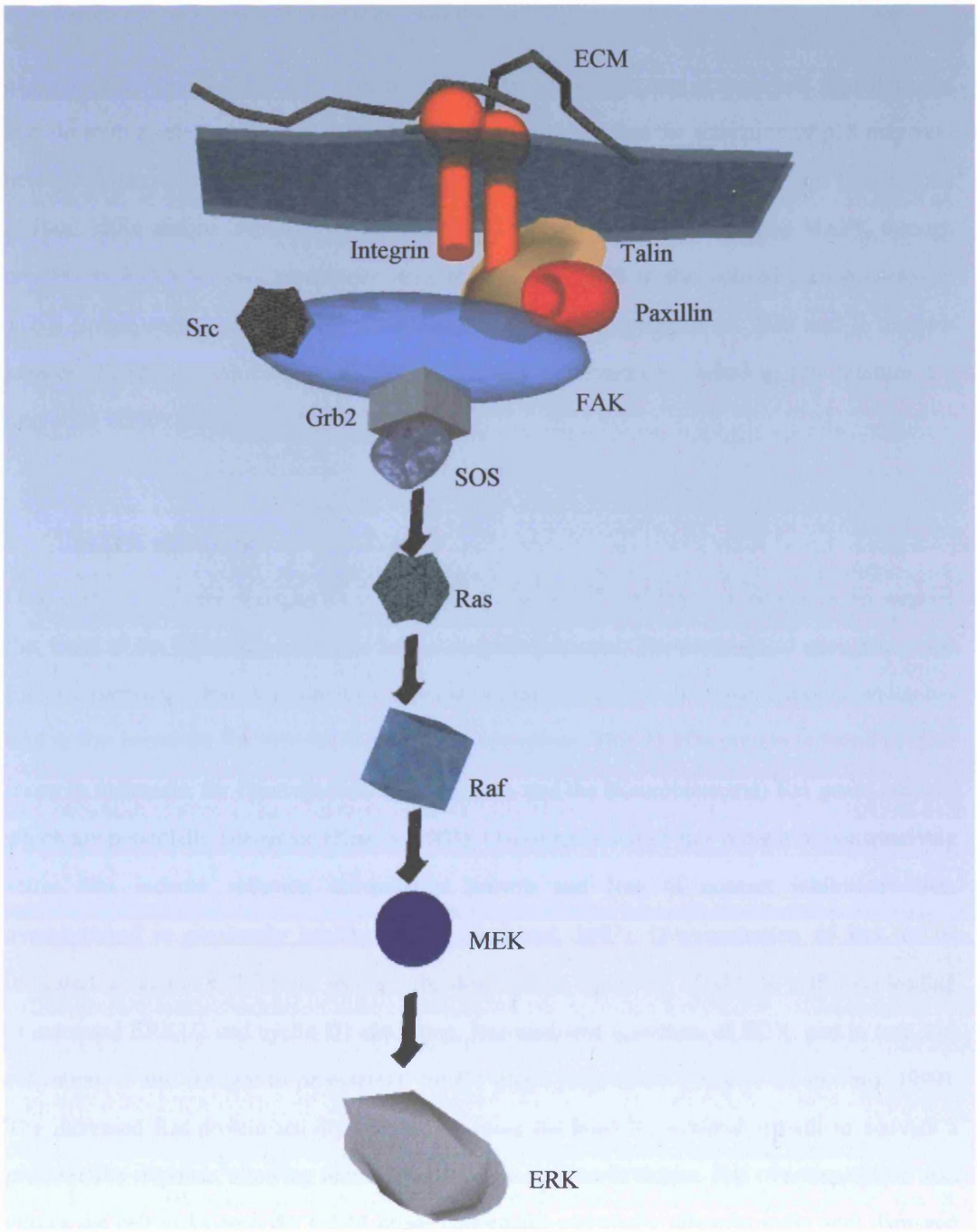

Figure 1.7 Diagram of the MAPK cascade. Integrin ligation causes a conformational change in its cytoplasmic region. The activated integrin binds talin and in turn paxilin and FAK. FAK is autophosphorylated due to its location at the membrane and initiates the kinase signalling cascade that eventually results in the downstream activation of ERK. Activated ERK is able to translocate into the nucleus and initiate transcription. Arrows represent phosphorylation events.

of stimuli (see above); for example many different growth factors may activate p38 signalling and may do so in a cell-specific way. Indeed, it has been observed that the activation of p38 may vary between cell types (Ono & Han, 2000). Nearly a hundred genes are regulated by this kinase (Ono & Han, 2000) and its importance is illustrated by the fact that deletion of p38 MAPK through creation of knockout mice results in embryonic lethality. p38 is also activated downstream of TGFβ (transforming growth factor β) receptor binding and activation of TβRI and II receptor kinases. TGFβ is a cytokine that controls many cellular functions including proliferation and migration via the Smad and p38 pathways.

MAPK and cancer

Due to the growth regulating/promoting nature of the MAPK pathways it comes as no surprise that many of the signalling molecules have oncogenic potential. The prototypical oncogene in the ERK1/2 pathway is Ras. Ras mutation is found in nearly a third of all human tumours, which has lead to Ras becoming the best defined of all the oncogenes. This 21 kDa protein is found in three forms in mammals: the H(arvey)-Ras, K(irsten)-Ras, and the N(euroblastoma)-Ras genes, each of which are potantially oncogenic (Krauss, 2003). Over-expression of Ras protein or constitutively active Ras induces substrate independent growth and loss of contact inhibition when overexpressed in previously healthy tissues (Barbacid, 1987). Overexpression of Ras, or its increased activation will in turn increase the downstream signalling of MAPK pathways leading to increased ERK1/2 and cyclin D1 activation. Ras-mediated activation of PI3K, and in turn Akt activation, is also thought to be essential for G1 phase progression (Gille & Downward, 1999). The increased Ras protein/activity in effect reduces the need for external stimuli to activate a proliferative response, allowing reduced dependence on growth factors. Ras over-expression also allows the cell to by-pass the G2-M phase checkpoint potentially allowing cells with damaged DNA to replicate and thus allowing mutations to accumulate and generate a transformed cell (Knauf *et al.*, 2006).

Src is also found to be oncogenic when over-expressed. Src was originally discovered as a viral protein (v-Src) that caused tumour formation. v-Src expression produces a characteristic transformed phenotype, showing anchorage-independent growth and changes in morphology/cytoskeleton (Irby & Yeatman, 2000). A homologue of v-Src, c-Src, was

subsequently found to be a native protein in animal cells. Unlike the viral protein, c-Src is a proto-oncogene and does not have intrinsic transforming ability unless dysregulated. The viral protein is thought to be constitutively active due to deletion of the regulatory c-terminal region. Src is a non-receptor tyrosine kinase that is involved in many intracellular signalling pathways involving cell growth and proliferation. Src is activated by tyrosine kinase receptors, including the growth factor EGF and PDGF receptors, and is also activated in response to integrin ligation, see review (Bjorge *et al.*, 2000). FAK recruitment to a focal adhesion causes recruitment and activation of Src. Src is responsible for the further phosphorylation of FAK and its functional activation, which is important in cell motility and resistance to anoikis (Chang *et al.*, 1995). Src expression and Src kinase activity are found to be elevated in numerous tumours, including breast and colon cancers, where it is essential in the turnover of focal adhesions (Muthuswamy *et al.*, 1994; Brunton *et al.*, 2005; Hiscox *et al.*, 2006). Src expression correlates with the metastatic phenotype so that as cells become more metastatic they increase Src expression. One consequence of increased Src expression or activation is the modulation of some K^+ channels (Brunton *et al.*, 2005): Src inhibits Kv1.3 and KCNQ channel current, but increases the activity of hERG. What significance this may have in tumour cells remains as yet unknown.

Ras and Src are just two examples of signalling proteins that are downstream of integrin signalling and when up-regulated cause a breakdown in the control of adhesion-dependent growth and/or survival signals. Some of these signalling proteins, e.g. Src, may also cause an increase in cell proliferation when over-expressed (Irby & Yeatman, 2000). The common feature of these proteins is the up-regulation of MAPK activation. Increased activation of the ERK1/2 MAPK pathway will increase the rate of cell proliferation, while reduction of active MEK or ERK1/2 reduces proliferation in NIH 3T3 cells (Roovers & Assoian, 2000). Activation of the MAPK pathway increases the expression of cyclin D both at the mRNA and protein levels; however ERK1/2 must remain activated for a given length of time to activate cyclin D (Roovers & Assoian, 2000). If the ERK1/2 activation is only transient then it will activate p21 (CDK inhibitor) to cause cell cycle arrest.

The p38 MAPK pathway has also been linked with cancer, and is also heavily involved in epithelial-mesenchymal transition (EMT); a process of de-differentiation of structured epithelial tissue into individual cells that are able to form new tissues in the body. On committing to EMT

polarised epithelial cells lose cell-cell contacts, such as tight junctions, and lose polarity. Cells also break down many of their stress fibres to aid cell motility and invasion, a process mediated by GTPases (Masszi *et al.*, 2003). Whilst EMT is an essential mechanism for normal wound healing, it is also involved in cancer metastasis (Kiemer *et al.*, 2001). The environment in which epithelial cells undergo EMT determines their fate. EMT during development, wound healing or transformation will produce mesenchymal cells, fibroblasts, or metastatic tumours respectively, see review (Kalluri & Neilson, 2003). The signalling processes that control EMT are not fully understood, however there is evidence to support the involvement of the cytokine TGF-β and the p38 MAPK pathway (Bhowmick *et al.*, 2001b; Bakin *et al.*, 2002). Upon TGFβ application to cultured epithelial cells it is common to see a loss of cell polarisation and for a new elongated spindle- or mesenchyme-like phenotype to develop (Bakin *et al.*, 2002). This has been shown to be mediated through RhoA/p160^{ROCK}-signalling in a variety of cell-lines, although this is not the case in NIH-3T3 cells (Bhowmick *et al.*, 2001a). Also TGF-β has been shown to increase cell migration in a wound healing assay via p38 MAPK in NMuMG mouse mammary epithelial cells and MDA-MB-231 human breast cancer cells (Bakin *et al.*, 2002).

Integrin expression profiles are altered in cancers

A common observation in malignant, transformed cells is the altered expression of integrins. This altered integrin profile is key to the migratory and invasive phenotype of these cells. Integrins of malignant cells can be either up-regulated or down-regulated. The laminin binding α6β4 integrin is found to be overexpressed in thyroid and papilloma carcinomas compared with healthy tissue (Hood & Cheresh, 2002). αvβ3 is also upregulated in cancerous tissue and its expression in melanoma cells is found to increase with increased metastatic phenotype (Mizejewski, 1999). Conversely, expression of the fibronectin binding α5β1 integrin reduces the metastatic potential of the host cell (Hood & Cheresh, 2002). In general there is an overall decrease in total integrin expression. Transformed cells may also change the localisation of the expressed integrins. In carcinomas the localization of integrins becomes disrupted and diffuse, which may affect focal adhesions as well as the cytoskeleton and signalling networks (Mizejewski, 1999). In the case of the α6β4 integrin, it is relocated from hemi-desmosomes to the leading edge of a migrating transformed cell, a process that requires PKC (Hood & Cheresh, 2002). This correlates with the observed loss of polarity of epithelial cells during transformation. Due to the aberrant expression

of integrins on cancer cells and the dependence of the cell on these integrins for migration and other functions, they are possible therapeutic targets. So far experiments have shown that blocking specific integrins with peptides or monoclonal antibodies (against ECM binding regions) is effective in reducing metastasis (Mizejewski, 1999). Park *et al.* (2006) have taken this a stage further and shown that anti-β1 antibodies can prevent tumour formation in mice injected with β1 integrin-expressing breast cancer cells. The antibody can also reduce tumour size in well established tumours *in vivo*, while having no discernible adverse effect on the host (Park *et al.*, 2006). It is evident that cell-cell and cell-ECM interactions via integrins are important for maintaining a normal healthy morphology, while aberrant expression of integrins or incorrect signalling downstream of normal integrin-ligand interactions are important in the development of a cancerous phenotype.

1.7 Involvement of hERG in macromolecular signalling complexes

Recent ion channel studies have started to uncover possible signalling roles for ion channels that are independent of their ion conduction properties (Kaczmarek, 2006). Effects of ion channel expression that cannot be solely explained by ion flux has been demonstrated for non-selective cation channels, Ca^{2+} channels and also K^+ channels (Kaczmarek, 2006). As already mentioned one of the best examples of this is the EAG channel, which has been shown to interact with the MAPK pathway component proteins independently of ion flux (Hegle *et al.*, 2006). In this study the authors used mutant channels to show that collapse of the channel pore did not affect the ability of EAG to influence cell proliferation. It was also demonstrated that mutant channels that preferred the open state configuration at resting membrane potentials decreased the proliferative effect of non-conductive channels (Hegle *et al.*, 2006). This important finding suggests that channel gating movements are important for cell signalling.

The similarity between the hERG and EAG channels suggests that the hERG channel may also be able to activate signalling pathways through direct protein-protein interactions. Below is a summary of the signalling proteins known to interact with the hERG proteins, and hence may be involved in hERG-mediated cell signalling. However, it is important to bear in mind that all the proteins mentioned below can reside at focal adhesions and their association with hERG has been

indicated through co-immunoprecipitation-based experiments. Therefore, these results may be misleading and the association of hERG with any of these proteins may consequently be indirect.

Many studies have shown that K^+ channels including hERG, are involved in macromolecular complexes at focal adhesion points (Hofmann *et al.*, 2001; Artym & Petty, 2002; Cherubini *et al.*, 2002; Baron *et al.*, 2003; Arcangeli *et al.*, 2004). Co-immunoprecipitation experiments and fluorescence resonance energy transfer (FRET) analysis have shown that K^+ channels (kv1.3, hERG, and GIRK) associate with β1 integrins on integrin binding to substratum (Artym & Petty, 2002; Cherubini *et al.*, 2002; Arcangeli *et al.*, 2004). Before reviewing evidence on the hERG-integrin interaction, I will give a brief overview of cell interactions with the extracellular matrix.

Structure of focal adhesions

The majority of cells within the body are organised into tissues and are dependent on interactions with other cells and the extracellular matrix (ECM). Cells interact with one another and transmit signals through these interactions such as contact inhibition of growth. One of the major proteins involved in cell-cell contacts are cadherins. Cadherins are membrane-spanning proteins that participate in cell-cell adhesion. Clusters of cadherins form adherens junctions between adjacent cells. At these sites cadherins bind to cadherins of the neighbouring cell on their extracellular side, and are linked to the actin cytoskeleton via catenin proteins on the intracellular side (Lodish *et al.*, 2003).

The ECM helps to localise cells together independently of cell-cell contacts and this is important for organ/tissue development. In fact association with the ECM is so important that (for healthy cells) detachment from the ECM is enough to trigger cell death in a process termed anoikis (Frisch & Francis, 1994; Frisch & Screaton, 2001; Reddig & Juliano, 2005). The ECM is made up of 3 major components, proteoglycans, collagens, and soluble adhesive proteins, such as fibronectin (FN) (Lodish *et al.*, 2003). The ratios and numbers of these proteins can be changed depending on the function the ECM is required to perform.

Cells use integrins for high specificity and high affinity binding to the substratum. The α and β sub-groups of integrins share a common structure, consisting of a large extracellular domain

linked to a smaller non-catalytic cytoplasmic domain through a single transmembrane region. Integrins exist as non-covalently linked αβ heterodimers 25 of which have been identified. These heterodimers are composed of 18 types of α and 8 types of β subunits. The α subunits may associate with a number of β subunits to give many combinations of integrins. The extracellular domains recognise specific amino acid sequences within their target molecules. In the case of fibronectin the target-binding region is one of the many RGD (Arg-Gly-Asp) repeats. This sequence is common to many other ECM proteins such as vitonectin, laminin and thrombospondin (Mizejewski, 1999). The cytosolic region of most integrins interacts with the actin cytoskeleton, allowing the cell to directly transfer mechanical strain from integrin binding, to its load bearing cytoskeleton.

For some time it was thought that integrins are purely adhesion molecules, however it is now widely accepted that integrins have an important role in signal transduction. Integrins can transmit both 'outside-in' and 'inside-out' signals:

Inside-out: The ability of a cell to modulate its binding to substrates is important for interactions with other cells and for processes such as migration and invasion. β1, β2, β3, and β7 integrin subunit binding affinities are known to be regulated by internal cell signalling (Hughes & Pfaff, 1998). Intracellular signalling pathways may result in modifying the conformation of the integrin binding site and affecting its binding affinity. Under normal conditions the integrin active site is partially blocked by the 'hinge' region, reducing the affinity for its ligand. Once activated however the hinge region moves out of the way of the active site and the integrin can bind with greater affinity (Aplin *et al.*, 1998). This change in conformation is recognised by some monoclonal antibodies that specifically bind activated integrins. Intracellular signalling molecules may activate integrins by phosphorylating the intracellular integrin subunit domains causing a change in conformation which is transmitted through the protein to the extracellular domain. However, the mechanism of integrin activation is not well understood.

Integrin binding, clustering and activation is the basis for focal adhesion formation. Focal adhesion sites form the nucleation centre for stress fibre formation, which will in turn lead to a change in the cytoskeleton and cell flattening. This interaction also occurs in reverse and the state of the cytoskeleton has important consequences for integrin activity.

Integrin affinity may also be influenced by interaction with other membrane proteins that may act on extracellular and transmembrane regions of the integrin molecule. The hERG K^+ channel has been reported to be linked with integrin function. Not only can hERG be co-immunoprecipitated with β1 subunit-containing integrins, but integrin-mediated adhesion has been demonstrated to cause long-lasting activation of hERG channels in some tumour cells (Cherubini *et al.*, 2005). However, the N-terminal truncated hERG1b channel is unable to associate with integrins. Cherubini and colleagues demonstrated that hERG current is necessary for the activation of the FAK protein downstream of integrin activation, thus linking hERG with the MAPK pathway (Cherubini *et al.*, 2005). hERG is also linked with Rac1 whose activation is elevated in hERG expressing cells relative to mock-transfected cells. This activation is dependent on both integrin attachment and hERG function (Cherubini *et al.*, 2005). While these observations imply that hERG is indeed heavily involved at the site of integrin adhesion there is presently no evidence to suggest that hERG directly interacts with any of these proteins. However, it is likely that hERG is involved with integrins due to co-localisation at focal adhesions. This interaction then affects downstream signalling proteins such as Rac1 and FAK most likely through an indirect mechanism. The fact that the application of a hERG specific blocker reduces the effect of hERG on the cell does not necessarily indicate that a K^+ ion flux is necessary. Drug block of hERG may cause a change in conformation, or prevent a conformational change that occurs in the native protein in response to membrane potential change. This alteration of the conformation of the channel may prevent specific associations of hERG with signalling molecules. Together these data suggest a role for hERG in integrin signalling, cell motility and cytoskeletal modulation.

Outside-in: External signals generated through integrin binding are important for many functions such as cell growth, division and survival (anoikis). On integrin binding to substrate, the protein undergoes conformational changes that alter the cytoplasmic tail region (Juliano, 2002), which is important for signalling and focal adhesion formation. Indeed, removal of the cytoplasmic region of the β1 integrin inhibited proliferation of fibroblasts (Walker & Assoian, 2005).

When an integrin interacts with the ECM it becomes localised at a fixed point in the membrane. If other integrins that also recognise the ECM bind close by, then the integrins start to cluster. Integrin clustering forms punctuate attachment sites at the plasma membrane. At these sites the

large number of integrins helps to localise signalling molecules and eventually forms a large complex termed a focal adhesion (Petit & Thiery, 2000). Integrin clustering and activation provides binding sites for the scaffolding protein talin. Talin is able to bind vinculin; an inherently inactive protein that undergoes a conformational change on binding talin exposing its active site. Activation of vinculin allows it to bind the actin binding protein α-actinin (Figure 1.8). The binding of actin monomers provides a nucleation site for its rapid polymerisation into filamentous strands, or F-actin. α-actinin is also involved in this process and helps to bundle the actin filaments by crosslinking them. These actin filament bundles originating from focal adhesions are called stress fibres. Stress fibres link the cytoskeleton with the external environment allowing the cell to use myosin motors to pull against them. This produces the flattened morphology characteristic of many cell types such as fibroblasts and epithelial cells. Indeed transformed cells that have reduced focal adhesions and actin filaments lose their fibroblastic shape and default to a more rounded spindle-like morphology. As will be mentioned in more detail later, focal adhesions and stress fibres are of key importance in the process of cell migration.

Talin is also able to bind paxillin, which in turn binds to FAK. FAK is a non-receptor tyrosine kinase located at (and involved in the maintenance of) focal adhesions at points of integrin clustering and attachment to the ECM. Focal adhesion localization allows autophosphorylation of FAK at Tyr-397, providing a binding site for Src kinase. Src then phosphorylates two more residues on FAK, creating a Src homology domain (SH2), allowing binding to other SH domain-containing adaptor proteins involved in the MAPK signalling cascade (such as Grb2, paxillin, $p130^{CAS}$, p85 subunit of PI3K, and Shc). Using these protein-protein interactions FAK acts as a scaffolding protein that is necessary for the development of focal adhesion complexes. Activated FAK is able to bind to and activate the membrane-associated Ras protein via the Grb2/SOS proteins. Activated Ras is now able to interact and activate a range of further signalling pathways including the MAPK/ERK pathway.

The overlap in signalling molecules between integrin signalling and receptor tyrosine kinase/MAPK signalling allows cross-talk between the two pathways downstream of the initial stimulus. There are also cases where integrins and growth factor receptors interact directly in the membrane (Bill *et al.*, 2004; Walker & Assoian, 2005). Integrins can thus modulate effects of

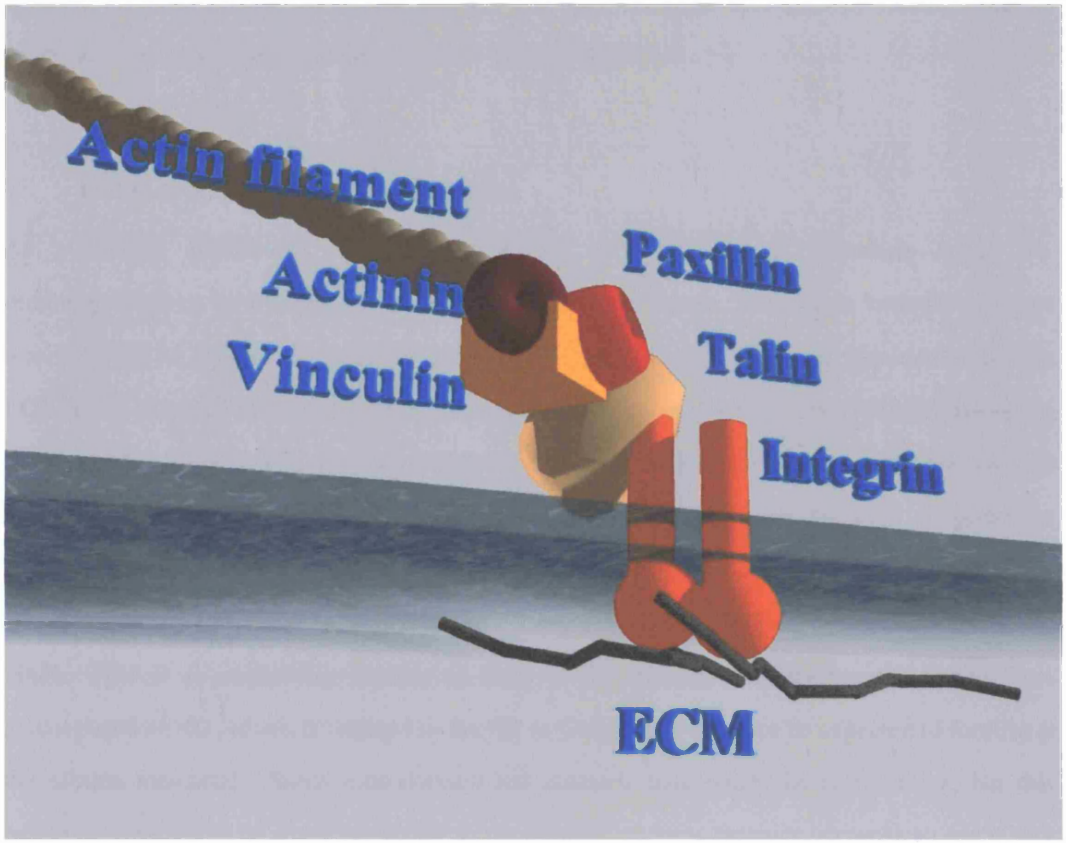

Figure 1.8 Integrins are linked to the cytoskeleton. Integrin adhesion to the ECM causes activation of the intracellular region of the integrin causing talin to bind. Paxillin then binds to talin. Vinculin and α-actinin also bind to the complex and provide a nucleation centre for actin filament assembly. The actin filament extends into the cytoplasm and links with the rest of the cytoskeleton.

receptor tyrosine kinase activation, and in this way integrins and growth factor receptors cooperate to ensure correct signalling for cell cycle progression.

hERG channels interact with integrins

As previously mentioned there are reports of a number of K^+ channels which co-immunoprecipitate with integrins. In the case of Kv1.3 channels, association with β1 integrins was found to be dependent on a functional current in the human malignant melanoma cell line LOX. If the channel is blocked then the two proteins dissociate (Artym & Petty, 2002). However, this study did not demonstrate a direct link between the integrin and channel, and there may be intermediate scaffolding molecules involved. The Co-immunoprecipitation experiments performed by Cherubini *et al.* (2005) showed that the immature form of the hERG channel also associates with β1 integrins in SH-SY5Y and stably transfected HEK293 cells (Cherubini *et al.*, 2005). This is an interesting finding as most of the immature asparagine (N)-linked, core glycosylated hERG protein is retained in the ER or Golgi and would not be expected to localise at the plasma membrane. Some core-glycosylated channels may reach the cell surface, but this would be expected to be a rare occurance as the stability of these channels is compromised (Gong *et al.*, 2002). This association of immature hERG and integrins may indicate that the association occurs before incorporation into the plasma membrane, maybe as early as the ER.

Not only do hERG channels and integrins associate, but there is also evidence that these proteins regulate one another. Attachment of cells to fibronectin and vitronectin increases hERG current density, in FLG 29.1 leukemic cells, without any increase in hERG RNA or modifications of hERG protein levels (Hofmann *et al.*, 2001). These authors also presented evidence that hERG current density can be increased by antibody-induced clustering of β1 integrins in suspended cells (Hofmann *et al.*, 2001). These data suggest that integrin binding regulates hERG channel activation; indeed, hERG channels are functionally activated by β1 integrins in neuroblastoma and leukaemia cells (Arcangeli *et al.*, 2004). This activation of hERG channels is sustained by β1 integrin subunit activation (Cherubini *et al.*, 2002). While these data would seem to suggest that a physical interaction occurs between hERG and integrins there may also be indirect mechanisms of activation involving MAPK or other signalling cascades. The case for an integrin-hERG interaction is strengthened by the evidence that hERG current is able to affect integrin expression.

In human preosteoclastic cells hERG channel block with the compound WAY-123,398 is sufficient to prevent the increase in $\alpha v\beta 3$ integrin protein expression on cell adhesion observed in control cells (Hofmann *et al.*, 2001).

The hERG channel is modulated by, and may directly interact with Src

The interaction between Src and hERG has been shown to be more than just a simple protein-protein interaction. Tyrosine phosphorylation of the hERG channel by constitutively active Src significantly increases the currents passed by the channel in the MLS-9 rat microglial cell line (Cayabyab & Schlichter, 2002). Src also produced a leftward shift in activation of the hERG channel, such that the channel is open at more negative membrane potentials. This may be important in non-excitable cells where hERG would not normally be activated due to the hyperpolarised V_{rest}. Activation of the channel and the increase in current was inhibited by protein tyrosine kinase inhibitors. Src and hERG proteins co-immunoprecipitate, and hERG has sequences that resemble SH2 and SH3 binding motifs used by the Src protein. In light of these data direct binding of the proteins would seem to be more likely than an indirect association via scaffolding molecules.

hERG and focal adhesion kinase (FAK)

FAK and hERG associate in co-immunoprecipitation assays and this association is increased on integrin ligation to fibronectin compared to suspended cells. The phosphorylation and association of FAK with hERG is dependent on integrin ligation (Cherubini *et al.*, 2005). The FAK-hERG association is reduced on specific hERG channel block with Way-123,398 or E4031 (Cherubini *et al.*, 2005). The phosphorylation of residue Tyr-397 and thus initial activation of FAK, is also reduced on hERG block. Phosphorylation of residue Tyr-925, normally phosphorylated by Src after phosphorylation of residue Tyr-397, was also concomitantly reduced on hERG block (Cherubini *et al.*, 2005).

FAK is activated simply by being localised to the membrane (Frisch *et al.*, 1996; Katz *et al.*, 2003). The increase in FAK phosphorylation with hERG expression may be due to membrane localisation by the hERG protein. While it is true that the FAK-hERG association is severely reduced in suspended cells relative to integrin bound cells the association is not absent altogether

(Cherubini *et al.*, 2005). This may suggest that a small amount of FAK-hERG interactions occur independently of integrin binding. The increased association seen in the pull-down assay on integrin ligation might also be non-specific, and arise from large signalling complexes linking FAK with hERG indirectly. To test this, a more direct assay of FAK and hERG association is needed. If FAK and hERG do constitutively interact and activate FAK then it would be expected that hERG expression would increase focal adhesion turnover. This would seem to be the case, at least in HEK293 cells models, where cell spreading is accelerated independently of integrin ligation (Cherubini *et al.*, 2005).

hERG and Rac1

Cherubini *et al.* (2005) have shown that hERG also immunoprecipitates with Rac1, but not with RhoA. While the specificity of this interaction can again questioned, like FAK and integrins, the Rac1-hERG association is modulated by integrin ligation and hERG blockade. Also the activity of Rac1 has been shown to be increased in hERG-expressing cells relative to mock-transfected cells. The translocation of Rac to the plasma membrane is sufficient for its activation, a function possibly provided by hERG channels. This interaction would be predicted to produce an increase in cell motility in hERG-expressing cells.

In conclusion, the interaction of hERG with any part of the focal adhesion complex, be this kinases, monomeric GTPase, or integrins, may be key to its role in cancer. The specific association of hERG at these signalling hubs suggests a role for hERG in cancer that can potentially be completely independent of its ion conductance activity. If hERG is able to activate FAK, or indeed any kinase downstream of integrin activation, then this may allow hERG to by pass the regulatory role of cell adhesion. Thus, the expression of hERG in so many cancer cells may have a role in generating the transformed phenotype, making hERG an oncogene rather than an epi-phenomenom, secondary to cell transformation.

1.8 Conclusion

As our understanding of ion channels has increased it has become evident that ion-channels have a bigger role to play in cell function than simply modulating ion flux. There is increasing evidence that ion channel expression is closely linked with the cell cycle. Ion channel activity may even

play a role in the regulation of the cell cycle. There is also a clear relationship between cancer development and altered ion channel expression profiles. It is not yet proven that ion channel expression precedes transformation. However, there is growing evidence that ion channels might be oncogenes in their own right.

The hERG channel has been associated with many different cancers, and it is proposed that it may have similar oncogenic properties to the closely related EAG ion channel. However, it is still unclear what the effect of hERG channel expression is having on non-excitable cells and its importance in cancer development.

1.9 Thesis aims

The aim of this investigation was to study the oncogenic potential of the hERG channel. hERG channels will be stably expressed in non-excitable cells and a range of studies performed to provide a detailed assessment of changes in cell proliferation, motility, contact inhibition, and the adhesion-dependency of growth. hERG channel blockers, trafficking inhibitors and dominant-negative hERG channel constructs will be employed to elucidate the role of the hERG channel and hERG current in non-excitable cells. The effect of hERG channel expression on cell signalling pathways will also be investigated to determine potential mechanisms by which hERG channels might induce their cell transforming effects.

Methods

Generation of stable cell lines

The DNA expression vector pcDNA3 was chosen for the generation of stable cell lines as it has a strong immediate/early cytomegalovirus promoter/enhancer complex (CMV promoter) (Figure 2.1). This vector is suitable for transient transfections and for high levels of hERG expression in a variety of cell lines (Zhou *et al.*, 1998b). pcDNA3 expresses the neomycin resistance gene which produces aminoglycoside 3β-phosphotransferase, which phosphorylates and inactivates G418. G418 inhibits protein synthesis making it toxic to both bacterial and mammalian cells. G418 could therefore be used as a selection tool for stably transfected cells that can be tested for hERG expression levels. Mammalian cell lines were permanently maintained in medium containing 500 $\mu g\ ml^{-1}$ G418. Cells stably expressing hERG were generated using HEK293, and NIH-3T3 cell lines.

After transfection (lipofectamine, see below) with either pcDNA3-hERG1, or pcDNA3 alone (to produce vector control), mammalian cells needed to be cultured in selection media so that only stably transfected cells survived. It was critical that the concentration of G418 was sufficient to kill non-expressing cells but not too great that it adversely affected cell growth of the stably transfected cells. In order to determine the ideal concentration of G418 for each cell line kill curves were generated. A kill curve was performed by culturing untranfected cells in media containing a range of concentrations of G418. The cells were observed over 3 weeks. A concentration of 500 $\mu g\ ml^{-1}$ G418 was found to kill off HEK and NIH-3T3 cells in just under 3 weeks, and so was added to cells 24 hrs after transfection. The cells were then permanently maintained in this concentration of G418 to force continued hERG expression and thus stable expression.

This project aimed to observe the changes in cell morphology/phenotype after hERG expression. In order to make the changes in cell phenotype more apparent, clones were produced from single cells within the population. Not only did this ensure that all the cells from a particular clone expressed hERG, but also that they expressed hERG at the same level. The use of more that one clone also allowed changes in hERG expression levels to be correlated with phenotype. After

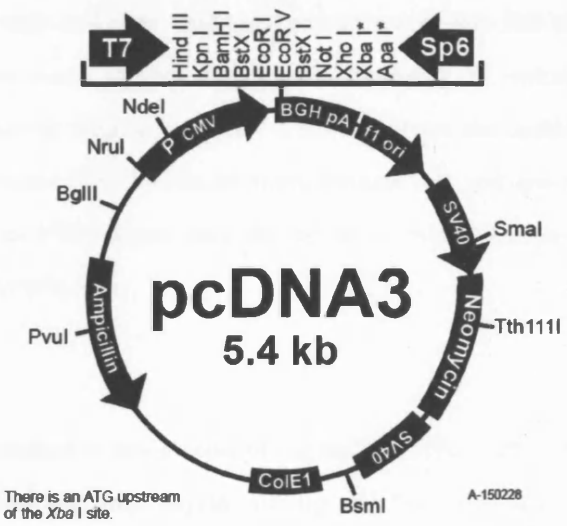

Figure 2.1 Map of pcDNA3 cloning/expression vector (adapted from Invitrogen website). The vector has a multi-cloning region with many restriction sites for inserting a gene of interest. The hERG1 gene was inserted into the EcoR1 and HindIII restriction sites. A CMV promoter drives the expression of the inserted gene. Ampicillin resistance allows use of this antibiotic as a selection tool, for bacterial amplification. An SV40 promoter drives the expression of the neomycin resistance proving resistance to G418. This enables selection of mammalian cells that have incorporated plasmid DNA into their genome and maybe stably expressing hERG.

transfection and 3 weeks of selection cells were plated into 96 well plates using serial dilution. Wells that contained a single cell were monitored and grown up into full size cultures. In some cases individual colonies were 'picked' from wells containing >1 colony. Here media was removed and a p10 Gilson tip used to scrape off a few cells from the center of the colony. Care was taken that these colonies were produced from a single cell and not the product and two smaller colonies. Wildtype (WT) clones were also produced from the same stock of cells as the hERG and vector control (VC) cells.

Cell culture

NIH-3T3 cells were maintained in low glucose (1 mg ml^{-1}) DMEM, with 10% fetal bovine serum and 50,000 units penicillin and streptomycin. 500 µg ml^{-1} G418 was also added to the culture media for clones stably expressing pcDNA3-hERG or pcDNA3 only (vector control). Cells were kept at 37 °C in an atmosphere of 5 % CO_2. To lift cells from the flask the culture medium was aspirated, and the cell monolayer washed with D-PBS. Cells were enzymatically dissociated from the culture flask using ~30 µl trypsin/EDTA per cm^2 of culture surface. After cells started to round up and loose adhesion (typically ~2 minutes after trypsin addition) fresh media was added to dilute the cells and allow passage at a ratio of 1:12. This was repeated every 3 days, or when cells reached 70 % confluency.

HEK293 cells were maintained in MEM alpha culture media supplemented with 10% fetal bovine serum and 50,000 units penicillin and streptomycin. 500 µg ml^{-1} G418 was also added to the culture media for clones stably expressing pcDNA3-hERG or pcDNA3 only (vector control). Cells were kept at 37 °C in an atmosphere of 5 % CO_2. Cells were passaged in a similar fashion to NIH-3T3 cells, although they were split at a ratio of 1:6 every 3 days. All cell culture reagents from Gibco.

Transient transfections

Transient transfection methods were used in the initial transfection of the stable cell lines. Transient transfection methods were also investigated for their ability to transfect NIH-3T3 cells with mutant hERG channels. All transient transfections included eGFP expressing plasmid at a concentration $1/10^{th}$ of the DNA of interest. This allowed a quick visual determination of the transfection efficiency.

Lipofectamine

Lipofectamine (Invitrogen, Paisley, UK) is a lipid based transfection technique that facilitates entry of DNA into the cytoplasm via endocytosis. Standard conditions suggested by the manufacturer were found to be optimal. Cells were cultured to 80% confluency on wells of a 6 well plate. 3 µl lipofectamine was added to 95 µl serum free media and incubated at room temp for 5 mins. 1µg DNA was added to the solution and allowed to complex with the lipofectamine for 20 mins. The DNA/lipofectamine complex was added to the cells in serum free media. After 5 hrs lipofectamine containing medium was exchanged for culture medium.

jetPEI

jetPEI (autogenbioclear, Wiltshire, UK) works in a similar manner to lipofectamine. This reagent was used in attempts to transfect NIH-3T3 cells as the product was believed to have a higher transfection efficiency in this cell line than lipofectamine. NIH-3T3 cells were cultured to 40% confluency in 96 well plates. 10 µl 150 mM NaCl containing 0.25 µg DNA and 10 µl 150mM NaCl containing 1 µl jetPEI were incubated separately at room temp for 5 mins. The solutions were then mixed and allowed to complex for a further 30 mins. The DNA jetPEI solution was then added to cells in no more than 100 µl culture media. Media was changed after 4 hrs.

Amaxa Nucleofection

Lipofectamine and jetPEI both rely on lipid based reagents to translocate DNA into cells. In an effort to improve transfection efficiency these lipid based transfection reagents can be combined with electroporation to help force DNA into cells, in a process developed by Amaxa (Cologne) called nucleofection. 10^6 NIH-3T3 cells were cultured and removed from the culture dish by trypsin/EDTA. Cells were pelleted by centrifugation (300 rpm, 2mins) and the media removed. The cell pellet was resuspended in 100 µl solution R. 2.5 µg of eGFP DNA was added to the cells before placing the cell solution into a nucleofection cuvette. The cuvette was placed into the nucleofector machine and run on program A24, or U30, or T20. The cell suspension was quickly moved into pre-prepared 6 well plates containing normal culture medium. After 24 hrs the media was exchanged for fresh media to remove traces of transfection reagents.

Generation of hERG channel mutants

The hERG mutants A561V and G628S used in this project needed to be generated by mutating the wild type hERG1 gene. However the production of the mutants was complicated by the fact that the hERG genes needed to be subcloned into the viral shuttle vector for adenovirus production. Also after generating the hERG mutants and their incorporation into adenoviral transfection vectors it will be important to investigate the expression of these mutants in the NIH-3T3 cells. The most efficient way to do this is via western blotting, however the available hERG antibodies lack sensitivity. A common method of increasing protein detection by antibodies is to introduce an epitope tag such as Myc, flag, or HA. Epitope tags are short sequences that code for a small number of residues that can be recognised by a high affinity antibody. The small size of the tag means that there is little effect upon the function of the original protein. The following strategy was used to generate the hERG mutant constructs.

WT-hERG was originally expressed in a pcDNA3 expression vector. Here the hERG1 gene was subcloned into the vector at HindIII and EcoR1 sites in the multi-cloning region. The pcDNA3 vector had previously been modified to remove its inherent Sal1 and BglII restriction sites. These sites are also present within the hERG gene and so their absence within the vector allowed specific restrictions within the hERG gene. These restriction sites also lie close to either side of the sites of mutation (Figure 2.2).

The hERG point mutations A561V and G628S were introduced via PCR. Using the Quickchange technique (Stratagene, La Jolla, CA, USA) PCR was used to make missense mutations (site directed mutagenesis), see later 'PCR' section. However PCR is not a perfect process and polymerases may introduce mutations, thus any DNA produced by PCR should be sequenced in order to check for unwanted mutations. Therefore in order to minimise the amount of synthesised DNA (and need for sequencing) a strategy was developed that allowed the generation of the mutants in a cloning vector, followed by removal of the region of interest (between the Sal1 - BglII restriction sites) and subsequent ligation into the an unaltered version of the WT-hERG1 gene (Figure 2.5). This meant that only a small amount of the DNA was affected by PCR and so only this region needed to be sequenced. This was performed at the same time as checking the Sequence of the insertion sites. The added advantage of this approach was that once a Myc-tagged

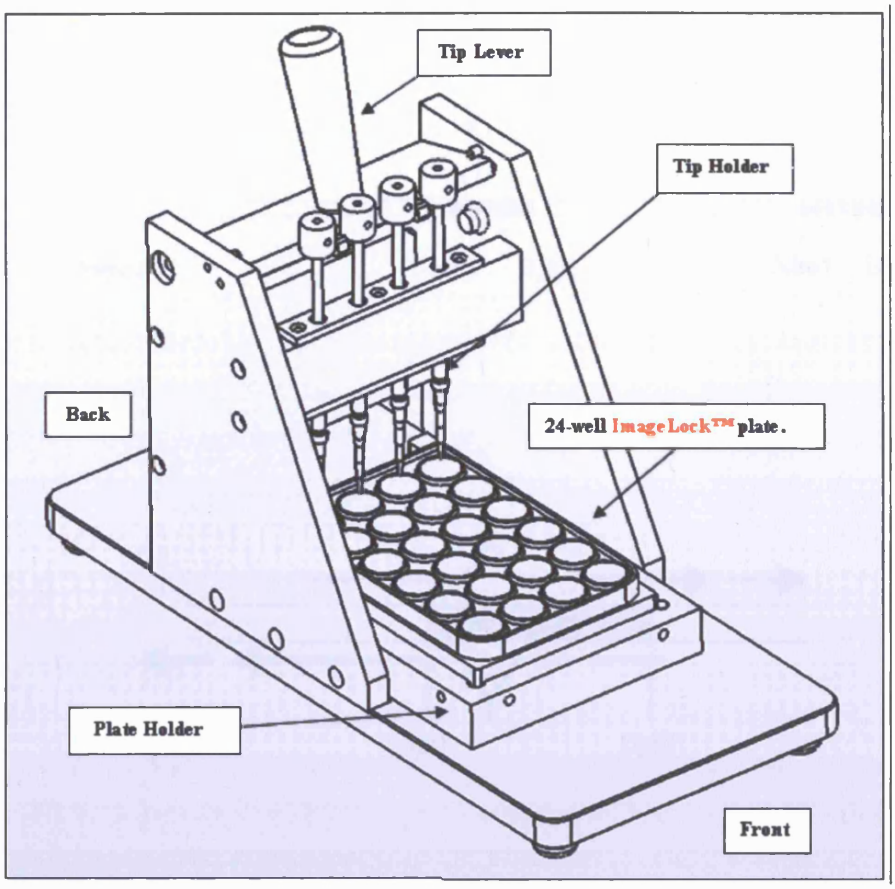

Figure 2.2 Diagram of Essen Woundmaker™ apparatus. The woundmaker™ allowed consistent sized wound to be made at the center of the ImageLock™ 24 well plates. This was necessary for the Incucyte™ system to recognise the wound, and produce automated measurement.

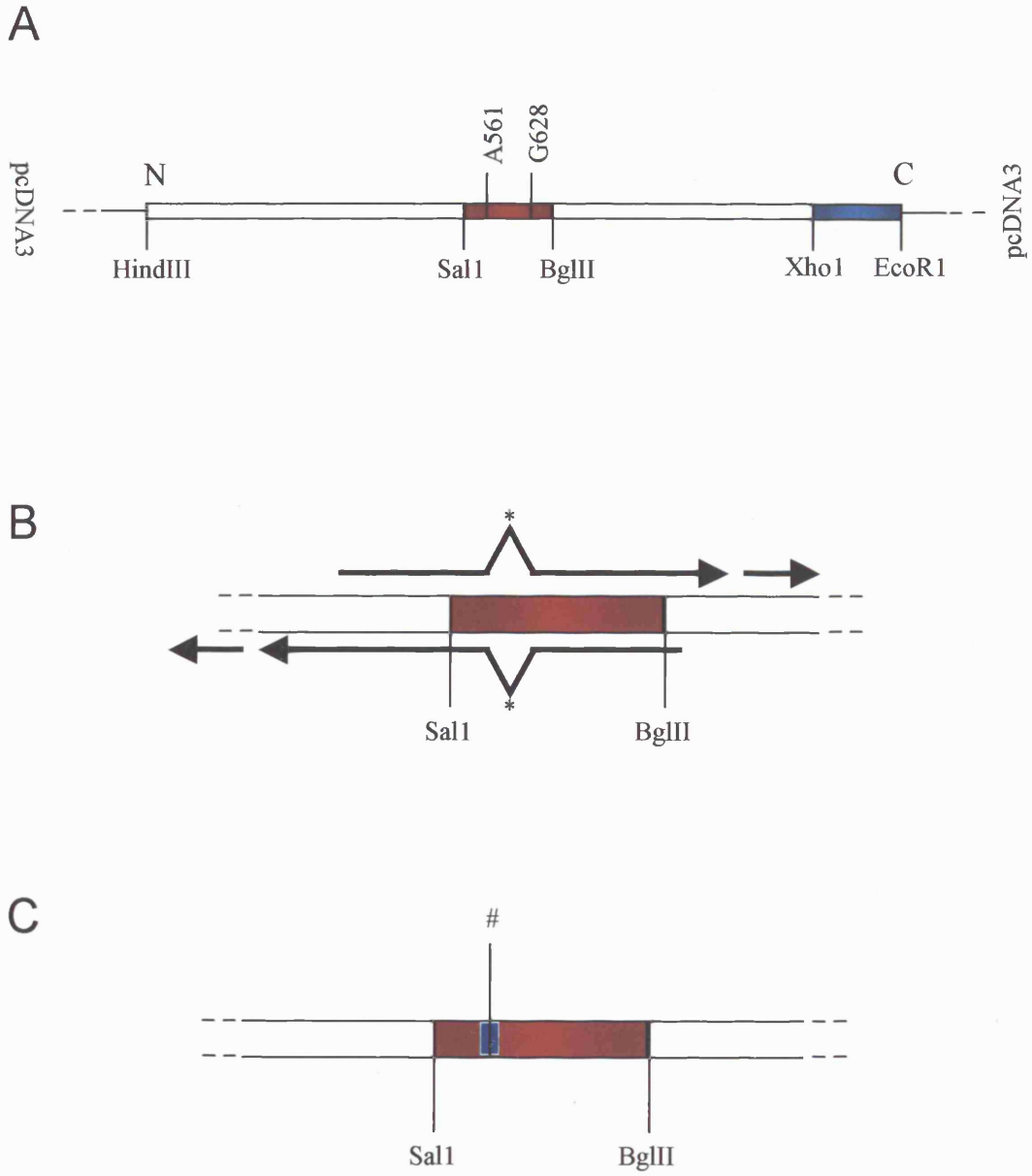

Figure 2.3 Site directed mutagenesis of A561V and G628S. **A:** Diagram of the hERG1 gene in the pcDNA3 expression vector. pcDNA3 is not shown for clarity, but flanks both sides of the hERG1 gene and forms a circular plasmid. A561V and G628S are located between the unique Sal1 and BglII restriction sites (red). The unique restriction sites HindIII and EcoR1 flank the hERG1 gene. **B:** PCR primers designed to introduce at mutation (*) were designed and used in a PCR reaction **C:** Newly generated DNA contains mutation at site directed by PCR primers (#).

version of the WT-hERG1 gene had been created the mutants could be directly subcloned into this gene. This avoided the need to engineer a Myc tag onto the mutant genes separately.

In this project a Myc tag was added to the C-terminal end of the hERG protein. The tag was added at the C-terminal to ensure that only fully transcribed proteins would be identified by the anti-Myc antibody. PCR primers were designed that amplified a small region of the C-terminal tail of the hERG1 gene. The Myc-Rev primer was designed so that it would remove the original EcoR1 restriction site and stop codon from the hERG1 gene. Instead a Myc epitope tag was added followed by a new stop codon (AUG) and then a new Xba1 site (Figure 2.4). The Myc-For primer was designed so that it annealed to the hERG1 gene just before the Xho1 restriction site. The position of the primers on the DNA meant that during PCR only the small region of DNA between the primers would be amplified. The PCR product was cut with the Xho1 and Xba1 restriction enzymes and gel purified. This fragment could then be subcloned into the WT-hERG1 gene in pcDNA3 between the Xho1 and Xba1 sites. This strategy meant that only a small region of the DNA was generated by PCR and thus needed to be sequenced. The Myc tag will also replace a small portion of the pcDNA3 vector containing the Not1, EcoR1 and BamH1 restriction sites. Therefore correct insertion was also confirmed by the absence of these restriction sites, and also by DNA sequencing of the insertion sites.

Each of the mutants and WT-Myc-tagged hERG1 were excised from the pcDNA3 vector using HindIII and Xba1 restriction enzymes and subsequently ligated into the pAD-Track CMV vector also cut with these enzymes. Thus the hERG gene was inserted in the multi-cloning region of the pAD-Track CMV vector directly after the CMV promoter. Both insertion sites were sequenced for each mutant and WT gene to check for random mutation.

Molecular Biology

Preparation of DNA

DH5α competent E.coli cells transformed with plasmid DNA of interest were cultured in LB broth with either 100 μg ml^{-1} of Ampicilin or 50 μg ml^{-1} kanomycin overnight at 37 °C in a shaking incubator 250 rpm. DNA was then recovered and purified by column purification using commercial kits (Quiagen, Chatsworth, CA, USA). Briefly, bacteria were lysed using strong

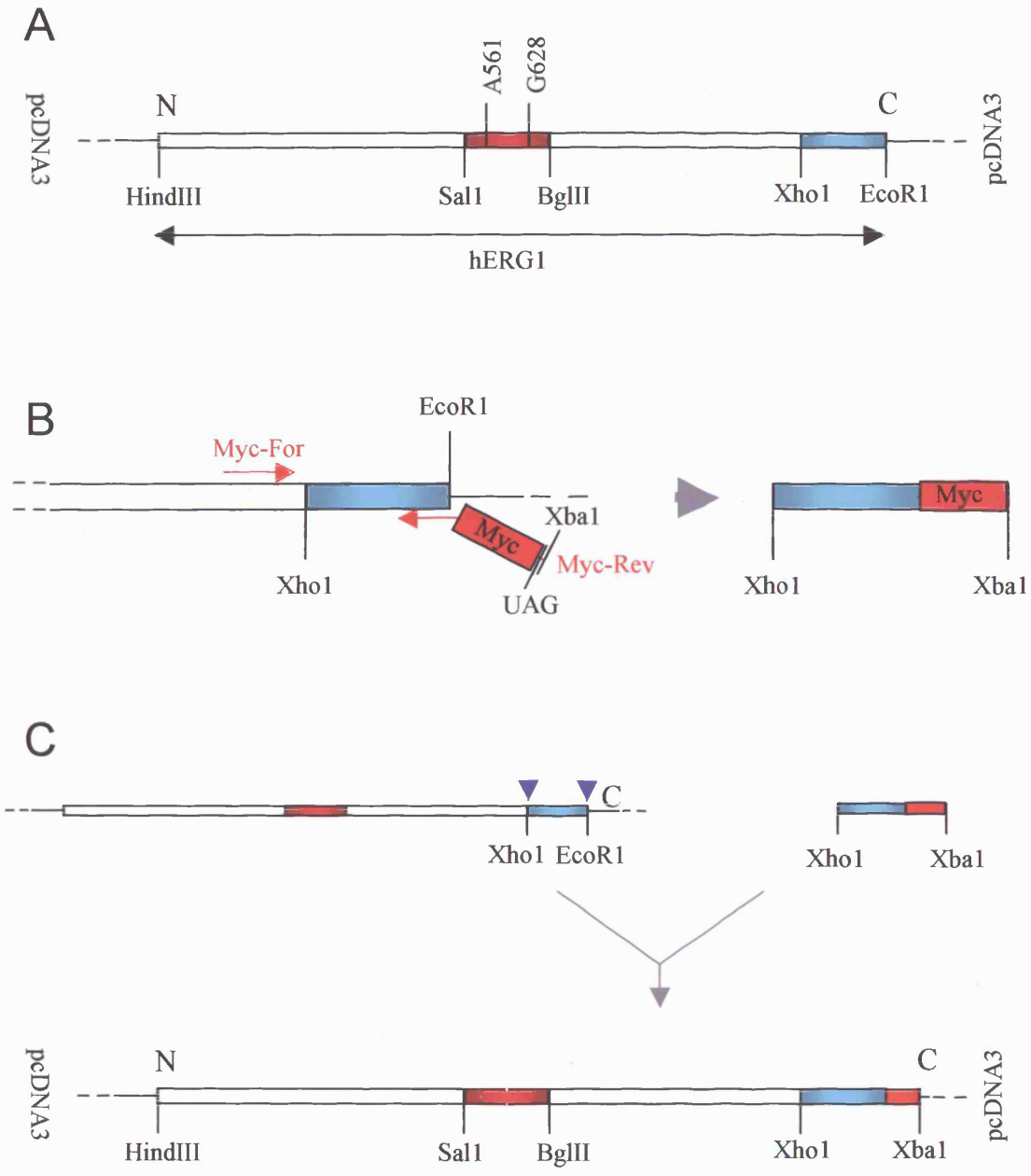

Figure 2.4 Addition of a Myc epitope tag to the C-terminal end of the hERG gene. **A:** hERG contained within the pcDNA3 vector (not shown for clarity). **B:** Myc-for and Myc-Rev primers were used in a PCR reaction that produced a small fragment the Myc tagged C-terminal tail of the hERG gene. **C:** The C-terminal tail of hERG was removed using restriction enzymes Xho1 and Xba1, the product of which was ligated with the Myc-tagged C-terminal fragment to give full length hERG in pcDNA3 with a Myc tag.

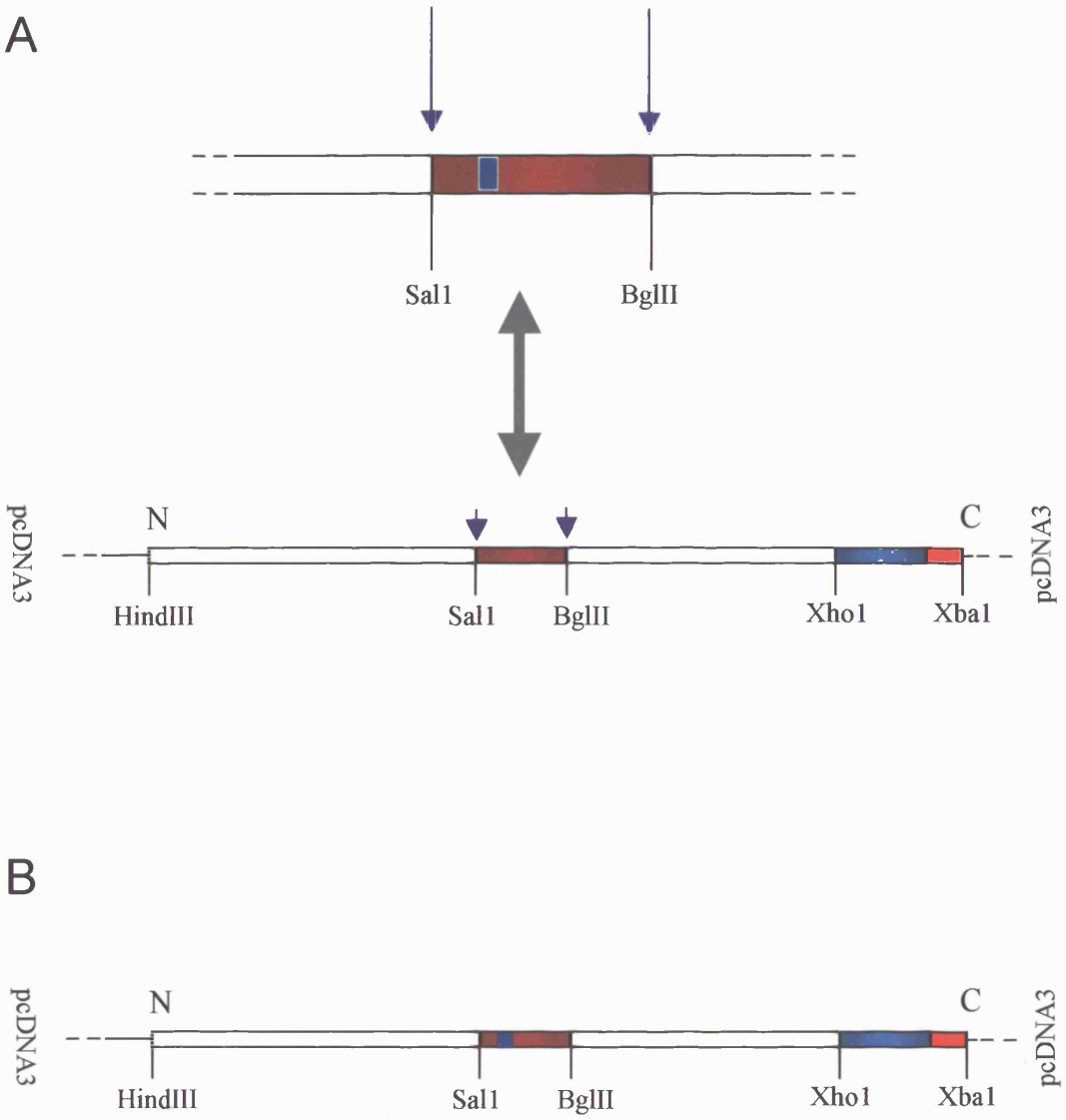

Figure 2.5 Subcloning of hERG mutation into Myc-tagged hERG1 gene. **A:** Mutated hERG1 genes and Myc-tagged-wildtype hERG1 genes were both digested by Sal1 and BglII enzymes (shown by blue arrows). The mutated fragment was then ligated into the wildtype Myc tagged hERG gene. **B:** After ligation the newly created hERG gene included either A561V or G628S mutations and also the Myc tag.

alkaline (NaOH). The lysis buffer was then neutralised and the salt concentration adjusted for column binding, this also caused Chromosomal DNA and protein to precipitate, whereas plasmid DNA remains in solution. The bacterial membranes/precipitate were pelleted by centrifugation. Cell lysates were added to the silica-based anion exchange resin. The resin properties allow the binding of specific DNA types (i.e. genomic and plasmid) at separate salt concentrations. In this way plasmid DNA could be bound to the column while genomic DNA and unwanted cellular components were removed. Finally plasmid DNA was eluted from the column. DNA was then run on a 1 % agarose gel with 0.003 % ethidium bromide. The ethidium bromide intercalated with DNA was visualised using a UV lightbox and the DNA quantified by comparison with DNA ladder of known size and quantity. DNA hyperladder 1 (Bioline, London).

DNA sequencing

DNA sequencing was outsourced to PNACL (Protein and Nucleic Acid Chemistry Laboratory, University of Leicester) who used an automated DNA sequencer (ABI PRISM Model 377). Sequencing was\performed to check constructs following ligations and site directed mutagenesis. Primers used for sequencing were designed to be ~100bp upstream of the target site. Criteria for primer design was; a) Primer length should be around 21 base pairs and begin with G or C. b) Melting temperature should be ≥ 55 °C. c) GC content should be ~ 60 %. d) DNA should be single stranded and not form any secondary structure or duplexes. Primers were purchased from Sigma Genosis (Poole, UK).

Restriction digests

Site specific DNA digestion with restriction site endonucleases was performed in accordance with the manufacturers (New England Biolabs, Hertfordshire, UK) protocols. Briefly, both DNA and restriction enzymes were combined with the correct buffer (supplied with the enzyme) as to give an appropriate overdigestion as specified by the for relevant restriction site enzyme. Restriction enzymes were chosen not only for their ability to cut the DNA sequence at the chosen site, but also for the manner in which they cut the DNA. Only enzymes that gave DNA overhangs ('sticky ends') were used. This ensured selective annealing of complimentary fragments and facilitated ligation of the DNA with minimal chance of random mutation. DNA/enzyme mixture was then incubated at 37 °C. The length of the incubation was dependent upon the overdigestion being

performed and the amount of enzyme used. 1 unit of enzyme is the amount needed to digest 1 µg of DNA in 1 hr; hence 0.5 units of enzyme would require 2 hrs to digest 1 µg of DNA. Care was taken to ensure that the amount of glycerol was not more than 5 % of the total volume to avoid non-specific digests (star activity). To confirm the digestion was complete DNA was electrophoresed on a 1% agarose gel and the size and number of fragments checked.

Transformation

DNA for molecular biology is produced in E.coli bacteria. This expression system allows high quantities of DNA to be generated quickly and accurately. In order for the bacteria to express and thus produce the DNA, it must be first introduced into the cells in a process called 'transformation'. E.coli cells are made to be competent via chemical treatment; a process that increases their ability to take up plasmid DNA. DNA of choice is then added to the cells and forced into the cells either through heat treatments or electroporation.

DH5α library efficiency competent bacteria (Invitrogen, Paisley, UK) were slowly thawed on ice to which DNA (no more than 100 ng) was added slowly. The mixture was incubated on ice for 30 minutes and then heatshocked by plunging tube into waterbath at 42 °C for 45 seconds, before returning to ice for a further 2 minutes and added to pre-warmed SOC (Salt optimised and carbon) media. Cells were then incubated at 37 °C in a shaking incubator 250 rpm for 1 hour, to allow plasmid driven expression of antibiotic resistance. Cells were plated onto pre-prepared LB agar agarose plates containing either 100 µg ml^{-1} Ampicilin or 50 µg ml^{-1} kanomycin (depending on the antibiotic resistance provided by plasmid DNA) and incubated overnight at 37 °C. The competence of bacteria was checked with known quantities of control plasmid DNA (puc18). To check for exogenous plasmid DNA contamination, ddH_2O was used as a negative control.

Ligation

The two pre-cut DNA samples to be ligated were mixed to give a molecular ratio of 5 molecules insert DNA : 1 molecule vector DNA. The pre-cut DNA samples each contained 'sticky ends' that had inter-fragment but not intra-fragment compatibility. 2 % T4 ligase and 1 x T4 buffer were also added to the solution. Control samples were also prepared: Control 'A' had no insert DNA to check that the vector DNA could not re-ligate to itself. Control 'B' had no vector DNA to check

that the insert DNA could not re-ligate to itself. Control 'C' had no T4 ligase to check that there was no uncut vector DNA in the DNA samples. The ligation mixtures were incubated at 16°C overnight and DH5α competent cells transformed with 5 µl of the mixture. Successful ligations would produce colonies on agar plates containing the appropriate selection marker (ampicilin or kanomycin), whilst producing no colonies for the three control samples.

DNA extraction from agarose gels

DNA fragments were separated by electrophoresis and extracted from gels using a QIAquick Gel Extraction Kit (Quiagen). Briefly, DNA bands were visualised by staining with 0.003% ethidium bromide and viewing on a UV lightbox. Bands of DNA were cut from the gel with care taken to minimise the amount of excess agarose. The gel slice was dissolved in heated (50 °C) QG buffer (at a 3:1 buffer volume to gel mass ratio). If DNA fragments are <500 bp or >4 Kb – 1 gel volume of isopropanol was added to increase DNA yield. The solution was passed through an anion exchange column via centrifugation (16,000 g for 1 min) to bind DNA, the column was washed and DNA eluted with 30µl elution buffer containing: 10 mM Tris-HCl, pH 8.5 (16,000 g for 1min).

PCR

The polymerase chain reaction (PCR) uses DNA polymerase enzymes to elongate DNA primers annealed to a complimentary site of template DNA. Using pairs of primers directed against the sense and antisense strands of the template DNA both strands can be copied. This allows exponential amplification of a known sequence of DNA and also allows mutations of the DNA to be engineered, using the Quickchange technique (Stratagene, La Jolla, CA, USA). The PCR machine is used to produce rapid and consistent temperature cycles. Firstly the sample DNA duplex is 'melted' apart by a high temperature. Secondly a new temperature is chosen to allow the annealing of the primers to the single-stranded DNA. This temperature varies depending on the sequence for each oligonucleotide primer and so a range of temperatures were used to find the optimal conditions. The temperature is then changed to 68 °C to allow optimal activity of the DNA polymerase enzyme and elongate the double stranded DNA thus producing new daughter copies of the original sample DNA. This cycle is then repeated many times to further amplify the DNA.

In order to generate the A561V and G628S mutations in the hERG gene primers were designed that were complimentary to the DNA sequence either side of the base(s) to be mutated. The primer sequence differed from the vector DNA at the site of mutation on both the sense and antisense strands (Figure 2.3). After elongation of the double stranded DNA in the PCR reaction the daughter strands would contain the mutation. The approach used for introducing the Myc-epitope tag is explained above (generation of hERG mutants).

PCR primers used in PCR were designed to have minimal secondary structure (via inter-strand base paring, e.g. hairpin loops) and minimal primer dimmer formation that would prevent efficient annealing. Primers were also designed to have a high GC content, which would provide strong binding and a higher melting point. This helps to give more specific primer adhesion to sample DNA. The ideal length for primers was between 25 to 40 bases long. Mutated bases are underlined.

A561V sense: GCGCTCATCGTTCACTGGCTA
A561V antisense: TAGCCAGTGAACGATGAGCGC

G628S sense: GTGGGCTTCAGCAACGTCTCTCCC
G628S antisense: GGGAGAGACGTTGCTGAAGCCCAC

Myc tag sense: CCCAACACCAACTCAGAGAAG
Myc tag antisense: AAATCTAGA**TTACAGATCCTCTTCAGAGATGAGTTTCTGCTC**
ACTGCCCGGGTCCGAGCCG (xba1, **stop codon**, **Myc epitope tag**, Sequence complimentary to hERG).

PCR reaction solutions were prepared as follows in 0.2 ml thin walled PCR tubes on ice: 1 x reaction buffer (Stratagene), 100 ng 5' primer, 100 ng 3' primer, 2 mM dNTP mix, 50 ng template DNA, 2 % DNA polymerase (either Pfu Ultra (Stratagene), or Bio-x-act long (Bioline) for the addition of the Myc tag). Control samples of primers and DNA templates known to amplify well were included with every experiment as a positive control. Tubes were transferred to the PCR machine. The following is a generalised temperature cycling protocol used for the PCR reactions:

Lid		104°C
1.	95°C (denaturation)	2 min
2.	95°C (denaturation)	0.5 – 1 min
3.	annealing temp	1 min
4.	68°C (elongation)	2 min / Kb plasmid length

Repeat steps 2-4 17 times (18 in total). Store product at 4°C until ready to digest.

The annealing temperature was often modified to allow optimal conditions for each individual reaction. Optimal annealing conditions were determined by the number and composition of base pairs formed between the primer and sample DNA. This was calculated using the equation:

$$Tm = 4(G + C) + 2(A + T)\ ^{\circ}C$$

'Hot starts' were also used to optimise conditions. At low temperatures below the melting point of the primer (such as at the very beginning of the PCR protocol) the primers may form dimers or non-specific interactions with the template DNA. Hot starts withhold the polymerase until the reaction mixture has reached 95°C thus preventing elongation of non-specifically adhered primer. Here the PCR reaction mixture was made up without the DNA polymerase enzyme and mineral oil layered on top to prevent evaporation. The samples were loaded into the PCR machine and the protocol started. Once the samples had reached temperature the DNA polymerase was added below the level of the oil. In some cases 1% DMSO was added to reduce any secondary structure or primer dimmer formation formed in the primers.

After the PCR reaction was complete the new DNA needed to be separated from the parent DNA from the original sample. Parental DNA produced in E.Coli is methylated by the bacteria, this can be digested by the Dpn1 restriction enzyme, whilst leaving the newly generated unmethylated DNA unharmed. Dpn1 enzyme was added (10 units per 50µl) and incubated for 1 hour at 37°C.

Ethanol precipitation

After production of the hERG mutants and subcloning into the pAD-Track CMV vector, the vector is linearised with Pac1 restriction enzyme. This linear DNA is now ready for transfection into HEK293 cells, however the Pac1 enzyme must be removed. In order to do this, and also

optimise DNA conditions for transfection, the DNA was ethanol precipitated. This allows the DNA to be resuspended in ddH_2O free of any PacI.

Sodium acetate (pH 5.2) was added to the DNA sample at a final concentration of 10% (V:V). 100% cold ethanol was added at 2.5 times the volume of the DNA/sodium acetate solution. The solution was maintained at -20 °C for at least 30 mins. The DNA solution was centrifuged at 16,000 g for 15 mins at 4 °C to pellet the precipitated DNA. The supernatant was removed and the pelleted DNA resuspended in 70 % ethanol at 4 °C. The DNA solution was centrifuged at 16,000 g for 5 mins. The supernatant was removed and the DNA pellet dried in a 37 °C incubator. DNA was then resuspended in ddH_2O.

Conventional patch clamp recordings, with glass microelectrodes

NIH-3T3 cells were cultured to 70% confluency. Cells were removed from the culture plate using enough trypsin to just cover the monolayer of cells. Cells were pelleted and resuspended in D-PBS. Cells were added to a recording chamber mounted on the stage of a inverted microscope (Eclipse TE300, Nikon, Surrey). Cells were allowed to adhere for ~20 mins. The whole cell patch clamp configuration was used to measure membrane currents elicited by voltage step protocols. Borosilicate glass microelectrodes were pulled and fire polished to give resistances of 3 - 5 MΩ Pipettes were pulled using a P-87 micropipette puller (Sutter Instrument Co., Novato, CA). Voltage clamp recordings were made with an Axopatch 200B amplifier (Molecular devices, Sunnyvale, CA) and recorded to computer for off-line analysis with digidata. Internal solution: 130mM KCl, 5 mM MgATP, 10 mM HEPES, pH 7.2. External tyrode solution: 140 mM NaCl, 1 mM $MgCl_2$, 4 mM KCl, 10 mM glucose, 5 mM HEPES, 2 mM $CaCl_2$, pH 7.4. pClamp software (Molecular devices, Sunnyvale, CA) was routinely used for generating voltage clamp protocols, data acquisition and analysis. The sampling frequency of recordings was 5 KHz and currents were in-line filtered at 1 KHz. The series resistance compensated by 70-80 %. Recordings were performed at room temp.

Automated planar electrode voltage clamp recordings

In order to assess the proportion of cells in each clone that expressed a hERG current many recording were needed to be representative of the population. To do this via conventional patch clamp techniques would not be feasible due to time considerations. However the relatively new

technology known as 'automated planar electrode voltage clamp' allows many hundreds of simultaneous recordings to be performed. Here an IonWorks^{TM} machine was utilised to measure hERG currents in both HEK293 and NIH-3T3 stable cell lines using methods similar to previously published work (Bridgland-Taylor *et al.*, 2006).

Cells were cultured to 70 % confluency in 75 cm^2 tissue culture flasks. Cells were washed twice in D-PBS and washed quickly in trypsin/EDTA. Trypsin/EDTA was added and incubated with the cells for minimum length of time needed for detachment of cells (usually ~2 mins). Cells were suspended in D-PBS and the cells pelleted by centrifugation (1000 g for 3 mins). The supernatant was removed and the cells resuspended in D-PBS. The cellular suspension was pipetted 70 times through a p200 Gilson pipette tip to separate the cells. Cellular suspensions were then loaded onto the Ionworks^{TM} (Molecular devices, Sunnyvale, CA) automated voltage clamp device.

The system performs a hole-test to check the resistance of the planar electrodes. 3 µl of cells are pipetted into each well. After applying suction to pull a cell onto the hole a seal test (-70 mV for 160 ms, then -80 mV for 160 ms) was performed to check the resistance between the electrode and cell membrane. Any cell that did not achieve a 20 MΩ seal were not analysed. The cell now isolates the fluid on the underside of the patch plate from that in the wells of the patch plate. 0.01% amphotericin in intracellular solution was perfused onto the lower side of the well only to permeabilise membrane exposed to the hole on the planar electrode and so gain electrical access to the inside of the cell. Electrodes in the intra- and extra-cellular solutions can then clamp membrane potential and measure current flow across cell membrane. Intracellular solution contained: 140 mM KCl, 1 mM $MgCl_2$, 1 mM EGTA, 20 mM Hepes, pH 7.25. Extracellular solution contained: PBS containing 1 mg Ca^{2+}, and 1mg/L Mg^{2+}. The sampling frequency of recording was 2.5 KHz. IonWorks V2 software was used for full automation including, generating voltage clamp protocols, data acquisition and analysis.

Optical determination of membrane potential changes

Optical recording of membrane potential has been demonstrated in cardiac myocytes (Hardy *et al.*, 2006) and was adapted here for measuring changes in membrane potential in NIH-3T3 cells in response to hERG channel blockers. Glass coverslips were treated with poly-L-lysine for 30 min. Excess poly-L-lysine was removed and cells added to the coverslips and allowed to attach by

culturing overnight in complete medium. NIH-3T3 cells were loaded with the potentiometric dye di-8-ANEPPS at a concentration of 5 μM for 20 min at room temperature, prior to washing in Tyrode's solution containing: 140 mM NaCl, 1 mM $MgCl_2$, 4 mM KCl, 10 mM glucose, 5 mM HEPES, 2 mM $CaCl_2$, pH 7.4. Coverslips were placed into a recording chamber mounted on the stage of an inverted microscope and superfused with Tyrode's solution at room temperature. Measurements were taken from groups of 3 - 7 cells. Cells were illuminated with excitation light of 460-500 nm and the resulting emission split and detected with two photomultiplier tubes. The ratio of emissions at 560 nM and 620 nM wavelengths was then calculated. In order to limit phototoxicity cells were excited with a 100 ms pulse every 10 seconds and sampled every 0.1 ms. Depolarisation causes an increase in emissions at 620 nm and a decrease at 560 nm. Ratios were measured in cells superfused with control Tyrode's solution, a high K^+ solution to take membrane potential close to 0 mV and in solutions containing 10 μm dofetilide to completely block hERG channels.

[^{3}H]-dofetilide binding assay

Radioligand binding assays allow the measurement of small amount of receptor that have a high affinity for the ligand and which the ligand binds to selectively. Homogenised cell membranes are incubated with the radioligand, washed, and the bound ligand quantified by scintillation counting. Due to the high sensitivity of radioactivity detection very small amount of bound ligand can be detected. For this reason the sensitivity of this assay is far greater than that of western blotting and is also more quantitative.

Membrane preparations

Culture medium was aspirated from confluent cells in 175 cm^2 flasks, which were washed with buffer 'A' (10mM HEPES, 0.9% NaCl, 0.2% EDTA, pH7.4). Fresh buffer A was then added and incubated at room temperature for around ten minutes to allow the cells to lift off the flask. Cells were pelleted by centrifugation the supernatant removed, and cells re-suspended in 5 ml of buffer 'B' (50mM Tris, 1mM EDTA, pH7.4) and homogenised using a Polytron (22,000 rpm, 5 second pulses). The homogenate was washed into a 50 ml centrifuge tube and the membrane fraction pelleted by centrifugation at 40,000g for 20 minutes, at 4 °C. The supernatant was removed and the membrane pellet re-suspended in minimum volume of buffer B, and again homogenised using

a Polytron. The membranes were pelleted as above and resuspended in 2 ml of assay buffer containing 71.5 mM NaCl, 60 mM KCl, 1 mM $CaCl_2$, 2 mM $MgCl_2$, 10 mM HEPES, pH7.4.

50µl of assay buffer was added to membrane preparations containing 75µg total protein. [^{3}H]-dofetilide was added at a final concentration of 10 nM. Tubes were vortexed, and incubated at room temperature for 120 min. The binding assay was terminated by filtration onto glass fibre filters (GF/C filters (Whatman) soaked in 0.25% polyethylimine (PEI)) under vacuum. Each tube was then washed in 3 x 2 ml of wash buffer (131.5 mM NaCl, 10 mM HEPES, 1 mM $CaCl_2$, 2 mM $MgCl_2$, pH 7.4). Filter discs were transferred to scintillation vials, and 4.2 ml of Emulsifier Safe scintillation fluid (Lumac, Holland) added. Radioactivity was determined via scintillation counting over a 3 minute period. Non-specific binding was determined by the addition of unlabelled dofetilide at a final concentration of 10 µM. The unlabelled dofetilide competes for the channel binding site, consequently any radioligand bound to these membranes represented non-specific binding to the membrane preparation. Non-specific binding to the filter was determined by repeating the assay in the absence of cell membranes.

To validate the assay, membrane preparations from a known high-level hERG expressing cell line (hERG-HEK293 stable cell line provided by Prof C. January, University of Wisconsin) were used as a positive control and wildtype-HEK293 cells were used as a negative control. Association curves of ligand binding versus incubation time showed that binding saturated at ~60 minutes. In order to insure complete association of receptor and ligand incubation times of 120 minutes were used for the assay.

Cell proliferation assays

[^{3}H]-thymidine incorporation assay

The standard [^{3}H]-thymidine incorporation assay used for attached cells was modified to limit errors produced during repeated washing of the cells. This was important given the weak adhesion of the HEK293 cells. Instead of the majority of the assay being performed in tissue culture plates, the majority of the assay was performed on glass fibre filters. Thus any washing steps could not remove cells from the assay. 100,000 cells were seeded into each well of a 24 well plate. After 24 hours the medium was changed for either serum-replete or serum-free medium. After 45 hours 0.5

μCi of [^{3}H] thymidine was added per well and incubated for 3 hours. The medium was aspirated and cells lifted using 0.5 ml of Trypsin-EDTA (Gibco) per well. Cell suspensions were placed onto GF/B filters (Whatman) and wells washed and contents transferred onto filters with a further 1 ml of Trypsin-EDTA. After removing the Trypsin-EDTA by filtration the filters were incubated in 5 % trichloroacetic acid for 5 min. 2 ml of ethanol containing 200 μM potassium acetate was added and allowed to evaporate. 1 ml of ethanol:diethylether (v:v ratio of 3:1) was added and allowed to evaporate. Filters were then placed into scintillation vials and 4.2 ml of Emulsifier Safe scintillation fluid (Lumac) added. [^{3}H] thymidine disintegrations were counted for 3 min.

Incucyte^{TM} measurement of cell confluency

The Incucyte^{TM} system uses an automated microscope camera housed within the cell culture incubator. The camera can be programmed to take images at specific time points over a given time period. The collected images are automatically analysed with on board software. The software uses algorithms to determine the difference between culture area covered by cells and the area left uncovered. From this the percentage confluency can be calculated. Assuming that cells remain at a given size a change in confluency corresponds to a change in cell number and thus gives a measure of proliferation. The system is designed for up to 6 multiwell plates. For this project 24 well plates were routinely used.

Due to the nature of the small culture wells, cells naturally seed towards the center of the well. This is not ideal for proliferation or scratch wound assays. In order to reduce this effect cells were left at room temperature for 1 hour after plating, before being moved to the incubator. Essen advise this treatment in order to reduce convection currents within the wells. In an attempt to further reduce the effects of cell seeding in the center of the well upon the measurements of proliferation, 4 images were taken per well. This allowed the images to be positioned off center, and increased the total area measured.

10,000 cells were plated into wells of 24 well plates. Culture plates were left at room temperature for ~1 hr in an attempt to achieve uniform cell dispersal. Cells were given > 6 hrs to adhere. The culture medium was aspirated and changed for modified medium containing drug additions or serum changes if required. Each experimental condition was performed on four wells. Culture

plates were then inserted into the Incucyte machine, within the culture incubator and maintained at standard culture conditions. The Incucyte system was then set to repeatedly take photographs of the same area of individual wells and monitor cell confluency over a period of at least 48 hrs. Algorithms within the software calculated confluency as the percentage surface area covered by cells. Data was exported into and analysed in Prism software. Confluency was plotted against time to produce a sigmoidal shaped growth curve. The gradient of the linear portion of the growth curve was used to give a rate of change in confluency. This prevented the need for cells to be of equal confluency at the start of the experiment in order for comparison, thus changes in cell seeding patterns will not affect the results.

Focus formation assay

Foci formation assays are a common way to evaluate the transformation of a cell line. Cells are plated at confluency and cultured for three weeks. Transformed cells will grow to a greater density than non-transformed cells. Dense areas of cells form large foci that are clearly visible after staining. $2x10^6$ cells were plated into 6 cm tissue culture dishes with medium containing 10 % serum. Clones were plated in duplicate. The medium was changed every 4 days. In some experiments 10 μM dofetilide was added once the cells had reached confluency to investigate whether hERG current was important for focus formation. After 21 days cells were washed once with PBS. After aspiration of the PBS 0.5 ml Leischman's stain (VWR, Leicestershire) was added for 5 min at room temp, in order to more clearly show any foci as dark spots against a lighter staining monolayer background. 1 ml of water was then added for a further 1 min. The solution was removed and the plates allowed to air dry (Kazansky & Rosen, 2001). Plates were then photographed, number of foci recorded and the morphology noted.

Wound healing

All metastatic cancers show enhanced motility, thus a change in motility may indicate that an oncogene has a role in metastasis. Scratch wound assays measure the movement of cells from regions of high cell density into areas devoid of cells.

Manual method

NIH-3T3 cells were plated in duplicate in normal culture medium at a density of 2 x 10^6 NIH-3T3 cells in a 6 cm dish. After 24 hrs the cells had attached and formed a confluent monolayer. The plates were incubated at 37 °C, 5 % CO_2 in a humidified atmosphere for 24 hrs. A wound in the cell monolayer was then scored using the tip of a P200 Gilson pipette. Photographs of the size of the wound at ≥ 5 separate marked points were then taken at 0 hrs after wounding and 10 hrs after wounding. Photographs were not taken at >10 hrs after wounding in order to reduce the effect of proliferation upon wound closure. Photographs of the wound were calibrated with a slide graticule imaged at the same magnification to allow measurements of wound width to be taken (Pritchard *et al.*, 2004). Wound width was plotted against time, and the gradient used as a measure of migration. Data were analysed using Prism software, and the statistics quoted are one-way ANOVA with a Dunnetts post test.

Automated Incucyte method

500 x 10^5 cells were plated in normal culture medium in wells of a 24 well ImageLock™ plate (Essen Instruments, Michigan). After 24 h the cells had attached, spread and formed a confluent monolayer. ImageLock plates have a crosshair marked on their lower surface that is used to guide the automated camera from the Incucyte to the same point each time a measurement is taken. Consequently the wound made in the cell monolayer must be directly over this region of the well. In order to do this the Woundmaker apparatus was used to wound the monolayer of cells (Figure 2.2). The media was changed to remove cells scraped off the plate by the wounding process. Compound additions were made at this point. The plates were inserted into the Incucyte system within the incubator and maintained in standard cell-culture conditions. 1 hr was allowed for the plates to reach temperature (and condensation on culture lids to disappear). The Incucyte system was then set to measure wound size every hour over a period of at least 10 hrs. Four wells of a 24 well plate were used per experimental condition.

Soft agar assay

An essential part of metastatic growth is the ability to grow in the absence of adhesion to a substrate. In order to assay this soft agar assays were developed that contain cells within a block of agarose. Cells are unable to adhere to the culture surface, and so growth in these conditions

indicates a transformed phenotype. Indeed soft agar assays are seen as the best indication that a test gene will form tumours in vivo (Shin *et al.*, 1975).

A base layer of 5 ml, 0.7 % low melting point (LMP) agarose (Sigma, Poole) in DMEM was poured into a 6 cm dish. The solution was cooled until set. 100,000 cells were re-suspended in 5 ml DMEM containing 0.35 % LMP agarose at no more than 40°C (pre-warmed in microwave). This middle layer was allowed to cool until set. A third layer of 5 ml DMEM containing 0.7 % LMP agarose was then added and cooled until set. Plates were incubated at 37 °C, 5 % CO_2 in a humidified atmosphere. Each cell sample was plated in duplicate. After 21 days cells were stained overnight for metabolic activity 2 ml of 20 mg ml^{-1} 3-[4,5-dimethylthiazol-2-yl]-2,5-diphenyltetrazoliumbromide (MTT; Sigma, Poole) in ethanol and diluted 1:200 with 1 x DMEM. In metabolically active cells the tetrazolium component of the MTT dye is reduced to form a deep blue coloured formazan product. Plates were then photographed and macroscopic blue stained colonies counted (Mercer *et al.*, 2002). Blue macroscopic colonies indicate viable cells, able to divide without adhesion to substratum. Ras transformed cells have been documented to grow in soft agar (Mercer *et al.*, 2002) and so NIH-3T3 cells were used here as a positive control. Results were only considered if colonies were obtained with NIH-Ras transformed cells. The mean (± SEM) number of colonies from each NIH clone were calculated and statistical comparisons with NIH-VC made using Prism software with a one-way ANOVA test with a Dunnetts post test.

Saturation density

This assay measures the number of cells that can grow on a given surface area. Cells are plated at confluency so that any net increase in cell number indicates that cells are overgrowing. However the assay does not take into account cell shape or proliferation rate that may differ from clone to clone. 1 x 10^6 cells were plated in medium containing 10% serum in a 6 well plate, and were confluent after 24 h. Cells were plated in duplicate. The plates were incubated at 37 °C, 5 % CO_2 in a humidified atmosphere. 24 hrs later the medium was changed and the plates incubated for a further 4 days. Cells were then lifted and counted using trypan blue viability stain. The protocol was adapted from the method of Kuo et al. (Kuo *et al.*, 2000). The mean (± SEM) number of cells from each plate were calculated and statistical comparisons with results from NIH-VC cells made. Data were analysed using Prism software, and the statistics quoted are 1-way ANOVA with a Dunnetts post test.

Immunocytochemistry

Changes in actin cytoskeleton and focal adhesions are characteristic to many oncogenes such as Ras and are a key indicator of transformation (Dartsch *et al.*, 1994). Immuno staining and phalloidin staining of the cell allows any changes in the actin cytoskeleton to be visualised.

Actin staining

Glass coverslips were treated with poly-L-lysine for 30 min. Excess poly-L-lysine was removed and cells added to the coverslips in complete medium. Coverslips were incubated at 37°C, 5 % CO_2 in a humidified atmosphere overnight. The culture medium was removed and the coverslips washed twice with PBS. Cells were fixed in 2 % paraformaldehyde (Sigma, Poole) in PBS at room temp for 15 min. Cover slips were washed 3 times with PBS, and 0.2 % Triton X-100 in PBS was added for 2 min to permeabilise the cells. Cover slips were washed 3 times with PBS. Cover slips were then incubated in 0.1 % BSA in PBS for 30 min. 100 µl of Texas-Red-conjugated phalloidin (Molecular Probes) diluted 1:500 in PBS containing 0.1 % BSA was added and incubated for 20 min, before washing for 20 min in blocking buffer (0.1 % BSA in PBS). Cover slips were then mounted using ProLong Gold antifade reagent (Molecular Probes). Actin staining was visualised via excitation with light at a wavelength of 650 nM.

Vinculin and actin co-staining

Cells were grow on coverslips, fixed and permeabilised as described above. The cells were blocked using 5% goat serum/PBS for 20 mins before washing with PBS. Coverslips were incubated with mouse monoclonal anti-vinculin (V9131, Sigma, Poole) for 1 hr at 37°C at a concentration of 1:100 in PBS containing 1% goat serum. Coverslips were washed in PBS containing 1% serum. Anti-mouse secondary antibody conjugated to Alexafluor 488 was added for 1 hr at 37°C at a concentration of 1:100 in PBS containing 1% goat serum. Coverslips were washed in PBS, and then incubated in 0.1% BSA in PBS for 30 min. For double labelling studies with actin, phalloidin staining was subsequently performed as described above. Cover slips were then mounted using antifade (Molecular Probes). Vinculin staining was visualised via excitation with light at a wavelength of 488 nM.

hERG staining

Glass coverslips were treated with poly-L-lysine for 30 min. Excess poly-L-lysine was removed and cells added to the coverslips in complete medium. Coverslips were incubated at 37°C, 5 % CO_2 in a humidified atmosphere overnight to allow cell spreading. The culture medium was removed and washed twice with PBS. 2 % paraformaldehyde (PFA) in PBS was added and incubated at room temp for 10 min. After a further 15 minute PBS wash cells were blocked and permeabilised for 30 minutes (10% goat serum, 0.5% Triton X-100 in PBS). After two PBS washes the coverslips were incubated with Anti-hERG primary antibody (A gift from G. Robertson (Roti *et al.*, 2002) raised against a C-terminal peptide corresponding to hERG aa residues 883-901, RQRKRKLSFRRRTDKDTEQ; Zymed Laboratories Inc., San Diego) diluted to 1:2,000 in PBS containing 10% goat serum, 4°C overnight. The following morning the coverslips were washed with PBS and incubated with an anti-goat secondary antibody conjugated to AlexaFluor 568 (Sigma) at a dilution of 1:1000 for 2 hrs at room temp. Slides were rinsed in PBS, then mounted in prolong Gold antifade reagent (molecular probes). Fluorescence was visualised via excitation using light of a wavelength of 650 nM. Mounted coverslips were imaged using a Nikon inverted fluorescent confocal microscope, with a x 40 oil immersion lens. Images were collected using Olympus FlowView camera and software.

Lowry protein assay

The Lowry protein assay is based on a two step process. The first step involves the reaction of the protein sample with copper in an alkaline environment (Biuret reaction). The second step amplifies the colour change via the reduction of the folin reagent by the copper treated protein (Lowry *et al.*, 1951). In brief, seven BSA standards were made in duplicate with a range (0 – 400 $\mu g\ ml^{-1}$) of known protein concentrations. Protein samples were diluted in 0.1 M NaOH to be within the range of the standards. 1 ml of $CuSO_4$ solution containing 2% Na_2CO_3 / 0.4% NaOH, 0.01 % $CuSO_4$, and 0.02 % Na^+/k^+ tartrate was added to all tubes vortexed and incubated for 10 mins. 100 µl of folin (Sigma, Poole) diluted 1:3 with ddH_20 was added, vortexed and then incubated for 20 mins. Absorbance at 750 nM was measured using a Beckman Du-65 spectrophotometer. The protein concentrations of the experimental samples could were determined from the standard curve from the BSA standard samples.

Western blotting

Analysis of hERG channel expression levels

Cells were plated in 6 well plates and cultured overnight to achieve ~70 % confluence. The media was aspirated off and cells washed with PBS, and incubated on ice for 15 mins with a minimum volume of RIPA buffer (Sigma, Poole). The lysed cells were then scraped off the plate and centrifuged at 16,000 g for 5 min at 4 °C. The pellet was discarded, and the supernatant analysed for protein concentration. Samples containing 30 µg of protein were added to loading buffer containing 5 % DTT and 2 x sample buffer (125 mM tris-HCL, 4 % SDS (w/v), 20 % Glycerol, 0.1 % Bromophenol blue) at a 1 : 2 (v:v) ratio. Samples were then heated for no more than 2 min at 60 °C to denature proteins. The samples along with a molecular weight marker (Bioline, London) were loaded on a 6 % SDS-polyacrylamide gel and separated by electrophoresis (200 V, 180 min) in TGS running buffer (BioRad, Hercules, CA) containing: 25 mM Tris, 192 mM glycine and 0.1 % SDS pH 8.3. separated proteins were transferred onto nitrocellulose membranes (Schleicher and Schuell, PROTRAN) using a current of 15 V for 20 minutes in transfer buffer containing: 50 mM Trizma Base, 40 mM Glycine, 1.3 mM SDS, 20% methanol, pH8.3. The blots were blocked by incubating in blocking buffer containing: 137 mM NaCl, 2.7 mM KCl, 25 mM Trizma Base and 0.1 % Tween-20, 5% Marvel non-fat milk powder, pH 8.0. After washing with wash buffer containing: 137 mM NaCl, 2.7 mM KCl, 25 mM Trizma Base and 0.1 % Tween-20, pH 8.0 (0.137 M TTBS) the membrane was incubated with rabbit overnight at 4 °C with anti-hERG serum antibody used at 1:1000 in wash buffer containing: 3 M NaCl, 27 mM KCl, 250 mM Trizma-Base, pH 8.0 (0.3 M TTBS). Anti-hERG serum antibody was raised in rabbit to the sequence TCNPLSGAFSGVSNIF on the intracellular C-terminal tail of the hERG channel). Blots were washed five times for five mins in 0.3 M TTBS for. Secondary anti-rabbit antibodies (Sigma, Poole) conjugated to horse-radish peroxidase (HRP) were incubated with the blots, 1:20000 in 0.3 M TTBS 5 % Marvel, for 1 hr at room temperature with rocking. The blots were washed a further five times in 0.3 M TTBS. Immuno-reactive proteins could then be detected by enhanced chemiluminescence (ECL) and exposure to Hyperfilm™ (Amersham Life Science).

To determine antibody specificity the primary serum anti-hERG antibody was incubated with a specific peptide blocker (1 µg of blocker per 1 µg primary antibody) overnight at 4 °C. The rest of the assay was performed as detailed above.

Analysis of ERK1 and ERK2 phosphorylation, PKCδ, PKCε, β-actin, and FAK expression levels before and after confluency

Low confluency (actively proliferating) lysates were generated by plating 250 x 10^3 cells in a 6cm dish for 24 hours. Overconfluent lysates were generated by similar methods to those used in the saturation density assay. 2 x 10^6 cells were plated on a 6cm dish and after 24 hours the media was changed. Cells were then cultured for a further 4 days. Media was aspirated and cells washed with PBS and incubated with minimum volume of Ripa buffer on ice with rocking for 15 minutes. 30μg of sample protein was prepared from cell lysates as described above. The samples along with a molecular weight marker were loaded on an 8% SDS-polyacrylamide gel and run in TGS running buffer. Equal protein loading was confirmed by staining with 0.3 M $CuCl_2$ for 15 mins to detect total protein. $CuCl_2$ staining was removed via destaining solution (0.25 mM Tris, 0.25 mM EDTA pH 8.0). Gels were blotted onto nitrocellulose membranes as described above. The blots were blocked by incubating in Blocking buffer. After washing with 0.137 M TTBS the membranes were incubated with a specific primary antibody:

Rabbit anti-ERK1 (Santa Cruz) diluted 1:500

Mouse anti-phospho-ERK1/2 (#9106, Cell Signalling,) diluted 1:2000

Mouse anti-FAK (#05-537 Upstate Biotechnology, Lake Placid, NY) diluted 1:1000

Mouse anti-PKCε (BD Bioscience, Belgium) diluted 1:1000

Mouse anti-PKCδ (BD Bioscience) diluted 1:500

Monoclonal mouse anti β-actin (Sigma) diluted 1:1000

Primary antibodies were incubated in 0.137 M TTBS for 1 hr at room temp. Blots were then washed with 0.137 M TTBS five times for five mins.

Secondary antibodies conjugated to horse-radish peroxidase (HRP) and specific for the host species of primary antibody, were incubated with the blots.

Goat anti-rabbit (Sigma) 1:20,000 in 0.3 M TTBS 5% Marvel, 1 hr room temp with rocking.

Goat anti-mouse (Sigma) 1:1000 in 0.137 M TTBS 5% Marvel, 1 hr room temp with rocking.

The blots were washed for a further 5 x 5min in 0.137M TTBS. Immuno-reactive proteins could then be visualised by ECL, as described above.

Expression of hERG dominant negative mutants by adenoviral gene transfer

Adenovirus gene transfer is a highly efficient process that provides a higher transfection efficiency with NIH-3T3 cells than more common lipid based mechanisms. The pAD-Easy system uses homologous recombination in bacteria to integrate a recombinant shuttle vector into the viral genome. The viral DNA is transfected into a packaging cell line (HEK293) to produce and amplify viral partials. The pAD-Easy genome lacks the E1 gene without which the virus cannot replicate, thus the virus will not replicate in infected cells. The exception are HEK293 cells which already express E1 and so provide an ideal background in which to generate virus. An overview of this process can be seen in Figure 2.6.

Production of competent bacteria for transformation by shuttle vector and homologous recombination

In order to produce adenovirus a recombinant shuttle vector needs to recombine with the viral genome. To do this BJ5183 competent bacteria already expressing the pAD-Easy-1 plasmid (viral genome) are transformed with the recombinant shuttle vector. Unlike the DH5-α competent bacteria used previously to amplify DNA, BJ5183 competent bacteria have a higher incidence of recombination.

BJ5183 bacteria expressing the pADEasy-1 plasmid were grown SOB media containing: 2 % tryptone, 0.5 % yeast extract, 8.6 mM NaCl, 10 mM $MgSO_4$, 10 mM $MgCl_2$, and 2.5 mM KCl and 30 μg ml^{-1} ampicillin. Cells were grown a high cell density while maintaining logarithmic growth (absorbance at 600 nm of 0.5 - 0.7). The following was performed in a cold room on ice. The bacterial suspension was cooled for 4 hrs on ice before being centrifuged at 4 °C 2500 g for 10 min. The supernatant was removed from the bacterial pellets which were then resuspended in 1 L 10 % cold glycerol in ddH_2O. The centrifugation and glycerol wash were repeated. The cells were pelleted by centrifugation at 4 °C 2500 g for 10 mins and resuspended in the minimum volume of 10 % cold glycerol in ddH_2O, aliquoted and stored at -80 °C.

Generation of adenovirus

hERG tagged on the C-terminus with a Myc epitope was subcloned into the pADtrack CMV shuttle vector (Figure 2.7) between HindIII and XbaI restriction sites (pAD-Track-hERG). This

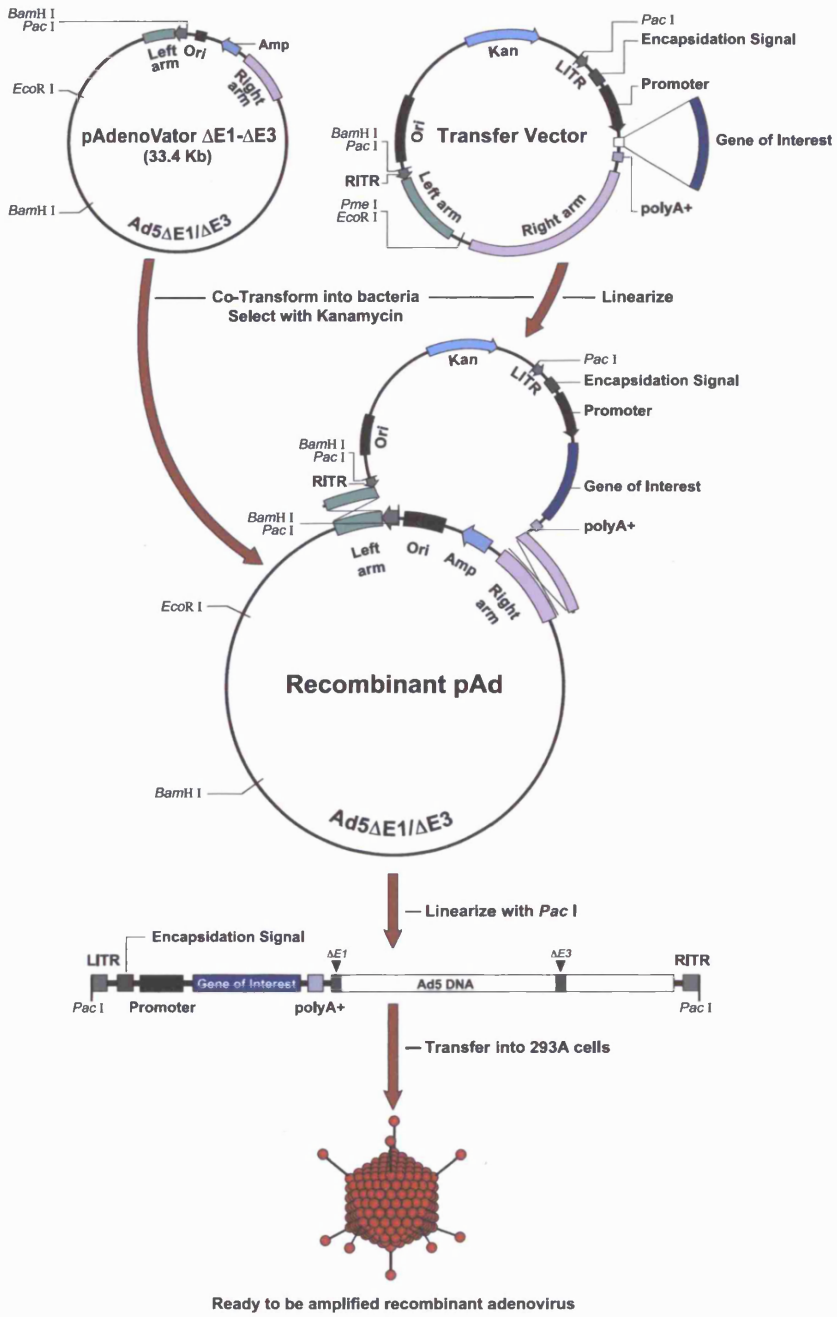

Figure 2.6 Diagrammatic overview of the pADEasy system. Once the hERG gene had been subcloned into the pADTrack-CMV shuttle vector this was transformed into BJ5183 competent bacteria containing the pADEasy-1 plasmid. After recombination and selection colonies were picked and DNA harvested. The resulting DNA was checked for size/correct restriction points and linearised with PacI. Linear DNA was transfected into HEK293 cells using Lipofectamine. After expression of the GFP protein the virus was harvested using a freeze-thaw method.

construct was then linearised with PmeI, ethanol precipitated, and resuspended in ddH_20. pAD-Track-hERG was electroporated into pAD-easy-1-BJ5183 strain of competent bacteria 1 mm electrode separation cuvette (molecular bio-products), 200 ohms, 1.8 kv, 25 uF (Micropulser, Bio-Rad). 1 ml of warm SOC media was added to the cuvette and mixed gently. Cells were moved to a 10 ml tube and placed into a shaking incubator (37 °C 250 rpm) for 1 hr to allow kanomycin resistance of transformed cells to develop. Cells were then plated onto LB agar plates with 50 μg ml^{-1} kanomycin and incubated overnight at 37 °C. Kanomycin resistance is conferred by the pAD-Track-CMV shuttle vector and so only those cells which have taken up the shuttle vector DNA will grow. Kanomycin resistant colonies were picked and DNA harvested from the resulting cultures. However kanomycin resistance is independent of recombination, consequently correct recombination needed to be checked via restriction digest. DNA was digested with PacI restriction enzyme and the resulting DNA fragments run on a 1 % agarose gel. A small band at either 4.5 kb or 3 kb will indicate proper recombination (Figure 2.8). After confirming the DNA sequence of the hERG, insert the viral DNA was transformed into DH5-α competent bacteria. This allowed amplification of the DNA with reduced risk of further recombination events. DNA was retrieved using midiprep kits and quantified on a 1 % agarose gel.

DNA was digested with PacI restriction enzyme to linearise the plasmid and expose the inverted terminal repeats. DNA was ethanol precipitated to purify the DNA and remove restriction enzyme ready for transfection. Sodium acetate was added at a final concentration of 0.3 M, pH 5.2 to adjust the salt concentration. 100 % cold ethanol was added at 2:1 (V:V) and incubated at -20 °C for >20 min. Precipitated DNA was pelleted (16,000 g for 10 min) before the supernatant was removed. DNA pellet was resuspended in Cold 70 % ethanol. DNA was pelleted by centrifugation (16,000 g for 5 min) and the supernatant removed. The pellet was air dried, and finally resuspended in ddH_2O. DNA was transfected into a single T25 cm^2 flask of ~60 % confluent HEK293 cells using lipofectamine (Invitrogen).

Amplification of adenovirus

Following successful transfection of HEK293 cells with viral DNA eGFP became visible under fluorescence after 24 hrs. After 3 – 7 days the cytopathic effect (CPE) of viral production became visable. Cells round up and detach from the plate and the nucleus grows to fill nearly the entire

A

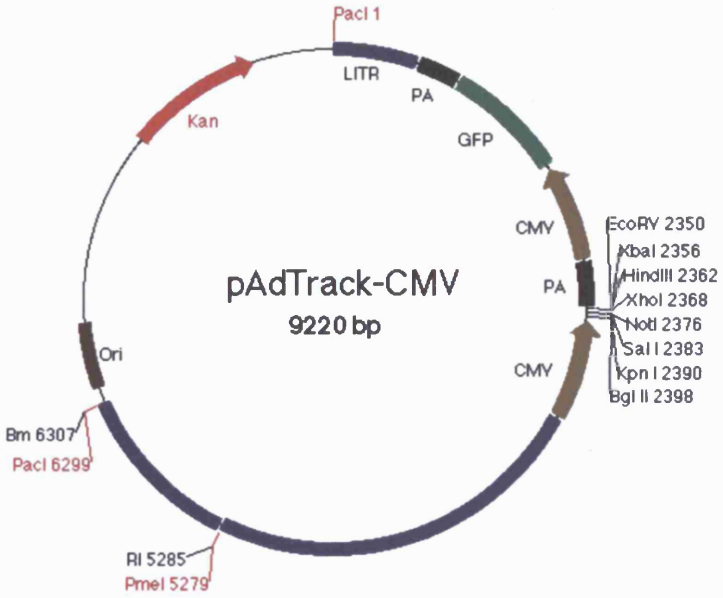

B

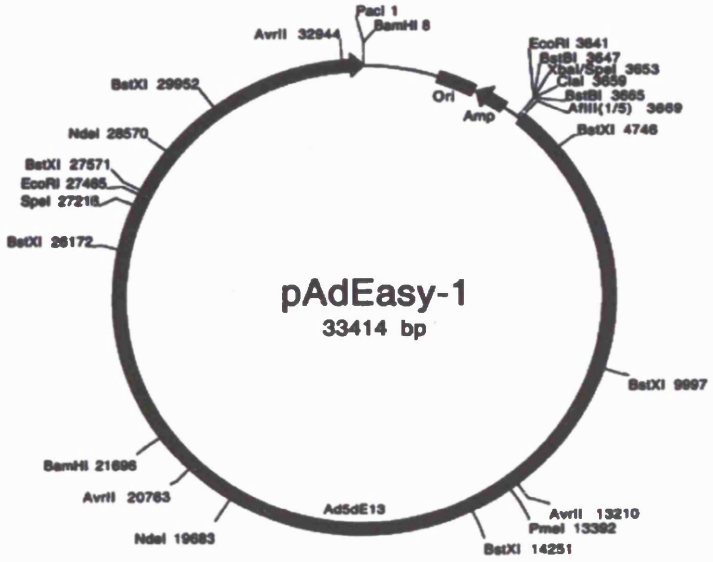

Figure 2.7 Vector maps for A) the pADTrack-CMV shuttle vector containing the GFP gene, and Kanomycin resistance. The WT and mutant hERG genes were inserted into the multi-cloning region between HindIII and XbaI. B) the pADEasy-1 viral DNA plasmid containing the ampicilin resistance gene, but lacking the E1 and E3 viral genes. Vector maps reproduced from National Academy of Sciences, U.S.A.

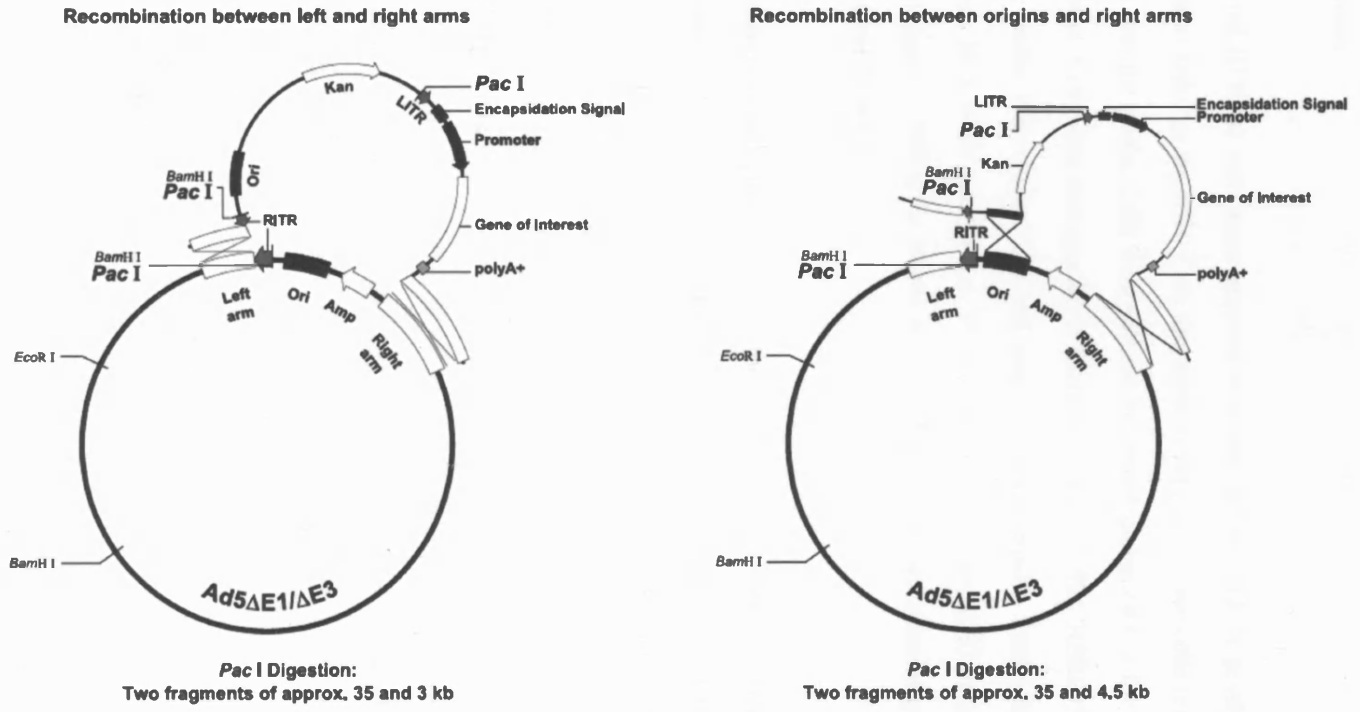

Figure 2.8 Diagrammatic over view of recombination events between shuttle vector (pAD-Track CMV) and viral backbone vector (pAD-Easy). There are two possible recombination events, producing fragments of 35 and 3 Kb or 35 (left) and 4.5 Kb (right). Reproduced from National Academy of Sciences, U.S.A.

cell. HEK293 cells were cultured in minimal media containing 2 % serum, to reduce viral particle binding to serum. After 50 % of cells had detached from the culture surface the virus was harvested.

Infected HEK293 cells were removed from the culture flask as gently as possible using culture media to dislodge the cells. Care was taken to keep the fragile cells intact and thus reduce loss of virus into the media. Cells were pelleted by centrifugation (400 g for 5 min) and the supernatant removed. Cells were resuspended in minimal volume of PBS. HEK293 cells were disrupted using three freeze thaw cycles. The cell suspension was rapidly frozen in liquid nitrogen and then thawed in a water bath set to 37 °C. The fractured HEK293 membranes were pelleted via centrifugation (2500 g for 10 min at 4 °C). The supernatant containing viral partials was removed and stored at -80 °C.

For amplification of the virus all of the viral lysates was used to infect (see below) a single T25 cm^2 culture flask of 80 % confluent HEK293 cells. After 24 – 48 hrs eGFP was visible under fluorescent illumination. The pattern of eGFP expression was indicative of viral titer. High viral titers would produce a speckled 'stars at night' appearance and would be ready to harvest 2 – 4 days after infection. Lower titers were characterized by the appearance of comet-like plaques of eGFP expressing cells, and would be ready for harvesting 7 – 10 days after infection. Further amplification steps used 100 % of the viral supernatant from the previous step to infect two T25 cm^2 flasks of 100 % confluent HEK293 cells. The virus was then amplified in two T75 cm^2 flasks, followed by ten T75 cm^2 flasks and finally fifteen T225 cm^2 flasks of 100 % confluent HEK293 cells.

Adenovirus infection

For proliferation assays cells were grown to ~20 % confluency. For saturation density and scratch wound assays the cells were grown to ~40 % confluency. Culture media was removed and the cells washed with PBS. Enough serum free OptiMEM media (Gibco) were added to cover the cell monolayer, and virus was pipetted directly into the media. The volume of virus added was determined by titration to find optimal transfection levels (number of GFP expressing cells) with minimum toxicity (toxicity determined by visual observation of dead floating cells 24 hr after

virus addition). For a single well of a 24 well plate volumes of 0.25 µl to 1 µl of virus were used (determined from percentage GFP expressing cells). Cells were incubated for 1-2 hours at 37°C in an atmosphere of 5% CO_2, after which minimal amounts of normal culture media was added. The media was changed the following morning.

Chapter 3 Characterisation of hERG expression in mammalian cell lines

Introduction

During early embryo development hERG is expressed throughout the body (Wang *et al.*, 1996), however, as cells differentiate, most lose hERG expression. Heart and nervous tissue is an exception to this rule, and express hERG in order to regulate their membrane excitability. Cancer cells of various origins have been shown to express hERG (Bianchi *et al.*, 1998; Cherubini *et al.*, 2000; Pillozzi *et al.*, 2002; Smith *et al.*, 2002; Lastraioli *et al.*, 2004; Masi *et al.*, 2005). In some cases (e.g. colon cancer) the level of hERG expression is directly proportional to the metastatic properties of the cancer (Lastraioli *et al.*, 2004). This expression pattern is similar to that of EAG, a known oncogene; lending support to the idea that hERG may also be oncogenic.

There are two possible approaches that could be used to study the oncogenic potential of hERG: 1) study cancer cell lines or primary tumour cells that already express hERG and investigate the effects of selectively manipulating hERG function and expression; 2) express hERG in a model cell that has clearly defined characteristics and investigate how hERG expression alters cell biology. The complex nature of cancer development, and mutation accumulation over time, could make it very difficult to assay the effects of hERG channel block or reduction of expression. Instead I chose to express hERG in cell lines that did not endogenously express the hERG channel. Any changes in these cells could then be directly attributable to the expression of the hERG channel. This method also allowed the generation of clones derived from the same parental cells and manipulated in the same way, but that have been stably transfected with constructs that lack the hERG gene. These so–called 'vector control' cells, allow direct comparison with the hERG expressing cells.

In order to assess the oncogenic potential of hERG it was important to study the channel in an appropriate model cell. Continuous cell line culture provided the opportunity to use many different cell types from various origins. The cell line of choice needed to demonstrate a consistent, healthy untransformed phenotype. The cell line of choice should also be easily

maintained in culture and easily transfectable with plasmid vectors. Two separate cell lines were chosen for use in this project. HEK293 (Human embryonic kidney) cells were chosen as they are easily transfectable with standard techniques and allow high expression levels of hERG (Zhou *et al.*, 1998b; Zhang *et al.*, 2003). HEK293 cells grow to form monolayers and maintain their fibroblast-like morphology.

The NIH-3T3 cell line was also chosen to assess the effects of hERG expression. These cells are well known for their well defined contact inhibition of growth upon reaching confluency. NIH-3T3 cells are derived from mouse fibroblasts and are often the cell line of choice for investigating oncogenic proteins (Jouanneau *et al.*, 1989; Dartsch *et al.*, 1994; Silberman *et al.*, 1997; Kuo *et al.*, 2000). This is due to the fact that NIH-3T3 cells are a partially transformed cell background that are susceptible to oncogenic transformation (Jainchill *et al.*, 1969). These cells have a large and very flat fibroblast morphology that is easy to image by conventional microscopy. They also strongly adhere to the culture substratum. Their properties are valuable for numerous cell biology assays.

Stable cell lines expressing the hERG protein are central to the project because transient transfections may not provide the continuous expression of the hERG gene necessary for the long incubation times that some assays may require. Clones stably expressing hERG also allow a better estimate of the relative levels of hERG expression and ensure that every cell is expressing the channel. I was interested in determining whether there is a threshold level of hERG expression that becomes oncogenic. In this Chapter, the production and characterisation of HEK293 and NIH-3T3 cell lines stably expressing the hERG1 gene is described.

Results

HEK293 and NIH-3T3 were transfected with pcDNA3-hERG1, and cells cultured in G418 selection medium. G418-resistant clones were numbered in the order that they were produced. hERG channel expression in each clone was initially quantified by [^{3}H]-dofetilide binding assay. A radioligand binding assay was chosen as the initial screen for hERG expression because it allows screening of many membrane preparations in one assay, and is relatively quick to perform. Most importantly the assay has high sensitivity compared to antibody-based techniques. This assay was validated using HEK-WT cells as a negative control and HEK-hERG cells (gift from C. January, GlaxoSmithKline, Stevenage, UK), which are known to express high levels of hERG (Zhou *et al.*, 1998b), as a positive control (Figure 3.1A). Thus, high specific binding values for dofetilide can be directly correlated with hERG protein expression levels. HEK-WT cells show similar levels of [^{3}H]-dofetilide binding in the presence and absence of competing unlabelled dofetilide, suggesting that any [^{3}H]-dofetilide binding is non-specific. This is confirmed by the result that [^{3}H]-dofetilide binding is unchanged when the cell membranes are omitted (filter blank). HEK-hERG cells show greater binding in the absence of competing unlabelled ligand. This specific binding (Total – NSB) is directly related to hERG protein in the sample. The assay was also demonstrated to be sensitive enough to detect specific binding in guinea-pig myocyte primary tissue (Figure 3.1A). However, hERG expression in SH-SY5Y cells was not detected (Figure 3.3). Eleven HEK293 clones from seventeen G418 resistant clones gave specific binding values that were larger than guinea-pig heart. Clones not used in this project are not shown. The clones 1, 5, 13, 14 and 16 were chosen for use in this project, providing clones with a wide range of specific binding values and hence hERG expression levels.

Binding assays were performed on membrane preparations produced by homogenization and centrifugation of cells, thus hERG protein localised in internal ER and Golgi membranes could contribute to the total ligand binding values. In order to determine the relative surface expression of the hERG channel western blotting was performed. hERG proteins run as two bands corresponding to molecular weights (MWts) of approx. 135 and 155 KDa. The lower MWt (faster migrating) band corresponds to immature, unglycosylated protein while the heavier band shows the fully glycosylated, mature channel protein (Zhou *et al.*, 1998b). It is widely accepted that the majority of the fully glycosylated form of the protein is found in the plasma membrane and the

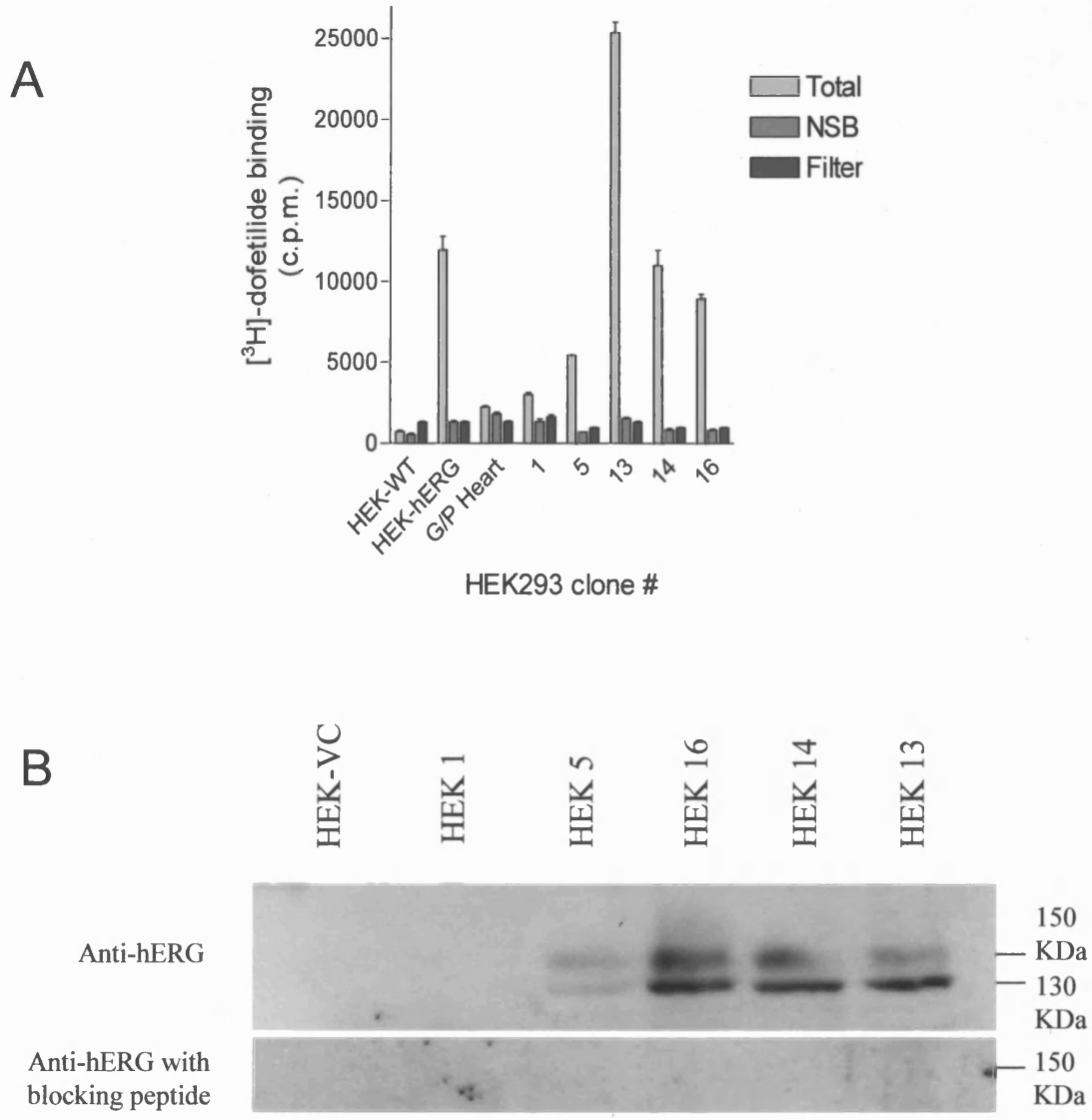

Figure 3.1 Quantification of hERG channel expression by [^{3}H]-dofetilide binding and western blot analysis. **A**: Membrane preparations of HEK293 clones were incubated with [^{3}H]-dofetilide for 120 min before being washed. Any remaining bound ligand was determined by scintillation counting over 3 min (Total binding). NSB (non-specific binding) was determined in the presence of 10 μM unlabelled dofetilide. Filter blanks represent the amount of ligand that bound to the filter in the absence of cell membranes. Graph represents mean ± SEM values measured in three samples from a single membrane preparation. **B**: Representative western blot. Total cell extracts were prepared and resolved on a 6% SDS-PAGE gel (see Materials and Methods). Proteins were probed with anti-hERG serum with (lower panel) or without (upper panel) pre-incubation with specific blocking peptide.

immature protein is mainly localised to the ER and Golgi. Thus, the presence of a band at 155 KDa provides evidence for surface-localised hERG channel expression. No bands were detected for the vector-control (HEK-VC) clone (Figure 3.1B), indicating that the antibody is specific for hERG at this MWt. To demonstrate further the specificity of the antibody, the western blot was repeated with the addition of a specific peptide blocker designed to compete for antibody binding. Figure 3.1B shows no bands for any of the HEK293 clones. Strong bands at 135 and 155 kDa were seen for HEK-hERG positive control cells (data not shown). No protein bands were seen for the HEK-1 clone or with guinea-pig ventricular myocyte lysates, which express relatively low levels of hERG (data not shown). However, clear double bands corresponding to 135 and 155 kDa hERG protein were detected for the clones 5, 13, 14 and 16. As predicted by the binding assay, the amount of hERG was lower in clone 5 than clones 13, 14 and 16. It can also be seen from this representative blot that while clones 13, 14 and 16 all have similar levels of immature hERG protein, the amount of mature hERG protein in clone 13 is lower than that for clones 14 and 16.

To determine if the hERG protein formed into functional channels, hERG channel currents were measured. The IonWorks voltage clamp platform was utilized as a high throughput method for measuring hERG current. IonWorks records from cells using the whole cell patch clamp method (Schroeder *et al.*, 2003; Bridgland-Taylor *et al.*, 2006). In the case of the HEK293 clones, cells were probed for hERG peak tail currents using the voltage protocol illustrated in Figure 3.2A inset. Cells were held at –90 mV for 80 ms and then –80 mV for 180 ms. The membrane potential was then stepped to a depolarised voltage of +40 mV for 500 ms to activate and inactivate the hERG channel. The voltage was changed to –30 mV for 2 sec, to release cells from inactivation and initiate deactivation. After this time the potential was dropped to the holding potential of –80 mV for a further 2 sec. hERG tail currents are generated after the rapid release from inactivation and the slow onset of deactivation. The hERG currents were measured before and after application of 3 μM cisapride, a potent hERG channel blocker. No cisapride-sensitive tail currents were observed in either HEK-WT or VC (Figure 3.2). CHO-S1 cells stably expressing high levels of functional hERG channels were used as a positive control. These cells demonstrated large cisapride-sensitive peak tail currents (data not shown). HEK-1 showed small (46 ± 39 pA) cisapride-sensitive peak tail currents. Clones 5, 13 and 14 showed similar cisapride-sensitive peak tail currents to one another (e.g. 0.45 ± 0.06 nA for clone 14). HEK-16 cells showed the largest cisapride-sensitive peak tail currents (0.76 ± 0.15 nA) (Figure 3.2).

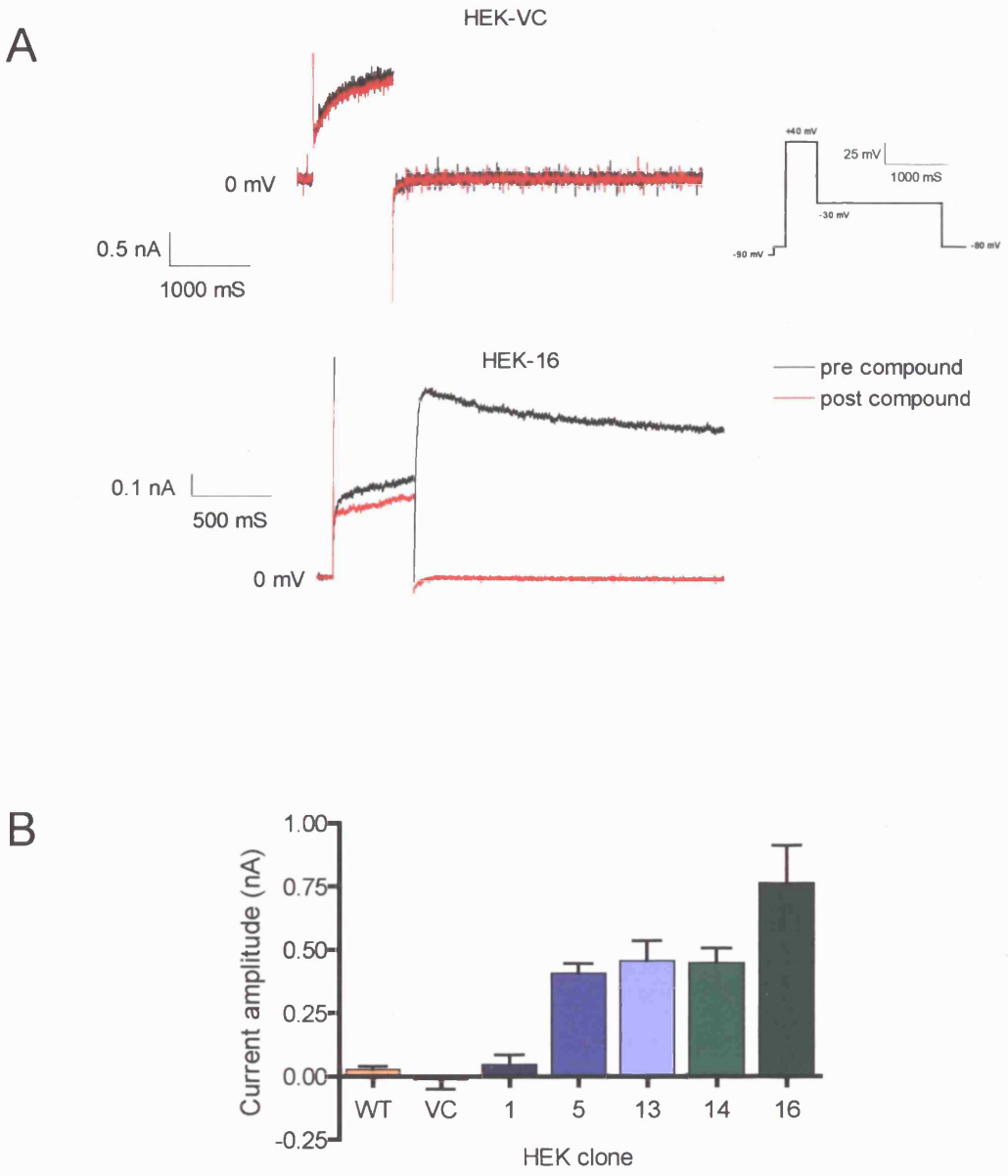

Figure 3.2 hERG peak tail currents measured in HEK cell clones. hERG currents were measured on the IonWorks platform using the protocol shown in the inset. Peak tail current amplitudes were measured before (black trace) and after (red trace) application of 3 μM cisapride. **A:** Representative traces of currents elicited from HEK-VC cell (upper panel) and 16 cell (lower panel). **B:** Average cisapride sensitive current amplitude are from indicated clones (WT n=2, VC n=3, clone 1 n=4, clone 5 n=27, clone 13 n=23, clone 14 n=17, clone 16 n=19). Data represented as mean ± SEM.

Stable, hERG-expressing NIH-3T3 cell lines were made in a similar fashion to the HEK293 cells. Again ligand binding assays using [^{3}H]-dofetilide were utilised to screen the clones for hERG expression. NIH-VC, WT and Ras clones showed no specific [^{3}H]-dofetilide binding. hERG-HEK cells were used in this assay as a positive control (specific binding ~12,500 c.p.m.). From nearly seventy NIH-3T3 clones I tested, only two exhibited significant specific [^{3}H]-dofetilide binding. The binding, and thus expression levels, are similar in the two positive clones; slightly greater than levels found in guinea pig cardiac myocytes (Figure 3.3). The binding values allowed us to estimate the number of hERG channels per cell to be in the region of 350,000 (however, a number of assumptions were made in this calculation, see appendix 4). hERG expression was shown to be stably maintained as [^{3}H]-dofetilide binding assays showed similar levels of specific binding at least until passage 30. Unfortunately, I was unable to demonstrate hERG expression using western blotting. Five separate hERG antibodies were tested without success. It seems that the western blotting assay using currently commercially available antibodies is not sensitive enough to detect this level of hERG expression.

NIH-3T3 cells with stably expressed V12-*Ras* (referred to as NIH-Ras) were a kind gift from Dr Julian Downward (MRC, Cancer Research Institute, UK). V12-Ras is a mutant form of the Ras G-protein that prevents the hydrolysis of GTP to GDP, resulting in constitutive activation of Ras. V12-Ras is a well documented oncogene that will transform NIH-3T3 cells amongst others. These cells will be used as a positive control for transformation in later assays.

Due to the problems with the western blots, immunocytochemistry was used in an attempt to determine hERG protein localisation. Cells were fixed and stained with the ERG1 antibody kindly provided by Dr G. Robertson (Roti *et al.*, 2002). HEK-hERG (C. January cell line) cells were used as a positive control and demonstrated staining that was localised to the plasma membrane producing a clear outline of the cell. Peri-nuclear staining, indicating hERG protein in the ER, was also visible (Figure 3.4). In the absence of primary antibody the staining became much fainter and diffuse throughout the cell, including the nucleus (Figure 3.4). WT-HEK cells used as a negative control showed no specific staining (data not shown). NIH-3T3 cells showed non-specific staining in the absence of primary antibody, however the NIH-VC, 16 and 50 clones also showed similar staining with primary antibody (Figure 3.4). The relatively high non-specific

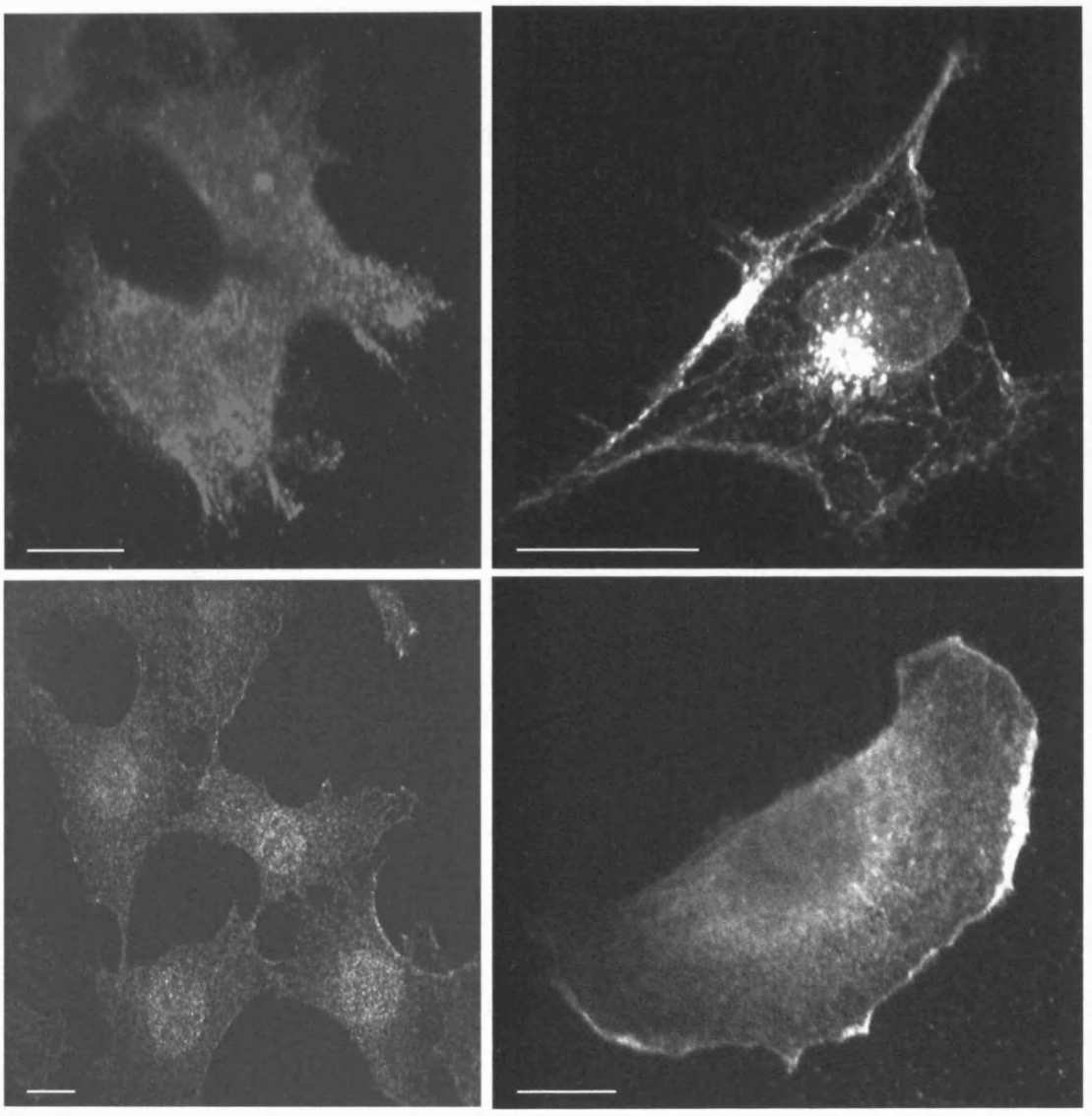

Figure 3.4 Detection of the hERG protein by immunofluorescence. Cells were fixed and labelled with anti-hERG antibody (see Methods). Top-left: hERG-HEK cells with secondary, but no primary antibody. Top right: hERG-HEK cells with primary and secondary antibodies (C. January - control cell line). Lower left: NIH-16 cells in the absence of primary antibody. Lower right: Representative image of staining characteristic to NIH-VC, 16 and 50 cells with anti-hERG antibody. Scale bar represents 25 μm.

background in these cells, coupled with similar staining patterns in hERG expressing clones meant I could not be confident I was detecting hERG channels.

In order to investigate the functional expression of hERG channels in the NIH-3T3 cells the IonWorks platform was used. The low levels of binding in the previous assay indicated that small hERG currents were to be expected in these cells. In order to maximise the measured current the recording conditions were modified. The currents were activated with a 5 sec depolarising pulse to +50 mV (Figure 3.5A inset). The membrane potential was then repolarised to -150 mV. The tail current elicited will be larger than for the previous protocol due to the increased driving force for K^+ at the tail current potential. NIH-VC cells showed no tail currents. Figure 3.5A shows representative current traces for NIH-16 and –50 clones pre and post application of cisapride, both of which show the characteristic hERG 'hook'. NIH-16 shows a shift in current at the holding potantial pre and post drug application, and is thought to be an artifact due to changes in leak. NIH-16 cells showed a mean cisapride-sensitive tail current at -150 mV of 0.80 ± 0.41 nA (n = 9). NIH-50 cells showed a mean cisapride-sensitive tail current at -150 mV of 0.15 ± 0.05 nA (n= 6) (Figure 3.5B). 100 nM cisapride was added in this series of recordings. Unfortunately, this did not cause a full blockade of the hERG currents and thus the values for mean cisapride-sensitive hERG current may be an underestimate of their true size.

While the IonWorks system allowed many parallel recordings from relatively large numbers of cells, it suffers from significantly lower resistance seals with the membrane, and recordings are not very stable. In addition there is a large reliance upon leak subtraction, and the software is unable to run I–V protocols. While the IonWorks system was appropriate for sampling current amplitudes for each clone, conventional whole-cell patch clamp methods were utilised for more detailed study of the hERG currents. An I–V protocol was used in which membrane potential was stepped to test potentials between -60 and +40 mV for 5 sec, and tail current recorded at -150 mV. The recorded currents from both NIH-16 and -50 show the characteristic 'hook' of the tail current. This is produced by rapid recovery from inactivation, producing a sharp downward deflection, followed by relatively slow deactivation that gives a slow decrease in current amplitude (Figure 3.6A). A plot of the normalised peak tail currents (Figure 3.6B) shows that NIH-16 and -50 have similar activation profiles. NIH-16 and -50 both activate at around -25 mV and have potentials for half-maximal activation ($V_{0.5}$) of 6.4 ± 1.0 mV (n=2) and -4.0 ± 0.45 mV (n=2), respectively.

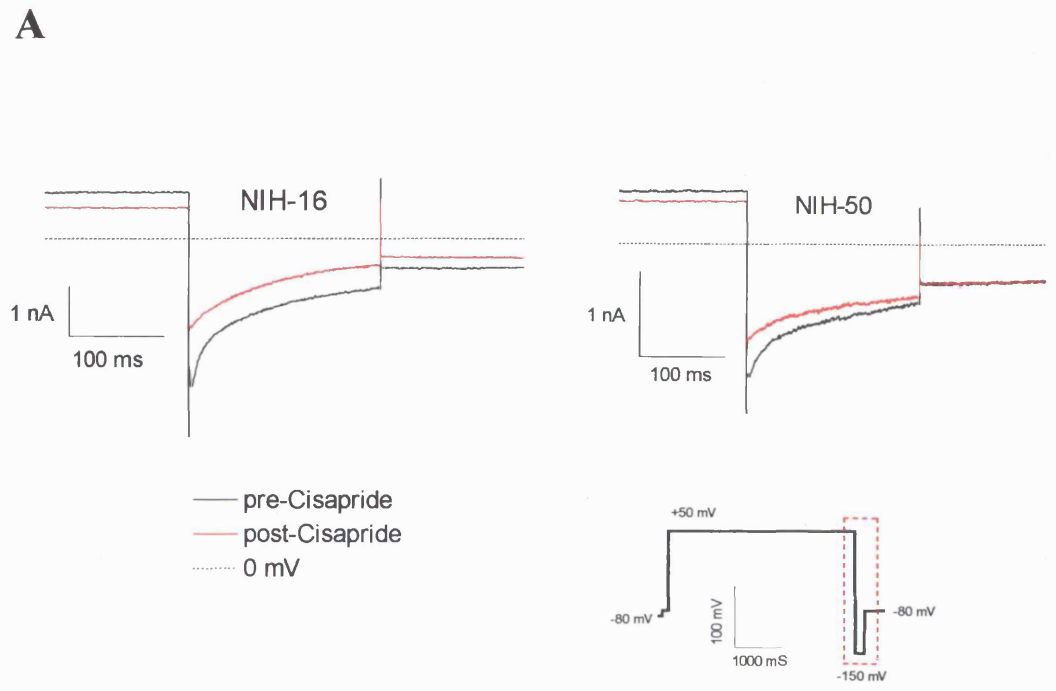

Figure 3.5 hERG current measured in NIH stable clones 16 and 50. **A:** Representative IonWorks recordings of NIH-16 and 50 cells. hERG currents were elicited by voltage protocol shown in inset (boxed section corresponds to traces). hERG current was measured before (black trace) and after (red trace) application of 100 nM cisapride. **B:** Mean (± SEM) data from 9 (NIH-16) and 6 (NIH-50) recordings.

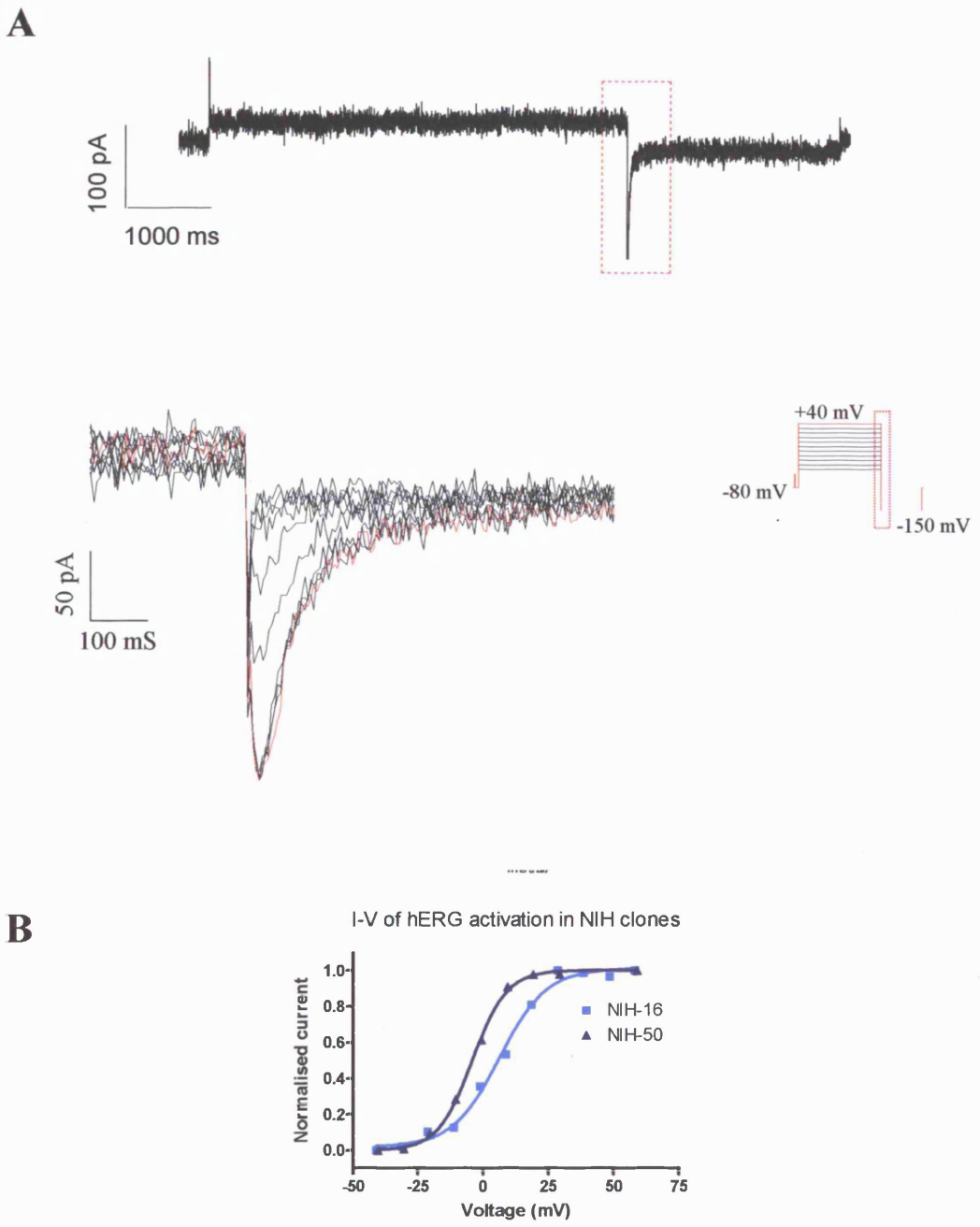

Figure 3.6 hERG current measured in NIH stable clones 16 and 50. **A:** Representative trace of hERG tail currents recorded from NIH-16 cell using conventional whole cell patch clamp. hERG currents were elicited by a voltage protocol shown in inset. Upper panel: whole trace after a depolarization to +40 mV. Lower panel: magnified view of hERG tail currents, corresponding to the boxed region of the voltage protocol. **B:** Representative current-voltage relationship for hERG currents in NIH-16 and 50 cells. peak tail current amplitudes were plotted against test pulse potential and fitted with a Boltzman function.

While performing patch clamp recordings it was noticed that there was relatively little voltage dependent endogenous currents, in the range of potentials used to activate hERG. However, to fully investigate the influence of I_{hERG} on membrane potential an optical recording method (Hardy *et al.*, 2006) was chosen to measure membrane potential changes in response to hERG channel blockers. Optical recording of membrane potential is a non-invasive approach that relies on a voltage-sensitive fluorescent dye, in this case Di-8 ANNEPS. The dye incorporates into the plasma membrane of the cells and can be excited at 460 – 500 nm. The ratio of the fluorescence emissions at 560 and 620 nm changes depending upon the potential difference across the membrane. Thus, the change in ratio is a measure of membrane potential change, and because it is a ratiometric dye the fluorescence signal is less sensitive to changes in cell size, morphology or dye concentration. Membrane potential can also be recorded whilst cells are substratum-attached, instead of in the rounded up, trypsinized state used in electrophysiology recordings. Groups of cells can be recorded from at any one time, allowing cells to maintain inter-cell interactions.

The fluorescence ratio signal was measured from a cluster of cells (2 – 5) perfused with Tyrode containing 4 mM K^+. After 5 min the perfused solution was switched to Tyrode containing 140 mM K^+ to remove the K^+ concentration gradient across the membrane. This will depolarise the membrane potential to around 0 mV (assuming NIH-3T3 cell membranes are primarily permeant to K^+). As can be seen in Figure 3.7 there was rapid and substantial fluorescence change in all of the clones. After solution change there is a delay of ~2 min before a fluorescence change is measured. This is due to the time taken for solutions to pass through the perfusion system and reach the cells. The mean fluorescence ratio during perfusion with 4 mM K^+ (between points A and B on Figure 3.8A) was subtracted from the mean fluorescence ratio during perfusion with 140 mM K^+ (between points C and D, Figure 3.8A) to give the change in ratio upon perfusion with 140 mM K^+. Changes seen with NIH-16 and -50 clones were normalised to NIH-VC (which was set as 100 %). Both of the hERG-expressing clones show a larger fluorescence change than NIH-VC. NIH-50 changes by 116 ± 14 % of NIH-VC and NIH-16 changes by 138 ± 10 % of NIH-VC. Upon returning the cells to control conditions a rapid decrease in fluorescence was seen in all clones. The application of 10 μM dofetilide to selectively block hERG channels had no effect on NIH-VC cells. In contrast, 10 μM dofetilide initiated a rapid increase in the fluorescence ratio of both NIH-16 and -50 clones. The change in fluorescence ratio induced by 10 μM dofetilide was

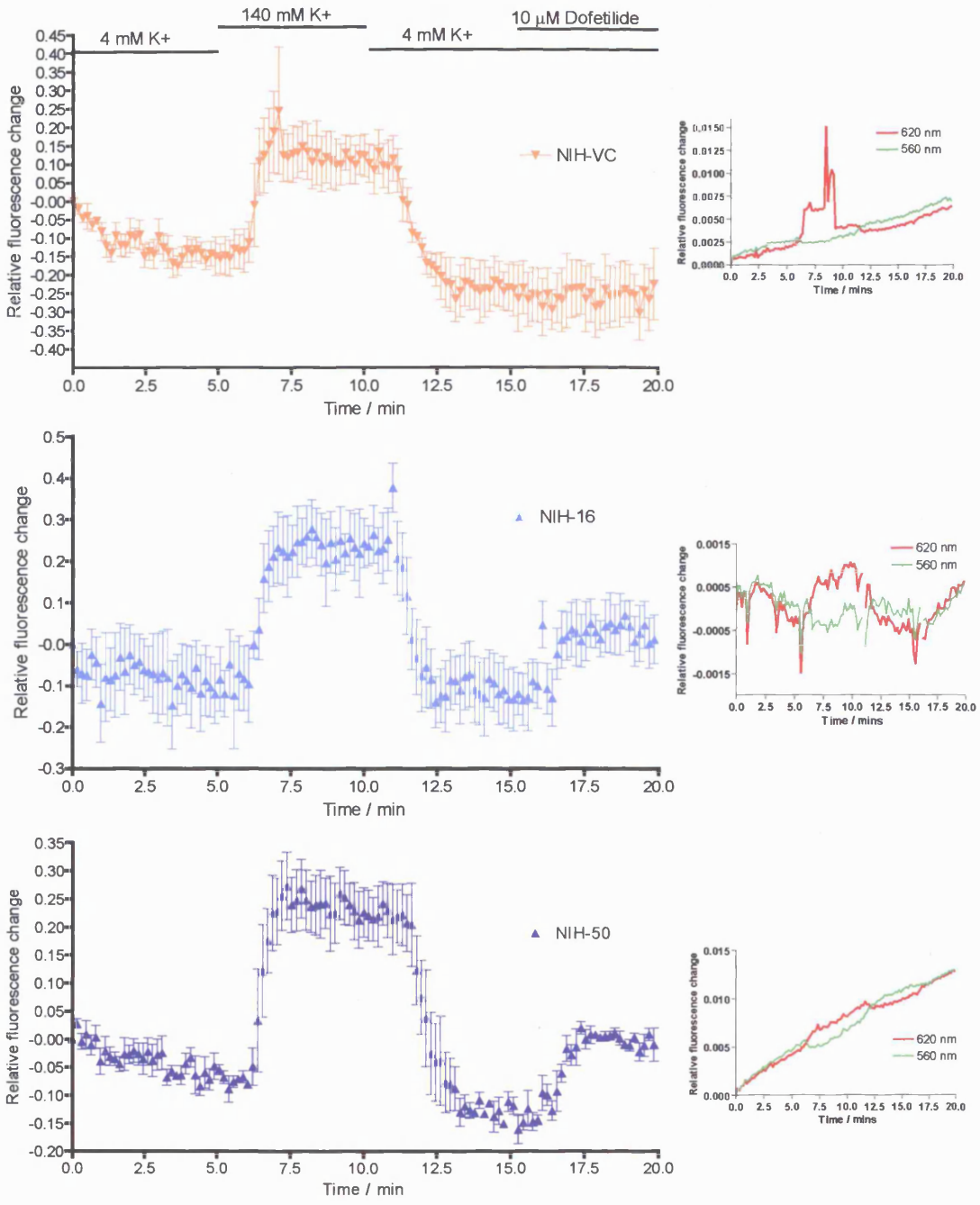

Figure 3.7 Effect of blocking hERG currents upon resting membrane potential. Change in fluorescence ratio recorded from NIH-VC, -16 and -50 clones using the membrane-sensitive dye, Di-8 ANEPPS (see Methods). Data are plotted as mean fluorescence ratio normalized to the beginning of the experiment. Cells were superfused with 4 mM K^+ Tyrode solution. After 5 min 140 mM K^+ was added to the external solution. After a further 5 min 4 mM K^+ Tyrode solution was used to wash the cells. After stabilization, 10 µM dofetilide was added in 4 mM K^+ Tyrode (n=3) for all clones. Inset shows changes in individual fluorescence signals at 620 nm and 560 nm.

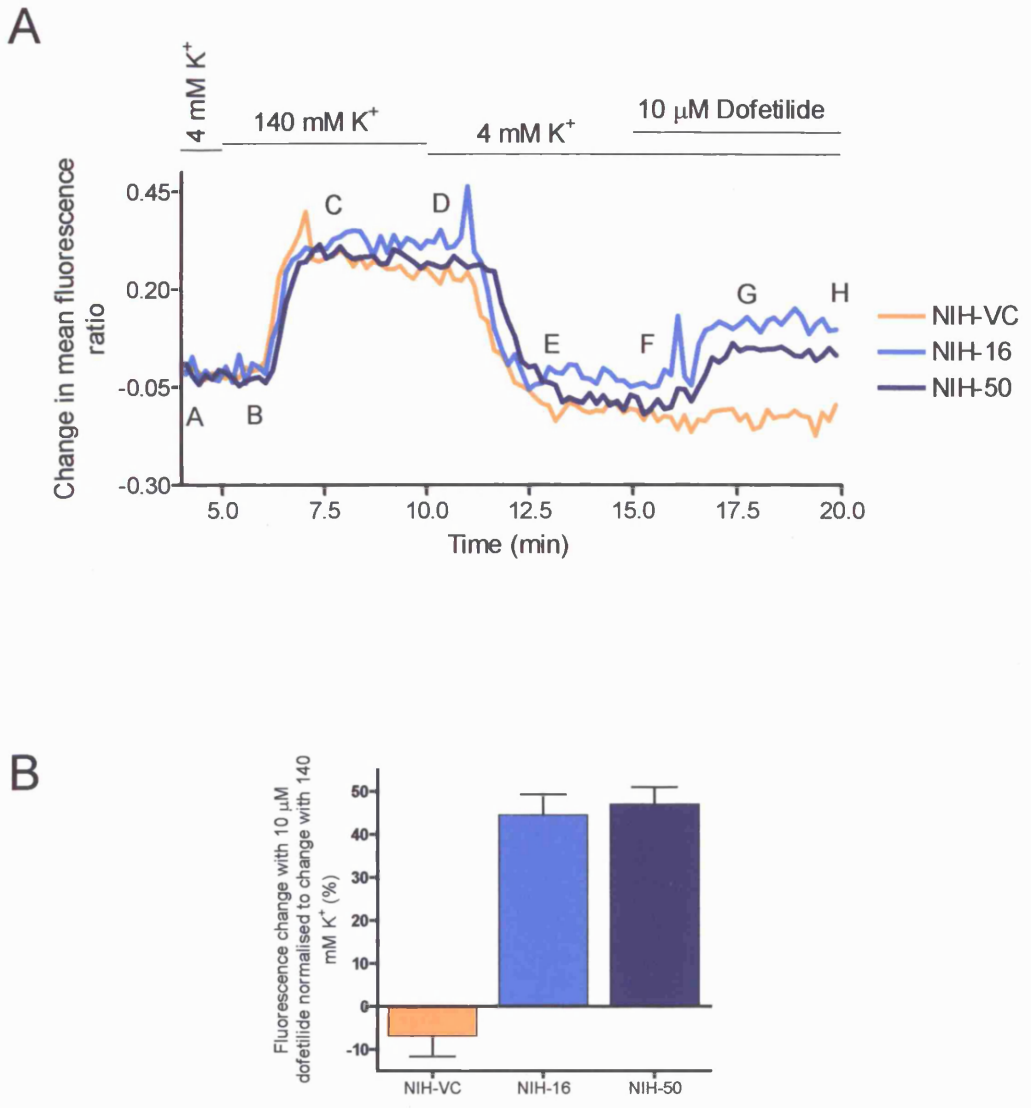

Figure 3.8 Effect of hERG expression upon resting membrane potential. **A:** Overlay of mean traces from Figure 4.7. Data are plotted as the mean fluorescence ratio normalized to the beginning of the experiment. **B:** Change in fluorescence ratio induced by 10 μM dofetilide represented as a percentage of the change in fluorescence induced by 140 mM $[K^+]_o$. Mean value of region G – H minus the mean value of region E – F was expressed as a percentage of mean value of region C – D minus the mean value of region A – B.

$$\frac{\text{(Mean value of region G – H) - (mean value of region E – F)}}{\text{(mean value of region C – D) - (mean value of region A – B)}} \times 100$$

calculated as a percentage of the change in fluorescence induced by 140 mM $[K^+]_o$ (Figure 3.7B). The increase in fluorescence ratio was similar for both clones and corresponded to ~50 % of that seen with 140 mM $[K^+]_o$.

In order to calibrate the system for a particular cell type it is necessary to patch clamp a cell and hold it at different membrane potentials, while simultaneously recording the change in fluorescence. Unfortunately, as yet the system does not have the resolution needed to record from single NIH-3T3 cells (data not shown). Nevertheless, what these experiments indicate is that hERG channels contribute to the resting potential of NIH-16 and -50 clones. The resting membrane potential of these cells is likely to be more hyperpolarised than NIH-VC cells.

Discussion

The current Chapter has characterised two separate cell types generated to stably express the hERG1 gene. Antibiotic-resistant cells were screened for hERG protein expression in ligand binding assays, with further confirmation by western blotting. The functional activity of the expressed hERG channel was also assayed using conventional patch clamp and planar electrode-based recording techniques. Finally the effect of hERG expression upon resting membrane potential (V_{rest}) was measured using optical recording techniques. The results demonstrate that the stable NIH-3T3 clones produced here express functional hERG channels and that their presence contributes to V_{rest}.

The generation of stable cell lines is in general a random process relying on the spontaneous incorporation of the gene of interest within the host genome under control of the CMV promoter. Thus, HEK clones with differing levels in hERG expression were found in the initial ligand binding screen. Five clones were selected to investigate whether the oncogenic potential of hERG1 was dependent on a threshold level of protein expression within the cell. In the case of NIH-3T3 cells, clones were selected that had similar hERG expression profiles not only to one another, but also close to that found in guinea-pig myocytes. This will allow the investigation of the effects of hERG expression at physiological levels. A dividing cancerous cell-line called SH-SY5Y with endogenous hERG expression was also used as a measure of physiological expression levels with which to compare the NIH-3T3 clones. However, hERG expression in these cells is known to vary considerably, and could not be confirmed using western blot or ligand binding analysis (Figure 3.3). Further cell lines with endogenous hERG expression were not avalible for comparison. The two selected hERG-expressing clones will also provide controls for one another, such that hERG-specific effects can be more easily distinguished, helping to avoid any potential artifacts of clonal variation. Importantly, neither the wild-type or vector controls of either cell type showed any specific [^{3}H]-dofetilide binding, confirming that there is no detectable endogenous hERG expression in these cell lines. This was also confirmed by patch clamp studies.

In general the western blots used to probe the cells for the hERG protein correlated with the [^{3}H]-dofetilide binding assay. In those clones that showed high levels of ligand binding a clear double band pattern could be seen that has been previously demonstrated for the hERG protein (Zhou *et*

al., 1998b). HERG protein could not be detected in clones with low specific [^{3}H]-dofetilide binding activities. The Western blot is a less sensitive and reproducible method of hERG detection than a radioligand binding assay. hERG expression for the HEK-1, and NIH-3T3 clones was below the level of detection of the former assay. This was also confirmed when western blotting was unable to show protein bands from guinea-pig myocytes, known to express hERG currents of ~100 pA at tail potentials of -30 mV (Hancox *et al.*, 1998). Although the binding assay detected the greatest amount of hERG protein in the HEK-13 clone, the western blots indicated that HEK-16 has a greater amount of mature, fully glycosylated protein. It is only the mature, fully glycosylated protein that is thought to reach the plasma membrane (Petrecca *et al.*, 1999). Hence, only these mature channels will generate any of the functional current in voltage clamp experiments. The greater amount of hERG protein reaching the plasma membrane in the HEK-16 clone correlates well with the increased hERG current seen in these cells. The lack of sensitivity of the anti-hERG antibodies in immunocytochemistry is also thought to be the reason why hERG channels cannot be effectively visualised.

Both NIH-3T3 clones exhibited a cisapride-sensitive current, however this current was only detectable in around 50 % of the population of NIH-16 and 20 % of the NIH-50 cells. The reason for this differential expression of I_{hERG} may be due to variations in the stage of the cell cycle that each cell is in. As mentioned in the Introduction, hERG channel expression, as well as the functional activity of the channels, has been demonstrated to vary during the cell cycle (Crociani *et al.*, 2003). This may mean that NIH-3T3 cells showing no detectable hERG current may be in stages of the cell cycle where hERG expression is low. The reason this is not observed in the HEK293 stable clones may be due to the greater expression of hERG in these cells. In the NIH-3T3 cells only a small decrease in current would need to take place for it go below the sensitivity of the assay. The HEK293 cells would need a much greater decrease in current to produce the same phenomenon. Alternatively, it is also possible that a portion of the cells do not express hERG.

During the course of the optical recording assays a slight and continual decrease in the fluorescence can be seen under control conditions. This is thought to be due to slow washout of the dye from the cell membrane. However, because the rate of decrease is slow and is constant

through the experiment it can be accounted for. An alternative ratiometric dye (Di-4 anepps) was also used in this assay to try and reduce this run-down effect, but with little success.

In this assay the dye responds to a depolarisation of the membrane potential, resulting in an increase in fluorescence ratio. The application of 10 μM dofetilide had no effect upon NIH-VC cells, but had a pronounced effect upon the hERG-expressing clones. hERG-block gave a depolarisation of the membrane potential equal to ~50 % of that seen with 140 mM K^+ solution suggesting that I_{hERG} is responsible for a significant part of the membrane potential in these cells. When 140 mM $[K^+]_o$ is applied to depolarise the membrane potential a large increase in the fluorescence ratio is seen, which is larger for NIH-16 and NIH-50 cells than for NIH-VC cells. Assuming that at 140 mM $[K^+]_o$ the membrane potential is roughly equivalent to 0 mV for all the clones, this suggests that in order to experience a greater depolarisation, NIH-16 and -50 must have started at a more hyperpolarised membrane potential than NIH-VC. Consequently, these data suggest that hERG expression results in a more hyperpolarised resting potential in NIH-3T3 cells. It may initially seem that these results contradict the previously proposed idea that hERG expression within tumours is responsible for a more depolarised resting membrane potential, due to the channels limited hyperpolarising power relative to other inwardly rectifying K^+ channels (Crociani *et al.*, 2003). However, many healthy cells from which tumours originate express other inwardly rectifying K^+ channels that maintain a hyperpolarised membrane potential (Crociani *et al.*, 2003). The expression of some inwardly rectifying channels is thought to decrease during tumour development, which in turn leads to a more depolarised membrane potential (Crociani *et al.*, 2003). Consequently, the depolarisation of the membrane potential seen in cancerous cells, relative to the healthy cells from which they were derived, is a product not only of hERG expression, but also of other inwardly rectifying K^+ channels. In contrast, very small endogenous currents were observed in the NIH-3T3 cell line when patch clamped. This suggests that NIH-3T3 cells do not have a large number of inwardly rectifying K^+ channels, although this was not rigorously examined. Expression of hERG within these cells causes a hyperpolarisation, rather than a depolarisation of the membrane potential, because it increases the resting K^+ conductance of the membrane.

In summary, this Chapter has evaluated the generation of clonal cell-lines in two cell types stably expressing the hERG channel. These different cell types and the differing levels of hERG

expression between the clones will enable the role of hERG in cell growth and migration to be carefully examined. The production of vector control clones for each cell type, as well as wild-type cells increase the probability that changes in cell behaviour seen with hERG expression are due to expression of this channel rather than random events or consequences relating to cell transfection or manipulation.

Chapter 4 Does hERG expression affect cell proliferation and adhesion independent growth and survival?

Introduction

The process of cell growth and division is a tightly controlled process that is regulated by a complex signalling network known as the cell cycle. This intricate system is responsible for identifying and preventing cancerous growth. Under normal conditions the cell cycle has a number of checkpoints that can be used as decision points for entry into the cell cycle or as barriers to further stages of the cell cycle that require specific conditions to be met. For example, under normal conditions a healthy cell will not commit to the cell cycle unless there is an external stimulus such as growth factors. Cells will also attempt to arrest their own division if they are damaged in some way and unable to complete division successfully, e.g. if the DNA is damaged or incomplete. If the damage is severe the cell may cause its own death in a process called apoptosis, rather than risk mutations that threaten the health of the organism as a whole.

Tumours are, by their very nature, composed of cells that do not follow the normal pattern of growth and division. Cancerous cells have a defect in their cell cycle signalling such that they are able to either ignore the effects of regulatory checkpoints, or have defects in the checkpoints themselves. Different oncogenes are known to have differing effects upon proliferation. Some oncogenes such as EAG are known to increase proliferation (Pardo *et al.*, 1999), while others such as Ras and Src may have little effect upon the rate of proliferation under normal conditions but may instead allow serum independent growth (Irby & Yeatman, 2000). Some oncogenes may have no effect upon proliferation and instead affect the cell in other ways, e.g. loss of contact inhibition, attachment independent growth or abnormal migration to name but a few.

The involvement of hERG in proliferation has been proposed by several authors. hERG deactivates at relatively depolarised membrane potentials compared with other inwardly rectifying potassium channels. It has been proposed that this helps maintain the depolarised resting membrane potential seen in many cancer cells (Arcangeli *et al.*, 1995). In turn this depolarised membrane potential may allow passage through cell cycle checkpoints, possibly via calcium influx (Wonderlin & Strobl, 1996). Levels of hERG expression also vary in accordance with the

cell cycle, showing a large increase at G1 (Crociani *et al.*, 2003). This cell cycle-dependent expression is thought to be further evidence for its involvement in proliferation, as it suggests that hERG expression is involved in key events in the cell cycle, such as progression through cell cycle checkpoints. However, as yet there is little in the way of direct evidence for an enhancement of proliferation as a direct result of hERG expression. Some studies have tried to block hERG channels in tumour cells and demonstrate a reduction in proliferation, however many have used very high drug concentrations that are up to two orders of magnitude greater than the IC_{50}, and may be causing non-specific effects (Crociani *et al.*, 2003). The question of whether hERG is involved in proliferation is far from fully answered.

Integrins and substrate independent growth

In normal healthy cells, attachment to the ECM is an essential requirement for growth. Integrin attachment to the ECM is quickly followed by integrin clustering. These clusters of activated integrins start the development of a macromolecular complex of signalling molecules surrounding the adhesion site. This complex or 'focal adhesion' is able to initiate the formation of stress fibers that link the focal adhesions with the actin cytoskeleton of the cell. In the absence of integrin ligation to the ECM, focal adhesions are unable to form and thus many important signalling pathways become silent. This has important consequences for the cell. In order to grow and pass through the G1 phase of the cell cycle a normal healthy cell must not only receive proliferative signals from growth factor receptors but also signals from integrin associated pathways. In fibroblast cells, loss of integrin signalling leads to cell cycle arrest, whilst in epithelial cells loss of integrin signalling causes a specialized type of apoptosis termed 'anoikis' (Wang, 2004).

One of the key markers of a transformed cell is adherence-independent growth. In order to metastasize and take over new areas of the body a transformed cell must not only be able to migrate away from its original site but it must also be able to survive whilst it travels in the blood stream. The mechanisms behind adhesion-independent growth vary for different oncogenes, however most seem to act through the PI3K, AKT pro-survival signalling pathway (Wang, 2004). Up-regulation of the pro-survival signalling is sufficient to rescue cells from apoptosis. The MAPK pathway is also documented to be involved in adhesion dependent growth, and constitutive activation of this signalling pathway can lead to a cancerous phenotype.

hERG expression is well documented in many cancerous tissues (Bianchi *et al.*, 1998). The expression level of the channel may correlate with the metastatic ability of the particular tumour. In colon cancer (Lastraioli *et al.*, 2004) and gliomas (Masi *et al.*, 2005) the channel and its functional current are increased in the later stage, metastatic, aggressive tumours. Thus it is tempting to speculate that hERG expression may help in the acquisition of a metastatic phenotype. The mechanism behind this may be linked with hERG channel interactions with focal adhesion signalling proteins. The hERG channel has been shown to interact with many of the components of focal adhesions such as FAK and β1-integrins (Cherubini *et al.*, 2005). hERG expression may also increase the phosphorylation and activation, state of the FAK protein (Cherubini *et al.*, 2005). FAK itself is known to be involved in transformation and increased activation is found in many cancers (Weiner *et al.*, 1993; Agochiya *et al.*, 1999; Xu *et al.*, 2000; van Nimwegen *et al.*, 2005). These findings have led us to propose that hERG expression may allow changes in signalling pathways that may present themselves as adhesion independent growth.

The aims of this chapter are to investigate the effects of hERG expression upon the growth characteristics of stably transfected HEK293 and NIH-3T3 cells. Initial experiments will determine whether hERG expression provides an advantage during proliferation under normal and growth factor depleted conditions. Further experiments will examine the effect of hERG expression upon attachment-independent growth. Together these results will help to elucidate whether hERG involvement in cancers extends to enhanced growth properties in conditions encountered by developing tumours such as loss of adhesion.

Results

The stable cell lines generated in the previous chapter allow a detailed investigation into the effects of hERG expression on proliferation. There are many different methods to assay proliferation such as MTT and BrdU based assays. However in order to investigate the effects of hERG expression on the rate of proliferation the [^{3}H]-thymidine incorporation assay was chosen. [^{3}H]-thymidine incorporation measures the amount of DNA synthesis - a process that is directly coupled with cell division. The [^{3}H]-thymidine incorporation assay was modified to reduce potential cell loss from wash steps as much as possible (see methods). This was necessary to exclude potential errors introduced by any changes in substrate adhesion due to hERG expression since during routine culture I noticed that hERG expression, especially in the HEK293 cells, reduced adhesion to culture plates.

Does hERG expression affect the rate of HEK293 proliferation?

Sub-confluent HEK293 clones cultured in medium containing 10 % serum showed similar [^{3}H]-thymidine incorporation (and thus proliferation) rates for HEK-WT, VC and the low level hERG expressing clones HEK-1 and -5 (Figure 4.1). In contrast, the high-level hERG expressing clones HEK-13, HEK-14 and HEK-16 showed significantly decreased rates of [^{3}H]-thymidine incorporation. The decrease in [^{3}H]-thymidine incorporation was in the order HEK-13 > HEK-14 > HEK-16. If this change in proliferation rate is compared with hERG expression it can be seen that [^{3}H]-thymidine incorporation correlates with the level of hERG protein expression (Figure 3.1A) rather than hERG current (I_{hERG}) expression levels (Figure 3.2) suggesting that the effects of hERG expression on proliferation may be less dependent on ion flux (and associated changes in membrane potential), and more dependent on the total amount of hERG protein expression.

HEK-WT, -VC and low-level hERG expressing HEK293 clones (HEK-1 and -5) show almost equal amounts of thymidine incorporation in the absence of serum as that shown by the high level hERG expressing clones HEK-13, -14 and –16 grown in the presence of serum (Figure 4.1). Thus HEK-WT, -VC, -1 and -5 clones show relatively high proliferation rates even in the absence of growth factors. Culture under serum-free conditions resulted in a decrease in [^{3}H]-thymidine incorporation in all HEK clones, however, there was a reduced affect in hERG-expressing clones HEK-13 and -16, and this achieved statistical significance in the case of HEK-16 (see Figure

A

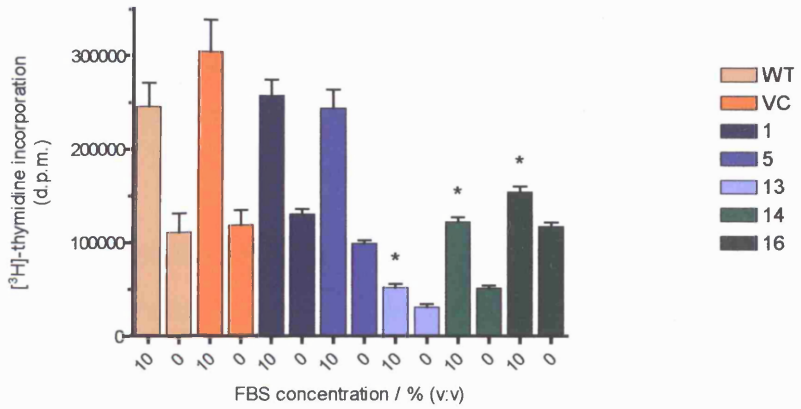

B

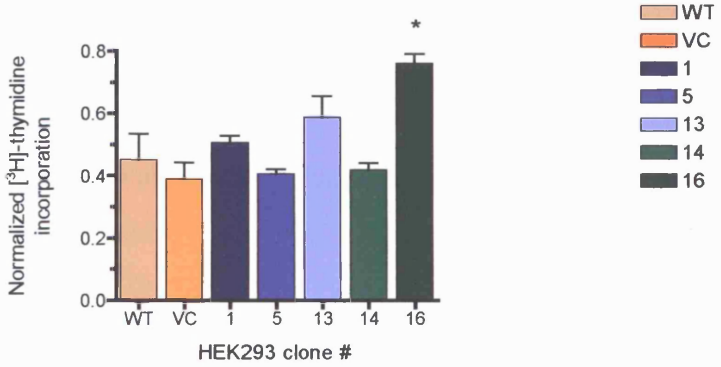

Figure 4.1 hERG expression decreases [^{3}H]-thymidine incorporation in HEK293 clones. **A:** stable HEK293 clones were grown in medium containing either 10 % or 0 % serum for 48 h. [^{3}H]-thymidine was added for the final 3 hrs. [^{3}H]-thymidine incorporated into the DNA was measured by scintillation counting. Data are presented as means ± range from least two experiments performed in triplicate. **B:** [^{3}H]-thymidine incorporation under serum-free conditions relative to that observed in the presence of 10 % serum. Data were analysed with GraphPad Prism software, using a one-way ANOVA analysis with Dunnett's post-test with reference to HEK-VC as control (*$p<0.05$).

4.1B). However, the HEK-14 clone did not seem to follow this trend. Thus, high levels of hERG expression in HEK293 cells tend to decrease proliferation rates and may lead to a decreased dependency on serum for proliferation.

Does hERG current play a role in HEK293 proliferation?

In order to investigate if hERG current is required for the effects upon proliferation, cells were grown in the presence of hERG channel blockers. Blockers were added to culture medium in the absence of serum. It was hoped that any potential effects of hERG channel block would be more evident under serum free conditions if hERG has a transforming effect upon proliferation.

Dofetilide is a potent, highly specific hERG open-channel blocker. Dofetilide was applied at concentrations of 10 nM, 100 nM, 1 μM, 10 μM and 100 μM. The IC_{50} of dofetilide against hERG has determined to be ~10 nM (data not shown), which agrees with previous studies using the [^{3}H]-thymidine incorporation assay (Diaz *et al.*, 2004). No significant effects upon proliferation were seen from 10 nM through to 10 μM dofetilide. Figure 4.2A shows the mean results with 10 μM dofetilide. There is <10 % change from control conditions after the addition of dofetilide for the hERG expressing HEK clones. There does seem to be a larger effect upon the HEK-WT and VC clones, however this is unlikely to be specific as dofetilide's effect upon [^{3}H]-thymidine incorporation is not concentration dependent for these clones (data not shown). Only when a concentration of 100 μM dofetilide is present is there a significant (~50 %) decrease upon the hERG-expressing clones (Figure 4.2A).

ERG-toxin was used as an alternative hERG blocker in a repeat of the [^{3}H]-thymidine incorporation assays. ERG-toxin is a scorpion toxin that unlike most hERG channel blockers does not bind to the central pore region, instead it binds to an amphipathic α-helix on the extracellular face of the channel (Pardo-Lopez *et al.*, 2002). The toxin is a closed-channel blocker, and does not rely upon activation of the channel in order to block the pore (Milnes *et al.*, 2003). rERG-toxin was applied to cells at 10 and 100 nM in the absence of serum, and [^{3}H]-thymidine incorporation measured (see figure 4.2B). HEK-WT and VC clones as well as HEK-1 were reduced to around 60 % of the thymidine incorporation seen under control, serum free conditions. It is not clear why there is a reduction in [^{3}H]-thymidine incorporation. However, the effect was not concentration

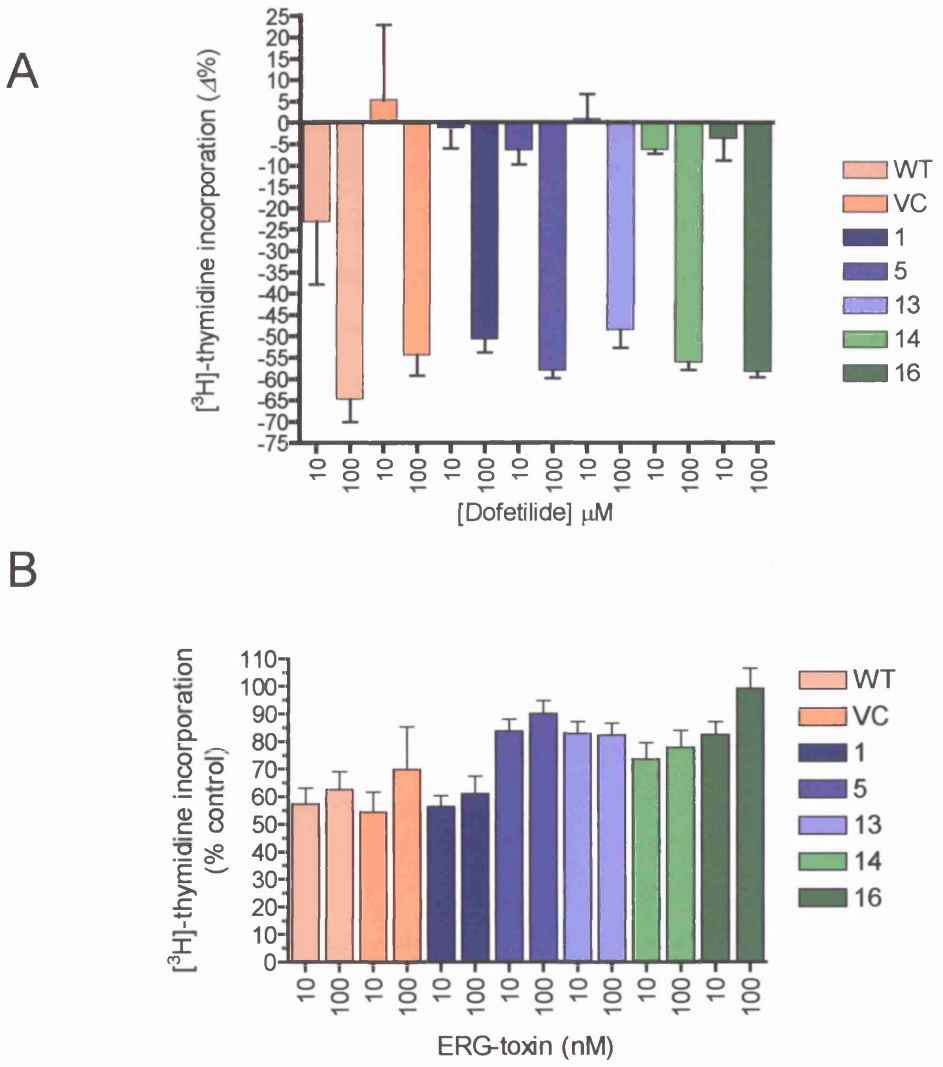

Figure 4.2 **A:** Effects of dofetilide on [^{3}H]-thymidine incorporation in HEK293 clones. Cells were cultured in serum-free medium containing 10 or 100 μM dofetilide for 23 hrs, and during the final 3 hrs [^{3}H]-thymidine was included in the medium. [^{3}H]-thymidine incorporation into the DNA was measured via scintillation counting. Data are plotted as percentage change (*Δ*%) in [^{3}H]-thymidine incorporation relative to that measured under serum-free control conditions. Bars represent means ± range from at least two experiments, performed in triplicate. **B:** Effect of rERG-toxin on [^{3}H]-thymidine incorporation in HEK293 clones. Cells were cultured in serum-free medium containing ERG-toxin for 23 hrs, the final 3 hrs of which [^{3}H]-thymidine was added. Data are plotted as percentage change in thymidine incorporation relative to that measured in serum-free control conditions with ERG-toxin vehicle.

dependent. In the hERG expressing clones thymidine incorporation was also reduced by ERG-toxin to between 74 and 99 % of control values. To demonstrate hERG channel block by this compound, HEK-13 cells were patch clamped by traditional whole-cell patch-clamp. After holding at -70 mV, cells were depolarised to 0 mV which activates and rapidly inactivates the hERG channels and then repolarised to -50 mV to produce tail currents (Figure 4.3 inset). After the currents had stabilised, ERG-toxin was perfused onto the cell. I_{hERG} was rapidly blocked such that after 60 secs 80 % of control peak tail current had been blocked. The control and ERG-toxin traces have different shapes on depolarisation, with ERG-toxin producing a gentle slope. This is suggests that the block of hERG by ERG-toxin is time dependent. hERG channel block was reversible, and after 5 mins of washout there was almost full recovery (Figure 4.3).

Dofetilide and ERG-toxin do not appear to alter the proliferation of HEK293 cells in a hERG dependent manner. Therefore it would seem that hERG current is not responsible for any hERG mediated effect upon proliferation in this cell type.

Does hERG expression affect the rate of NIH-3T3 proliferation?

In order to check if these findings were cell type specific, similar assays were carried out in the stable NIH-3T3 cells generated in the previous chapter. 1 % and 5 % serum conditions were added to this assay to give more information on the serum dependence. NIH-WT, VC and hERG expressing clones show a similar amount of [^{3}H]-thymidine incorporation in response to growth in different serum levels (Figure 4.4A). Each clone showed a relatively linear relationship between serum concentration and proliferation rate. Under serum-free conditions NIH-WT, VC and hERG expressing clones (NIH-16 and 50) show 27 - 36 % of the [^{3}H]-thymidine incorporation seen in the presence of 10 % serum. The transformed NIH-Ras cells show a reduced [^{3}H]-thymidine incorporation in comparison to that of NIH-WT and VC in 10 % serum medium. However, [^{3}H]-thymidine incorporation levels in the NIH-Ras clone appear to be serum-independent (Figure 4.4A). It would seem that the oncogenic properties of NIH-Ras that allow this clone it grow independently of growth factors are not reproduced following hERG expression in NIH-3T3 cells.

In order to further validate the [^{3}H]-thymidine incorporation data, proliferation rates were also measured using the Incucyte system. This equipment has the advantages of high throughput

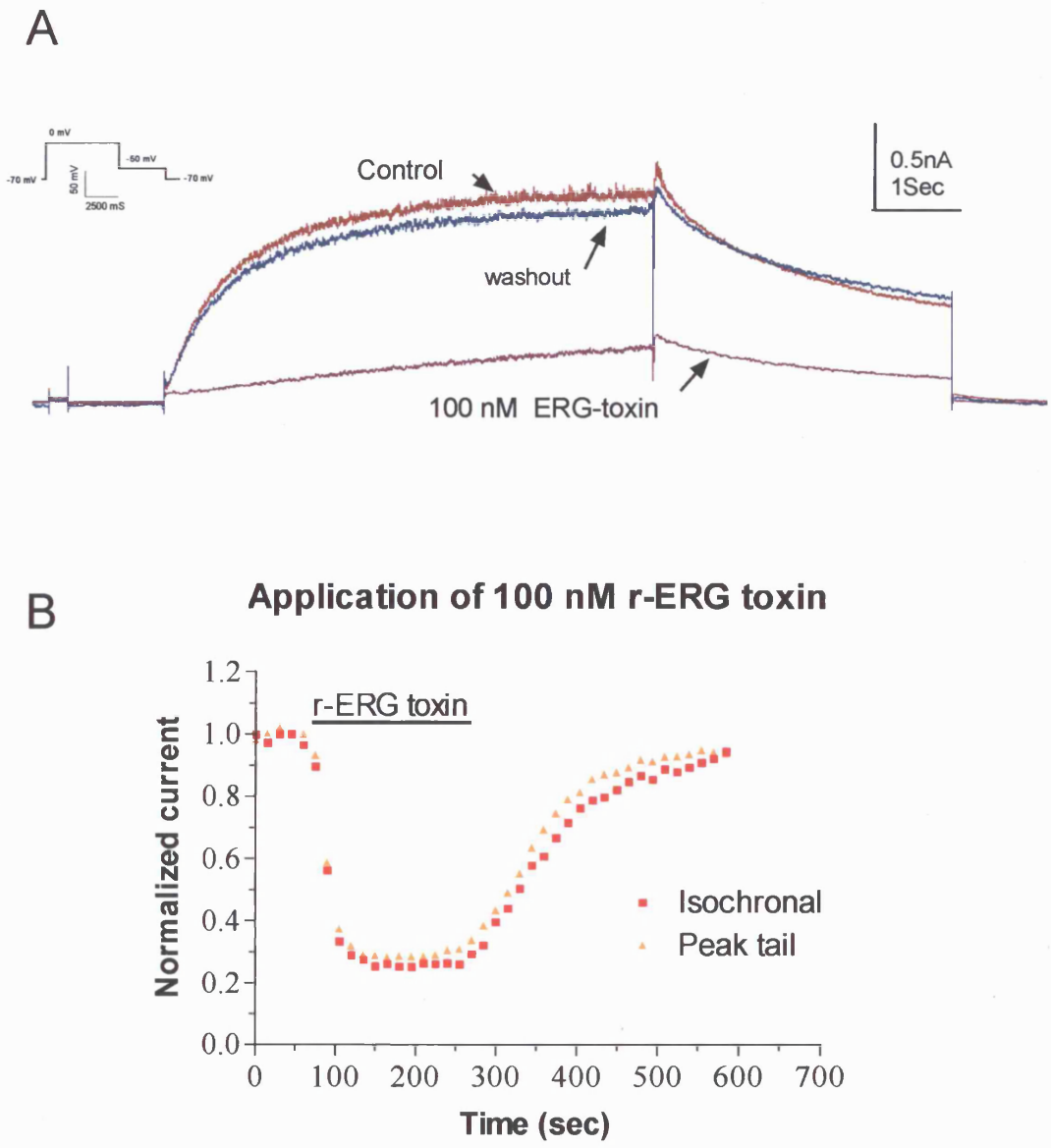

Figure 4.3 Representative hERG currents were recorded from a HEK-13 cell, stably expressing hERG, using whole cell patch clamp. **A:** Membrane potential was depolarised to 0 mV for 5 sec followed by a repolarisation to -50 mV to induce a tail current. 100 nM of hERG toxin was perfused onto the cell for 3 min and then washed off. ERG-toxin was able to block 80 % of hERG current at 100 nM. **B:** hERG isochronal end-pulse currents and peak tails were normalized to control. hERG block by rERG-toxin has rapid onset and was readily reversible on removal of the compound.

A

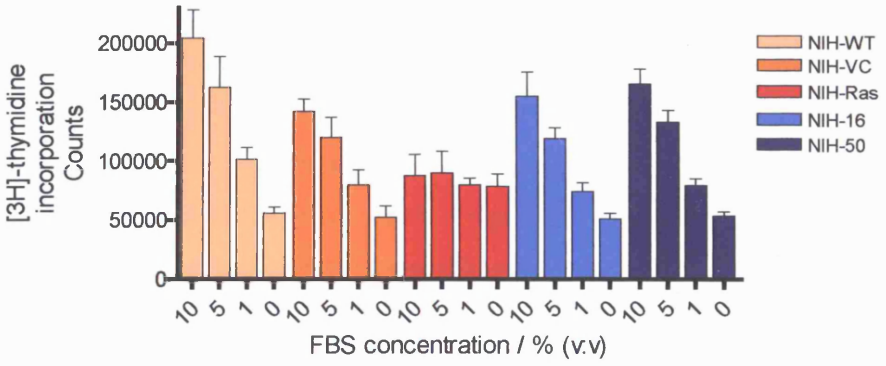

B

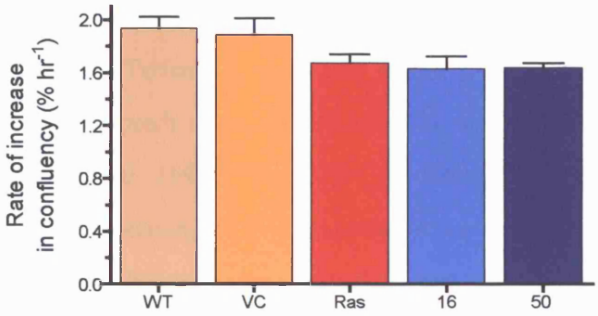

Figure 4.4 **A:** Stable NIH-3T3 clones were grown in medium containing either 10, 5, 1 or 0 % serum for 48 hrs. [^{3}H]-thymidine was added for the final 3 hrs. [^{3}H]-thymidine incorporated into the DNA was measured by scintillation counting. Data represent means ± range values from at least two experiments, performed in triplicate. **B:** Confluency was measured using the Incucyte microscope system (see Methods), under standard (10 % serum) conditions over a period of 24-48 hrs. Data were analysed with Prism software, using a one-way ANOVA analysis with Dunnett's post-test with NIH-VC as control.

(multi-well format) and the entire assay is performed within a cell culture incubator. The Incucyte system was used to measure the rate of change in confluency of NIH-3T3 cells in 10 % serum over 48 hrs. In this assay the control clones and hERG expressing clones grew at a similar rate. Whilst the growth rate of the NIH-50 clone is significantly different from that of NIH-VC ($p < 0.01$), this difference is not substantial (Figure 4.4B). In contrast to the thymidine incorporation assay, the Incucyte system did not detect a significant difference in the rate of proliferation between control clones and NIH-Ras. Overall it appears that hERG expression has little effect on proliferation in NIH-3T3 cells.

Does inhibiting hERG current alter NIH-3T3 cell proliferation?

To determine if hERG channel conductance had a role in proliferation of NIH-3T3 cells, the effect of terfenadine was tested. Terfenadine is another highly hERG specific and potent open-channel blocker, with an IC_{50} in patch clamp studies of ~300 nM in oocytes and ~200nM in cardiac myocytes (Taglialatela *et al.*, 1998; Crumb, 2000). In these experiments terfenadine was added to standard culture media containing 10 % serum. Serum contains growth factors that are important for cell division. Serum is known to depolarise the resting membrane potential of fibroblast cells (Postma *et al.*, 1996). This was also observed in my experiments where serum addition caused intracellular Ca^{2+} responses in NIH-3T3 cells, suggesting membrane depolarization (data not shown). Similarly Archangeli et al. describe cycling cells as having a more depolarized membrane potential than quiescent cells (Arcangeli *et al.*, 1995). A depolarised membrane potential will increase the chances of hERG activation and the possibility of seeing hERG driven effects.

As with all the experiments in this study the effects of compound addition were performed in parallel to controls (in the absence of compound). In this dataset the values for the control samples are similar to those presented previously in Figure 4.4B. However, NIH-Ras cells seemed to increase growth towards confluency faster in this dataset (Figure 4.5A) than in Figure 4.4B. This difference is unlikely to represent a genuine change in cell behaviour. Figure 4.5A shows only those controls that were performed alongside the test compounds ($n = 3$), while Figure 4.4B shows all control values from many different datasets ($n = 9$).

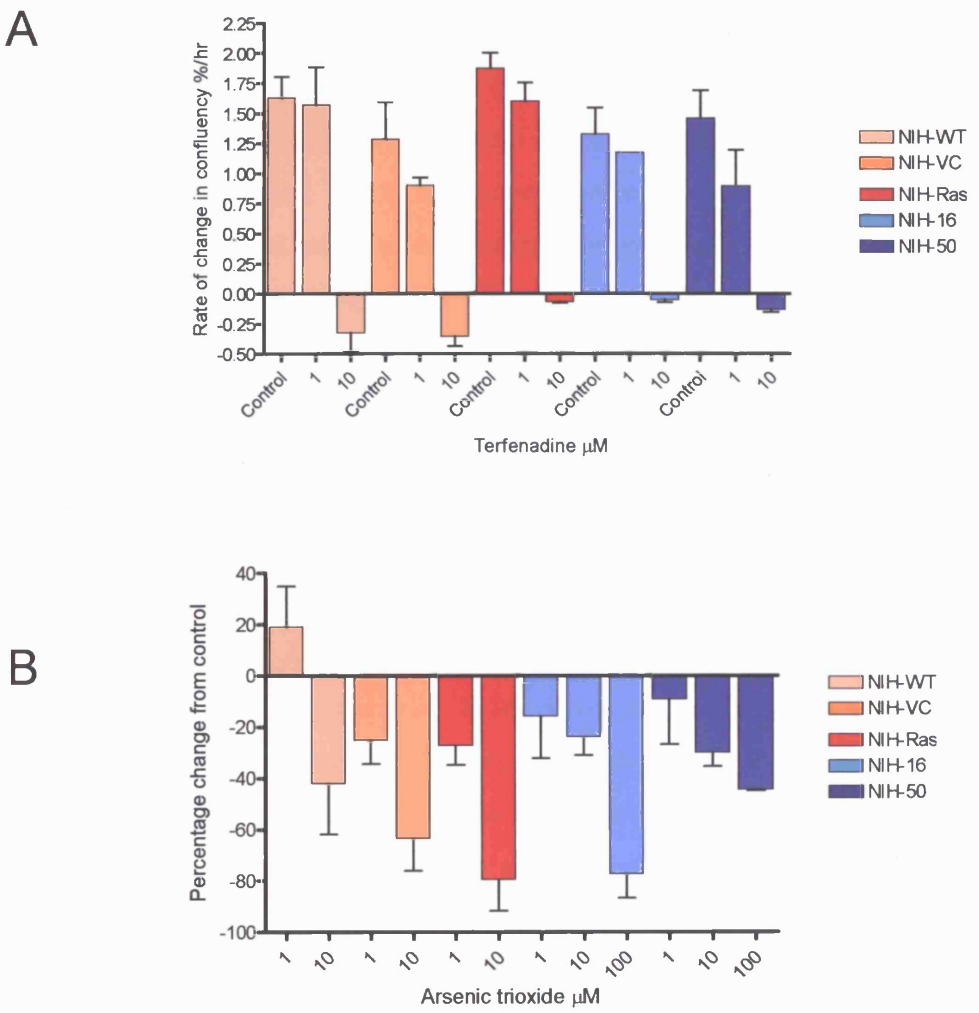

Figure 4.5 NIH-3T3 cells were plated at low density in 24 well plates and left to adhere for >6 hrs. Medium was changed for medium containing either 0, 1 or 10 μM terfenadine **(A)** or 0, 1, 10 or 100 μM arsenic trioxide **(B)**. Plates were inserted into the Incucyte™ machine. Confluency was measured at regular intervals over >24 hrs and a growth curve generated. Data represent mean ± range values from two separate experiments, performed in quadruplet. **B:** data plotted as change in rate of change in confluency normalized to control values. Data were analysed with Prism software, using a one-way ANOVA analysis with Dunnett's post-test.

At 1 μM terfenadine there was little effect on rate of increase towards confluency for any of the clones, with NIH-50 showing the greatest, not statistically significant, decrease. Therefore, inhibition of hERG with 1 μM terfenadine does not alter proliferation in a hERG expression-dependent manner. However, 10 μM terfenadine produced a pronounced negative effect on growth in all the clones, indicating that this concentration of terfenadine may be toxic to the cells (Figure 4.5A). The cell morphology clearly indicated toxicity and so it was not necessary to look for apoptotic markers such as DNA laddering and caspase activation.

Does removal of the hERG channels from the plasma membrane affect proliferation?

Since the previous assays indicate that hERG channel block has no effect on the cells, the next logical question was to ask whether removal of the hERG protein from the membrane would have any effect upon the cells. Arsenic trioxide is known to have an inhibitory effect upon hERG trafficking to the membrane (Ficker *et al.*, 2004). Arsenic trioxide was added to the cell culture medium (10 % serum) at 1, 10 or 100 μM and proliferation recorded for at least 48 hrs using the Incucyte system. Again control values were similar to those previously recorded (data not shown). Incubation of cells with 1 μM Arsenic trioxide gave between 9 ± 17 % and 27 ± 8 % decrease in confluency relative to control in all the clones except NIH-WT, which actually showed an increase (19 ± 16 %) (Figure 4.5B). Application of 10 μM Arsenic trioxide produced a large decrease in confluency change in NIH-WT, VC and Ras clones. Interestingly the decrease in confluency change seen in the hERG-expressing clones was much reduced in comparison. 100 μM arsenic trioxide was required for NIH-16 and 50 clones to produce the same decrease in confluency seen with NIH-WT and VC (Figure 4.5B). I tentatively conclude that hERG-expressing NIH-3T3 cells are less sensitive to the effects of arsenic trioxide.

Does co-expression of a dominant negative hERG channel affect NIH-3T3 cell proliferation?

In order to address potential issues surrounding the stability, and potential non-specific effects of the hERG-blocking compounds, dominant negative mutant-hERG channels were generated to block ion conduction through the pore (see methods). The single point mutation G628S has been demonstrated to cause a disruption of the selectivity filter of the hERG channel, preventing ion flux through the pore. This particular mutation also has a dominant negative mode of action and

when co-expressed with the WT hERG gene severely reduces hERG current (Sanguinetti *et al.*, 1996). Thus one mutant subunit per tetrameric channel is sufficient to block conduction (Sanguinetti *et al.*, 1996). The conduction-defective hERG mutant G628S channels are trafficked to the cell surface as normal (Zhou *et al.*, 1998a). It is proposed that this mutant adopts a conformation so close to that of the WT channels that it is not recognised as abnormal by the chaperones. This is likely to be because the mutation is buried deep within the folded protein (Ficker *et al.*, 2003). Thus the decrease in current is not due to changes of channel expression on the membrane and instead is due to dysfunction of the selectivity filter.

Here, our aim was to compare proliferation in cell lines expressing WT-hERG alone and cells expressing WT and G628S hERG. In order to evaluate whether mutations in hERG channels could reverse the effects seen upon hERG channel expression, the mutant channel first had to be expressed. NIH-3T3 cells are known to be difficult to transfect using traditional lipid based methods. Indeed lipofectamine gave only ~20 % transfection efficiency (Figure 4.6). AMAXA™ nucleofection and jetPEI (polyplus) were also tried. Although both of these reagents gave better transfection efficiencies (~40 % and 60 % respectively, see figure 4.6) they both killed a large proportion of the cells, and those that were left appeared unhealthy. Given enough time to recover the cell population would return to normal morphology, however this treatment could have serious unseen consequences. In order to get high transfection efficiencies with low cell death, we generated adenovirus constructs to express G628S hERG channels (see methods) and characterised hERG channel function and cell proliferation.

Adenovirus were constructed to express a WT-hERG channel as a control, and also to ask the question of whether transient expression of hERG was sufficient for transformation. Unfortunately this virus did not cause the expression of high enough levels of the hERG protein to be useful in this project (data not shown). 'Empty' adenovirus was produced that expressed no hERG protein and was used as a vector control. Two separate G628S hERG expressing adenoviruses were produced, (termed here G628S and G628Sa) to help control for any artifacts generated by the virus transfection. All viruses produced high levels of GFP expression in infected NIH-3T3 cells. Optimal infection conditions (see methods) gave ~80 % transfection efficiency with G628S and G628Sa viruses (Figure 4.6). ~60 % transfection efficiency was achieved with the empty virus. The production of hERG protein was verified through western

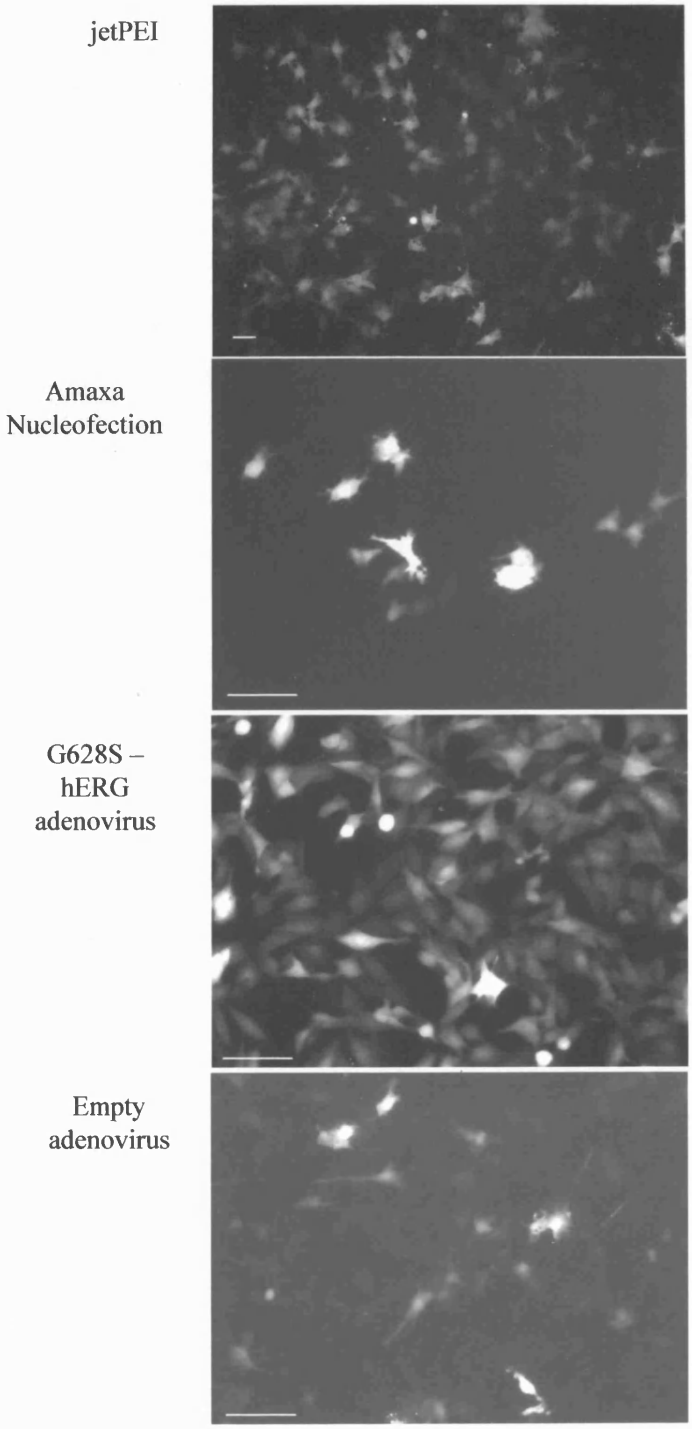

Figure 4.6 Representative GFP expression patterns of NIH-3T3 cells using various transfection methods. Cells were plated for 24 hrs prior to transfection. Photographs were then taken of the confluent monolayers after 48 hrs, which is sufficient time to allow for GFP expression. Viruses were applied for 2 hrs. Scale bars are 100 μm.

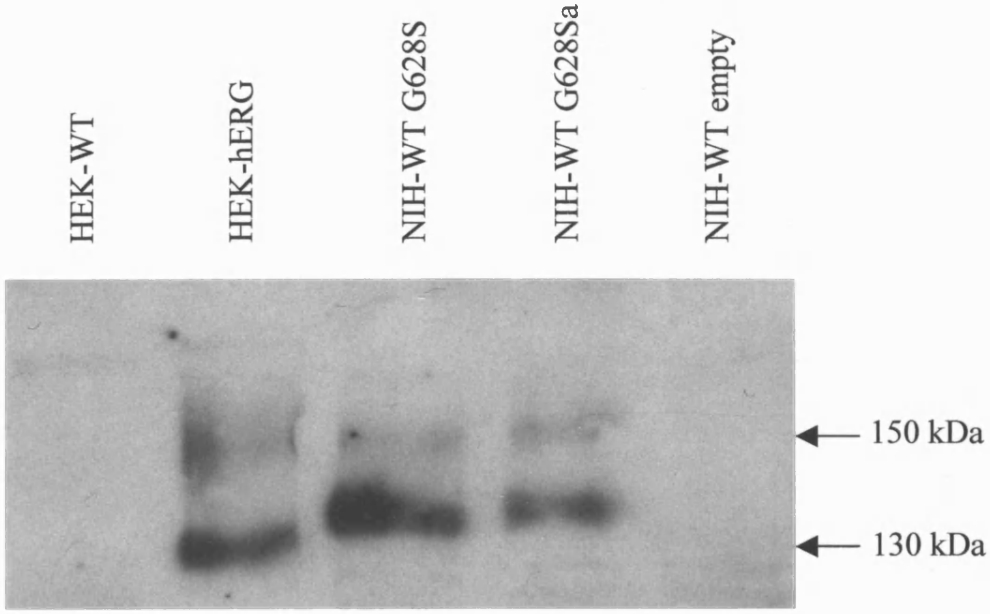

Figure 4.7 Adenoviral hERG expression. NIH-WT cells were plated on a 6 well plate and infected with either 4.5 µl G628S hERG-virus, 12 µl G628Sa hERG-virus, or 50 µl empty virus. After 48 hrs cells were solubilised. Total cell extracts were prepared and resolved on a 6 % SDS-PAGE (see Materials and Methods). Proteins were probed with an anti-hERG antibody.

blotting (Figure 4.7). Here the empty virus shows no hERG-specific bands confirming the absence of the protein. G628S and G628Sa viruses each produce two bands can be seen that migrate at ~150 and 130 KDa. The bands also correspond to those seen in a sample of WT-hERG protein expressed in HEK-hERG cells. The slight difference in apparent weight is likely due to the Myc tag added to the mutant channels.

Dominant negative suppression of channel function was investigated by measuring hERG current. Initially the effects of the viruses were monitored on hERG expressing CHO stable cell line, CHO-S1, which exhibits large hERG currents. Using a high level expression system to characterise the virus allowed the change in I_{hERG} to be monitored more easily. The IonWorks automated patch clamp system was used record from large numbers of cells. Membrane potential was held at –90 mV and hERG current elicited with a 500 ms step to +40 mV. The voltage was changed to –150 mV for 200 ms, to release cells from inactivation and initiate deactivation. After this time the potential was dropped to the holding potential of –80 mV. hERG tail currents are generated after the rapid release form inactivation and the slow onset of deactivation. To confirm that the tail current was predominantly through hERG channels, 1 μM cisapride was applied, a potent hERG channel blocker. G628S and G628Sa both reduced the tail current amplitude (Figure 4.8A). hERG current was calculated as cisapride sensitive current measured as the difference between peak tail currents before- and after-application of 1 μM Cisapride. The G628S virus gave a significant ($P < 0.01$) decrease in average I_{hERG} relative to the control sample, that was greater than the decrease with addition of the empty control virus (Figure 4.8A). This corresponded to a decrease in average cisapride sensitive current of 31 ± 7 %. The G628Sa virus also caused a large and significant ($P < 0.01$) decrease in average cisapride sensitive current of 46 ± 5 %. Nevertheless, this was less than expected for a dominant negative mutant. To investigate suppression of hERG current by G628S in more detail we looked at the distribution of current amplitude within the population of cells. Figure 4.8E shows the distribution of cisapride sensitive currents within the populations of cells. The virus increased the proportion of cells with small currents. Thus G628S and G628Sa viruses caused a 29 and 33 % increase in cells with current amplitudes ≤0.5 nA of current. In general, the viruses reduced the number of cells in all bins with amplitudes >1.5 nA.

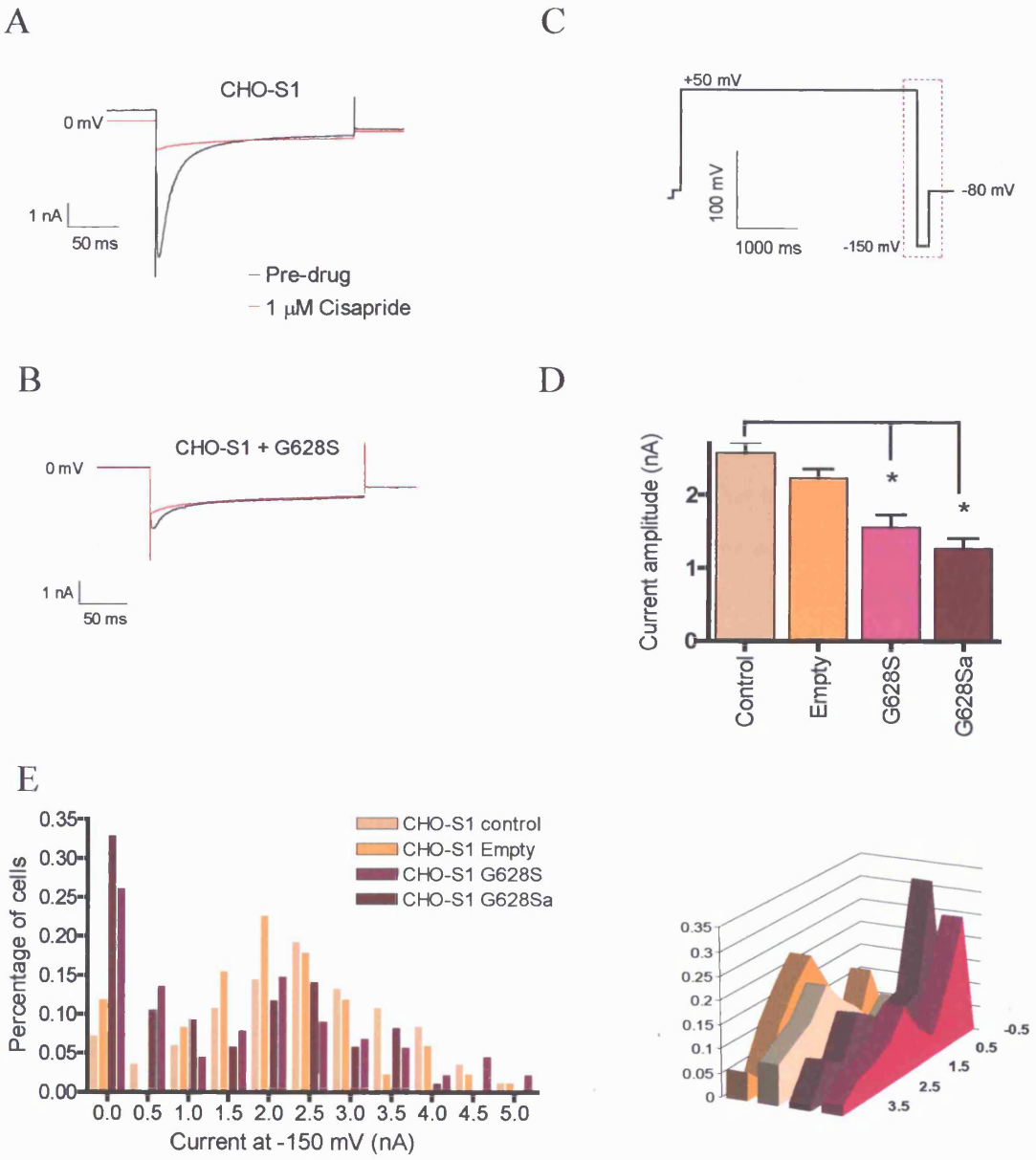

Figure 4.8 Effect of dominant-negative G628S hERG mutants upon I_{hERG} in CHO-S1 cells. Cells were infected with virus encoding the channel protein and left for 48 hrs. Cells were loaded onto the IonWorks platform and currents measured before and during application of 1 μM cisapride, a hERG-selective blocker. Representative tail current traces with **(A)** and without **(B)** co-expression of G628S. Traces correspond to boxed region of protocol. **C:** Voltage pulse protocol. HERG tail currents measured with hyperpolarization to -150 mV. **D:** mean ± SEM cisapride-sensitive current amplitude at -150 mV, n = 83 (control), 84 (Empty), 85 (G628S) and 88 (G628Sa). Data were analysed with Prism software, using a one-way ANOVA analysis with Dunnett's post-test (*$p<0.05$). **E:** Histogram, in which cisapride-sensitive current amplitudes are binned according to size. Inset 3D histogram of same data.

It was now important to demonstrate that the viruses would also reduce hERG currents in the NIH-3T3 cells. In these cells the smaller hERG currents necessitated a triple pulse protocol to maximize the observed hERG currents. Membrane potential was held at –80 mV and stepped to a depolarised voltage of +50 mV for 4000 ms to fully activate and inactivate the hERG channels. The voltage was changed to –150 mV for 20 ms, to release cells from inactivation and hERG current measured at the beginning of the third pulse to +50 mV. This final step allows relatively large currents to flow before they rapidly re-inactivate. Cisapride completely blocked the current during the third pulse (Figure 5.9B). Peak tail currents were measured as the difference between the maximum current passed after the third pulse, and the current after it had reached steady state. Cisapride sensitive currents were measured as the difference between peak tail currents measured pre- and post- application of 1 μM cisapride. In the NIH-3T3 clones both the G628Sa and G628S viruses caused a significant decrease (a decrease of 66 ± 6 and 69 ± 7 % respectively, $p < 0.01$ for both viruses) in average I_{hERG} (Figure 4.9). This corresponds with an extra >21 % (G628S) and 27 % (G628Sa) of the population showing <0.05 nA of current.

From these experiments it would seem that the G628S and G628Sa hERG-encoding viruses give reliable high level infection and hERG protein expression levels that correlate with a significant reduction in mean hERG current.

Does the G628S dominant negative hERG mutation have any effect upon proliferation?

After infection the proliferation of NIH-3T3 clones was measured using the Incucyte system. The empty control virus caused a decrease in rate of change in confluency in all clones (~-25 % for NIH-16, -50 and -VC), which was most pronounced and statistically significant ($p<0.05$) in NIH-WT and NIH-Ras clones (>50%) (Figure 4.10). Preliminary experiments have shown that NIH-WT, -VC, and -50 clones show no change in proliferation after infection with either the G628Sa or G628S viruses. NIH-16 and NIH-Ras clones show decreases in rate of change of confluency (proliferation) however these decreases are no larger than that seen with empty virus infection. Overall, there appears to be no clear evidence that reduction of hERG conduction has any influence on proliferation in hERG expressing cells.

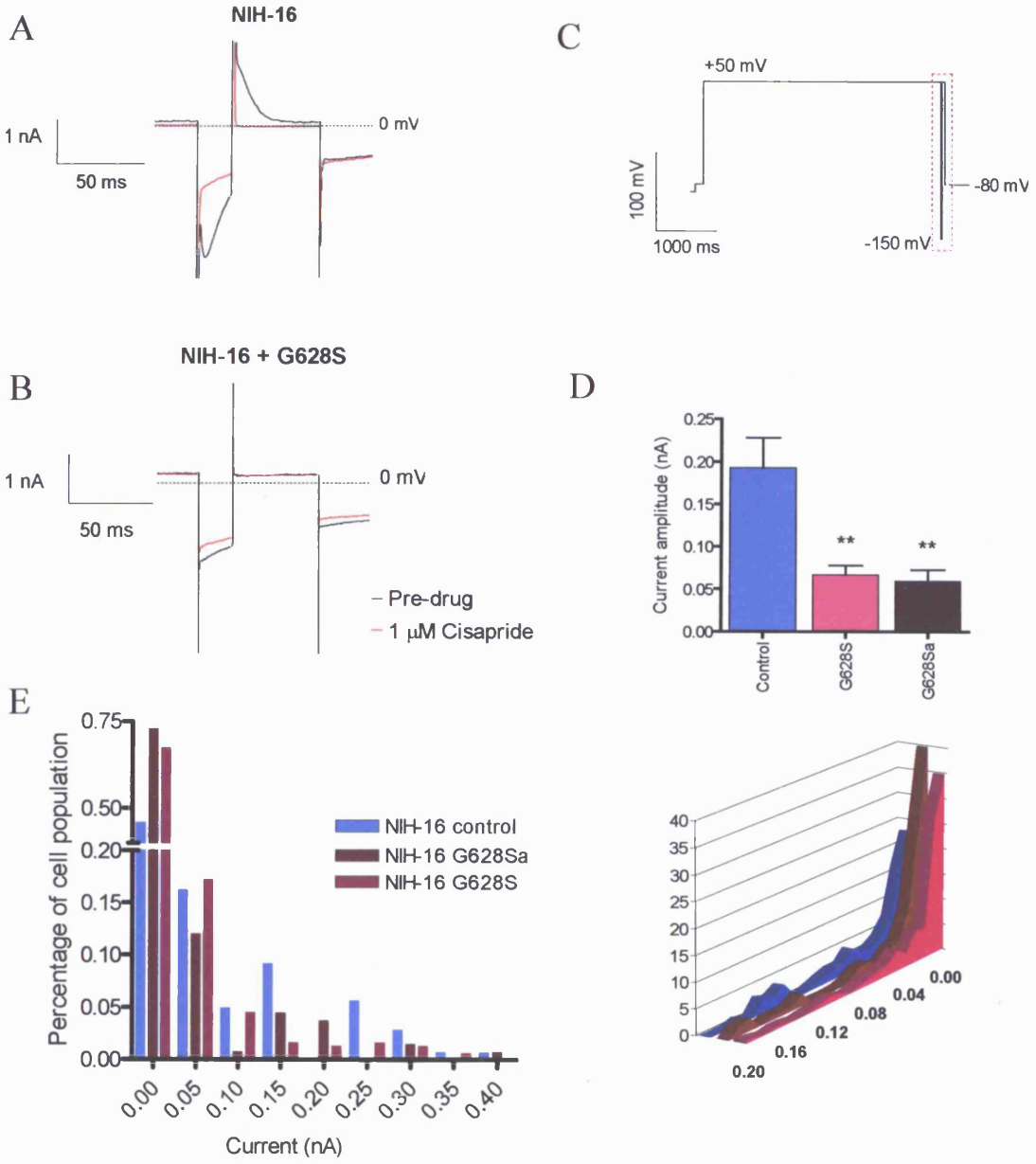

Figure 4.9 Effect of dominant-negative hERG mutants on stable $I_{hERG.}$ Cells were infected with virus encoding the channel protein and left for 48 hrs. Cells were loaded onto the IonWorks platform and currents measured before and during application of 1 μM cisapride. **C:** Voltage pulse protocol. hERG tail current measured with hyperpolarization to -150 mV and then depolarization to +50 mV where hERG currents were recorded. Current traces of hERG peak tails with **(B)** and without **(A)** co-expression of G628S. Traces correspond to boxed region of protocol. **D:** Mean ± SEM cisapride-sensitive current amplitude at +50 mV. Data were analyzed by a one-way ANOVA analysis with Dunnett's post test (**$p<0.01$, n=141 (control), 307 (G628S) or 133 (G628Sa). **E:** Histogram, in which current amplitudes are binned according to size. Inset, 3D histogram of same data.

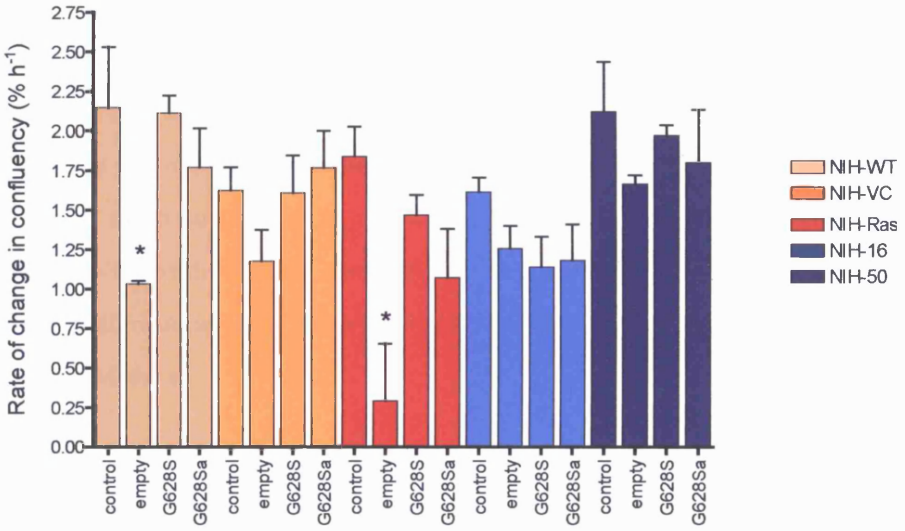

Figure 4.10 Cells (1 x 10^4 per well) were plated in 24-well plates. Cells were allowed at adhere for >6 rs and then infected with 1 µl G628S-virus, 3 µl G628Sa-virus, or 10 µl empty virus. Medium was changed the following morning. Plates were inserted into the Incucyte machine and measurements of confluency taken every 2 hrs over a >48 hrs period. Data represent the means ± range from two experiments with four replicates per experimental condition. Data were analyzed with Prism software, using a Students paired *t*-test. (*$p<0.05$).

Adhesion independent growth

To date there is little direct evidence to suggest that hERG expression has any effect upon the growth rate of cell/tumours. However there is increasing evidence that hERG expression is greater in metastatic cells relative to non-metastatic early-stage cancers (Lastraioli *et al.*, 2004; Masi *et al.*, 2005) and levels of hERG expression may correlate with a severity of the cancers. Even though hERG may have a limited effect upon proliferation rate, it could potentially permit proliferation in environments that would not normally support cell growth. Many transformed cells have the ability to grow in an adherence to substratum independent manner that would normally inhibit growth or cause apoptosis. To explore this possibility, the ability of hERG expression to allow attachment independent growth was evaluated using a soft agar assay (see Materials and Methods).

HEK-WT and VC cells were able to form thousands of viable colonies in the soft agar assay, making this cell background inappropriate for this type of experiment. NIH-WT and VC cells on the other hand always failed to grow in soft agar (Figure 4.11 and 4.12). Thus the NIH-3T3 cell line provided a good cell background in which to test the adhesion dependence of growth. NIH-Ras cells formed 147 ± 13 viable (MTT staining) colonies (Figure 4.12). NIH-16 also formed viable colonies however these were fewer (12 ± 2) and smaller in size. In contrast, NIH-WT, -VC and -50 cell-lines failed to show colony formation in soft agar.

Initially soft agar was made up to contain the anti-fungals amphotericin (1 %) and nystatin (0.8 %) because the long incubation times of the assay pre-disposed it to infection. Nystatin and amphotericin are both ionophores that increase the permeability of cell membranes to monovalent cations. This was deemed unsuitable when studying the effect of an ion-channel on cell biology. When the experiments were repeated in the absence of these compounds there was little effect upon the negative controls (NIH-WT and VC clones), and they still failed to form viable colonies. However, the number of viable colonies formed by NIH-Ras cells doubled to 306 ± 55 when these compounds were omitted (Figure 4.12). Omitting Nystatin and amphotericin also caused a large (although not significant) increase in the number of colonies formed for NIH-16 and -50. NIH-50 colony forming ability was now comparable to that of NIH-16. NIH-16 and 50 clones clearly showed the capacity to form a small number of colonies in the absence of attachment. In Figure 4.11 a number of macroscopic colonies can be seen and are indicated by arrows. These colonies

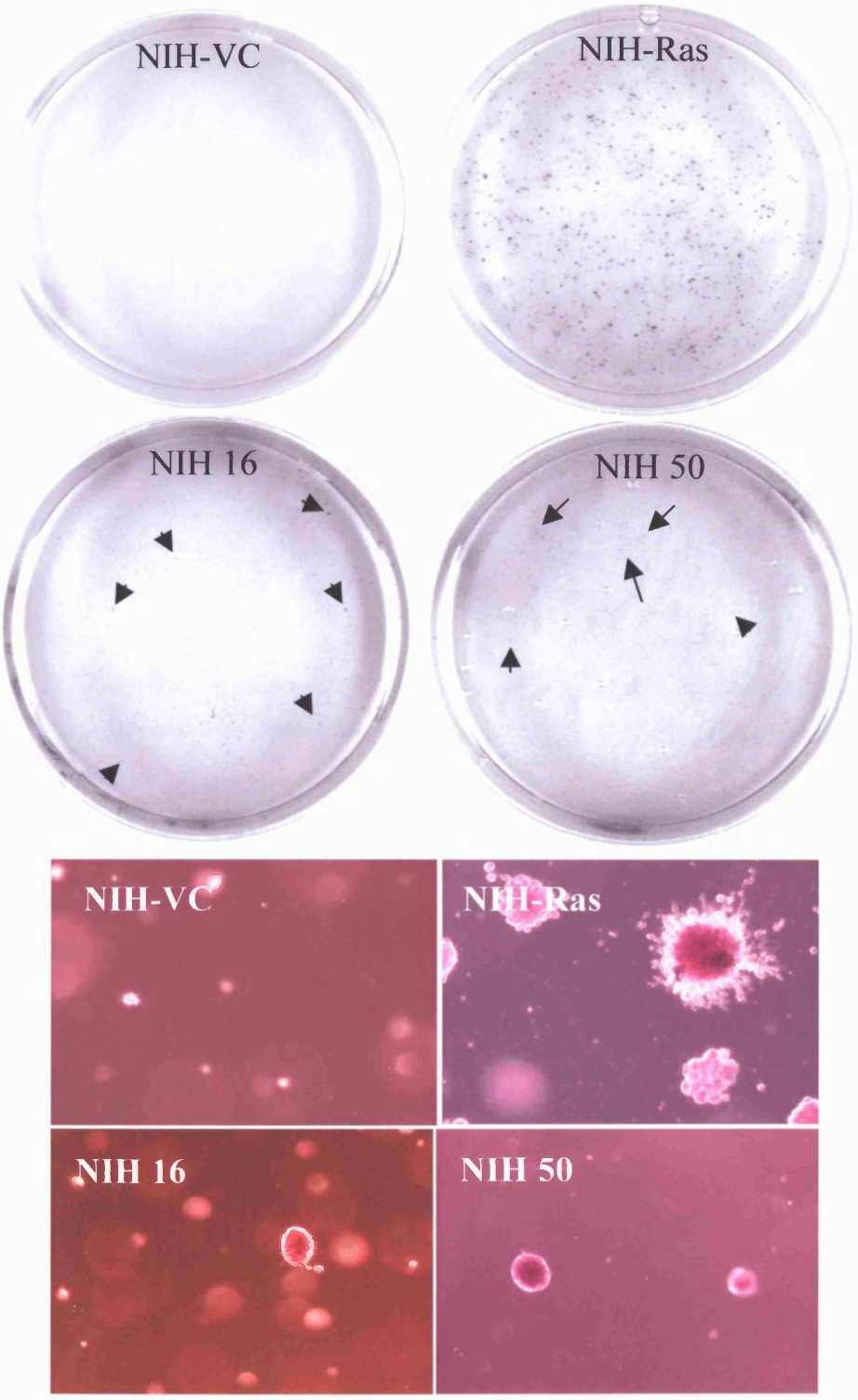

Figure 4.11 Cells were grown in soft agar (no antifungal agents) to prevent attachment to the culture surface (see Methods). After 21 days the colonies of cells were stained with the vital dye MTT. Upper panel: Representative photographs of whole plates in which the indicated cells were grown. Arrows indicate viable colonies. Lower panel: Representative photographs of viable colonies at higher (x10) magnification.

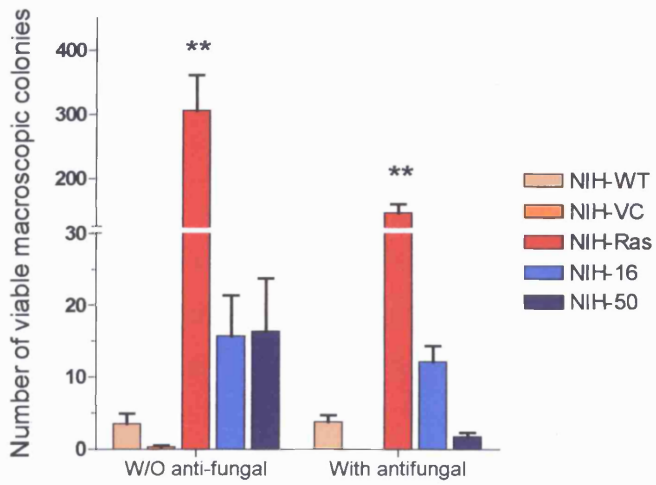

Figure 4.12 Cells were grown in soft agar to prevent attachment to the culture plate (see Methods). After 21 days cells were stained with the vital dye MTT and the number of viable macroscopic colonies per plate counted. Experiments were performed both in the absence and presence of the antifungal compounds amphotericin and nystatin. Data represent means ± SEM from 4 experiments performed in duplicate. Data were analyzed with Prism software, using a one-way ANOVA analysis with Dunnett's post-test (**$p < 0.01$, n=6).

are smaller than those formed by the Ras cells, but are no less viable and stain well after MTT application. 10 to 20 colonies were formed by the hERG expressing cells (Figure 4.12). NIH-VC plates show no macroscopic colonies, and under magnification the individual cells show absence of MTT staining.

In summary stable hERG expression confers the ability to grow in the absence of adhesion to a culture surface. Antifungal agents commonly used in this assay caused a reduction in colony forming ability for Ras and hERG expressing NIH-3T3 clones.

Discussion

hERG is closely related to the EAG oncogene which is known to give a dramatic increase in proliferation rate (Pardo *et al.*, 1999; Hegle *et al.*, 2006). This finding combined with previous studies showing that block of K^+ channels inhibits proliferation (Wonderlin & Strobl, 1996; LeppleWienhues *et al.*, 1996; Pardo *et al.*, 1999; Abdul & Hoosein, 2002b; Crociani *et al.*, 2003), led us to investigate whether hERG expression could increase proliferation. To measure the effects of hERG expression on cell proliferation, the proliferative rates of two different cell types (HEK293 and NIH-3T3) was recorded via two separate methods.

The data produced indicates that the effects of hERG expression on proliferation are dependent on the level of expression of the protein. hERG expression at physiological levels seen in the NIH-16 and -50 clones, and HEK-1 and -5 clones has little effect upon proliferation rate. However, "supra-physiological" levels of hERG protein expression, as seen in HEK-13, -14 and -16 clones, decreased proliferative rates to below that of the NIH-WT and VC controls. This decrease in proliferation may be due to a hyperpolarisation of the membrane potential (see Figure 3.7), which may cause problems for passing through cell cycle checkpoints, as it is commonly thought that the depolarisation seen in many transformed cells, relative to their healthy cells of origin, may increase proliferation (see Chapter 1). This depolarisation was in some cases thought to be mediated by the expression of hERG. However, as previously mentioned the NIH-3T3 cell line has very few native hyperpolarising currents, thus the expression of hERG causes a hyperpolarisation of the resting membrane potential where normally it would cause a relative depolarisation.

The proposal that hERG affects growth by membrane potential would seem unlikely in light of the results obtained with channel blockers. In this study there are no hERG-specific effects observed upon application of the hERG-channel blockers dofetilide, terfenadine or ERG-toxin. Both terfenadine and dofetilide only produced effects upon proliferation at high concentrations (100 μM) and these effects were observed in hERG and non-hERG expressing clones. At this concentration cell death was obvious in the case of terfenadine, producing a negative growth rate (Figure 4.5), while dofetilide caused a marked decrease in proliferative rates in all clones. These data emphasize the importance of using appropriate drug concentrations in these experiments, and helps to explain why many studies using high concentrations of drugs have reported hERG-

specific effects upon growth (LeppleWienhues *et al.*, 1996; Macfarlane & Sontheimer, 2000; Pillozzi *et al.*, 2002; Crociani *et al.*, 2003). For example Crociani et al. use between 50 – 200 μM of WAY-123,398 and E4031 inhibitors to reduce the proliferation of the hERG expressing cell line SH-SY5Y (Crociani *et al.*, 2003). These concentrations are up to two orders of magnitude greater than the IC_{50}, and are likely to produce non-hERG specific side effects. In another study up to 200 μM WAY-123,398 was used to inhibit proliferation in a leukemia cell line, with the authors arguing that this concentration was necessary to compensate for depletion/degradation of the drug over the course of the experiment (Pillozzi *et al.*, 2002). The studies mentioned here use cancer cell lines and thus cannot use non-hERG-expressing clones of similar origin as controls. Hence, they are unable to gauge accurately the non-specific effects of drugs used to inhibit proliferation. In my study the generation of stable cell lines allowed the parallel generation of vector control and wild-type clones all from the same original cell stock.

The overall effect of ERG-toxin seems to have been a non-specific reduction in [^{3}H]-thymidine incorporation. ERG-toxin has a greater effect upon non- or low-level hERG expressing cells when compared with HEK-13, 14 and 16 Clones. However, changes in proliferation do not display the concentration-dependency that would be expected if this was a hERG specific response. In light of this it would seem that ERG-toxin has no specific effects upon reduction of [^{3}H]-thymidine incorporation and thus proliferation.

Expression of the dominant negative hERG channel G628S (via adenovirus infection) showed little or no effect upon the proliferation of NIH-3T3 cells. These data help to confirm the results from the studies using hERG channel blockers. Unfortunately the empty adenovirus gave a decrease in proliferation that was, in some cases, large. This is probably due to either the toxicity of the virus *per se* or contaminants that may have been carried through the amplification steps in the production of this virus. These data suggest that the empty virus will be of little use in this assay unless its toxicity can be eliminated (e.g. by production of batches of higher titre adenovirus). While the G628S/G628Sa hERG viruses had only partial effects on the hERG-expressing NIH clones, they did not affect proliferation of NIH-WT and -VC control clones, indicating that they are not toxic to the cells.

This chapter demonstrates that hERG channel blockers and dominant negative hERG channels have little effect upon the proliferation of stably hERG expressing cells. This may seem at odds with previous studies suggesting that hERG blockers reduce proliferation. However, there are a few important points that must be taken into account before these results can be compared: 1) many studies have used very high concentrations of drugs to exert these effects. This by itself may be enough to cause a non-specific decrease in proliferation. 2) This is the first study to investigate the proliferative effect of hERG expressed in a recombinant cell line. In this study hERG expression was not shown to increase the proliferation rate. In all other studies hERG channel block is investigated in transformed cells that already display an enhanced rate of proliferation, which may or may-not be linked with hERG expression. Consequently, any conditions not optimal for cell growth would likely cause a decrease in growth, which will be more evident in the faster growing transformed cells. Further experiments with siRNA to directly knockout hERG channel expression are needed to confirm a role for hERG *per se*.

It is possible that the reduction in proliferation seen with high-level hERG expression in the HEK293 clones may be due to hERG protein interactions within the cell that are independent of ion conductance. As mentioned in Chapter 1, hERG has been shown to co-immunoprecipitate with many other signaling molecules that are involved in growth processes. The preliminary western blots shown in Figure 3.2A indicate that the effect of hERG expression upon growth (Figure 4.1A) correlates with protein level rather than functional current. However, more work is needed in this area before this can be confirmed.

Any signaling interaction of the hERG channel would most likely occur at the plasma membrane. To investigate this arsenic trioxide was used to cause retention of hERG in the endoplasmic reticulum (ER) and inhibit trafficking to the plasma membrane (Ficker *et al.*, 2004). The effects of arsenic trioxide were not very specific and a general reduction in proliferation was seen in all clones. However, it can be seen that NIH-16 and -50 behave differently from the control clones, with their proliferation being less affected by 10 μM arsenic trioxide. However, there are a few problems with the arsenic trioxide approach. Firstly, we were unable to demonstrate a reduction in hERG channel trafficking in the NIH-3T3 clones due to the limited sensitivity of western blots not being able to reproducibly detect the low level of hERG protein expressed in the NIH-3T3 clones. Future studies could help to clarify this issue by measuring any changes in hERG current density

upon arsenic trioxide application, and/or using biotinylation studies to monitor hERG expression at the cell surface. Secondly, while it has been shown that arsenic trioxide can remove a large percentage of the hERG current, studies still show a sizable proportion of mature channels in western blots even at 10 μM As_2O_3 (Ficker *et al.*, 2004). In an attempt to decrease hERG trafficking further 100 μM As_2O_3 was used, however the effects here are likely due to toxicity rather than specific hERG-trafficking effects. Ideally this assay would be repeated in the presence of other hERG-trafficking inhibitors preferably with fewer off-target side-effects. In an attempt to remove hERG from the membrane, expression of A561V dominant negative channels that retain nascent hERG channels in the ER or golgi (Kagan *et al.*, 2000; Ficker *et al.*, 2000) was attempted. However, the construct was not functional. RNA interference is another possible future approach that could be used to reduce functional expression, and has been effectively used in the study of the EAG channel (Weber *et al.*, 2006).

Attachment independent growth

Using the soft agar method to prevent cells attaching to a solid culture surface we demonstrated that hERG expressing clones were capable of attachment independent growth whereas NIH-WT and -VC control clones were not. The ability of the hERG expressing clones to grow in agar suspension, independently of substrate adhesion/contact was observed as marcroscopic colonies that were stained with a viability die. Attachment independent growth is an important step in the development of a metastatic phenotype. Hence the ability of hERG expression to increase growth in soft agar agrees with studies that have found hERG expression to correlate well with the metastatic ability of primary cancers (Lastraioli *et al.*, 2004; Masi *et al.*, 2005). This phenotype was also seen in CHO cells expressing the EAG channel (Pardo *et al.*, 1999). It is also interesting to note that in some plates NIH-16 and 50 cells were found attached to the bottom of the cell culture plate, beneath the agarose layer. Due to the nature of the assay it is impossible for the cells to accidentally have been plated here, because cells were added to the plates after a lower layer of agarose had already been applied to the plates (see methods). The cells at the edge of the agarose look to have migrated down the sides of the dish. This phenomenon was not seen on any of the NIH-WT, NIH-VC or NIH-Ras plates, and indicates that hERG expression is allowing a greater degree of motility/ability to migrate. Increased motility is also characteristic of a transformed phenotype and is discussed in Chapter 6.

The reduction in colony forming ability of the NIH-3T3 cells in the presence of nystatin and amphotericin has shown the importance of precluding these compounds from any of the cell culture assays. These compounds affect the NIH-Ras cells as well as the hERG expressing cells, non-specifically reducing colony numbers in all clones. Hence it is unlikely that this is a hERG-specific effect, and it is more likely that they cause a general decrease in viability of NIH-3T3 cells. The ability of these compounds to disrupt the membrane conductance and alter the membrane potential suggests that their use in cell culture assays involving the study of ion-channels should be avoided. For this reason I have not used any anti-fungal treatments in any of the assays in this report.

The finding that simple over-expression of the hERG gene can cause attachment-independent growth means that it is likely that the observed hERG expression in primary cancers precedes the change from a benign to a malignant phenotype. Previous to this it was unknown whether hERG expression was simply a bi-product of cancer development. This result opens up the possibility that hERG may influence metastasis and thus might be an important drug target in cancer. The mechanism of induction of adhesion independent growth via hERG expression has not yet been investigated. The soft agar assay could be extended in future experiments to include hERG channel blockers, trafficking inhibitors and RNAi to attribute the functional expression of the hERG channel directly to adhesion independent growth.

It has been observed that nearly all oncogenes are unable to retain adhesion-independent growth upon PI3K inhibition (Wang, 2004). Thus the PI3K/PKB survival signalling pathway is likely to be utilised by the hERG protein; indeed hERG channels gating is affected PKB (Zhang *et al.*, 2003). hERG is also known to co-localise with focal adhesions and their signalling molecules, including FAK. FAK and hERG associate in co-immunoprecipitation assays, and FAK phosphorylation (activation) is also increased in hERG transfected cells relative to mock transfections (Cherubini *et al.*, 2005). FAK over-expression is seen in a number of cancers and is essential for their metastatic phenotype (Weiner *et al.*, 1993; Agochiya *et al.*, 1999; Xu *et al.*, 2000; van Nimwegen *et al.*, 2005). FAK is important for pro-survival signals during adhesion independent growth, and is known to directly activate PI3K and PKB/AKT (Frisch & Screaton, 2001). FRNK expression (and thus reduction of FAK activation) in breast cancer cells was shown

to cause apoptosis (Xu *et al.*, 2000). Concurrently overexpression of activated FAK is sufficient for adhesion independent growth of MDCK cells and their tumour formation in nude mice (Frisch *et al.*, 1996). Future experiments could be used to investigate the potential role of hERG channel associations with signalling molecules such as PI3K to elucidate the mechanism of action by which hERG channel expression contributes to attachment independent growth.

In summary this chapter has investigated the role of hERG expression in proliferation of HEK293 and NIH-3T3 cells. Whilst hERG expression appears to have minimal effect upon proliferation under normal cell culture conditions, its effects were increased in more demanding environments such as low serum and arsenic trioxide treatment. Thus hERG expression in cancers may allow increased survival in the harsh conditions encountered by early stage cancer formation. An important finding was the promotion of viable colonies in adhesion-independent cultures. hERG expression appears to, in some way, bypass signalling pathways that inhibit proliferation and induce apoptosis in non-adherent fibroblast cells.

Chapter 5 hERG expression removes contact inhibition of growth.

Introduction

In order to form tissues and organs it is important that differentiated cell growth patterns are tightly controlled. As explained in Chapter 3, cell growth and division are influenced by serum- and adhesion-dependent mechanisms. A further regulation of growth seen in most of the tissues within an organism is the process of contact inhibition of growth. Contact inhibition of growth is a mechanism whereby cells will stop proliferating once they have formed cell-cell contacts. Just like attachment-dependency, contact inhibition provides a control against unregulated proliferation. Contact inhibition of growth is thus very important in the control against cancer formation. This mechanism of contact inhibition is thought to be initiated by cell membrane messengers/receptors, such as contactinhibin, a membrane glycoprotein expressed by confluent cells in culture (Wieser *et al.*, 1990). Contactinhibin binds to and activates its own receptor and in turn initiates contact inhibition of growth (Wieser *et al.*, 1985). This initial receptor ligation links through an as yet undetermined signalling mechanism, to cause growth arrest at G1 phase of the cell cycle. There have been many investigations into the signalling pathways involved in contact inhibition and so far there is good evidence that PKCs (Heit *et al.*, 2001), MAPKs (Faust *et al.*, 2005; Wayne *et al.*, 2006) and even the redox state of cells are all important (Hutter *et al.*, 1997; Pani *et al.*, 2000; Wayne *et al.*, 2006).

Transformed cells show the ability to disregard or downregulate contact inhibition signals, and consequently are able to continue proliferating after confluency of the cell layer has occurred. Cells overgrow and can happily continue proliferating even when several layers deep. This is essential for enabling these cells to proliferate in the cramped conditions found in the center of growing tumours. Transformed cells have been shown to have altered redox states (Hutter *et al.*, 1997), increased p38 activation (Faust *et al.*, 2005) and altered PKC expression levels relative to normal healthy cells (Heit *et al.*, 2001). These changes in signalling proteins have helped to corroborate their involvement in the process of contact inhibition.

The EAG channel has been shown to transform CHO cells and, in turn, to remove contact inhibition of growth, allowing cells to form tightly packed foci in conditions that allow only monolayer formation in wildtype cells (Pardo *et al.*, 1999). The similarity between EAG and hERG may suggest that hERG also affects contact inhibition. As demonstrated in the previous chapter hERG expression did not have advantageous effects upon growth under normal culture conditions. However, hERG expression did allow increased growth in conditions not usually viable for growth such as low serum and adhesion independence, suggesting that hERG may also play a role in overcrowded conditions also found in developing cancers.

The aim of this chapter is to investigate the effects of hERG expression upon the process of contact inhibition of growth. Whether these effects can be attributed to a functional hERG current or simply the presence of the channel protein will also be examined. These experiments will help to determine if hERG expression is sufficient to disrupt contact inhibition signalling.

Results

This ability of a cell to inhibit growth upon reaching confluency can be demonstrated in a foci-forming assay. Here, cells are cultured for 21 days past the point of confluency, and macroscopic changes in the population observed (see methods). NIH-WT and VC clones produced a monolayer of cells, which when stained with Leischmans stain gave a uniform, light stain over the entire plate (Figure 5.1A). This was also true when the cells were viewed at higher magnification (Figure 5.1B). NIH-VC cells form a contact inhibited monolayer with a cobble-stone appearance, which did not change after confluency (Figure 5.2A). In contrast to this, the transformed NIH-Ras clone showed uneven staining with very dark spots (foci), representing overgrowing cells that are many cells deep (Figure 5.1A). The hERG expressing clones, NIH-16 and 50, produced a phenotype that was different to both sets of control cells. Here the cells produced a staining pattern that was not uniform, showing regions of dense, overgrowing cells surrounding regions of less dense, lighter stained cells (Figure 5.1A). This staining pattern was even more evident at higher magnification as 'ridges' of dense cells surrounding regions of lighter staining (Figure 5.1B). This staining pattern was almost identical between NIH-16 and –50 clones. The lack of discreet foci means that a quantitative value, normally associated with this assay, cannot be attributed to these results.

When the foci-forming plates were viewed under high magnification it was noted that the hERG expressing clones had changed their morphology to something resembling the NIH-Ras cells. Previously under subconfluent culture conditions the differences in cell morphology between NIH-WT, VC, 16 and 50 were not notable. There appears to be a cell density dependent change in morphology, which can be seen in Figure 5.2. NIH-VC cells present a classic flattened fibroblast morphology, with a clear boundary between cells in a monolayer. Cells can be seen to form a uniform monolayer that changes little between the day of confluency and two days post-confluency. NIH-WT cells show an identical phenotype (data not shown). NIH-VC cell morphology is stable over time, and this can also clearly be seen in time-lapse movies of cell growth (see movie-1 on included CD). In movie 1 NIH-VC cells can be seen to spread out after initial plating and attachment to the culture plate. Soon after cell division begins, cells move to maximise the number of cells that can be supported by the area. Eventually, after confluency has been reached, the cells rapidly reduce proliferation. Any cells that do happen to divide (presumably as they had already committed to the cell cycle before confluency was reached)

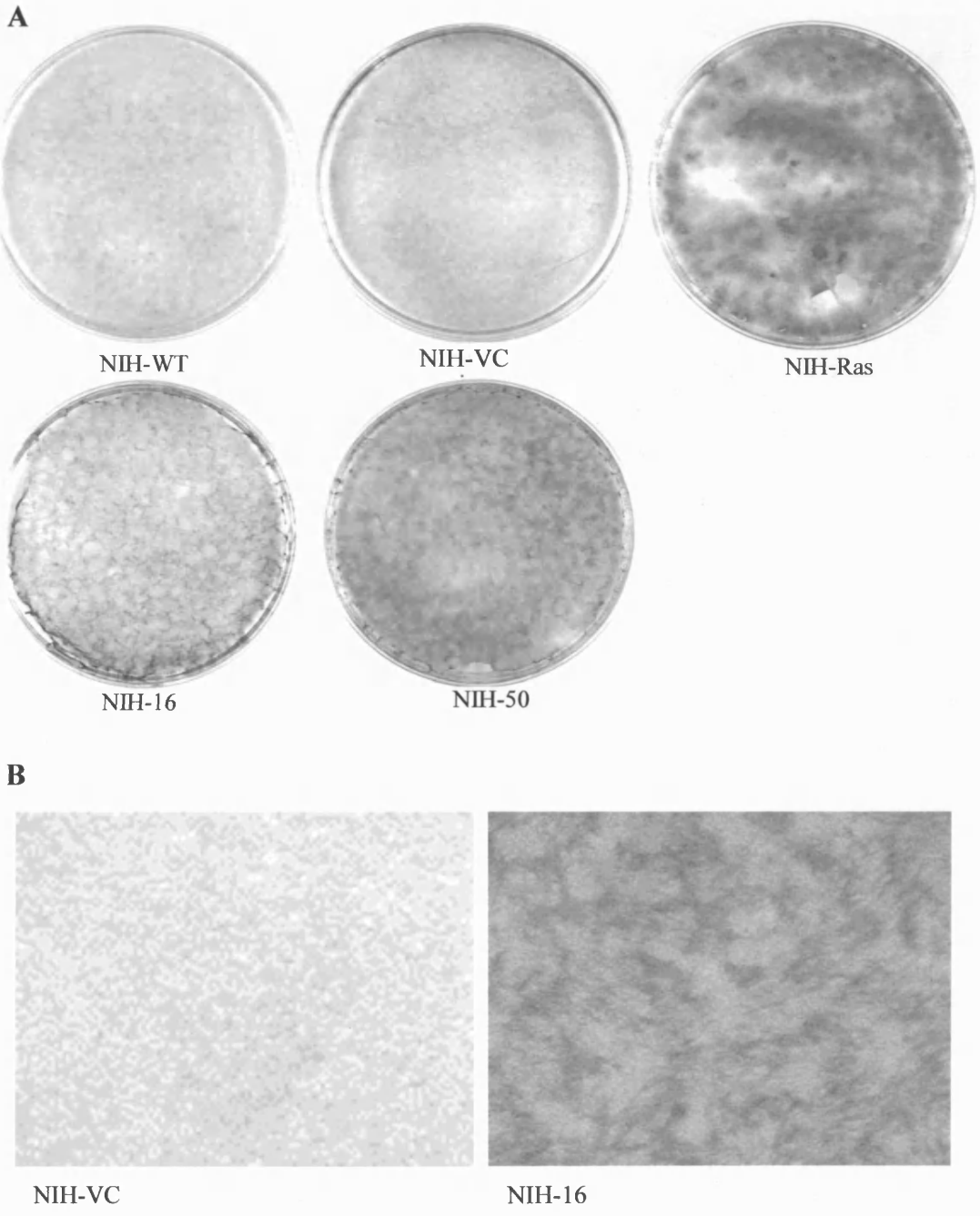

Figure 5.1 Foci formation in NIH-3T3 cells. NIH-3T3 cells were plated at confluency and cultured for 21 days with regular media changes. On day 21 cells were washed and stained with Leischmans stain. **A:** Representative images of whole plates. Cells were plated in duplicate and repeated at least twice. **B:** representative images of 5 times magnification of the cell layer.

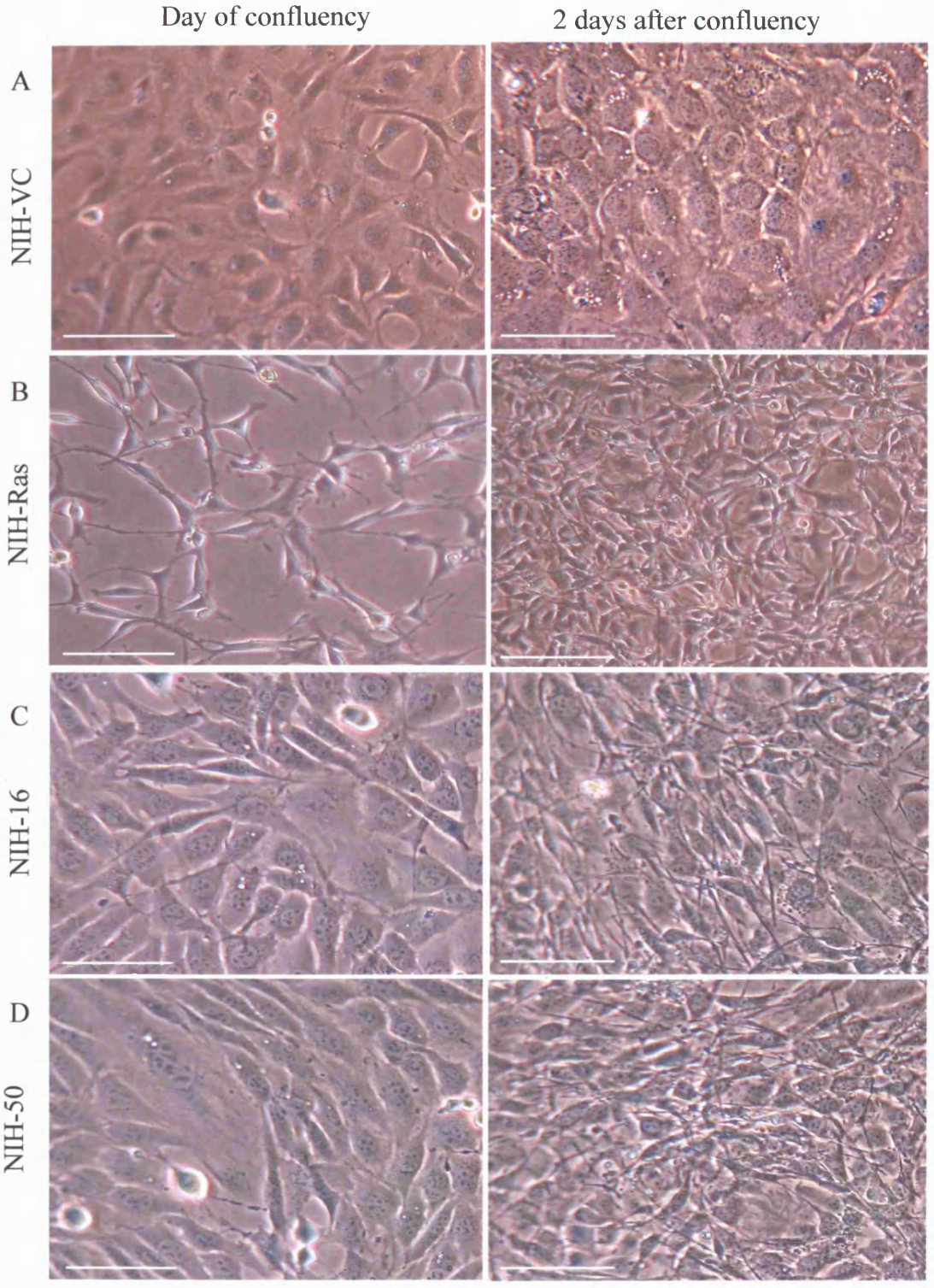

Figure 5.2 Images of live NIH-3T3 cells growing in culture. Cells were cultured under normal, control conditions and imaged either after reaching confluency (left) or 2 days post confluency (right). Pairs of images represent the same plate of cells. Scale bars represent 100 μm.

produce daughter cells that are unable to adhere to the plate and are released into the culture media. This can be seen as a rounded phase-bright object above the monolayer of cells. Movie 2 shows NIH-WT cells displaying almost identical morphology to that of NIH-VC, although here the cells do seem to pack together slightly tighter. No overgrowth or gross morphology change upon confluency is seen.

NIH-Ras cells (Figure 5.2C) show a typical transformed phenotype of long, thin, spindle-like cells that appear to have only a few small areas of the cell attached to the culture surface. The cells have a rounded cell body and look smaller under phase contrast, although cell volumes were not quantified. The overgrowth and loss of contact inhibition can be seen two days post-confluency where it is hard to visualise individual cells (Figure 5.2C, right panel). Cells can be seen to grow over one another, and there does not appear to be any ordered structure. In movie 3, NIH-Ras cells can be seen to grow and take up much of the available space as they proliferate. Unlike the NIH-VC cells, the NIH-Ras cells start to overgrow before confluency has been reached. By the end of the movie the cells are many cells deep on the culture plate. Dividing cells can still be seen even at this stage, and unlike the NIH-VC cells, the daughter cells maintain adhesion to neighbouring cells and are not lost into the medium.

The hERG expressing clones show a similar phenotype to that of the NIH-VC cells at the point of reaching confluency. The cells are flattened and have formed a monolayer, whilst still maintaining clear cell-cell boundaries (Figure 5.2C, left panel). However the change in cell morphology two days after confluency is dramatic. The hERG expressing clones have started to overgrow and criss-cross one another making it hard to identify single cells. Cells have also developed morphology more akin to that of NIH-Ras. Cells have become more spindle-like, and long extensions can be seen that pass over neighbouring cells (Figure 5.2). Time-lapse movies of these cells clearly demonstrate this change in morphology at confluency. Movie 4 and movie 5 show NIH-16 and -50 respectively. In both movies the cells start with a NIH-VC-like morphology; the cells are flattened and move round the culture area to allow a monolayer to form by about half way through the movie. However, both clones continue to show dividing cells well after the monolayer has formed. These cells are not lost to the media and remain anchored to neighbouring cells. As with the foci-forming experiment, the NIH-16 and -50 clones behave in a similar manner. The increase in the cell population and density seems to induce a morphology change in

the cells. In movie 4 NIH-16 cells change from a large flattened morphology to a smaller more rounded cell shape with less substratum contact. The cells also produce long protrusions to give a spindle like appearance. Cells can be seen to overlap one another as they overgrow. Movie 5 shows NIH-50 displaying much of the same traits as NIH-16. However, in this view it is possible to see some cells that do not display the spindle-like morphology. At the end of the movie there are some clearly transformed cells that surround a few larger flatter cells. The flatter cells do not appear to divide in this dense population.

Does hERG expression affect the morphology of HEK293 cells?

In order to study contact inhibition of growth cells are cultured at greater density than routinely maintained cultures. The HEK293 clones were inappropriate for the foci forming assay for two reasons. Firstly, the wild-type clones could, at least to some extent, continue to proliferate once a monolayer had been reached. This means that it would be much more difficult to dissect out the effects of hERG expression from the native phenotype in this assay. Secondly, the HEK293 cell-line is widely accepted to possess quite poor adhesion to unmodified cell culture surfaces. This became even more evident as the cells became overconfluent, and would cause the cells to dissociate from the culture plate upon media changes, or during staining. For these reasons no data for the HEK293 clones are presented.

The HEK293 cells did, however, show a change in morphology when hERG was expressed (Figure 5.3). Under subconfluent culture conditions HEK-WT and VC cells showed a flattened morphology. As they proliferated the cells divided to fill the available space, producing a monolayer. In contrast to this, hERG expressing cells showed a more elongated spindle-like appearance, with a more rounded cell body. This makes the cells appear smaller because part of the cell extends out of the plane of focus. Changes in cell size were not measured in this project. hERG-expressing HEK293 cells also grew on top of one another rather than migrating to cover the entire culture area. This is demonstrated in Figure 5.3B; here the cells have space available to migrate into and colonise, yet they have formed themselves into small colony-like formations that are many cells deep. Under these non-confluent conditions it can be inferred that hERG expression favours a more transformed phenotype. The degree to which cell morphology is changed correlated with the amount of hERG expression. HEK-1 and 5 show very little change in

phenotype, whereas the more highly hERG expressing HEK-13, 14 and 16 clones all show overgrowth in sub-confluent conditions to a similar extent.

Does hERG expression increase allow overgrowth, and increase cell density?

In order to quantify the degree to which hERG expression can increase post-confluency cell division the saturation density was measured. Saturation density is a measure of the number of cells that can be supported by a given culture surface area. Whilst this assay does not take into account variations in cell size or shape it is still able to quantify the overgrowth of cells to some degree. NIH-3T3 cells were plated in a 6 cm culture dish at a density sufficient to produce a confluent monolayer (1 x 10^6 cells). After 4 days there was no net increase in the number of NIH-VC cells (Figure 5.4A). When viewed under the microscope a confluent monolayer was observed with no overgrowth. Therefore, >1 x 10^6 cells will indicate that the cells have either started to overgrow, or have changed shape to allow more cells per unit area. NIH-WT grew to a greater density than NIH-VC in this assay (Figure 5.4A). The reason for the difference is not clear, although it was a consistent observation. In some plates there were small groups of cells that did show a spindle-like morphology, but they did not make up a significant proportion of the cells. NIH-Ras cells were able to grow to approx. three times the density of NIH-VC cells ($p<0.01$, n=14). The cells appeared very overgrown when observed under the microscope. The hERG-expressing clones showed an ability to grow to a cell density greater than either NIH-WT or NIH-VC. The cell number for NIH-16 was 2.75 (± 0.08) x 10^6, ($p<0.01$, n=22 versus NIH-WT and -VC), and almost as great as that of NIH-Ras. NIH-50 grew to a population of 2.30 (± 0.09) x 10^6 ($p<0.01$, n=22 versus NIH-WT and -VC). NIH-16 and -50 clones showed morphology similar to that shown in Figure 5.2, indicating that the increase in cell density was attributable to overgrowth of the cells.

The measurement of viable cell number recorded in the saturation density assay was supported by measurements of total protein. Protein measurements were taken from cells cultured at sub-confluency and also cells cultured for four days post confluency. The experiment was similar to the saturation density assay, except that at the end of the assay cell lysates were produced and the protein content quantified with a Lowry assay (rather than counting cell number as in the saturation density assay). Cells were plated at ~40 % confluency (250 x10^3 cells) for 24 hrs to

A

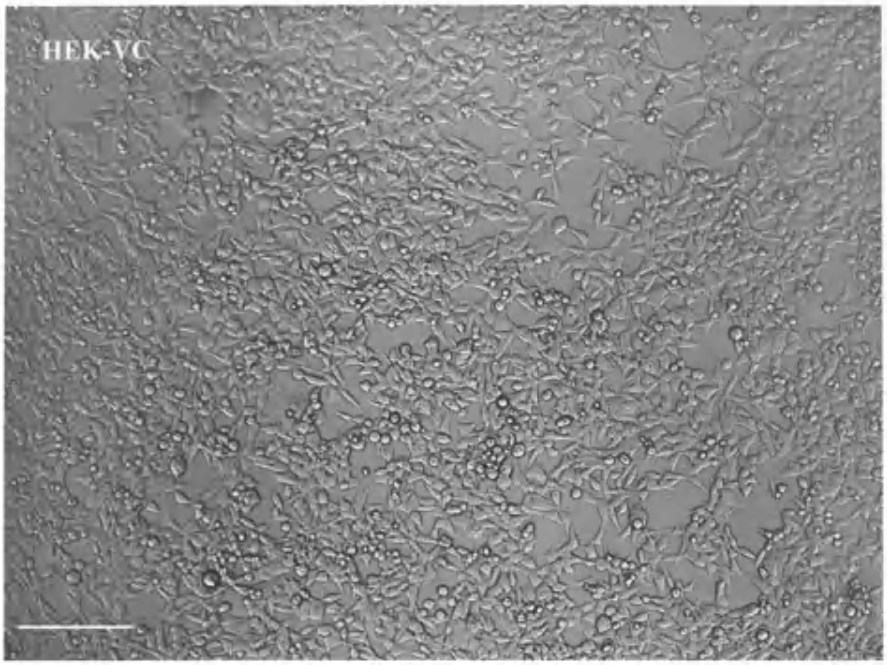

B

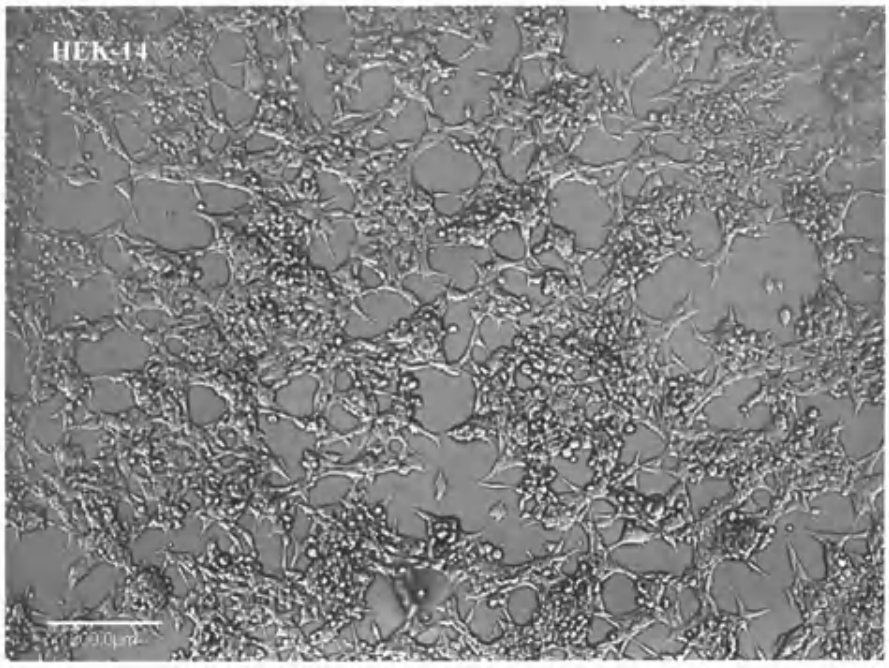

Figure 5.3 Images of HEK293 cells growing in culture. HEK293 Cells were plated under subconfluent culture conditions and left to grow for 48 hrs. Pictures were taken using phase contrast on an inverted microscope. Scale bars represent 200 μm.

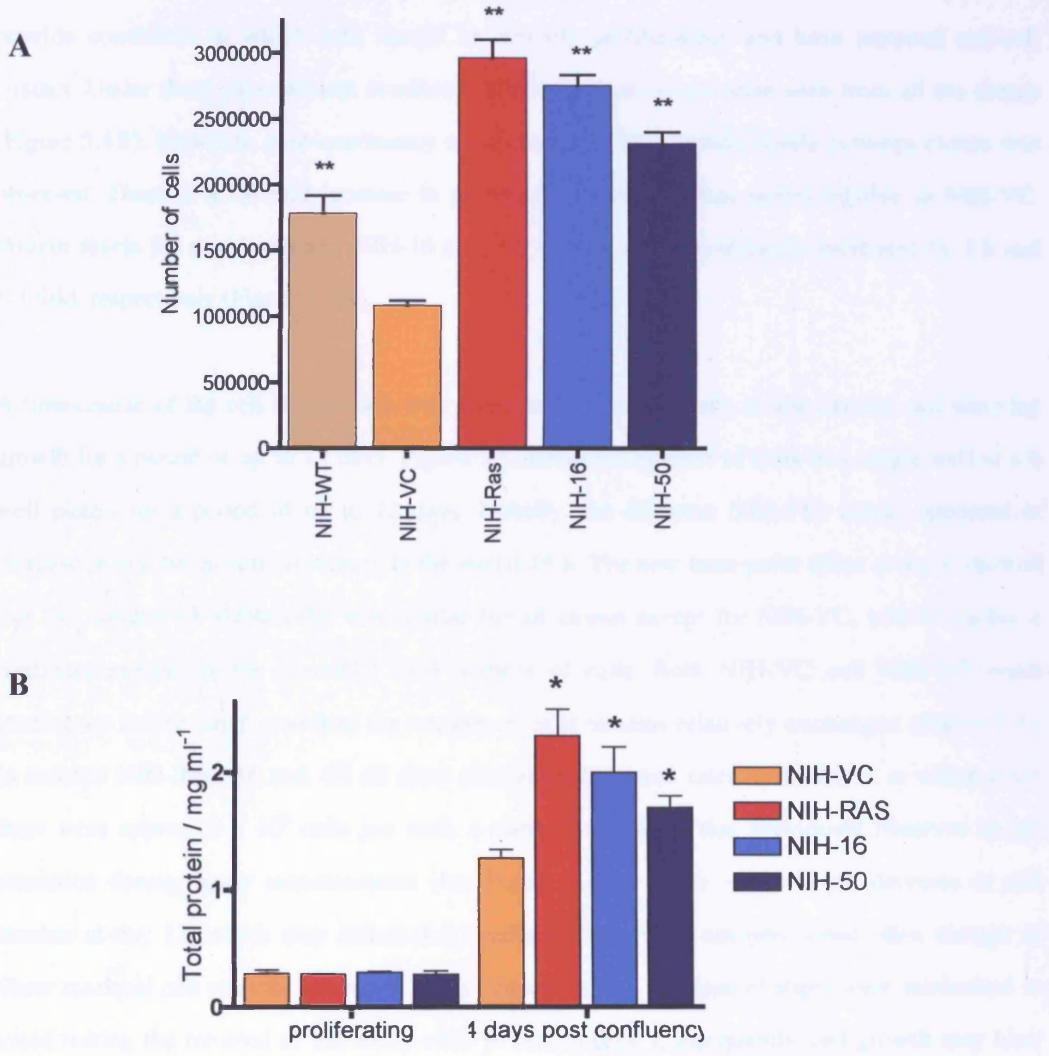

Figure 5.4 Changes in cell density upon hERG expression. **A:** 1 x 10^6 cells were seeded at confluency in 6 well plates. After 4 days, viable cell numbers were detected with trypan blue and counted. Data represent means ± SEM for at least seven experiments performed in duplicate. **B:** 'Proliferating' samples – 250 x 10^3 cells were plated (~40 % confluency) and after 24 hrs solubilised with RIPA buffer. 'Post-confluent' samples - cells were plated at confluency and cultured for 4 days. Cells were solubilised with RIPA buffer. Total protein was determined using the Lowry method. Bars represent mean ± SEM from 5 experiments. Data were analysed with Prism software, using a one-way ANOVA analysis with Dunnett's post-test with HEK-VC as control (*$p<0.05$; **$p<0.01$).

provide conditions in which cells would be actively proliferating, and have minimal cell-cell contact. Under these subconfluent conditions similar protein levels were seen from all the clones (Figure 5.4B). However, post-confluency a difference in total protein levels between clones was observed. There is a 1.8 fold increase in protein levels in NIH-Ras clones relative to NIH-VC. Protein levels for post-confluent NIH-16 and -50 clones were significantly increased by 1.6 and 1.3 fold, respectively (Figure 5.4B).

A time-course of the cell overgrowth was generated by plating cells at low density and allowing growth for a period of up to 12 days. Figure 5.5 shows the number of cells in a single well of a 6 well plate over a period of up to 12 days. Initially, the different NIH-3T3 clones appeared to increase in number at similar rates over the initial 48 h. The next time-point taken at day 6 showed that the number of viable cells was similar for all clones except for NIH-VC, which reaches a confluent monolayer for a smaller total number of cells. Both NIH-VC and NIH-WT reach confluency before day 6, and then the number of cells remains relatively unchanged (Figure 5.5). In contrast NIH-Ras, -16 and -50 all show similar proliferation rates up to day 9, at which point there were approx. 3 x 10^6 cells per well, a number similar to that previously observed in the saturation density assay measurements (see Figure 5.4A). There was a slight decrease in cell number at day 12, which may reflect that media changes were not performed often enough to allow maximal cell growth. However, it was important that medium changes were minimised to avoid risking the removal of too many cells in the process. Consequently cell growth may have been limited. Nevertheless, it was clear that while NIH-WT and NIH-VC clones were confluent by day 6, hERG expressing clones continued to divide to at least day 9, and the total number of cells was substantially larger.

The standard saturation density assay was repeated with different levels of serum in the medium to check the serum-dependence of proliferation under conditions of cell confluency (Figure 5.6). A decrease in serum levels to 5 % had little effect upon viability in NIH-WT and -VC clones. However, in 1 % serum a decrease in total cell number was seen, which was significant in the case of NIH-VC ($p<0.05$), but not NIH-WT. It is important to note that because NIH-VC was plated at confluency and did not overgrow, any decrease in cell number relative to control is caused by net cell death. Thus a decrease in saturation density with 1 % serum indicates cell death rather than changes in contact inhibition. Decreases in serum concentration reduced the number of NIH-Ras

provide conditions in which cells would be actively proliferating, and have minimal cell-cell contact. Under these subconfluent conditions similar protein levels were seen from all the clones (Figure 5.4B). However, post-confluency a difference in total protein levels between clones was observed. There is a 1.8 fold increase in protein levels in NIH-Ras clones relative to NIH-VC. Protein levels for post-confluent NIH-16 and -50 clones were significantly increased by 1.6 and 1.3 fold, respectively (Figure 5.4B).

A time-course of the cell overgrowth was generated by plating cells at low density and allowing growth for a period of up to 12 days. Figure 5.5 shows the number of cells in a single well of a 6 well plate over a period of up to 12 days. Initially, the different NIH-3T3 clones appeared to increase in number at similar rates over the initial 48 h. The next time-point taken at day 6 showed that the number of viable cells was similar for all clones except for NIH-VC, which reaches a confluent monolayer for a smaller total number of cells. Both NIH-VC and NIH-WT reach confluency before day 6, and then the number of cells remains relatively unchanged (Figure 5.5). In contrast NIH-Ras, -16 and -50 all show similar proliferation rates up to day 9, at which point there were approx. 3 x 10^6 cells per well, a number similar to that previously observed in the saturation density assay measurements (see Figure 5.4A). There was a slight decrease in cell number at day 12, which may reflect that media changes were not performed often enough to allow maximal cell growth. However, it was important that medium changes were minimised to avoid risking the removal of too many cells in the process. Consequently cell growth may have been limited. Nevertheless, it was clear that while NIH-WT and NIH-VC clones were confluent by day 6, hERG expressing clones continued to divide to at least day 9, and the total number of cells was substantially larger.

The standard saturation density assay was repeated with different levels of serum in the medium to check the serum-dependence of proliferation under conditions of cell confluency (Figure 5.6). A decrease in serum levels to 5 % had little effect upon viability in NIH-WT and -VC clones. However, in 1 % serum a decrease in total cell number was seen, which was significant in the case of NIH-VC ($p<0.05$), but not NIH-WT. It is important to note that because NIH-VC was plated at confluency and did not overgrow, any decrease in cell number relative to control is caused by net cell death. Thus a decrease in saturation density with 1 % serum indicates cell death rather than changes in contact inhibition. Decreases in serum concentration reduced the number of NIH-Ras

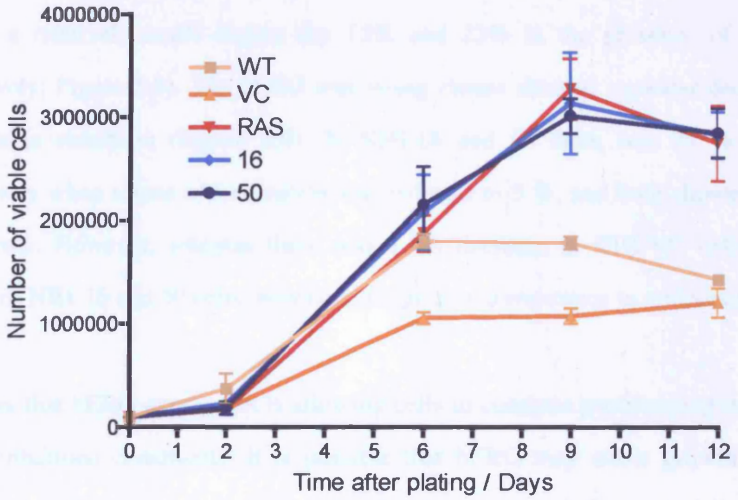

Figure 5.5 Time course of saturation density. Cells were plated at low density (100,000 cells per well on a 6 well plate) and allowed to proliferate for up to 12 days. Media was changed every 4 days. At days 2, 6, 9, and 12 viable cells were counted after trypan blue exposure. Data represent mean ± SEM, n = 3.

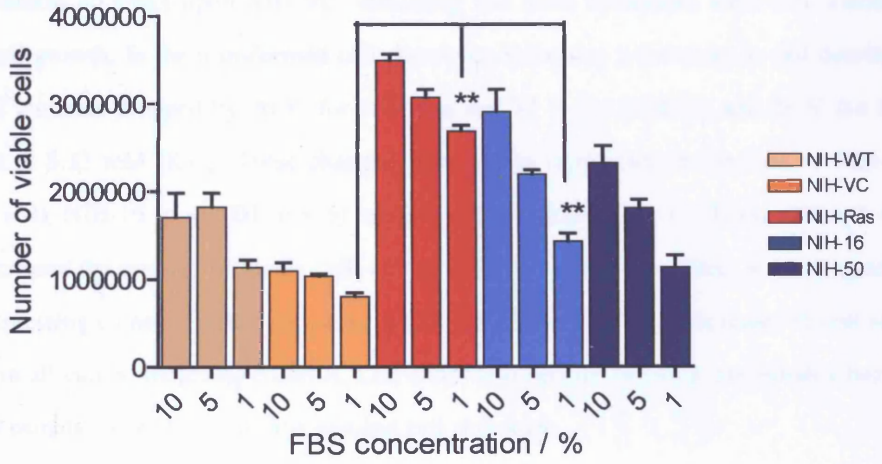

Figure 5.6 Effect of serum concentration upon saturation density 1 x 10^6 cells were plated and after an initial 24 h in 10% serum, cells were grown in medium containing the indicated amount of serum (1, 5 or 10 %). Viable cells were counted after 4 days. Data represent mean ± SEM from three experiments performed in duplicate. Data were analysed with Prism software, using a one-way ANOVA analysis with Dunnetts post test with NIH-VC as control (** $p < 0.01$).

cells to a relatively small degree (by 12% and 23% in the presence of 5% and 1% serum, respectively; Figure 5.6). The hERG expressing clones showed a greater decrease in cell number upon serum reduction (Figure 5.6). In NIH-16 and 50 there was 24 % and 22 % decrease respectively when serum concentration was reduced to 5 %, and both showed a 51 % decrease in 1 % serum. However, whereas there was a net decrease in NIH-VC cells in 1 % serum, the number of NIH-16 and 50 cells increased, suggesting a resistance to apoptosis in low serum.

It appears that hERG expression is allowing cells to continue proliferating independent of normal contact inhibition constraints. It is possible that hERG may allow growth of cells under post-confluent conditions via modulation of membrane potential. To investigate this, the membrane potential of the cells was altered via the addition of KCl to the medium to cause a depolarisation of the membrane potential, via an influx of K^+ ions. The greater the membrane conductance to K^+ ions the closer the membrane potential will follow E_K. Thus cells expressing a high density of hERG channels are likely to be more depolarized by high $[K^+]_o$ than control cells. An increase in $[K^+]_o$ from 5.3 mM to 10 mM produced a small increase in saturation density in all clones (Figure 5.7). A further increase in $[K^+]_o$ (40 mM) showed an increase in saturation density for NIH-WT and had almost no effect upon NIH-VC; indicating that these conditions were still conducive to normal cell growth. In the transformed cells however, there was a decrease in cell density at 40 mM. Cell numbers dropped by 20 % for NIH-Ras and 32 % for NIH-16, and 28 % for NIH-50 compared to 5.33 mM $[K+]_o$. These changes were highly significant in the case of NIH-Ras ($p < 0.01$, $n = 4$), NIH-16 ($p < 0.001$, $n = 6$) and NIH-50 ($p < 0.001$, $n = 6$). Thus, although 40 mM $[K+]_o$ decreased the number of viable cells for transformed clones, the effect was not specific for hERG expressing clones. Further increases in $[K+]_o$ showed very large decreases in cell numbers (>80 %) in all clones, including controls. Cell death also became obvious, presumably because of increased osmolarity of the media and ensuing cell shrinkage.

hERG current effects upon contact inhibition were also investigated by repeating assays in the presence of hERG channel blockers. The foci-forming assay was repeated in the presence of dofetilide (10 μM). No significant changes were documented for any of the clones (data not shown) and the resulting staining patterns appeared the same as previously seen in Figure 5.1. NIH-16 and 50 cells still showed the characteristic ridges of overgrowing cells that lead to regions of dark staining, surrounding regions of lighter staining. However, the qualitative nature of the

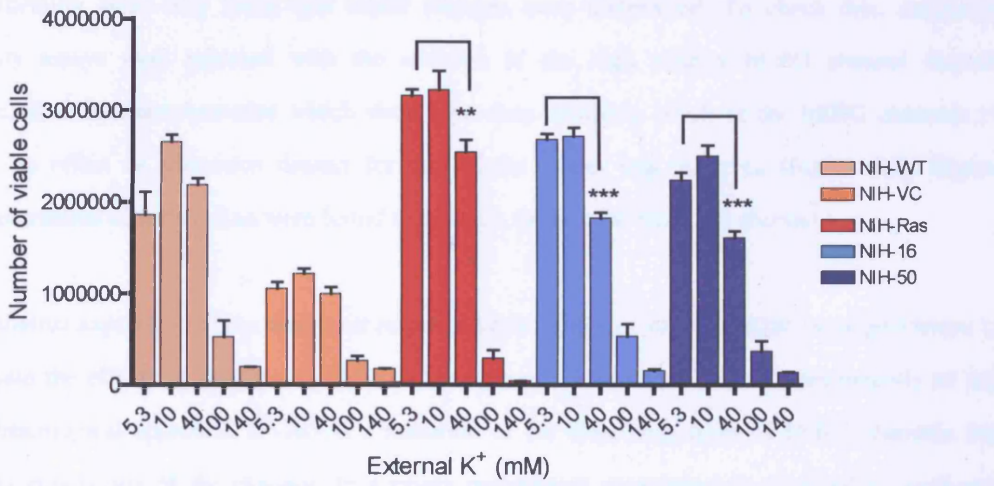

Figure 5.7 Effect of $[K+]_o$ on saturation density of NIH-3T3 clones. Cells were plated at confluency, see methods. After 24 hrs media was replaced with indicated external [KCl]. Viable cells were counted after 4 days. Bars represent duplicate wells from three experiments, mean ± SEM. Data were analysed with Prism software, using a two-way ANOVA analysis (** $p < 0.01$, *** $p < 0.001$).

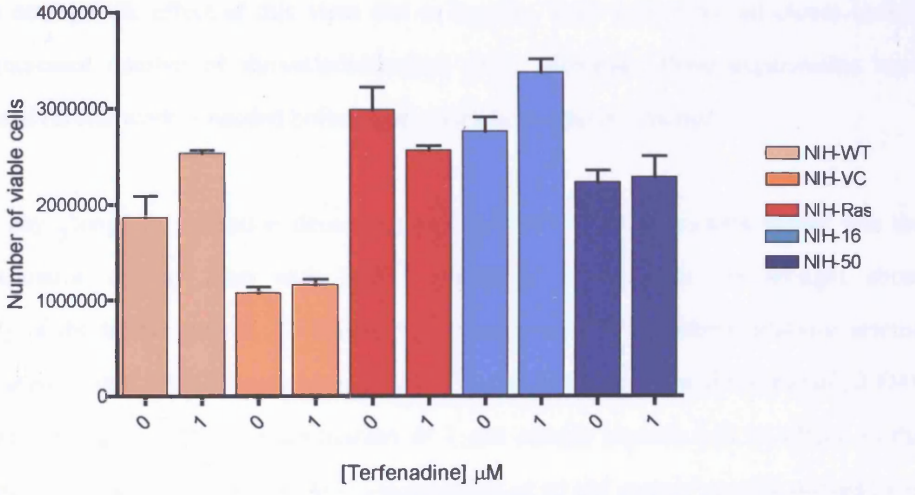

Figure 5.8 Effect of terfenadine upon saturation density of NIH-3T3 clones. After 24 hrs, cells were grown in medium containing terfenadine. Viable cells were counted after 4 days. Bars represent mean ± SEM number of cells counted in duplicate wells from two experiments. Data were analysed with Prism software. No significant differences found.

foci-forming assay may mean that subtle changes were undetected. To check this, saturation density assays were repeated with the addition of the high affinity hERG channel blocker terfenadine: at a concentration which should produce complete block of the hERG channels (1 μM), no effect on saturation density for any of the clones was observed (Figure 5.8). Higher concentrations of terfenadine were found to be toxic to the cells (data not shown).

Adenovirus expression of the dominant negative hERG channel mutant G628S were performed to evaluate the effects of reduction of hERG current upon contact inhibition independently of any pharmacological approach. G628S is a mutation of the selectivity filter of hERG channels that blocks conduction of the channel. In a single preliminary experiment (performed in duplicate) adenovirus was used to infect subconfluent cultures of NIH-3T3 cells. After 48 h the cell cultures were confluent and >90 % of cells expressed GFP with the G628Sa virus (see Methods) and >80 % for G628S virus. Unfortunately the empty virus gave very poor infection levels and only ~10 % of cells showed GFP expression (data not shown). Infection with G628S encoding virus gave mixed results. There was very little, if any, effect upon NIH-VC or NIH-16, whilst there was a loss of 60 % of cells from the NIH-50 culture (Figure 5.9). Infection with the G628Sa-encoding virus produced a clear decrease in the total cell number for all the cell-lines tested (Figure 5.9), suggesting a non-specific effect of this virus due to toxicity, since cells from all clones looked unhealthy (increased number of shrivelled/detached cells). However, these experiments were preliminary and further work is needed before firm conclusions can be reached.

The lack of any change in saturation density upon addition of hERG blockers means that the increased saturation density seen with hERG expression is likely to be brought about independently of the hERG current. To further test this, the hERG trafficking inhibitor arsenic trioxide was used to limit hERG channel expression at the plasma membrane (Ficker *et al.*, 2004). As can be seen in Figure 5.10A the application of 1 μM arsenic trioxide had no effect on the saturation densities of any of the clones. At a concentration of 10 μM arsenic trioxide proved to be toxic. Interestingly, the toxicity of arsenic trioxide seemed to be reduced in the hERG expressing NIH-3T3 clones compared with NIH-VC (Figure 5.10B). However, at present we have no direct evidence that arsenic trioxide influences surface expression or conduction of hERG channels in our NIH-3T3 clones.

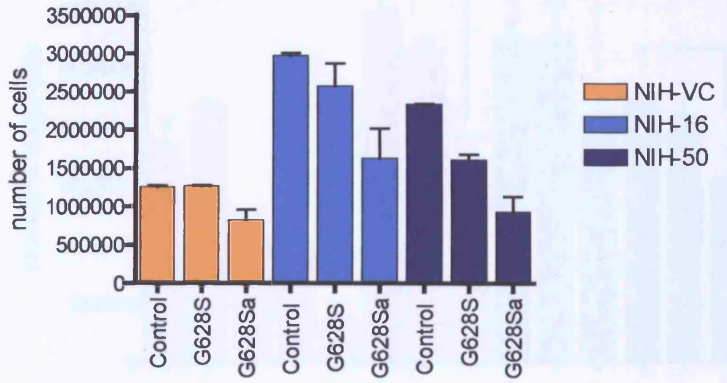

Figure 5.9 NIH-3T3 cells (100,000) were plated per well of 6 well plate. After adhesion, cells were infected with one of the following viral constructs: G628S-hERG (4.5 µl), G628Sa-hERG (12 µl), or "empty" virus (50 µl). After 24 and 48 h cells were washed in fresh medium. Plates were incubated at 37 °C in 5 % CO_2:air for four further days. Control samples have no virus addition. Viable cells were counted. Data represent means (duplicate plates from a single experiment) ± range.

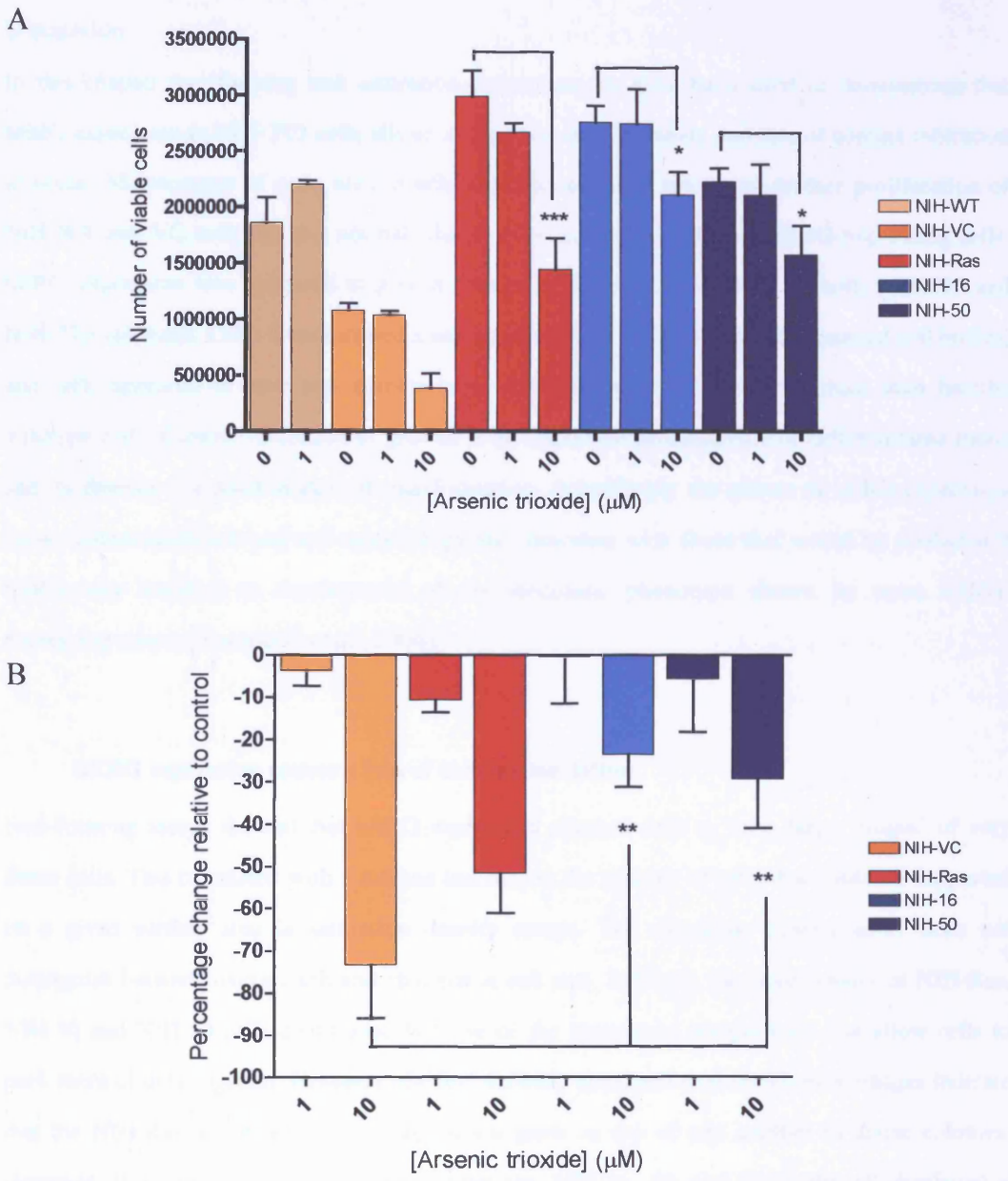

Figure 5.10 Effect of arsenic trioxide upon saturation density. Cells were plated at confluency. After 24 hrs media was replaced with media containing arsenic trioxide (1 or 10 μM). Viable cells were counted after 4 days. Bars represent duplicate wells from at least two experiments, means ± SEM. **A:** total number of viable cells. Data analysed using a Two-way ANOVA (* $p < 0.05$, *** $p < 0.001$). **B:** percentage change after drug additions relative to control values (no As_2O_3 addition). Data were analysed with Prism software, using a one-way ANOVA analysis with Dunnetts post test with NIH-VC as control (** $p < 0.01$).

Discussion

In this chapter foci-forming and saturation density assays have been used to demonstrate that hERG expression in NIH-3T3 cells allows an increase in cell density and loss of contact inhibition to occur. Maintenance of cells once confluency was attained, prevented further proliferation of NIH-WT and VC cells but did not halt the proliferation of NIH-Ras or hERG-expressing cells. hERG expression also appeared to give a change in cellular morphology in both HEK293 and NIH-3T3 cell lines. Cells demonstrated a more spindle-like morphology with rounded cell bodies, and cells appeared to have less surface area in contact with the culture surface than healthy wildtype cells. Contact inhibition of growth is an important characteristic of differentiated tissue and its absence is a good marker of transformation. Accordingly the effects of hERG expression upon contact inhibition and cell morphology are consistent with those that would be predicted if hERG was involved in development of the metastatic phenotype shown by some hERG-expressing cancers (Lastraioli *et al.*, 2004).

hERG expression causes a loss of contact inhibition

Foci-forming assays showed that hERG expression allowed cells to form large 'ridges' of very dense cells. This correlated with a marked increase in the number of cells that could be supported on a given surface area in saturation density assays. The saturation density assay does not distinguish between overgrowth and changes in cell size. In theory the high density of NIH-Ras, NIH-16 and NIH-50 cells could arise because of the changes in morphology that allow cells to pack more closely together. However, the foci-forming assay and post confluency images indicate that the NIH-Ras and hERG expressing clones grow on top of one another in dense colonies. However, it is important to note that whilst the NIH-16, 50 and Ras cells all displayed a transformed spindle-like morphology NIH-VC only displayed classical fibroblast 'flat' morphology and only very few of the NIH-WT cells ever appeared slightly spindle-like shape. In the assays performed in this Chapter, NIH-VC have been used as the "control" cell-line, however NIH-16, -50 and -Ras cell-lines all grew to cell numbers significantly greater than both NIH-VC and -WT cell-lines.

A potential complication in interpreting the results of the saturation density assay is the difference in number of cells between NIH-WT and NIH-VC. NIH-WT grew to a significantly greater cell

number than NIH-VC, without displaying the transformed phenotype seen in NIH-16, -50, or -Ras clones. Instead the NIH-WT cells shared the same basic appearance to NIH-VC except that the cells appeared smaller. The reason for the decrease in cell size of NIH-WT cells relative to NIH-VC is unknown. There were however, some instances of spontaneous transformation of the NIH-WT clone. This has been previously documented in this cell line and it is known that prolonged culture of NIH-3T3 cells in confluent conditions can lead to spontaneous transformation (Grundel & Rubin, 1992; Ellison & Rubin, 1992). It is not clear why NIH-WT should present more of these spontaneous transformations than NIH-VC, especially as they originated from the same cell stock. However, a possible explanation is that NIH-VC cells were generated from a single cell, whereas NIH-WT cells represent a heterogeneous population that may include a small percentage of transformed (or more prone to transformation) cells. The fact that NIH-VC does not show any transforming events provides good evidence that the transforming effects seen in NIH-16 and -50 are due to hERG expression rather than spontaneous events. This is also backed up by the fact that NIH-16 and -50 have similar phenotypes that are different from that of any spontaneously transformed NIH-WT cells.

Total protein levels in sub confluent populations of NIH-VC, -16, -50 and -Ras were identical 24 hrs after plating at the same cell number (Figure 5.4B). Assuming that the amount of protein per cell is consistent between the clones, this provides further support for the earlier finding that hERG expression has little effect on proliferation rate in the NIH-3T3 clones. Furthermore, the significant increases in protein observed post-confluency in NIH-16, -50 and -Ras clones (relative to NIH-VC) further demonstrate their loss of contact inhibition.

In the previous chapter hERG expression was shown to reduce the serum dependence of growth in the high expressing HEK293 clones (clones 13, 14 and 16). However, there was no evidence of serum-independence of proliferation in the NIH-3T3 clones. In this Chapter, 1% serum caused a decrease in cell number in NIH-VC cultures, whereas hERG-expressing clones continued to proliferate (although saturation density was significantly reduced). hERG expression causes loss of contact inhibition but not loss of growth factor dependency of cell division. It seems that rather than initiate growth and proliferation, hERG expression allows continued proliferation in conditions that would normally halt this process and where cell death/apoptosis might occur.

hERG expression causes changes in morphology of confluent cells

hERG expression produced a dramatic change in morphology upon reaching confluency. hERG expressing NIH-3T3 cells changed from a NIH-VC-like flattened morphology to something more akin to NIH-Ras cells. Upon confluency hERG expressing cells rounded up and became more spindle-like in appearance. The cells also gained the ability to grow on top of one another. The time-lapse movies (see included CD) generated from the NIH-16 and -50 clones demonstrate a clear change in cell morphology just after the point of confluency. This is unlike the NIH-VC and Ras clones which maintain their phenotype through this transition.

NIH-50 showed a subpopulation of cells that did not change morphology after reaching confluency. Highly transformed cells could be detected surrounding a relatively normal monolayer. Perhaps the non-transformed looking cells are not expressing hERG at this time. Data from Chapter 3 shows that not all cells express detectable amounts of hERG current all of the time. This is especially true in the NIH-50 clone. NIH-Ras can also be seen to exhibit a sub-population of these non-dividing flat cells (movie 3).

In the HEK293 cell line overgrowth of cells appears to correlate with the level of hERG channel expression. Whilst control cells spread out and cover the available culture surface, those clones with high levels of hERG channel expression (such as HEK-14) seem to reduce migration into new regions of uncolonised culture area. Instead cells prefer to grow on top of one another, giving the appearance of colonies of cells even when the cell population is far from confluent. This suggests not only loss of contact inhibition, but altered migration patterns.

During normal culture of the NIH-3T3 cells it was noticed that NIH-Ras cells had a decreased adhesion to the culture plate. This was observed as a decrease in the time taken for trypsin to "lift" cells during routine culture, as well as increased accidental removal of cells during medium changes. Under normal sub-confluent culture conditions hERG expressing clones did not show any sign of a change in adhesion. However, during the foci forming and saturation density assays (where the cells were grown to high density) the cells became noticeably less adherent. This can be seen in the pictures of the foci plates for NIH-16 and 50 (Figure 5.1). Around the edge of the plate cells have started to lift off in 'sheets'. The change in morphology of NIH-16 and 50 after reaching confluency is likely to be the cause of this change in adhesion. The observed changes in

NIH-16 and 50 morphology upon confluency were so striking and indicative of a transformed phenotype that they warranted further investigation. In the following chapter the changes in morphology are more fully characterised in relation to cell structure and effects upon migration.

Saturation density of transformed cells is reduced by membrane depolarisation

Membrane potential is thought to be important for regulation of checkpoint progression and passage through the cell cycle; its modulation by K^+ channels is also thought to be important (LeppleWienhues *et al.*, 1996). Thus hERG expression could conceivably remove contact inhibition through modulation of the membrane potential, such that cells were able to pass through cell cycle checkpoints independently of contact-inhibition. In order to investigate the importance of the membrane potential in contact inhibition the membrane potential was changed by manipulating $[K^+]_o$ (Figure 5.7).

NIH-WT and -VC clones both appeared unaffected by 40 mM $[K^+]_o$, indicating that this concentration was not toxic. However, NIH-Ras, -16 and -50 all showed a decrease in cell number correlating to 20 - 32 % of total cell number. This response is opposite to the prediction that depolarisation favours proliferation (Arcangeli *et al.*, 1995; Smith *et al.*, 2002; Crociani *et al.*, 2003). The observed decreases in cell proliferation were not dependent upon hERG expression since NIH-Ras cells also showed this decrease in saturation density. It seems likely that 40 mM $[K^+]_o$ causes a general decrease in proliferation rate in all clones. A general slowing of proliferation would be unlikely to affect the saturation density of NIH-VC cells because they are plated at a density approximating confluency and under normal conditions show no net growth. A decrease in proliferation rate would prevent NIH-16, -50 and -Ras clones from reaching the higher density normally seen within this time-frame. Further experiments are needed to investigate the effects of increasing $[K^+]_o$ upon proliferation rate. It would be interesting to extend the length of the experiment to see if, given longer for proliferation, these cells could still reach saturation densities seen at 5.3 mM K^+. Together this data suggests that either membrane potential is not important for cell cycle control or that contact inhibition has a dominant regulatory role.

Unfortunately, the interpretation of data from this assay is complicated by the effects of increasing the extracellular solute concentration. High $[K^+]_o$ will not only have effects upon membrane

potential but will also affect the osmolarity of the culture solution. Thus effects upon cell volume may contribute to changes in saturation density. A common method to mitigate against any artifacts caused by osmolarity changes is to balance the osmolarity of the test solutions with a non-permeant ion, such as choline or NMDG. From the presently available data it is unclear whether $[K^+]_o$ is affecting contact inhibition, cell survival, cell death, or proliferation rate. Thus, further experiments are required to investigate each of these processes in more detail.

hERG channel block does not reverse hERG-induced overgrowth

In order to more specifically analyse the effects of hERG current upon contact inhibition, hERG channel blockers were applied in the saturation density assay. Terfenadine failed to have any effect upon saturation density of NIH-16 and -50 clones at concentrations that should fully block the hERG channel. Unexpectedly there was a small increase in the saturation density of NIH-VC and WT clones with 3 μM fluoxetine. This increase could be due to one of the many non-specific effects of fluoxetine such as Ca^{2+}, K^+ and Cl^- ion channel block (Hahn *et al.*, 1999; Maertens *et al.*, 1999). Dofetilide did not alter the morphology or overgrowth of any of the clones, in an obvious manner, in the foci-forming assay. It therefore is unlikely that hERG current contributes to a loss of contact inhibition seen with hERG channel expression.

The stability of terfenadine, fluoxetine and dofetilide may be called into question in such a long assay (4 days). Pillozzi et al. have previously suggested that 200 μM of the hERG inhibitor Way123,398 was required in a 10 day assay due to depletion or degradation of the compound (Pillozzi *et al.*, 2002). However, dofetilide and fluoxetine (Prozac) were developed for clinical use, and were designed to be stable within the body (Allen *et al.*, 2002). Indeed dofetilide is so stable that the major cause of active drug loss from the body is though secretion of the unmodified compound into the urine. Hence, it is unlikely that drug stability will have a significantly effected these results. It was also important that drugs were not applied at toxic concentrations, as was seen with 100 μM terfenadine (data not shown). The advantage of this study relative to previous studies on cancer cell lines is the use of a vector control cell line made in parallel to the stable cell lines. The vector control allows a clear distinction to be made between hERG-specific effects and non-specific toxic effects due to compound addition. Despite my confidence in the pharmacological approach used, I also aimed to use an alternative method to reduce current; the

development of a dominant-negative mutant hERG channel. Preliminary experiments using adenovirus to infect NIH-3T3 cells with G628S hERG channels showed that the reduction in hERG current achieved was not able to influence saturation density. The G628Sa encoding virus produced a decrease in cell number and unhealthy looking cells. Thus care needs to be taken that viral toxicity is not the underlying mechanism for effects on cell biology. The data presented here for dominant negative hERG channel expression clearly needs to be repeated, and the amount of G628Sa used for infection reduced. However, these results strongly suggest that dominant negative suppression of hERG current does not affect the saturation density, and thus contact inhibition properties of NIH-3T3 cells. These results also corroborate those seen upon the addition of hERG channel blocking compounds. From this data it would appear that hERG current is not responsible for the loss of contact inhibition observed in NIH-3T3 cells expressing hERG. It follows that hERG expression is unlikely to cause a loss of contact inhibition via a simple change in membrane potential and that a conductance-independent signalling mechanism is involved (Hegle *et al.*, 2006).

hERG trafficking inhibitors do not reverse hERG-induced overgrowth

While it is clear that hERG channel blockade did not reinstate contact inhibition in hERG-expressing cells, the effects of the hERG trafficking inhibitor arsenic trioxide is a little harder to interpret. It is thought that As_2O_3 interacts with the thiol groups on chaperones Hsp70 and Hsp90, reducing their ability to fold hERG, resulting in ER retention due to quality control mechanisms (Ficker *et al.*, 2004). Effects of As_2O_3 upon hERG are limited to trafficking inhibition, as no direct block of hERG is documented with acute application arsenic trioxide at concentrations up to 10 μM (Ficker *et al.*, 2004). In this study low concentrations of arsenic (1 μM) had no effect upon any of the clones. This is perhaps not surprising, as previous research has shown that a significant proportion of the hERG channels remain in the membrane even after treatment with 10 μM As_2O_3 (Ficker *et al.*, 2004). Unfortunately it was not possible to confirm that hERG trafficking had indeed been disrupted in NIH-3T3 clones. At higher concentrations (10 μM) all the clones were affected to a similar degree. A decrease in cell number of ~70% for the NIH-VC cell-line strongly suggests that exposure to this concentration of As_2O_3 is toxic and results in significant, net cell death. Hence the decrease in cell number of NIH-Ras, -16 and -50 samples is not due to the re-appearance of a contact-inhibited phenotype, but instead, is caused by increased cell death.

Interestingly the toxicity of 10 μM As_2O_3 was greater in NIH-VC and -Ras clones compared with NIH-16 and -50 clones. This seems to suggest that hERG expression reduces cell death in response to As_2O_3. As explained above, even with 10 μM As_2O_3 a significant proportion of channels would be predicted to reach the membrane; thus, residual hERG expression at the cell surface may be involved in a process of cell survival signalling, separate from contact inhibition. To speculate further, the increased cell survival of NIH-16 and -50 cell-lines might arise due to increased NF-κB pro-survival signalling, with which hERG has been associated via interactions with the upstream receptor TNFR (Wang *et al.*, 2002). However, this would be at odds with other observations that NF-κB activity is inhibited by As_2O_3 to a greater extent in hERG-expressing cell-lines, such as SHSY-5Y, relative to non-hERG-expressing cell-lines (Woo *et al.*, 2006). Furthermore, oncogenic Ras is also associated with NF-κB signalling, yet does not show the As_2O_3-resistance exhibited by the hERG-expressing clones.

The increased survival of the hERG expressing clones might alternatively be linked with pro-survival signalling through the AKT/PKB/PI3K pathway (Datta *et al.*, 1999). While AKT/PKB signalling may involve NF-κB, there are also alternative signalling routes by which it may modulate apoptosis and increase survival (Datta *et al.*, 1999). hERG is known to co-immunoprecipitate with FAK. In turn FAK is able to directly activate AKT/PKB, which is an important pro-survival signalling molecule (Frisch & Screaton, 2001). The hERG channel is also known to be directly modulated by AKT/PKB (Zhang *et al.*, 2003). However, activation of this pathway is not unique to hERG expressing cells and is also observed with oncogenic Ras in mouse fibroblast cells via increased $PI(3,4,5)P_3$ levels (Rodriguez-Viciana *et al.*, 1997). These results help to bolster the argument that hERG expression in cancer cells is important for pro-survival mechanisms. Future experiments are required to elucidate the mechanisms and test the role of AKT/PKB signalling.

Summary

hERG expressing NIH-3T3 clones exhibited a very different cell morphology, that was potentiated by cell-cell contact. The morphology of over-confluent hERG expressing NIH-3T3 cells appears transformed and parallels a decrease in adhesion to the culture plate substratum. hERG expression also allows a greater cell density to be reached on a given surface area, through

the loss of contact inhibition of growth. Whilst morphology and cell overgrowth showed hERG dependency, the effects of hERG expression could not be substantially reversed by channel block or attempts to reduce channel expression at the membrane. While this may indicate a conduction independent signalling mechanism, further work is needed to definitely attribute changes in contact inhibition to expression of the hERG channel at the plasma membrane.

Chapter 6 hERG expression alters cytoskeletal organisation and affects cellular motility

Introduction

Cell migration is essential in development of tissues and organs in the developing embryo. In adult animals migration is necessary for many processes, such as wound healing and angiogenesis. Whilst motility is readily seen in development it is a property not often observed in differentiated cells, instead most cells (e.g. epithelial cells) stay firmly anchored in a fixed position. However, these cells do retain the ability to migrate if required to do so. For example, if there is a wound to surrounding tissue epithelial cells will change phenotype, reduce cell-cell and cell-substrate bonds and migrate into the wound to heal the tissue in a process called the epithelial to mesenchymal transition.

Cells migrate in a process called 'treadmilling'. This can be thought of as a two-stage process. First, the cell must extend its membrane in protrusions called lamellipodia and attach to the substratum ahead of the main body of the cell. Then the cell must relinquish contact with the substratum at the rear of the cell, releasing tension on the membrane and allowing the cell to extend further forward. The process of membrane extension is believed to be dependent on the polymerisation of actin filaments. By modifying the actin cytoskeleton the cell can push against the ECM in order to move forward. At the leading edge of the cell, actin filaments are rapidly polymerised perpendicular to the membrane. The filaments thus push against the membrane and force it to extend. This can be observed as a highly complex network of parallel actin filaments in phaloidin stained lamellipodia (Resch *et al.*, 2002).

Retraction of the rear of the cell is so important for cell migration that cells migrate slower on very adhesive substrates. Cells migrate fastest on substrates where their binding affinity is intermediate (Hood & Cheresh, 2002). On substrates where the affinity is low the cell is unable to maintain sufficient traction for efficient movement. To retract the rear of the cell membrane a cell must release contacts with the substrate. Here I will focus on integrin dissociation, which can happen through two separate mechanisms. The first (faster) method involves mechanical

dissociation. If the cell is able to produce enough force it can fracture the integrin-ECM bonds (Palecek *et al.*, 1999; Hood & Cheresh, 2002). The second (slower) mechanism involves proteolysis of integrins. This mechanism is used in cases where integrin-ECM binding is too strong for the cell to mechanically dissociate. The principal enzyme involved here is calpain, a calcium-activated protease that cleaves the integrin-cytoskeleton link. As the cell migrates the integrin becomes torn from the membrane leaving a trail in the wake of the cell (Palecek *et al.*, 1999; Hood & Cheresh, 2002).

Spatially regulated volume changes are thought to be important for the process of migration. It has been demonstrated that a polarized expression of ion channels allows a local cell swelling at the migrating edge of the cell, whilst also generating shrinkage at the rear of the cell (Schwab, 2001). This was been demonstrated with K^+ channel blockers that will only inhibit movement when applied to the rear of migrating cells. Schwab and colleagues propose that cell shrinkage, mediated by K^+ channels at the rear of the cell is important for cytoskeleton reorganization and integrin detachment (Schwab, 2001). The polarization of ion flux has been explained both by changes in localised channel activity (with a uniform spread of ion channels), and also by polarized ion channel location (Schwab, 2001).

Increased motility is a common characteristic of transformed cells. This phenotype is linked to the cytoskeletal organization and focal adhesion formation which are dramatically different in transformed cells when compared to healthy normal cells (Pritchard *et al.*, 2004). The reduction in focal adhesion numbers seen in transformed cells allows the cells a greater rate of migration. The retraction of the rear of the cell can be rate limiting in the process of migration and thus if focal adhesion numbers are reduced then there is a smaller barrier to motility (Wozniak *et al.*, 2004). The reduction in focal adhesions also affects cell motility through a reduction in stress fiber formation. Focal adhesions are used as nucleation centers for the initial (unstable) formation of actin stress fibers. A reduction in focal adhesions provides less nucleation points for actin stress fibers to form. In turn this decrease in F-actin generates a larger pool of monomeric actin available for polymerisation at the leading edge of the cell. The increased motility of cancer cells allows them to invade other tissues and this is a key aspect of metastasis. Thus an increased migratory phenotype and the morphology changes that are associated with this (such as cytoskeleton reorganization) are a marker of more highly developed tumours.

As has already been described in previous Chapters the expression of the hERG channel results in a change in morphology that correlates with decreased adhesion. The spindle-like shape that hERG-expressing NIH-3T3 cells adopt upon reaching confluency suggests a reduced number of cell-substrate contacts. These observations, along with many other studies describing hERG channel interactions with focal adhesion proteins (Cherubini *et al.*, 2002; Arcangeli *et al.*, 2004; Cherubini *et al.*, 2005), suggest that hERG may interact with, and alter the actin cytoskeleton. This may also have consequences for the motility of the cells. Therefore, the aim of this chapter is to investigate the effects of hERG channel expression upon the structure of the actin cytoskeleton. The influence of hERG channel expression upon migration rate will also be investigated in wound healing assays.

Results

Does hERG expression affect focal adhesion and cytoskeleton formation?

The spindle-like appearance of the NIH-Ras clones is likely due to a reduced number of focal adhesions (and thus stress fibers) that in turn reduce the ability of the cells to spread fully on a substrate. This effect of oncogenic Ras has been previously described (Dartsch *et al.*, 1994). The hERG expressing NIH-3T3 cells show a clear morphological similarity to the Ras expressing clones but only after confluency has been achieved. The rounded spindle-like morphology suggests the loss of stress fibers, whose scaffolding effect maintains the flat fibroblast morphology in normal cells. For this reason the actin cytoskeleton of the cells was investigated immunocytochemically.

The NIH-3T3 cell line is excellent for the study of the actin cytoskeleton with cells forming very distinct stress fibers under normal cell culture conditions. As can be seen in Figure 6.1, NIH-VC exhibited clearly defined stress fibers. These stress fibers stretch throughout the cytoplasm. As the cells approach confluency, there is little effect upon the cytoskeleton, with cells still maintaining their stress fibers. NIH-WT showed a similar staining pattern (data not shown). The NIH-Ras clone on the other hand shows a much more diffuse phalloidin staining pattern and the numbers of stress fibers are dramatically reduced. The actin staining of the NIH-Ras clone remains unchanged at and post-confluency (Figure 6.1). The hERG expressing NIH-3T3 clones 16 and 50 both share a similar actin staining pattern to the NIH-VC and -WT cells when plated sparsely. However, this phenotype dramatically changes upon confluency. The cells loose their flat, fibroblast shape and adopt a more spindle-like shape. Concomitant with this the stress fibers become less prominent against the diffuse cytosolic staining (Figure 6.1). Thus, hERG expression alters the actin cytoskeleton, an effect which seems to be augmented by cell-cell contact. In contrast to the NIH-3T3 cells, HEK293 cells displayed only cortical actin staining around the perimeter of the cell with no defined cytoplasmic stress fibers. This made it impossible to see any subtle changes in actin filament formation in this cell line (data not shown).

The dramatic change in the morphology and cytoskeleton organisation of the hERG expressing cells on reaching confluency could be caused by changes in focal adhesion formation. With this in

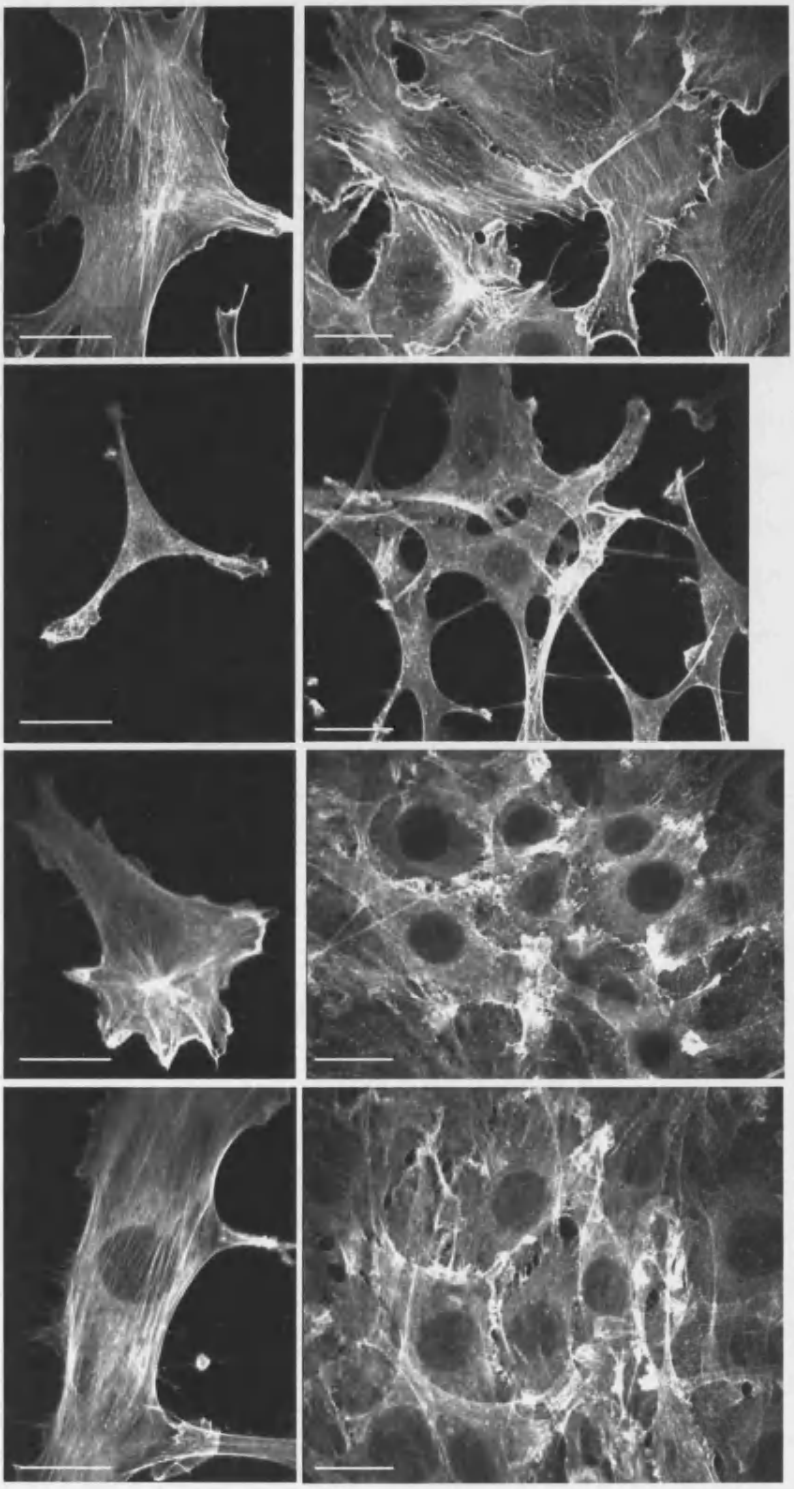

Figure 6.1 Cells grown on coverslips were fixed, permeabilised and Texas-red conjugated phalliodin used to stain actin filaments. Coverslips were imaged using a confocal microscope. Scale bars represent 25 μM. Left column presents sparsely plated cells; right column post-confluent cells.

mind, cells were fixed and stained for vinculin. Vinculin is an important component focal adhesion and stress fiber complexes, and is used to localise focal adhesions. NIH-WT and -VC clones show bright punctate vinculin staining at the ends of stress fibers, both throughout the cytoplasm and at the edges of the cell (Figure 6.2, NIH-WT data not shown). The focal adhesion pattern of individual cells was quantitatively similar after cells had reached confluency, helping these cells to maintain their flat morphology once a monolayer is formed. Ras transformed NIH-3T3 cells have very few punctate stained regions and a more diffuse labelling pattern was observed. The cytosolic labelling appears to be brighter than the equivalent regions in the NIH-VC or -WT cells, especially in the over-confluent samples. The hERG expressing NIH-3T3 clones NIH-16 and -50 displayed a similar punctate staining pattern to the NIH-VC cells when plated sparsely (Figure 6.2). This indicates that the focal adhesions in isolated NIH-3T3 cells are relatively unaffected by hERG expression and explains why these cells continue to display the WT-like flat morphology. The change to a more spindle-like morphology on reaching confluency suggests that hERG expressing cells have reduced numbers of focal adhesions. Indeed NIH-16 and 50 both displayed a distinct reduction in punctate vinculin staining after reaching confluency (Figure 6.2). The confocal images make it difficult to attribute specific vinculin staining to any cells growing on top of one another. There may also be vinculin staining from 'ghost' cells. During cell movement integrins, membrane patches and even vinculin can be torn from the membrane as the rear of the cell retracts (Palecek *et al.*, 1996). Obviously this staining will appear independent of actin filaments.

In order to get a more complete picture of vinculin staining images were captured using an inverted epiflourescence microscope. The increased depth of field shows the combined staining from many cells growing on top of one another in the overgrowing cells (Figure 6.2). In these images a greater density of diffuse vinculin staining in the cytosol can be seen in dense cell populations of NIH-16, 50 and Ras clones relative to NIH-VC. However it is possible that the high density of cells seen in the Ras and hERG-expressing clones may restrict washout of the antibody. Thus, the increased vinculin staining seen in dense cell clusters may be an artifact of the staining rather than an upregulation of vinculin expression. Nevertheless, there is a distinct reduction in the amount of punctate labeling, suggesting that the number of focal adhesions is reduced once the NIH-16 and -50 cells reach confluency.

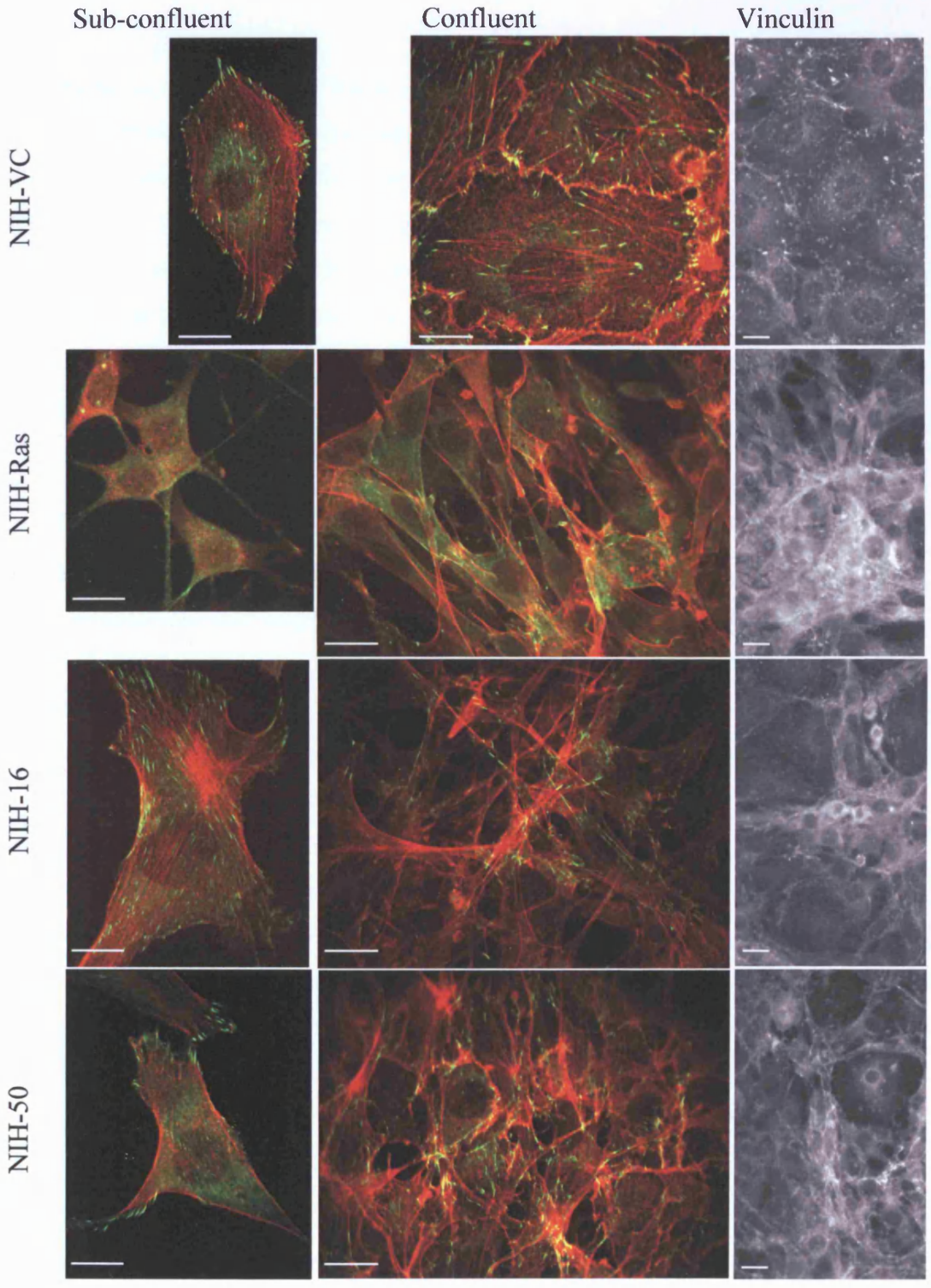

Figure 6.2 Cells were cultured on glass cover slips, fixed and permeabilised. Cells were antibody labelled for vinculin (green) and phalloidin-labelled for actin fibers (red). Left column: sparsely plated cells. Middle column: post confluency. Right hand column: vinculin staining only, in post confluent cells, imaged with epifluorescence inverted microscope. Scale bar represents 25 μM.

In an attempt to examine changes within the cells that may lead to the observed changes in morphology, Western blots were performed for FAK and β-actin proteins. Levels of β-actin were consistent between the various clones and were not dependent upon confluency (Figure 6.3). This suggests that the loss of actin stress fibers seen in NIH-Ras, -16, and -50 clones is not due to a downregulation of the actin protein. Instead the depolymerised stress fibers will directly contribute to the pool of monomeric actin, potentially allowing an increased rate of migration. Total FAK protein expression levels were found to be consistent in all the clones and this was not dependent on the confluency state of the cells (Figure 6.3).

Is hERG expression in NIH-3T3 cells responsible for a change in motility?

The observed change in cytoskeletal organisation and focal adhesion formation observed in NIH-16 and -50 upon confluency suggested that these cells may exhibit increased motility. Indeed an increase of motility is apparent even in subconfluent cells, before the changes in morphology are clear. In the proliferation movies mentioned previously (Chapter 4), NIH-WT and -VC cells move in classical fibroblast fashion. A large lamellipodia is formed that can be seen to ruffle as the cell moves (Figure 6.4B, Movies 6 and 7). NIH-Ras, -16, and -50 share a common phenotype that is very different from that of NIH-VC. The cells are much more motile and move around the culture plate even in the absence of cell-cell contact. The increase in motility can clearly be seen in time-lapse movies of the cells (Movies 8, 9 and 10). Some cells can be seen to migrate very fast in one direction such that they almost appear to 'jump'. In (Figure 6.4B) an initially flattened cell (indicated with arrow) develops a small lamellipodia at one end of the cell. Very soon after the initial formation of the lamellipodia the main cell body appears to reduce contact with the culture surface apart from the leading lamellipodia and a single focal adhesion at the rear of the cell. The front of the cell migrates very quickly in one direction, while the rear of the cell quickly retracts behind the leading edge. However, the rear contact point is not broken and causes a long thin 'tail' to form. Eventually this contact point breaks (not shown in Figure 6.4A), releasing the tail, which 'snaps' back. This gives the cells the appearance that it has 'jumped' when viewed in the time-lapse movie.

A scratch wound assay was used to compare migration properties of the different NIH-3T3 clones. This assay involves the measurement of cells migrating into an artificially created wound

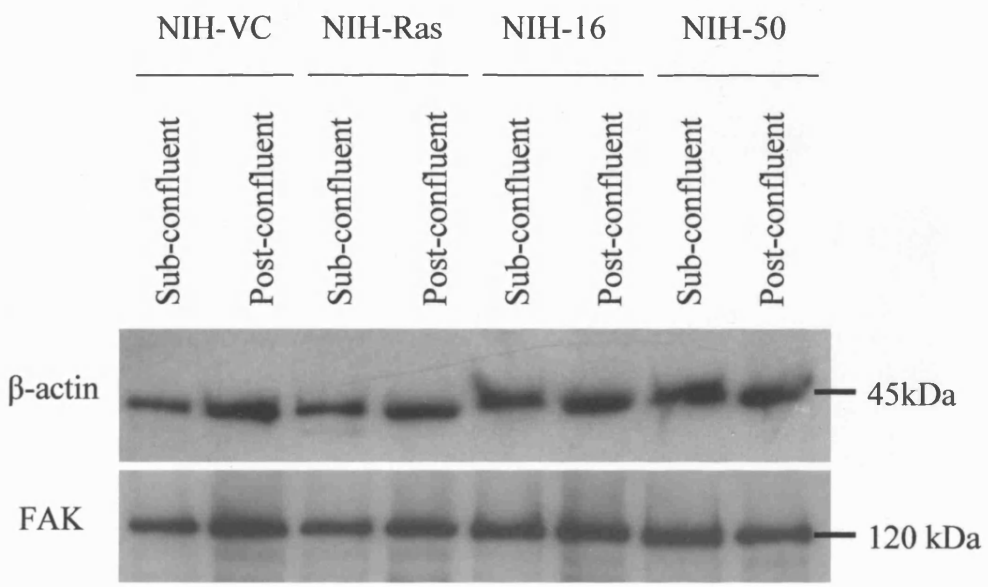

Figure 6.3 Effect of hERG expression and cell confluency upon levels of cytoskeletal proteins. Cells were plated at either 2.5 x 10^5 (sub-confluent) or 2.0 x 10^6 (confluent) cells per well. After 24 hrs subconfluent cells were solubilised with RIPA buffer. Post confluent samples were cultured for 4 days before solubilisation with RIPA buffer. Samples were normalised to obtain equal protein levels and separated on a 8 % SDS-PAGE gel. Protein was transferred to a nitrocellulose membrane and probed with anti β-actin or anti FAK antibodies. Blot shown is representative of three similar experiments.

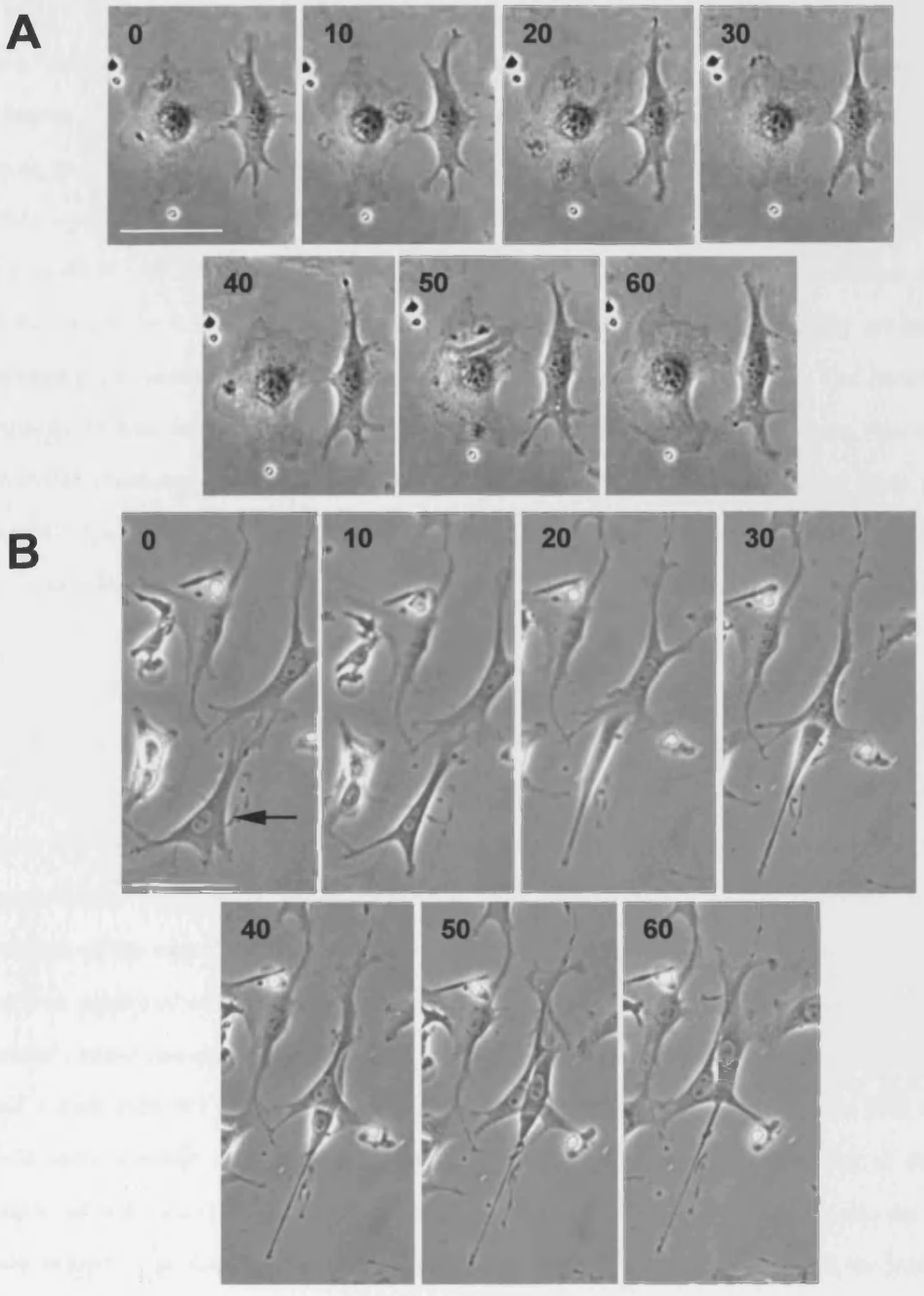

Figure 4 Imaging of individual cell movement. Images were taken using the Incucyte system every 10 mins. Scale bar represents 50 μm. **A:** NIH-VC cells: cell on the left shows large lamellipoda formation with membrane ruffling. Only small net movement is seen. **B:** NIH-16 cells: cell at bottom left of initial image (arrow) has a small lamellipodia at upper edge that moves very rapidly pulling the cell over a neighbouring cell. Focal adhesion at rear of cell does not detach resulting in an elongated cell.

in a confluent monolayer. In order to measure wound closure the Incucyte system mentioned in Chapter 5 was utilized. The system takes phase contrast images at specified time points at the same position on the wound and calculates the mean distance between the leading edges from each image. Thus, closure of the wound can be measured as a function of time. The results produced by the system were validated by conventional measurements from images calibrated with a graticule in an independent series of experiments and also by manually measuring and analysing the wound size from images generated by the Incucyte system. The benefit of the incucyte system was not only its ability to take regular measurements without removing cells from the incubator, but also the measurement of wound width was calculated from the entire wound edge (Figure 6.5), rather than at discrete predetermined points along the wound (as occurs for manual measurement).

Figure 6.7A shows the relative rates of wound closure. NIH-WT and -VC clones migrate at similar rates (30.8 ± 0.9 μm hr^{-1} and 32.8 ± 1.1 μm hr^{-1} respectively). NIH-Ras migrated into the wound at a significantly faster rate (53.9 ± 1.4 μm hr^{-1}; $p<0.01$; $n>32$). NIH-16 and -50 clones close the wound at similar rates to one another (47.6 ± 0.8 μm hr^{-1} and 44.4 ± 1.3 μm hr^{-1} respectively), which were also significantly faster than NIH-WT or -VC ($p<0.01$, $n>32$). An example of the migratory patterns is shown in Figure 6.5. The NIH-VC cells show a much more uniform pattern of wound closure compared to the more disorganized NIH-16 cells. The pattern of wound closure can also be clearly differentiated in time-lapse movies (see included CD). Movie 6 and 7 show NIH-WT and VC clones closing a wound over a period of 16 hrs. In both cases, the cells move together and maintain a flattened, fibroblast morphology, appearing to move as a 'sheet' of cells (also see Figure 6.6). As cells at the edge of the wound migrate into the void, the cells behind them move to take up the extra space. 4 or 5 layers of cells behind the leading edge can be seen to increase in size (spread out) as the wound is closed and more room becomes available. NIH-Ras cells move into the wound almost independently of one another (Movie 8). Cells can be seen to crawl over the top of one another giving a disorganized motion. Cells also leave gaps behind the leading edge of the wound.

NIH-16 and -50 clones showed similar phenotypes to one another during migration into the wound. Cells at the edge of the wound very quickly change from an initial compact cell, to a longer and thinner morphology (Figure 6.6, Movies 9 and 10). After 17 hrs cells appear to be

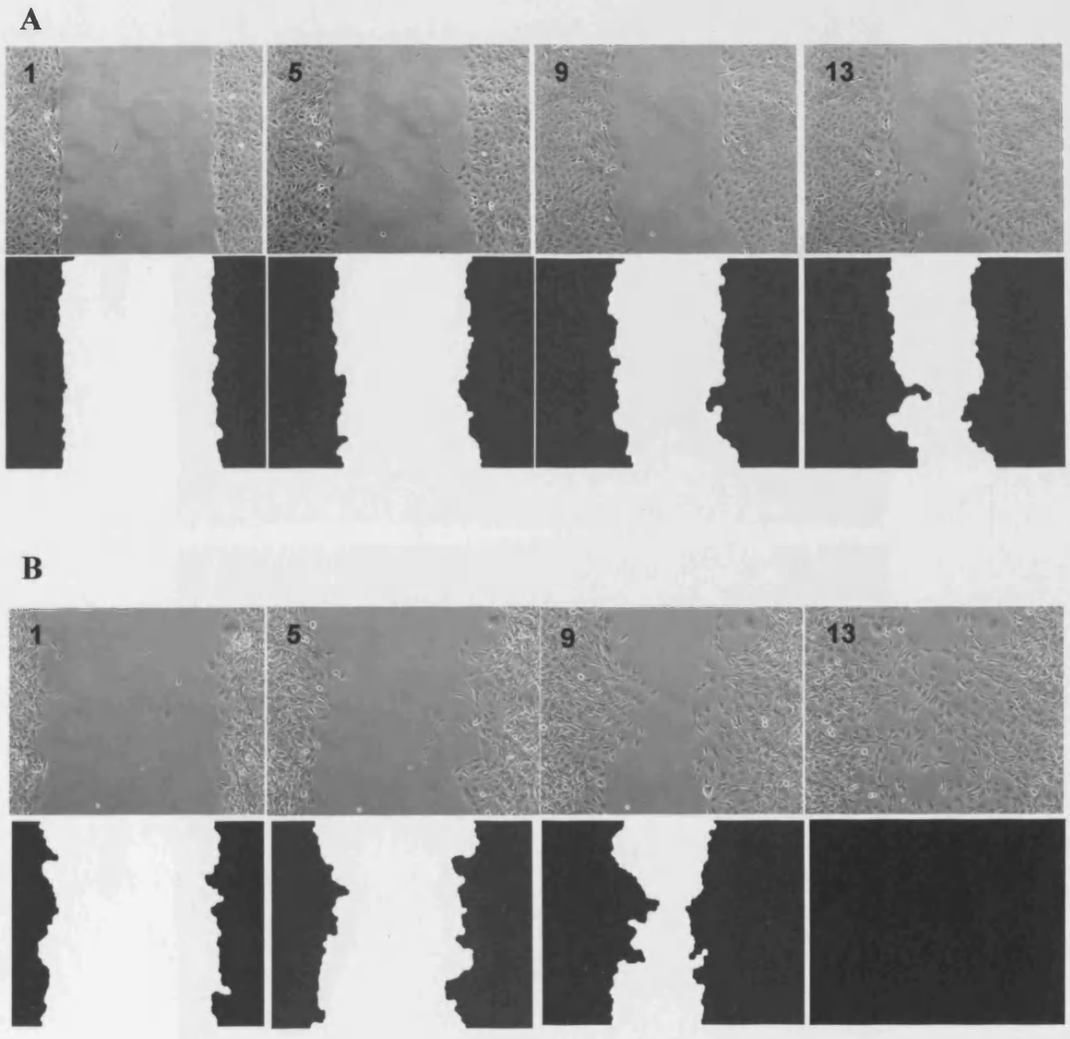

Figure 6.5 Incucyte analysis of wound closure. NIH-3T3 clones were plated at confluency overnight on 24 well ImageLock™ plates. The cell monolayer was then scratched and medium changed, see methods. Images were collected every 4 hrs using the Incucyte system (upper row). Wound size was automatically calculated and a wound map generated (lower row). **A:** NIH-VC, cells migrate as an organised sheet. **B:** NIH-16, cells migrate in a more disorganised pattern and the scratch wound is healed more rapidly than NIH-VC cells.

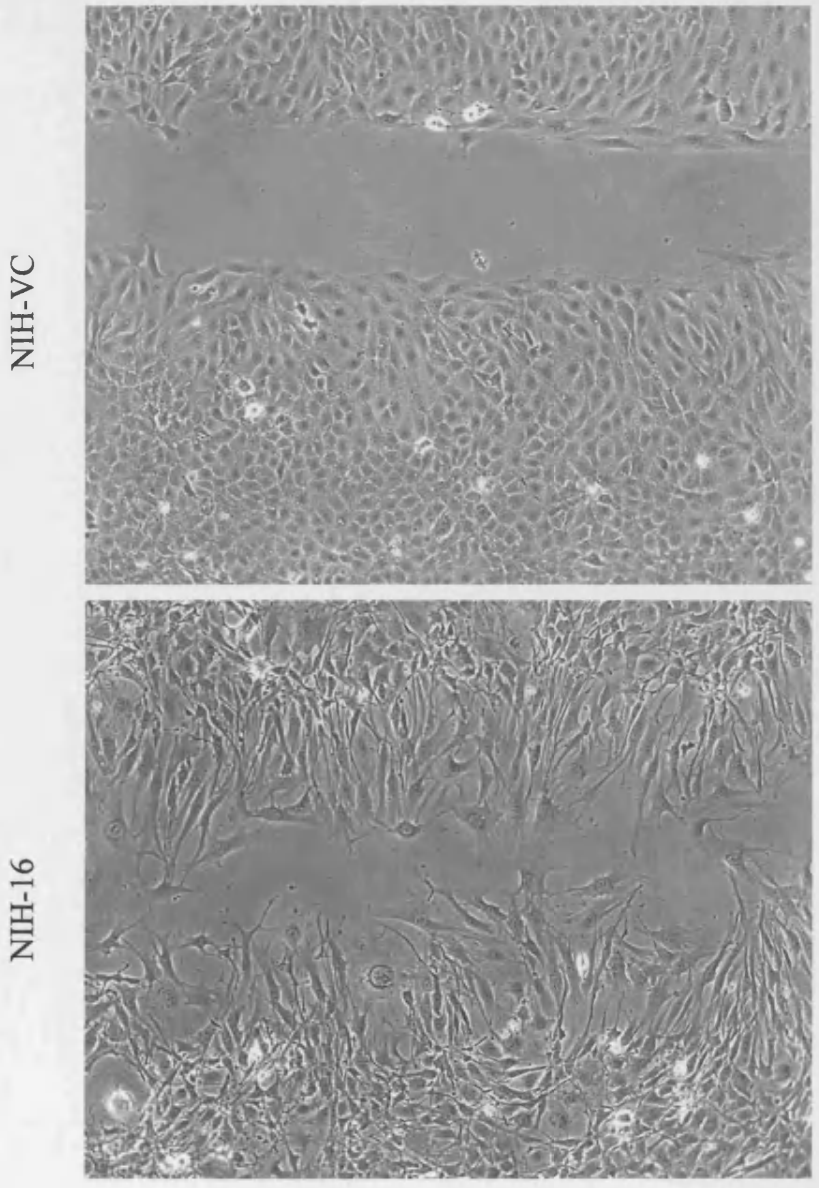

Figure6 .6 Images of wound edge in NIH-VC and NIH-16 clones were plated at confluency overnight in 24 well ImageLock plates. After the scratch wound was made, images were collected every hour using the Incucyte system over a period of 17 hrs, images show wound 17 hrs after wounding. Initial wound sizes were not equivalent in each sample, nevertheless, the images demonstrate clear differences in the migration pattern in the hERG expressing cells.

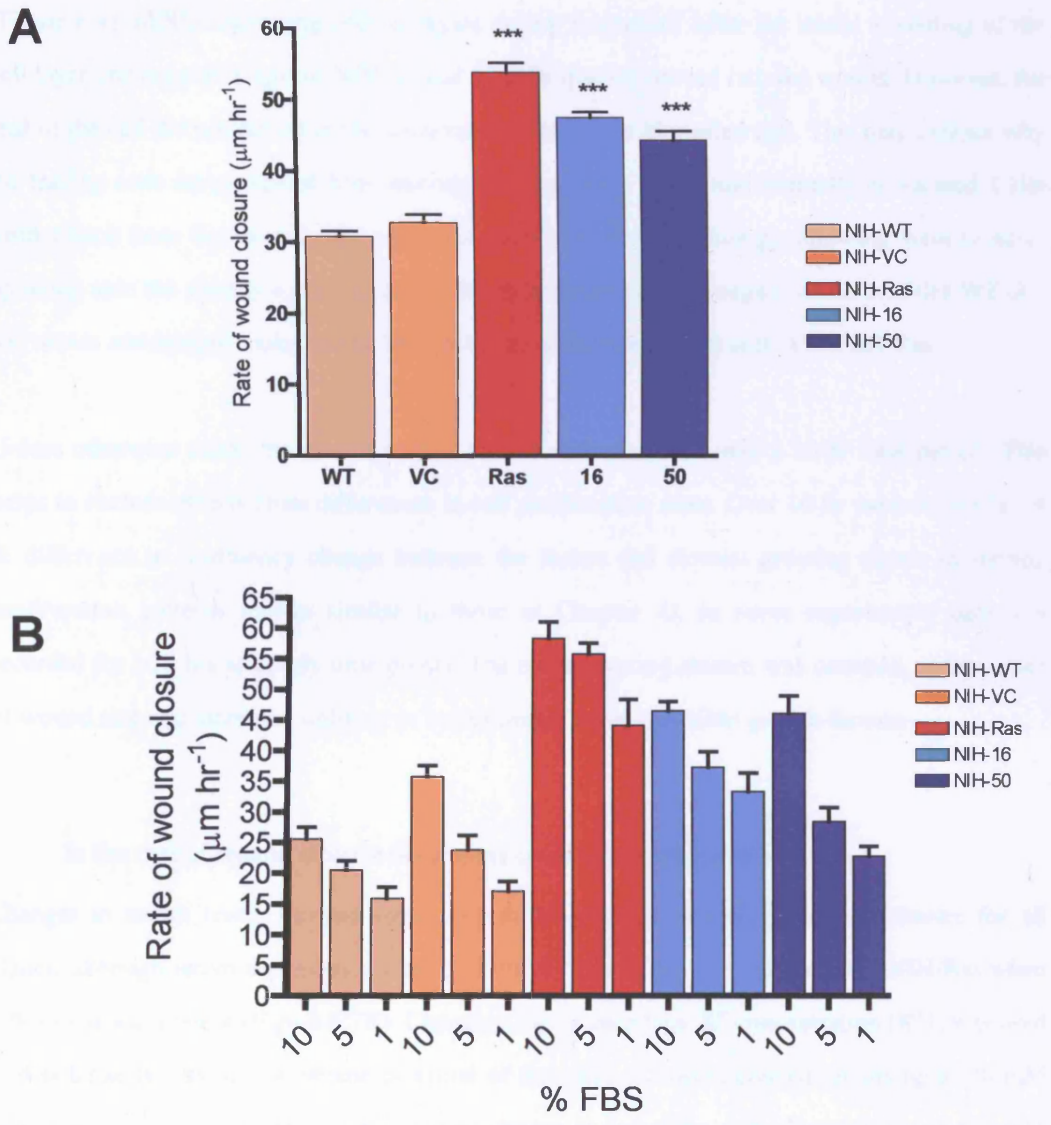

Figure 6.7 Rate of wound closure in NIH-3T3 clones. Cells were plated at confluency and left overnight. A scratch was made in the monolayer using the Woundmaker apparatus. The size of the wound was measured over 10 hrs using the Incucyte system. **A:** Mean (± SEM) wound closure rates under standard culture conditions (n >32 wounds). Data were analysed with GraphPad Prism software, using a one-way ANOVA analysis with Dunnett's post-test with reference to HEK-VC as control (*** $p < 0.01$). **B:** Mean rates of wound closure with different serum conditions (n = 8 wounds from 2 experiments).

lined up with each other, perpendicular to the wound edge. As was seen with individual cells (Figure 6.4), hERG expressing cells elongate during migration. After the initial wounding of the cell layer, the exposed edges of NIH-16 and 50 cells quickly moved into the wound. However, the rear of the cell did not retract at the same rate producing an elongated cell. This may explain why the trailing cells are prevented from moving into the space that would normally be vacated. Cells further back from the wound edge adopt the same extended morphology, allowing them to move up along side the already extended cells. This movement is not as organized as the NIH-WT or -VC clones and instead looked more like the disorganized movement seen with NIH-Ras.

Unless otherwise stated the rate of wound closure was measured over a 10 hr time-period. This helps to exclude effects from differences in cell proliferation rates. Over 10 hr there would be ~4 % difference in confluency change between the fastest and slowest growing clones (assuming proliferation patterns remain similar to those in Chapter 4). In some experiments data was recorded for >20 hrs at hourly time points. The rate of wound closure was constant, independent of wound size and therefore, unlikely to be dependent upon diffusible growth factors.

Is the rate of wound closure dependent upon serum concentration?

Changes in serum levels showed serum dependent changes in rates of wound closure for all clones, although serum dependency was significantly ($P < 0.01$, $n > 4$) reduced in NIH-Ras when 5 % serum was present (Figure 6.7B). Changing the extracellular K^+ concentration $[K^+]_o$ was used to depolarise the resting membrane potential of the cells. At media concentrations up to 40 mM there were no significant effects upon wound closure in any of the cells (Figure 6.8). At 100 mM $[K^+]_o$ there were significant ($P < 0.01$, $n > 4$) effects upon NIH-Ras, -16 and -50, but no significant changes for NIH-WT or -VC. 100 mM KCl reduced the rate of wound closure in NIH-Ras (-51.2 ± 2.4 %), -16 (-28.4 ± 2.8 %) and -50 (-37.6 ± 4.2 %) to the rates observed for NIH-WT and -VC cell-lines (Figure 6.8). 140 mM proved to be toxic to the cells, causing rounding up of the cell and inhibiting wound closure.

Are hERG induced motility changes dependent upon hERG current?

In order to test the involvement of hERG current in migration, hERG channel blockers were added to the culture medium, and incubated for 1 hr before measurements were taken. The

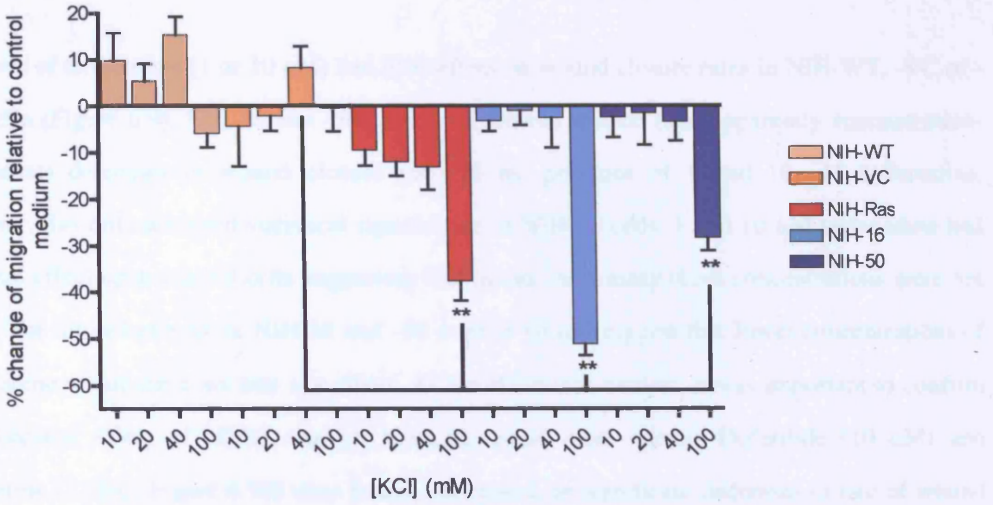

Figure 6.8 Effect of external [KCl] upon migration. NIH-3T3 cells were plated at confluency and left overnight. A wound was made using the Woundmaker apparatus. Media was changed for media containing different $[K^+]_o$. The size of the wound was measured at intervals over 10 hrs using the Incucyte equipment. Mean (± SEM) migration rates (n = 8 wounds from 2 experiments). Data were analysed with GraphPad Prism software, using a one-way ANOVA analysis with Dunnett's post-test with reference to HEK-VC as control (** $p < 0.01$).

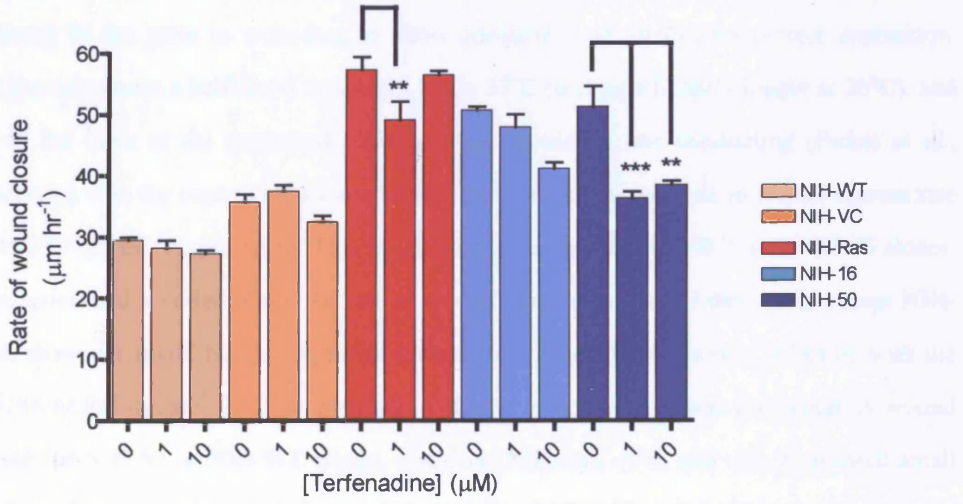

Figure 6.9 Effect of terfenadine upon migration. NIH-3T3 cells were plated at confluency and left overnight. A wound was made in the monolayer using the Woundmaker apparatus. Terfenadine (1 or 10 μM) was then added to the culture medium. The size of the wound was measured over 10 hrs using the Incucyte system. Mean (± SEM) migration rates (n = 8 wounds from 2 experiments). Data were analysed with GraphPad Prism software, using a two-way ANOVA (** $P < 0.01$, *** $P < 0.001$).

presence of terfenadine (1 or 10 μM) had little effect on wound closure rates in NIH-WT, -VC or -Ras cells (Figure 6.9). NIH-16 and -50 cells both showed modest (and apparently concentration-dependent) decreases in wound closure rates in the presence of 1 and 10 μM terfenadine, however, this only achieved statistical significance in NIH-50 cells. 1 and 10 μM terfenadine had minimal effect upon control cells suggesting that in this short assay these concentrations were not toxic. The limited effects on NIH-16 and –50 even at 10 μM suggest that lower concentrations of terfenadine would have not had any effect. As the effect was modest, it was important to confirm the potential effect of hERG channel blockade using other agents. Dofetilide (10 μM) and fluoxetine (3 μM) (Figure 6.10) were tested, but caused no significant decreases in rate of wound healing for any of the clones. Thus, the influence of hERG on cell migration may occur independently of its ion conductance activity.

To reduce hERG current, the G628S hERG mutant was transfected into the NIH-3T3 clones using adenovirus. GFP expression (which was used as a marker of G628S expression) resulting from adenovirus expression was monitored before and after the experiment and showed little change. This is good evidence that G628S expression was consistent throughout the experiment. Cells were infected 48 hrs prior to wounding to allow adequate time for G628S protein expression. hERG is known to have a halflife of around 11 hrs at 37°C (and significantly longer at 26°C), and so after 48 hrs most of the expressed hERG protein should be non-conducting (Ficker *et al.*, 2003). Infection with the control empty adenovirus showed a slight increase in wound closure rate in all NIH-3T3 clones (Figure 6.11). This was most pronounced in NIH-WT and NIH-50 clones. G628S infection had no effect upon the rate of wound closure for any of the clones except NIH-VC which showed a small, but non-significant decrease in wound closure rate. Infection with the other G628S-hERG mutant, G628Sa, resulted in similar effects. There was no change in wound closure rate for NIH-50 or NIH-WT clones, however, NIH-Ras, -VC, and -16 all showed small but significant decreases in the rate of wound closure ($P < 0.05$, 0.05, and 0.001 respectively).

Is hERG channel expression at the plasma membrane responsible for its effects upon motility?

It is possible that hERG channel expression may affect migration of NIH-3T3 cells via a direct interaction with cell signaling pathways, independently of ion flux through the channel. In order

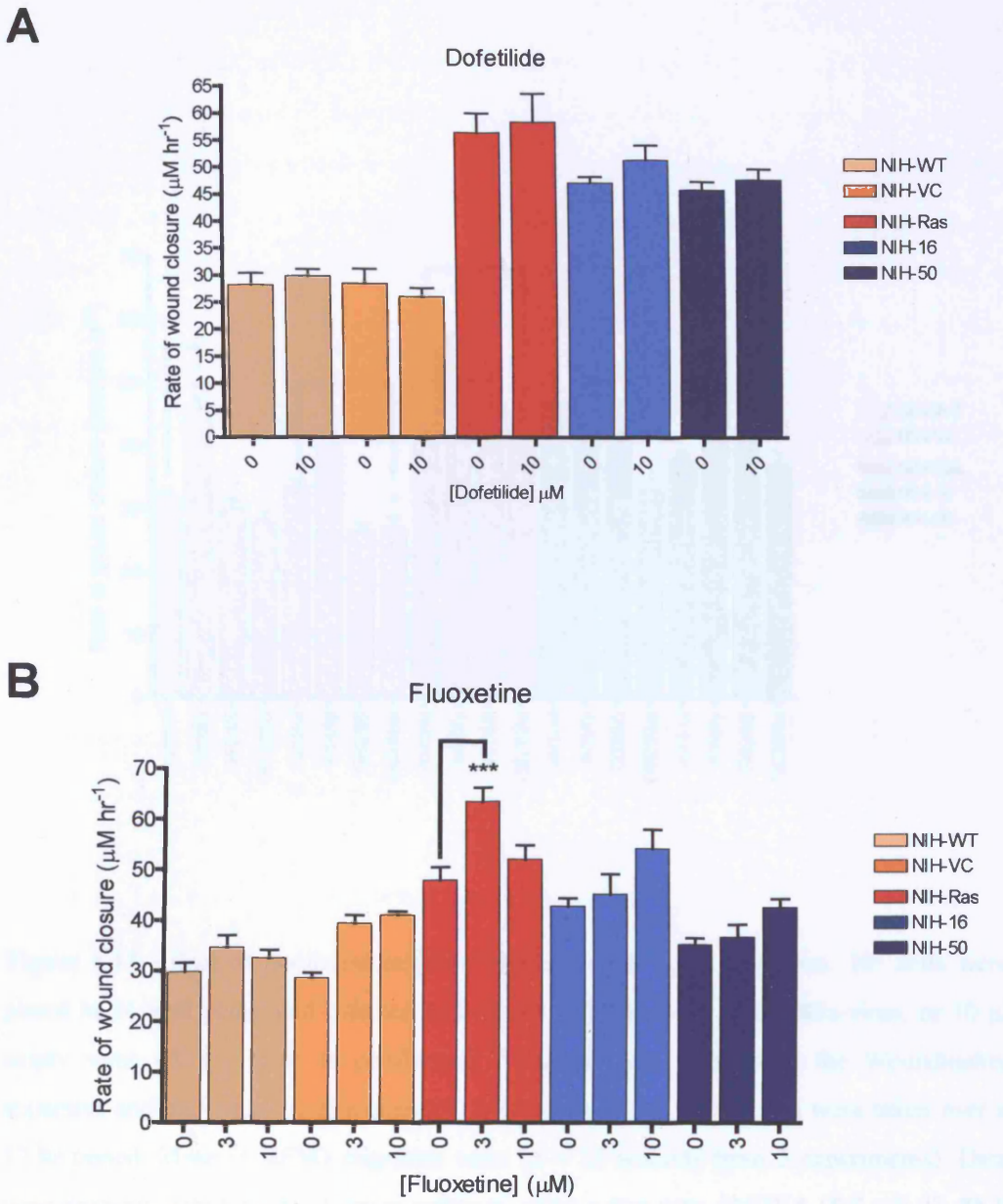

Figure 6.10 Effect of hERG channel drug block upon wound closure. NIH-3T3 cells were plated at confluency and left overnight. A wound was made in the monolayer using the Woundmaker apparatus. Dofetilide (A) or Fluoxetine (B) were added to the culture medium at indicated concentrations. The size of the wound was measured at intervals over 10 hrs using the Incucyte system. Mean (± SEM) migration rates (n = 8 wounds from 2 experiments). Data were analysed with GraphPad Prism software, using a two-way ANOVA (*** $P < 0.001$).

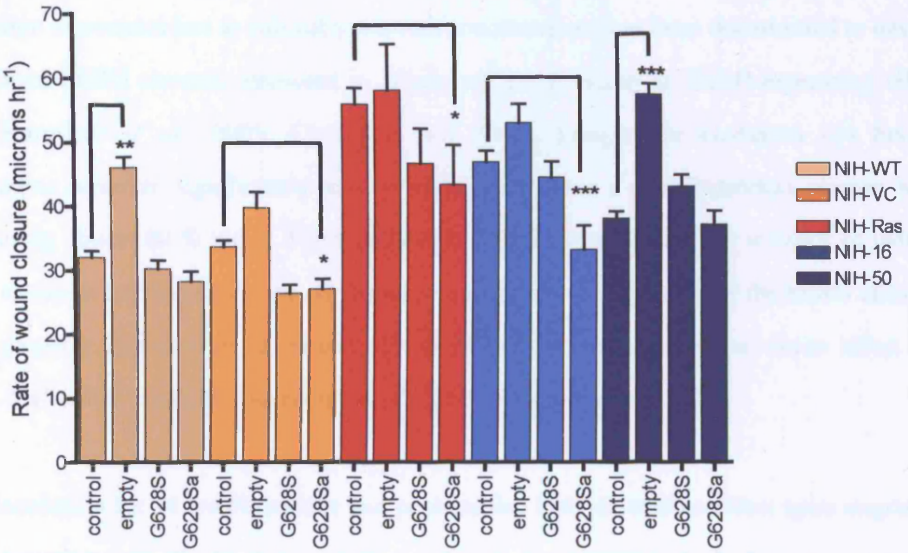

Figure 6.11 Effect of dominant negative hERG mutant upon migration. 10^5 cells were plated in 24 well plates and infected with 1 µl G628S-virus, 3 µl G628Sa-virus, or 10 µl empty virus 48 hrs prior to confluency. Wounds were made with the Woundmaker apparatus and the culture media changed. Measurements of wound size were taken over a 10 hr period. Mean (± SEM) migration rates (n = 12 wounds from 3 experiments). Data were analysed with GraphPad Prism software, using a two-way ANOVA (* $P < 0.05$, ** $P < 0.01$, *** $P < 0.001$), only significant changes are indicated.

to test this hypothesis trafficking inhibitor compounds were applied to the scratch wound assay. Removal of hERG channels from the membrane should inhibit the interactions of channels with any potential signaling pathways. As well as using fluoxetine and arsenic trioxide to inhibit hERG trafficking (as described previously), pentamidine was also utilized in this assay. Acute application of pentamidine at clinically relevant concentrations has been documented to have little effect upon hERG currents measured in whole-cell patch clamp on hERG-expressing HEK293 cells (Kuryshev *et al.*, 2005; Cordes *et al.*, 2005). Longer pre-incubation (24 hrs) with pentamidine however, significantly reduces hERG currents in a dose dependent manner, with 10 μM causing almost 80 % block. The reduction in hERG current is not due to block of individual hERG channels but instead can be attributed to a reduction in the ability of the hERG channels to traffic properly. Pentamidine has effects only on hERG and has been reported not to affect Kv1.5, Kv4.3, Na^+ or Ca^{2+} channels (Kuryshev *et al.*, 2005; Eckhardt *et al.*, 2005).

After incubation for 24 hrs Fluoxetine and pentamidine both showed no effect upon migration up to concentrations of 10 μM (Figure 6.10 and 6.12A respectively). At higher concentrations of pentamidine cells appeared unhealthy, indicating that this concentration may be toxic to the cells. This is also seen as a decrease in rate of wound closure for NIH-WT, -VC, and -Ras clones. These clones should not be affected by pentamidine and so any effects are likely to be attributable to non-specific interactions of the drug. 1 μM Arsenic trioxide had no effect upon NIH-Ras, but did induce a small change upon NIH-WT (-15.4 ± 2.6 %), -16 (-13.6 ± 6.0 %), and -50 (-19.2 ± 5.1 %) clones, which in the case of NIH-50 was significant ($P < 0.05$, $n = 8$) (Figure 6.12B). 1 μM Arsenic trioxide was shown to cause a significant ($P < 0.01$, $n = 8$) increase in NIH-VC migration. At higher concentrations (10 μM) arsenic trioxide gave significant decreases in wound closure rate for all clones except NIH-WT, the largest decreases were for NIH-VC (-25.1 ± 3.1 %, $P < 0.01$, $n = 8$) and NIH-Ras (-53.9 ± 2.3 %, $P < 0.001$, $n = 8$), suggesting that this concentration of compound was toxic. It appears that pentamidine and arsenic trioxide do not affect migration in a hERG-specific manner, and that the compounds quickly become toxic when used at higher concentrations. However, without the benefit of western blott data to confirm the reduction in hERG channel trafficking we cannot say whether hERGs effects upon migration are dependent on its localisation to the plasma membrane.

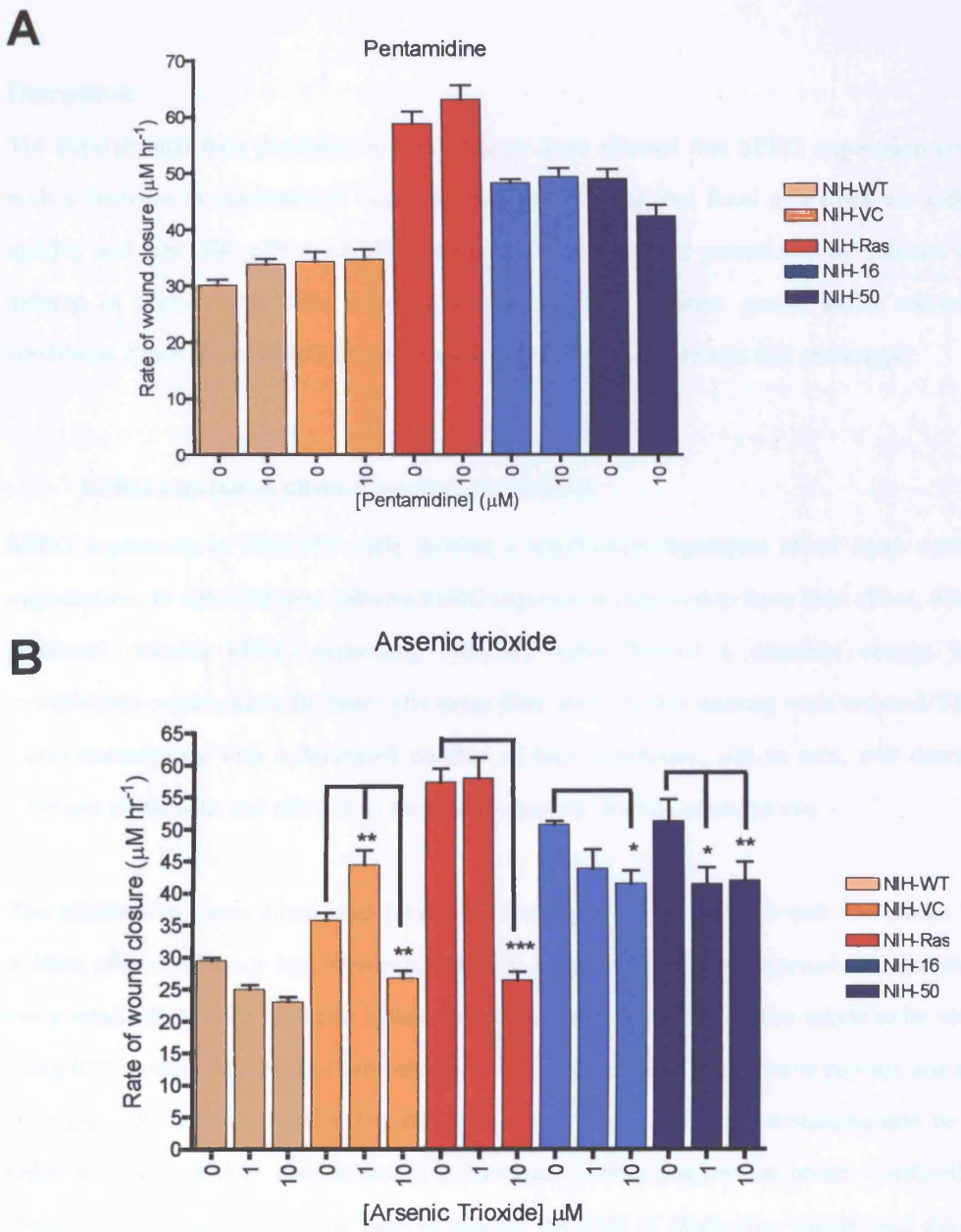

Figure 6.12 Effect of hERG trafficking inhibitors upon wound closure. NIH-3T3 cells were plated at confluency and left overnight. A wound was made in the monolayer using the WoundmakerTM apparatus. hERG trafficking inhibitors were added to the culture media. The size of the wound was measured over 10 hrs using the Incucyte equipment, see methods. Mean (± SEM) migration rates (n = 8 wounds from 2 experiments). **A:** addition of pentamidine to the culture medium. **B:** addition of Arsenic trioxide to the culture medium. Data were analysed with GraphPad Prism software, using a two-way ANOVA (* $P < 0.05$, ** $P < 0.01$, *** $P < 0.001$).

Discussion

The experimental data presented in this Chapter have showed that hERG expression correlates with a decrease in cytoskeleton organisation; not only this, but focal adhesions are reduced in number and size. The effects of hERG expression appear to be potentiated by cell-cell contact, helping to explain why cells retain a normal appearance when grown under sub-confluent conditions. Once again, hERG current does not appear to play a role in this phenotype.

hERG expression alters the actin cytoskeleton

hERG expression in NIH-3T3 cells showed a confluency dependent effect upon cytoskeletal organisation. In sub-confluent cultures hERG expression appeared to have little effect, whereas in confluent cultures hERG expressing NIH-3T3 cells showed a dramatic change in actin cytoskeleton organisation. In these cells stress fibre and vinculin staining were reduced. This most likely corresponds with a decreased number of focal adhesions, and in turn, will decrease the adhesion of the cells and allow the observed increase in the rate of migration.

The decrease in stress fibers and focal adhesions seen in the NIH-16 and -50 clones is most evident after confluency has been reached. It is possible that hERG expression in isolated cells has a small effect upon the actin cytoskeleton/focal adhesions that are too subtle to be visualized using ICC methods. Individual cell imaging is by its very nature a subjective process and also low throughput. With this in mind subtle effects in actin staining and vinculin staining may be missed. Other methods could be used in future experiments to help confirm the results displayed in this project. FACs analysis could be used to analyse the level of phalloidin staining and thus give a measure of stress fiber formation in each clone (Pritchard *et al.*, 2004).

hERG expressing NIH-3T3 clones also seemed to move in a different manner to control clones, with the front of the cell moving forward rapidly, with the rear failing to retract normally. This produced long thin membrane protrusions not seen in control cells. This extended morphology was seen in both isolated cells and those in the densely packed scratch wound assays. The fact that NIH-Ras also displays this feature may suggest that this is not a hERG-dependent effect and may instead be a consequence of the increased migration rate. In future experiments hERG localisation using ICC methods could potentially be used to see if hERG was somehow excluded

from this region of the cell. The concept of ion channel localisation to the front/rear of the cells has been previously demonstrated (Schwab, 2001).

The migration rate of NIH-3T3 cells increases following the stable expression of the hERG channel

The rate of wound closure was increased with hERG expression and these cells moved in a much less organised way. Instead of moving as a sheet of cells (as seen with NIH-WT and VC clones) hERG expressing cells moved as individuals. This phenotype is similar to that observed with the NIH-Ras cells. The change from sheet-like 'collective' migration to individual cell migration via loss of cell-cell contacts is a well documented process in cancer cells (Friedl *et al.*, 2004). In collective migration cells at the leading edge form lamellipodia, these cells 'pull' trailing cells behind them, maintaining cell-cell contacts. NIH-Ras, 16 and 50 clones do not maintain an organised wound edge, and individual cells migrate in different directions. Cells can even be observed migrating over the top of one another. The cells at the wound edge migrate faster than those directly behind them. This allows gaps to form between those cells at the front of the wound and those further back. The gaps that open up allow cells not at the wound edge to form lamellipodia, again another classical transformed phenotype (Friedl *et al.*, 2004). It would be interesting to examine this observation more fully; possibly by looking at integrin expression via ICC. It has been documented that β1 and β3-integrins are often only expressed by the leading cells in collective migration (Friedl *et al.*, 2004; Friedl, 2004), with trailing cells having reduced expression of these integrins. This may be the case in NIH-WT and VC clones; however, from these results NIH-Ras, -16 and -50 clones would be expected to show an increase in β1 and β3-integrins in all cells.

hERG channel expression induced changes in motility were not dependent upon hERG current

The dramatic changes in cell morphology and motility with hERG expression were not dependent upon hERG current. Three different channel blockers were tested. Terfenadine seemed to have a small effect in NIH-16 and –50 clones, however, dofetilide and fluoxetine were without effect. These data suggest that the effects seen with terfenadine were unlikely to be specifically brought about through hERG channel block. Experiments are required to confirm the stability of the

compounds in the culture medium over the assay period. However, the rate of wound closure remained constant over the whole assay with the drugs applied. If the drugs had been subject to degradation (and showed only a transient effect upon the rate of migration) then it is likely that this would have shown up as a change in the rate of wound closure during the time-course of the assay. The use of adenovirus to express G628S and reduce hERG current provided further evidence that functional hERG currents are not required for the observed changes of motility.

Despite drug block of hERG channels not affecting wound healing, raising the concentration of external K^+ did have an effect. High $[K^+]_o$ produced a significant decrease in wound healing in all the transformed clones. This decrease was not accompanied by any visible changes in morphology or viability. The observation that NIH-Ras clones were affected to a similar degree to hERG expressing clones, suggests the decrease in rate of wound closure upon increase in $[K^+]_o$ are likely to be due to non-hERG mediated effect. Why though do the transformed cell lines seem to be more susceptible to these changes in $[K^+]_o$? In order to answer these questions it would be important to know the relative levels of expression of other ion channels. Normal healthy tissue including excitable and non-excitable cells (e.g. epithelial cells) can express IRK channels to control V_{Rest}. It has been documented that a decrease in IRK channels correlates with increases in hERG channel expression in some cancer cell development (Crociani *et al.*, 2003). It remains to be investigated whether the up-regulation of hERG could affect other ion channel expression. It is possible that the transformed cells have lost the ability to decrease their volume sufficiently due to hERG-mediated down-regulation of IRK K^+ channels. Increases in cell volume will alter cytoskeleton organisation and membrane tension (Raucher & Sheetz, 2000). As I have previously described, these changes could have major effects upon a cells ability to migrate.

In saturation density assays raising $[K^+]_o$ to 40 mM was required to show differences between transformed and non-transformed clones; however, in the scratch wound assays 100 mM $[K^+]_o$ was needed. This is likely due to the difference in the duration of the assays. Wound healing is assayed over ten hours and so a larger K^+ gradient is needed to see similar effects to those seen in saturation density assays. This would also explain why 100 mM $[K^+]_o$ does not seem to kill the cells in the scratch wound assay.

hERG trafficking inhibitors also had little effect upon wound closure rate, however there are a number of problems with these compounds. As mentioned in the previous Chapter, fluoxetine at 10 μM gives only a small reduction in hERG protein trafficking, but even at this concentration may be exerting a non-hERG-dependent effect. Studies using pentamidine and arsenic trioxide have also demonstrated that there is still a large amount of mature hERG protein expressed at the membrane even at concentrations of 10 μM (Ficker et al., 2004; Cordes et al., 2005). Consequently, even though these compounds have not reversed the effects of hERG expression in the scratch wound assay, this may just be because the compounds were not sufficiently effective in reducing hERG protein trafficking to the membrane. Western blots or ICC methods are required to determine the level of trafficking inhibition in these cells. In future experiments a dominant negative trafficking deficient hERG mutant channel would prove very useful in helping to verify that the hERG channel was responsible for the effects seen upon the cytoskeleton and motility. These results would also be complemented by studies using RNAi approaches to manipulate hERG expression levels.

Unfortunately, we were not able to image hERG protein with ICC methods. If this became possible in the future (either through better antibodies or the use of cells expressing greater amounts of hERG) then it would be very interesting to monitor the localisation of hERG channels with respect to vinculin staining. Indeed it has been announced that preliminary experiments in SHSY-5Y cells have shown that hERG and paxillin (a major component of focal adhesions) co-localise, although these results have not been published (Cherubini *et al.*, 2002). hERG channels have been shown to co-localise with β1-integrins in co-immunoprecipitation and FRET experiments (Hofmann *et al.*, 2001; Artym & Petty, 2002; Cherubini *et al.*, 2002; Baron *et al.*, 2003; Arcangeli *et al.*, 2004). Integrins are fundamental to focal adhesion formation and so if hERG associates with integrins it should co-localize with vinculin. This is especially true as hERG-integrin interactions are enhanced by integrin-substrate adhesion (Cherubini *et al.*, 2005). There is also evidence for hERG-FAK and hERG-Src interactions, again placing hERG at focal adhesion complexes. Whilst there is much evidence for this focal adhesion localisation of hERG there have not yet been any studies studying the situation in over-confluent cells.

The evidence for a hERG-FAK interaction may be important in the regulation of focal adhesion formation/disassembly, and also stress fiber formation. FAK is known to be essential for the

deconstruction of focal adhesions. Increased FAK activity therefore generates a much faster turnover of focal adhesions which not only decreases the nucleation centers for actin stress fiber formation but also allows the cell to treadmill (migrate) faster (Katz *et al.*, 2003). Western blots show that there is no change in actin or FAK protein levels upon confluency, or any differences between the clones (Figure 6.3). Unfortunately no data was produced to confirm the activation states of the FAK protein. However, the decrease in vinculin (focal adhesion) staining seen in NIH-16 and -50 clones upon confluency would suggest that FAK activation is increased. This would correlate with previous studies that have shown that FAK activity is increased upon hERG expression in HEK293 cells (Cherubini *et al.*, 2005). Future experiments are needed to analyse the activation state of the FAK present in the different clones. This could be performed with either western blotting with antibodies specific for phosphorylated forms of the molecule, or via kinase assays to test the activity of the protein directly. It would be expected that NIH-Ras, -16 and -50 clones would have an increased FAK activity compared with NIH-VC and -WT clones. As mentioned previously, FAK can link to MAPK pathways and so increased FAK activation may also increase MAPK signalling It is for this reason that increased FAK activation might facilitate attachment-independent growth (Frisch *et al.*, 1996); a property also documented in the NIH-16 and -50 clones. Unfortunately FAK kinase inhibitors of high specificity were not available for use in this project. FRNK (FAK-related non-kinase domain), a dominant-negative alternative transcript of FAK has been cloned and remains a possible route to extend the present investigation.

In summary, results presented in this Chapter show that expression of hERG channels in NIH-3T3 cells alters the actin cytoskeleton and focal adhesion formation in a confluency dependent manner. These changes in cytoskeleton also affect cell morphology and motility. Indeed hERG expression seems to reduce vinculin staining and produces reduced adhesion, increased migration and less cell spreading. Interestingly these are the same effects that have been demonstrated in Balb/C 3T3 cells when vinculin expression was reduced via RNAi methods (Rodriguez Fernandez *et al.*, 1993). This study by Rodriguez Fernandez *et.al.* (1993) also demonstrates that reduction in vinculin expression is responsible for adhesion independent growth in Balb/C 3T3 cells. It is likely then that the growth in soft agar seen in chapter 5 of this Thesis is also related to a reduction in vinculin in hERG expressing clones. It seems likely that the hERG channel may be

closely linked with focal adhesion proteins and signalling pathways that regulate the cytoskeleton and focal adhesion formation.

Chapter 7 Are hERG channel effects on growth and migration mediated by interactions with intracellular signaling cascades?

Introduction

In this project hERG expression has been shown to enhance the oncogenic properties of HEK293 and NIH-3T3 cell lines. hERG-expressing cells demonstrate a dramatic change in morphology that coincides with a change in migratory capacity, loss of contact inhibition, and attachment-independent growth. hERG is expressed in many tumours and its expression seems to be linked with the metastatic potential of the tumour (Bianchi *et al.*, 1998; Cherubini *et al.*, 2000; Lastraioli *et al.*, 2004). Whilst this evidence provides a compelling argument for the role of hERG channels in cell transformation, mechanistic information on the pathway(s) linking hERG to transformation remains scant.

Some researchers have proposed that the role of hERG in cancer is through providing transforming cells with a necessary/permissive functional current (LeppleWienhues *et al.*, 1996; Macfarlane & Sontheimer, 2000; Pillozzi *et al.*, 2002; Crociani *et al.*, 2003). I_{hERG} (and the downregulation/absence of inward rectifier K^+ currents) is proposed to generate a relatively depolarised membrane potential that causes cells to divide (through the influx of Ca^{2+}, which has many signalling roles) irrespective of extracellular conditions/signalling. There is no direct evidence for this however, and several studies have only shown effects of hERG channel blockers at concentrations that may have non-specific effects or be deleterious to the cell. Indeed, experiments in this report show that application of hERG channel blockers failed to reverse any of the phenotype changes seen with hERG expression.

There is now mounting evidence that the hERG channel may exert its effects upon the cell via interactions with signaling pathways. hERG has been shown to associate with β1-integrins (Hofmann *et al.*, 2001; Cherubini *et al.*, 2002; Arcangeli *et al.*, 2004), FAK (Cherubini *et al.*, 2005), and Src (Cayabyab & Schlichter, 2002) proteins, all of which are components of focal adhesions. Thus hERG could be a constituent of a macromolecular complex formed at focal adhesions. The closely-related EAG channel has been shown to influence proliferation via direct

protein interactions that are independent of ion flux (Hegle *et al.*, 2006). These signalling interactions are dependent upon the conformation of the channel and suggest that the voltage-sensor acts as a molecular switch. It is possible that this mechanism is conserved in the hERG channel. EAG is also closely associated with the cytoskeleton; and the disruption of this interaction alters the electrophysiological properties of the channel (Camacho *et al.*, 2000).

The aim of the work described in this Chapter will be to investigate the signalling pathways by which expression of the hERG channel is coupled to the morphology and transformed phenotype of NIH-3T3 cells.

Results

Is protein kinase C signalling affected by hERG expression?

Protein kinase C (PKC) expression levels have been previously found to change in NIH-3T3 cells depending on the degree of confluency and are thought to be involved in the processes of contact inhibition (Heit *et al.*, 2001). PKCδ is thought to posses tumour suppressor characteristics while PKCε may have oncogenic properties. hERG channel gating is known to be affected by PKC, via direct phosphorylation (Cockerill *et al.*, 2006). Western blots for PKCδ showed a single band in all clones (Figure 7.1). NIH-VC showed an increase in band intensity in post-confluent relative to pre-confluent cultures and this pattern was observed in all clones. Under sub-confluent conditions, PKCδ levels were similar in NIH-16 and -50 to that of NIH-VC. Post-confluent cultures showed an increase in PKCδ that was also similar to that of the NIH-VC clone. PKCε expression levels for NIH-VC were greater in post-confluent cells relative to non-confluent cells. In contrast, in NIH-Ras cells PKCε expression levels were low and not greatly affected by cell density. NIH-16 and -50 clones showed similar band patterns and intensities to one another (Figure 7.1). For both clones PKCε expression was slightly lower in pre-confluent cultures relative to NIH-VC cells. However, PKCε levels increased substantially in post-confluent cells.

To investigate whether PKCδ and/or PKCε activation was necessary for the transforming effect of hERG expression, PKC inhibitors were added to the culture medium in saturation density and scratch wound assays. Application of the broad spectrum PKC inhibitor bisindolylmalemide I (BIS-I) and the negative control bisindolylmalemide V (BIS-V) (both at 1 μM) had no effect on the saturation density for any of the NIH-3T3 clones (Figure 7.2A). Application of BIS-I or BIS-V had similar effects on scratch wound closure in all clones, causing small, but significant increases in the rates of wound closure relative to untreated cells, in NIH-VC, -Ras, -16 and –50 clones ($P < 0.05$) (Figure 7.2B). Rottlerin has been reported to be a selective PKCδ isozyme inhibitor. When applied to a scratch wound assay, rottlerin (3 μM) significantly increased the rate of wound closure in the NIH-Ras clone (Figure 7.2B). At a higher concentration (30 μM) rottlerin caused a slowing of wound closure rates in all clones (Figure 7.2B).

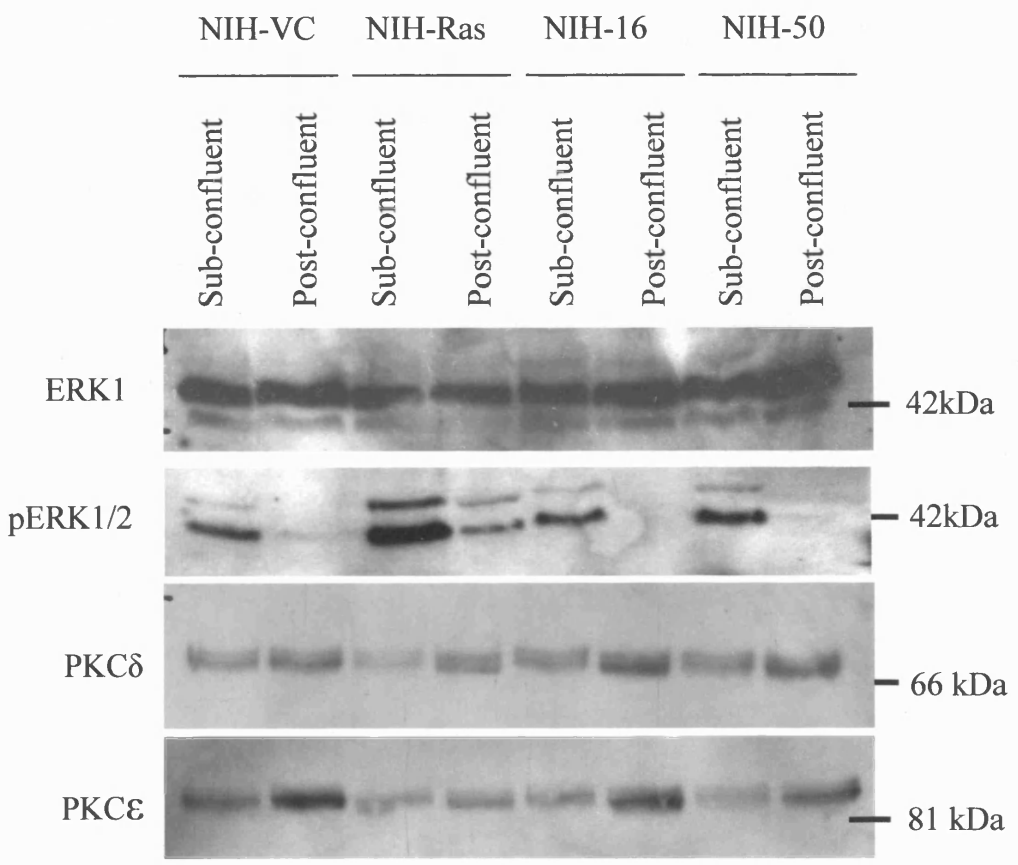

Figure 7.1 Effect of cell confluency on expression/activity of ERK and PKC proteins. 'sub-confluent' samples - Cells were plated at ~40 % confluency and cultured for 24 hrs. For 'Post-confluent' samples cells were plated at confluency and cultured for 4 days. Cells were solubilised with RIPA buffer, total protein determined with the Lowry assay and equivalent amounts of protein applied to each lane. After running on an 8 % SDS-PAGE gel, separated proteins were transferred to nitrocellulose and samples probed with antibodies against phospo-ERK, total ERK, PKCδ and PKCε. Blots are representative of at least four experiments.

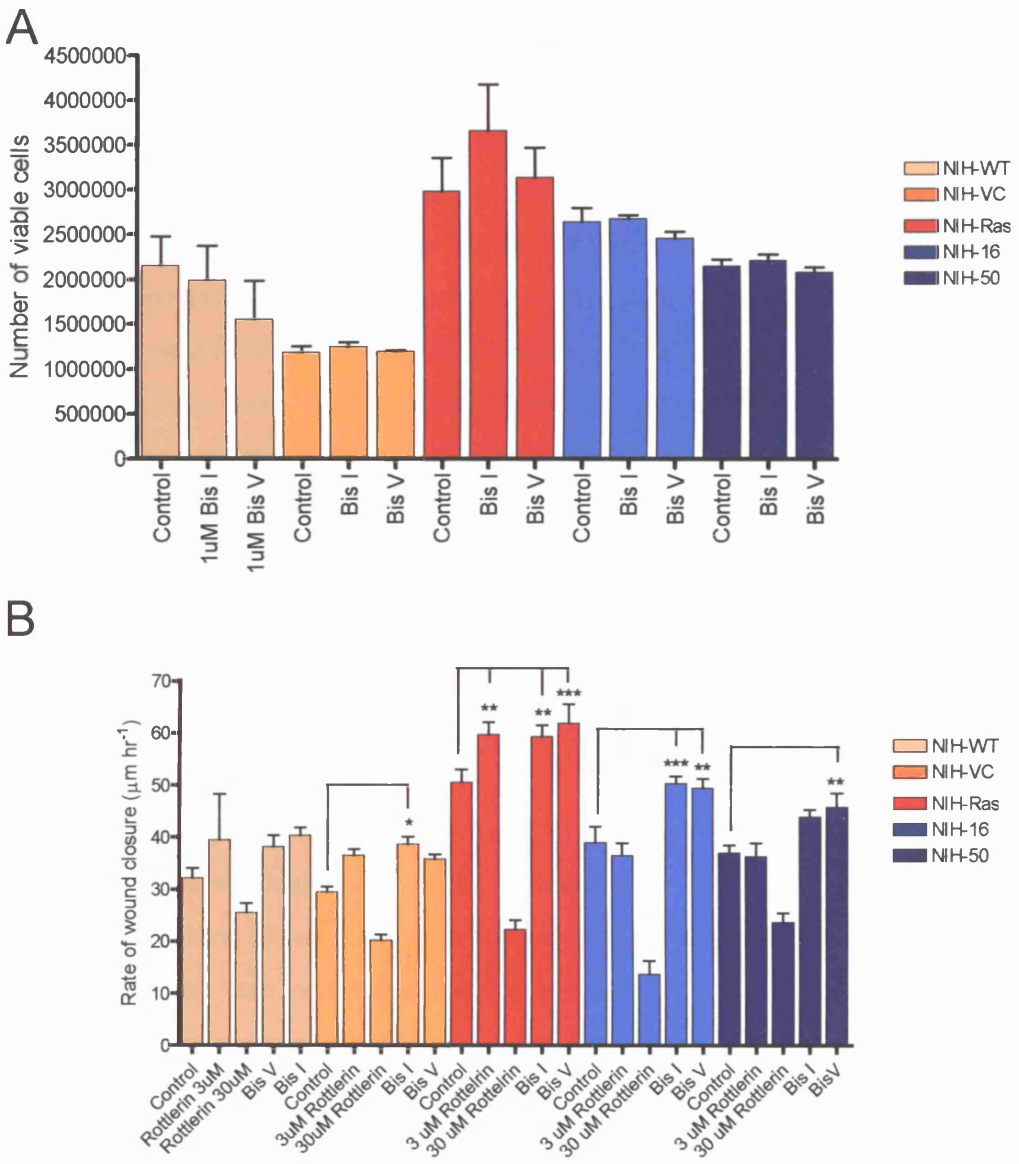

Figure 7.2 Effect of PKC inhibition in saturation density **(A)** and wound healing **(B)** assays. **A:** cells were plated at confluency. After 24 hrs the media was changed and Bis-I (1 µM) or Bis-V (1 µM) were added. Plates were incubated for four further days and viable cells counted. Data represents mean ± SEM of duplicate plates repeated twice. **B:** Wounds were made with the Woundmaker apparatus in a confluent monolayer of cells. Bis-I (1 µM) or Bis-V (1 µM) were added and plates inserted into the Incucyte machine. Measurements of wound size taken over a 10 hr period. Data represent the mean ± SEM of 4 separate wells repeated on two separate occasions. Data were analysed using GraphPad Prism software; two-way ANOVA (*$p<0.05$; **$p<0.01$; ***$p<0.001$).

ERK1/2. Inhibition at the level of MEK1/2 should inhibit all upstream signals, including those from Ras, altering ERK activity. Therefore, the NIH-Ras clone, in which Ras is constitutively active, provided a useful positive control. The MEK1/2 inhibitor U0126 was chosen due to high specificity for MEK1/2 over other cellular kinases (Davies *et al.*, 2000). The availability of an inactive analogue was also valuable as a negative control. 10 μM UO126 (MEK inhibitor) or the inactive analogue UO124 had no significant effect upon the rate of wound closure for NIH-WT or -VC clones (Figure 7.3). U0126 significantly ($P < 0.001$) slowed the rate of wound closure in NIH-Ras cells towards that observed in NIH-WT and -VC clones, whereas U0124 caused a small, yet significant ($P < 0.05$), increase in the rate of wound closure (Figure 7.3). NIH-16 and -50 clones both showed a small decrease in rate of wound closure in the presence of U0126, however, this did not attain statistical significance (Figure 7.3).

Are the transforming effects of hERG expression dependent upon p38 MAPK signalling?

I next investigated the possible involvement of the p38 MAPK pathway. As discussed earlier, p38 MAPK signalling is involved in stress responses, as well as growth, migration and contact inhibition processes. In NIH-3T3 cells expressing EAG channels p38 MAPK inhibitors can reduce proliferation rates down to those seen in non-transfected cells (Hegle *et al.*, 2006). EAG expression also increased the activity of p38 MAPK even when the channel was rendered non-conducting by a mutation within the pore region. In the current hERG study, proliferation assays performed using the Incucyte equipment showed that there was no significant change in proliferation rate on the application of 10 μM SB202190, a potent and selective inhibitor of p38 (Davies *et al.*, 2000), or inactive compound SB202470 (Appendix 1).

In previous studies, p38 MAPK has also been linked with the endothelial to mesenchymal transition (EMT) and cell migration (Ono & Han, 2000; Bakin *et al.*, 2002). p38 signalling has also been shown to be dependent upon β1-integrin adhesion in instances where ERK1/2 appears unaffected (Bhowmick *et al.*, 2001b). We were interested to determine if p38 may play a role in hERG mediated changes in cell motility. SB202190 and SB203580 are both active compounds that were tested in scratch wound assays. Neither compound had a pronounced effect on the rate of wound closure at 10 μM, although SB202190 did produce a significant decrease in NIH-VC, -

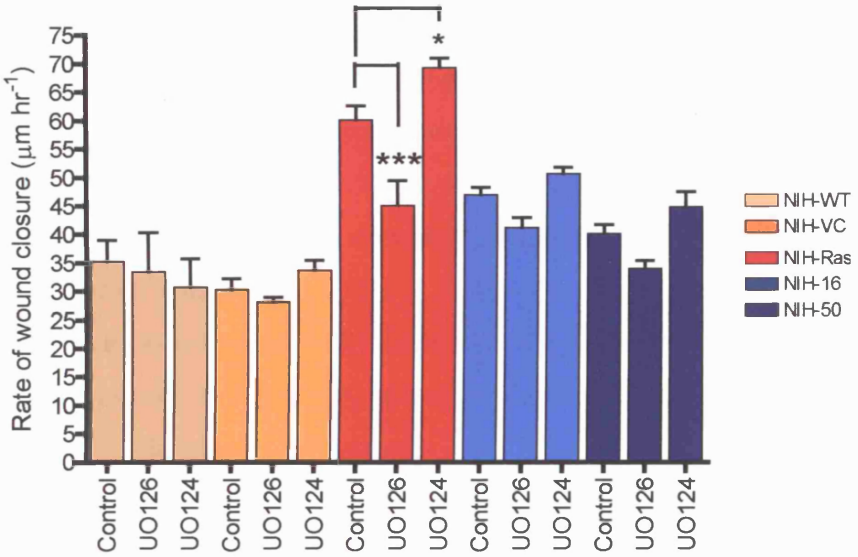

Figure 7.3 The effect of MEK inhibition upon hERG-influenced increases in rate of migration. Wounds were made with the Woundmaker apparatus and 10 μM UO126 or UO124 added. Plates were inserted into the Incucyte machine and measurements of wound size taken over a 10 hr period. Data represent the mean ± SEM of 4 separate wells repeated twice. Data were analysed with GraphPad Prism software; two-way ANOVA (*$p<0.05$; ***$p<0.001$).

Ras and -16 clones (Figure 7.4A and Appendix 2). SB202474 (10 μM), an inactive, chemically-related analogue, was generally without effect, however, this compound did cause a modest (though significant; see Figure 8.4A) effect in the NIH-VC cell-line.

The p38 MAPK pathway also has a role in the process of contact inhibition of growth. Activated p38 increases in confluent cells and inhibitors cause fibroblasts to grow to greater densities (Faust *et al.*, 2005). It is thought that p38 mediates contact inhibition through upregulation of the cyclin dependent kinase (Cdk) inhibitor $p27^{kip1}$, which correlates with a loss of Cdk2 activation and a corresponding dephosphorylation of the retinoblastoma protein, which is important in cell cycle checkpoint regulation (Faust *et al.*, 2005). It is also documented that loss of p38 MAPK production correlates with increased ERK1/2 activation (Faust *et al.*, 2005). This is supported by evidence that an increase in p38 MAPK activity can cause a reduction in active ERK1/2 via activation of protein phosphatases (Westermarck *et al.*, 2001). It is hypothesized that the hERG channel may be interacting with the p38 pathway to allow an increase in saturation density.

To investigate the role of p38 MAPK in contact inhibition the p38 inhibitor SB202190 was used alongside the inactive/less active analogue SB202474 in saturation density assays. NIH-VC cells showed no change in saturation density on application of the p38 inhibitor, or inactive analogue (Figure 7.4B). NIH-Ras showed a dramatic and significant decrease in saturation density following p38 MAPK inhibition; however, clear interpretation of this finding was complicated by the fact that SB202474 (at 10 μM) also caused a marked effect (Figure 7.4B). NIH-16 and -50 clones both presented a similar phenotype to NIH-Ras with dramatic and significant ($P < 0.001$) decreases in the number of viable cells in the presence of the p38 MAPK inhibitor. In the case of the hERG-expressing clones, SB202474 had no effect in NIH-50, but had a modest, though significant effect in the NIH-16 clone (Figure 7.4B). As was observed previously, the NIH-WT demonstrated a higher saturation density than the NIH-VC cells, however, evidence of spindle-like morphology was absent.

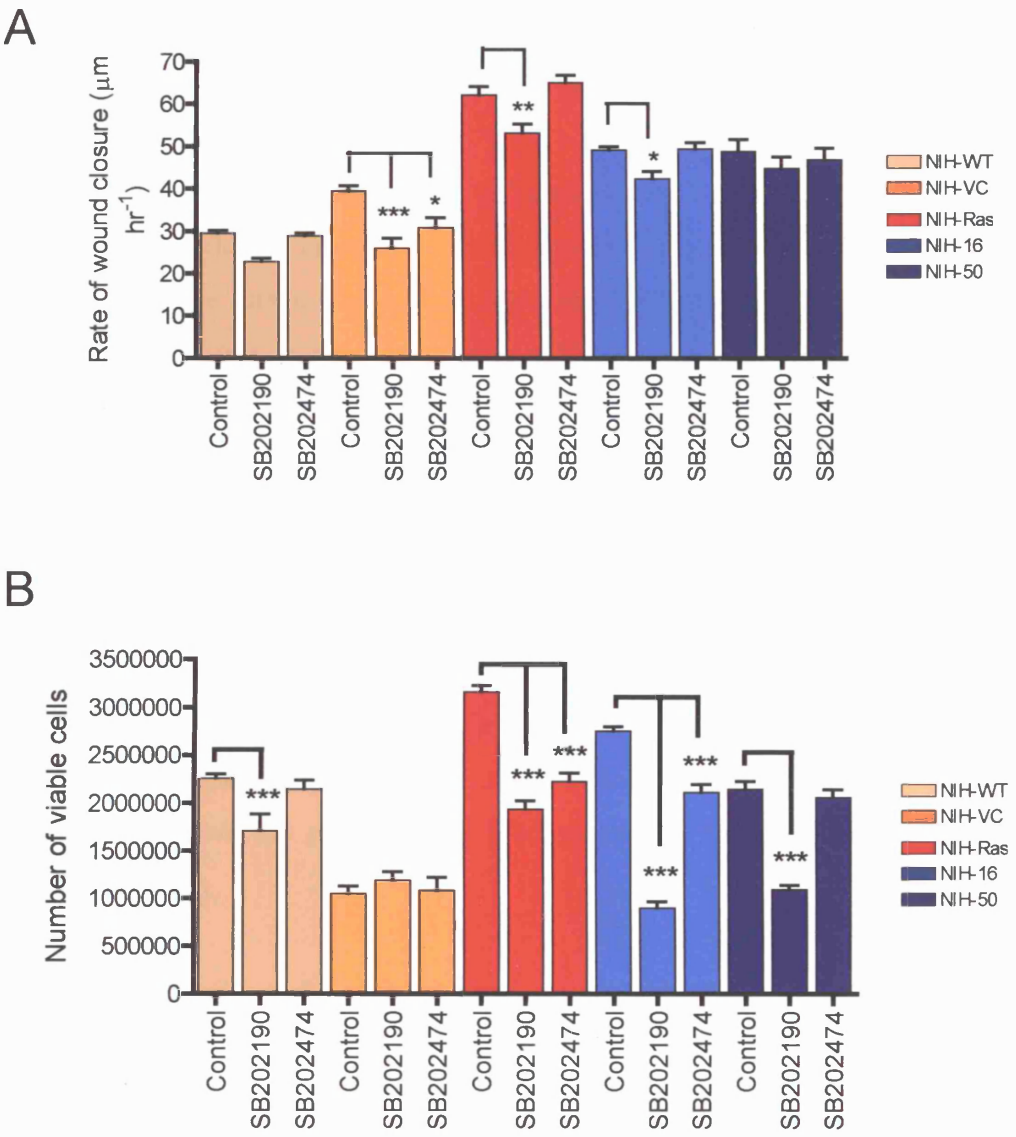

Figure 7.4 Does p38 inhibition affect wound healing **(A)** or saturation density **(B)** ? **A:** Wound healing experiment as described in Figure 8.3. 10 µM SB202190, a selective p38 inhibitor or 10 µM SB202474, an inactive analogue, were added to the media. Data represent the average of 4 separate wells repeated twice ± SEM. **B:** Saturation density assay as described in Figure 8.2. 10 µM SB202190 or SB202474 were added to the media. Data represents mean of duplicate plates repeated twice ± SEM. Data were analysed with GraphPad Prism software; Two-way ANOVA (*p <0.05, ** p <0.01, ***p<0.001).

Does Src kinase inhibition affect the transforming effect of hERG channel expression?

Src has been shown to interact directly with the hERG protein (Cayabyab & Schlichter, 2002). Src modulates hERG channel gating (by shifting activation to positive potentials) such that the channels pass more current (Cayabyab & Schlichter, 2002). Src activation is associated with cytoskeletal remodeling, increased cell motility and enhanced cell proliferation. The importance of Src signalling in hERG-expressing cells was investigated using the Src kinase inhibitor PP2. PP2 (10 μM) was added at the start of cell proliferation experiments performed using the Incucyte technique. PP2 caused a large and significant ($P < 0.001$) decrease in the rate of change in confluency for NIH-WT and -VC clones (Figure 7.5A). NIH-Ras also showed a decrease after PP2 application, although this smaller than that seen with NIH-WT and -VC and was not statistically significant. The rate of change in confluency of these clones was unaffected by PP3 (10 μM; an inactive analogue of PP2), added in parallel experiments. Interestingly, NIH-16 and -50 clones showed no change in the rate of change in confluency in the presence of either compound, suggesting that proliferation of hERG-expressing cells may not involve Src kinase activity.

PP2 and PP3 were also used in saturation density assays (Figure 7.5B). The saturation density of NIH-VC, -WT and -Ras clones remained relatively unchanged upon PP2 addition. In contrast, NIH-16 and NIH-50 showed a highly significant ($P < 0.001$) decrease in saturation density upon PP2 addition. In the case of NIH-50 this corresponded with a loss of ~125,000 cells, and 48 % of cells (Figure 7.5B). The PP3 had no effect on saturation density for all clones, except that it caused an apparent increase in cell number in the NIH-WT cells. PP2 and PP3 compounds were also used to analyse the effect of Src kinase inhibition on wound closure. In this assay it was found that PP2 produced a dramatic (>45 %) and highly significant ($P < 0.001$) decrease in the rate of wound closure for all clones, whereas PP3 was without effect (Appendix 2). The results with the Src inhibitor, PP2, suggest that the involvement of Src kinase activity in proliferation and high-density cell division are very different in hERG-expressing cells from the NIH-VC and -Ras clones.

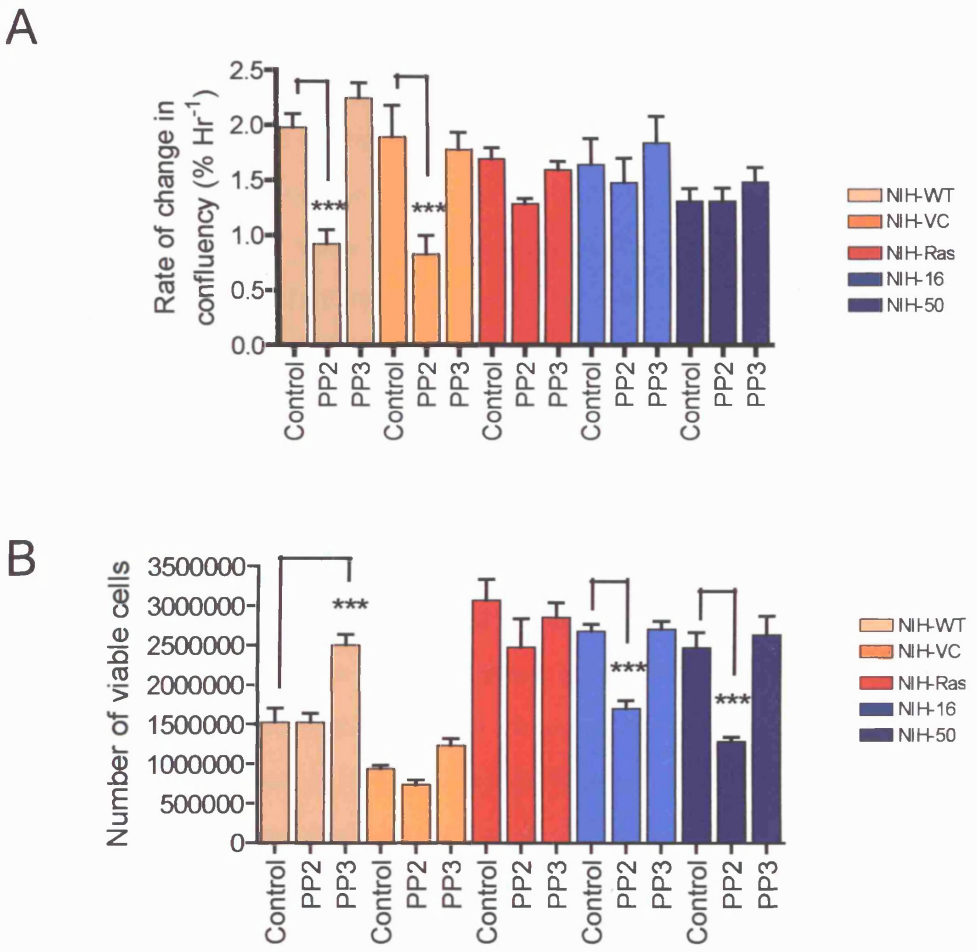

Figure 7.5 Effects of Src inhibition on **(A)** proliferation and **(B)** saturation density assays. **A:** Cells were allowed at adhere and spread before adding drugs (10 μM PP2 or PP3). Measurements of confluency were taken over a >48 hr period. Data represent the mean ± SEM of 4 separate wells in experiments performed on two separate occasions. **B:** Saturation density assay performed with 10 μM PP2 or PP3 added to the media. Plates were incubated for four further days and viable cells counted. Data represents mean ± SEM of duplicate plates in two seperate experiments. Data were analysed with GraphPad Prism software, using a two-way ANOVA (***$p<0.001$).

Does inhibition of PI3K alter the transforming effect of hERG channel expression?

Phosphoinositide 3-kinases (PI3Ks) are a class of lipid kinase known to be involved in cell proliferation, survival, and motility. PI3K is important in the activation of survival proteins, such as PKB/AKT and NF-κB (Fresno Vara *et al.*, 2004). PI3K activity prevents apoptosis and has an important role in cancer where oncogenes, such as Ras are able to up-regulate this kinase (Vivanco & Sawyers, 2002). PI3K activity is also key to the ability of nearly all cancer cell types to grow in a substratum-independent manner (Wang, 2004). Here, I wanted to investigate whether hERG expression can influence the survival ability of NIH-3T3 cells through PI3K signalling. This would help to explain why hERG expression increases growth in soft agar and reduces cell death in response to arsenic trioxide (see Figures 4.5B and 4.12).

The PI3K inhibitor LY294002 was tested in saturation density assays. The application of LY294002 (10 μM) reduced the saturation density of NIH-WT and -VC clones by 18 ± 4 % and 25 ± 2 %, respectively, although this did not achieve statistical significance in either case (Figure 7.6). The saturation density of NIH-Ras and NIH-50 clones was reduced to a greater extent (40 ± 3 % and 41 ± 5 % respectively), and was greater still for NIH-16 (52 ± 2 %). These reductions were all highly significant (see Figure 7.6). The inactive control compound LY30511 (10 μM) had minor, non-significant effects in all clones.

The PI3K inhibitor LY294002 was also assessed in cell proliferation assays in parallel with the inactive compound LY303511. LY294002 caused decreases in rate of change in confluency in all clones, with effects ranging from 23 ± 19 % (for NIH-16) to 45 ± 8 % (for NIH-Ras) (Appendix 1). LY30511 had no significant effect upon rate of change in confluency for any of the clones. Finally, the effects of LY294002 and LY30511 were also assessed in scratch wound assays. LY294002 significantly decreased the rate of wound closure in all clones, whilst the inactive analogue LY30511 showed only small effects on the rate of wound closure for any of the clones (Appendix 2). These results indicate that while PI3K inhibition decreases rates of wound closure and cell proliferation in all clones, the ability of hERG-expressing cells to grow at high densities appears to be highly dependent on PI3K activity.

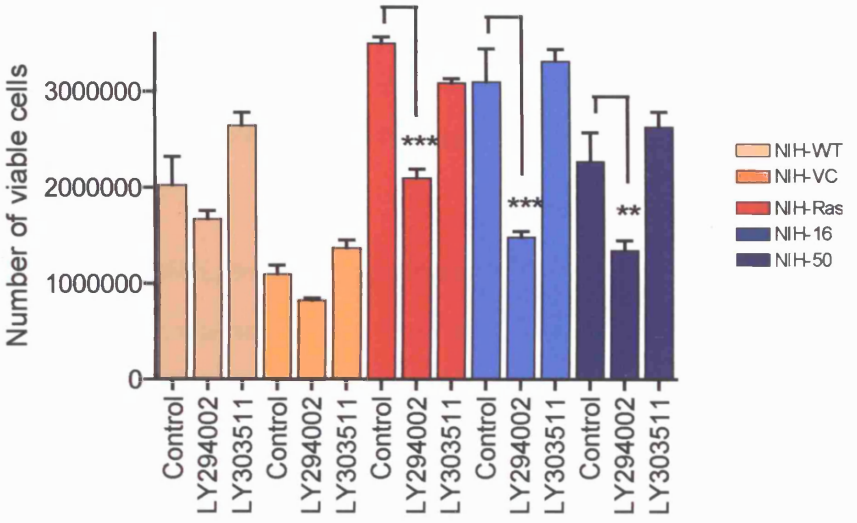

Figure 7.6 Effect of PI3K inhibition in saturation density assays. LY294002 (10 μM; PI3K inhibitor) or LY303511 (10 μM; inactive analogue) were added and cells incubated for four days before counting the number of viable cells. Data represents mean ± SEM of duplicate plates in two separate experiments. Data were analysed with GraphPad Prism software; Two-way ANOVA (** $p < 0.01$, *** $p < 0.001$).

Discussion

This Chapter has used a range of pharmacological protein kinase inhibitors to investigate the potential signalling pathways that hERG channel expression may influence in NIH-3T3 cells. My results indicate that pathways involving p38 MAPK, Src kinase, and PI3K kinase may all be necessary for the transforming effects of hERG expression.

hERG expression and PKC signalling

Stable hERG expression seemed to have little impact on the expression of PKCδ and PKCε isoenzymes. In all clones PKCδ levels increased in post-confluent cultures relative to sub-confluent cultures. This agrees with studies by Heit *et al.* (2001) who demonstrated that PKCδ is important for contact inhibition in NIH-3T3 cells and that its expression increases at cell confluency. Initiation of contact inhibition via PKCδ may be through interaction with cyclins D and E and may also involve regulation of p27 (a CDK inhibitor) (Heit *et al.*, 2001).

These data suggest that the tumour-suppressive effects of PKCδ have either been lost in NIH-Ras, -16 and -50 clones; or that these cells are able to negate growth inhibition signalling via up-regulation of a competing pathway(s). PKCε has been shown to be potentially oncogenic and its overexpression can lead to growth in soft agar, an increase in saturation density and tumour formation *in vivo* (Mischak *et al.*, 1993a). However, PKCε levels were not found to differ between control and hERG-expressing NIH-3T3 clones in this study. Thus, it seems unlikely that hERG removes contact inhibition of growth through PKCε signalling. Further evidence that PKC signalling is not involved in the loss of contact inhibition was obtained using the broad spectrum PKC inhibitor Bis-I, which had no effect in any of the NIH-3T3 clones in the saturation density assay.

Whilst PKC signalling does not seem to be involved in hERG-induced overgrowth, its role in cell motility was less clear. On the one hand rottlerin, a PKCδ-selective inhibitor, increased cell motility rates of NIH-VC, -WT, and -Ras clones, but had no effects on NIH-16 or -50 clones, suggesting a hERG expression-dependent difference. However, the specificity of rottlerin has been questioned, with at least one report suggesting that PKCδ inhibition by rottlerin is indirect

(Soltoff, 2001), and another reporting that even at 20 μM rottlerin is unable to significantly affect PKCδ activity (Davies *et al.*, 2000). Also both BIS-I and BIS-V produce small but significant increases in motility rates in all clones, suggesting a non-specific effect of these compounds. The potential lack of specificity of the protein kinase inhibitors used here means that further experiments are needed to establish fully a role for PKC signalling in hERG-transformed cells. Future studies could involve kinase assays used in parallel experiments to confirm the inhibition of PKC isoenzymes, or non-pharmacological approaches to (selective) PKC inhibition.

hERG and ERK-MAPK signalling

The phosphorylation, and by inference, activation state of ERK1/2 did not show any dramatic changes in NIH-16 or -50 clones relative to NIH-VC control cells, however, ERK1/2 activation was clearly evident in the NIH-Ras clone. Like NIH-VC cells, the NIH-16 and -50 clones showed marked decreases in phospho-ERK1/2 immunoreactivity upon reaching confluency. This result suggests that hERG expression does not lead to an increase in signalling through the MAPK pathway. NIH-50 did show a consistent (although small) increase in ERK1/2 activation relative to NIH-16 and -VC clones, but this may be due to clonal variation and may not be functionally important, since it did not correlate with saturation density results (where NIH-16 reaches a greater density). In all the clones tested the total ERK1/2 expression was similar in pre- and post-confluent cells. Thus, any changes in ERK1/2 phosphorylation are not attributable to changes in ERK1/2 expression levels. These results suggest that hERG expression does not reduce contact inhibition of growth through modulation of the ERK1/2 pathway.

ERK is known to have a role in the release and disassembly of focal adhesions, in turn allowing an increase in cell migration (Hood & Cheresh, 2002; Orr *et al.*, 2002). Indeed ERK activation is known to be important for the increased cell motility of Ras transformed cells (Bar-Sagi & Hall, 2000). The results from the use of the MEK inhibitor are in agreement with these previous findings and show a significant decrease in the rate of NIH-Ras migration on application of UO126. NIH-16 and NIH-50 both showed a small decrease in the rate of wound closure in the presence of U0126, but this was not different to the effect of this agent in NIH-VC cells. The decrease in rate of wound closure is not as substantial as might be expected. A possible concern is the stability of U0126 in culture medium at 37°C, as this compound is known to be unstable in

solution. Thus, it is possible that degradation of the inhibitor was significant over the course of the experiment. Although I was unable to confirm the continued activity of the inhibitor, I did observe that the rate of wound closure was linear with respect to time. This suggests the inhibitor remains at an effective inhibitory concentration throughout the experiment, however further work needs to be performed in order to confirm this.

p38 MAPK signalling is essential for hERG-induced overgrowth

EAG channel expression has been reported to cause an increased proliferation rate in NIH-3T3 cells via a mechanism that is sensitive to p38 MAPK inhibitors, but not MEK1/2 inhibitors (Hegle *et al.*, 2006). However, as has already been established, hERG channel expression has different effects on cell properties to EAG. This is most obvious in terms of cell proliferation, where in contrast to EAG, hERG expression failed to cause any significant enhancements in the NIH-3T3 clones. In cell proliferation assays and scratch wound healing assays the p38 MAPK inhibitors had no effect, whilst p38 inhibitors failed to affect cell proliferation and motility in NIH-3T3 clones. SB202190 caused a dramatic decrease in saturation density of the hERG expressing cells (Figure 7.4B). Since NIH-VC showed no decrease in saturation density with the p38 inhibitor it appeared that the concentration of SB202190 used was not toxic. SB202190 reduced the saturation density of both NIH-16 and -50 clones to similar levels to NIH-VC, suggesting that p38 MAPK activity is required for hERG to increase saturation density, and block contact inhibition. This result seems to be at odds with previous studies that have shown p38 to be a critical signalling protein in the mechanism of contact inhibition. Faust *et al.* (2005) showed that in FH109 human fibroblast cells p38 MAPK inhibition by SB203580 was sufficient to reduce contact inhibition. The authors also showed that a p38-deficient mouse embryonic fibroblast (MEF) cell-line was able to grow to a greater density than wildtype MEF cells (Faust *et al.*, 2005).

Why does p38 MAPK inhibition cause a decrease in saturation density in the hERG-expressing NIH-3T3 clones used in this study? The observation that SB202190 had no effect with NIH-VC suggests that in this NIH-3T3 cell-line p38 MAPK might not be responsible for regulating normal contact inhibition. A further possible explanation for the decrease in saturation density in NIH-Ras, -16 and -50 clones on application of SB202190 is the inhibition of the CMV promoter. A study by Bruening *et al.* (1998) reported that activation of the JNK and p38 (stress activated

MAPK) pathways increases transcription from the CMV promoter, whereas the p38 inhibitor SB203580 dramatically reduced transcription from this promoter (Bruening *et al.*, 1998). It is possible that the decrease in saturation density shown for NIH-Ras, -16 and -50 clones (Figure 7.4B) were due to a reduction in Ras and hERG transcription (under the control of CMV in these clones) rather than through p38 MAPK-dependent effects on contact inhibition. This effect may not be seen in the cell proliferation or migration assays due to their shorter assay lengths. This needs to be further investigated by using alternative means to decrease endogenous p38 MAPK activity and/or by examining effects of SB203580 on mRNA levels and functional expression of Ras and hERG in the NIH-Ras, -16 and -50 clones. In addition, if p38 MAPK signalling is indeed responsible for the increased saturation density of hERG-expressing NIH-3T3 cells then it would be expected that p38 activation would be greater in hERG-expressing cells relative to wild-type cell-lines.

hERG expression allows growth independently of Src activity, while the ability of hERG to increase saturation density is blocked by Src inhibitors

In this Chapter the involvement of Src kinase in hERG mediated-transformation was assessed using the Src inhibitor PP2 and its inactive analogue PP3. PP2 was shown to cause a decrease in the rate of wound closure in all clones and hence any differences in Src signalling relating to migration upon hERG expression could not be determined. This is perhaps not surprising as Src is known to be important for FAK phosphorylation and focal adhesion turnover during migration (Slack *et al.*, 2001; Brunton *et al.*, 2005).

Proliferation assays in the presence of PP2 have shown that the NIH-WT and -VC control clones, as well as NIH-Ras are dependent upon Src signalling for cell proliferation. In contrast, cell proliferation rates in the hERG-expressing clones NIH-16 and -50 were unaffected by PP2 application. These data suggest that hERG expression increases/activates a growth-inducing pathway that is independent of Src kinase activity, yet is not additive under normal culture conditions. In contrast to the effects of PP2 seen in proliferation assays, the hERG-expressing clones seem to be affected to a much greater extent than NIH-WT, VC or Ras clones in saturation density assays. Thus, it was found that in hERG-expressing clones PP2 reduces the saturation density to levels comparable with those of NIH-WT and VC clones. NIH-WT and -VC show

relatively little effect upon PP2 application; however, a decrease in cell number for NIH-WT and -VC might indicate decreased cell viability rather than a decrease in contact inhibition. Together these results suggest that hERG-induced release from contact inhibition is dependent on Src signalling.

Src is a non-receptor tyrosine kinase of known oncogenic potential that when over-expressed leads to loss of contact inhibition. Although a direct mechanistic link between Src activation and contact inhibition of growth has yet to be established, the idea that tyrosine kinases and the phosphorylation states of cell-cell adhesion molecules (e.g. cadherins) are important in the regulating contact inhibition is well accepted (Pani *et al.*, 2000). From my data it would seem reasonable to propose that hERG expression increases the activity of Src and this in turn is essential for loss of contact inhibition. hERG and Src proteins have been shown to interact in co-immunoprecipitation experiments and to interact functionally (Cayabyab & Schlichter, 2002); however, further experiments are needed to confirm the role of hERG in modulating Src activity.

PI3K inhibition reinstates contact inhibition in hERG-expressing NIH-3T3 cells

PI3K signalling does not seem to be altered in hERG-expressing NIH-3T3 clones at least in terms of cell migration or proliferation assays. In these assays, PI3K activity appears to be essential for wound closure and cell proliferation in all the clones tested, and this correlates well with previous studies that demonstrated the importance of PI3K activity (and thus PKB/AKT activity) in cell survival and proliferation (Vivanco & Sawyers, 2002). Interestingly, the PI3K inhibitor LY294002 reduced the saturation density of NIH-Ras, -16 and -50 clones to a much greater degree than the small decrease in saturation density seen in NIH-WT or -VC clones (Figure 7.6). Whilst a decrease in proliferation rate may help to explain this result (NIH-WT and -VC are plated at their saturation density and so will not be affected) it cannot account fully for such a dramatic decrease in saturation density.

The signalling pathways involved in contact inhibition of growth are still poorly understood and there are not yet any studies on the role of PI3K in this process. However, the data reported in this Chapter correlates well with a study that showed PI3K to be essential for cell-cell contact-initiated

proliferation. In an elegant set of experiments Nelson and Chen have isolated cell-cell contact from cell spreading in epithelial and smooth muscle cells (Nelson & Chen, 2002). Here the authors demonstrate that cell-cell contact is responsible for an increase in proliferation, and that this proliferation is reduced by the PI3K inhibitor LY294002. However, the authors go further and state that the phenomenon of contact inhibition could be caused by a change in cell spreading that is independent of the proliferative effect of cell-cell contact (Nelson & Chen, 2002). The idea that cell spreading is important for growth has been demonstrated in similar experiments with endothelial cells (Huang *et al.*, 1998). This theory does not agree with the observation that cell membrane proteins from confluent cultures of human fibroblast cells are sufficient to induce contact inhibition in sparsely plated cells (Wieser *et al.*, 1990; Gradl *et al.*, 1995). Whilst the results in this chapter have demonstrated that PI3K activity is essential for hERG and Ras induced overgrowth of NIH-3T3 cells, further studies will be needed before this mechanism can be thoroughly defined.

Conclusion

This Chapter has used a wide range of pharmacological kinase inhibitors (where possible with a closely related inactive control compound) and transformation assays to try and identify signalling pathways that may be influenced by hERG expression. Western blot experiments failed to show any substantial changes in NIH-3T3 cells after hERG expression. This suggests that while hERG may influence cell transformation via signalling pathways it does not do this via changes in expression levels of either ERK or PKC. Further assays have provided data to suggest a role for p38 MAPK, Src and PI3K signalling in mediating the transforming effects of hERG expression. Crucially, these experiments help to validate the idea that hERG channels may signal through protein kinase cascades. How precisely hERG is coupled to these intracellular signalling pathways needs further investigation.

Chapter 8 Concluding Discussion

The aim of this research project was to investigate the oncogenic potential of the recombinant hERG protein, expressed in a model cell background. Using a variety of assays I have investigated the effect of stable hERG channel expression on cell proliferation, morphology, cytoskeletal organisation, cell motility and contact inhibition in both NIH-3T3 and HEK293 cell backgrounds. hERG channel blockers, dominant-negative mutants, hERG channel trafficking inhibitors, changes in cell culture conditions, and protein kinase inhibitors have all been employed to investigate the changes in cell signalling that occurs with hERG channel expression.

hERG channel expression has similar transforming effects to the EAG channel, but is not involved in proliferation

Interest in the involvement of hERG in cancer development was sparked by the observation that hERG expression was increased in tumour cells relative to the healthy cells from which they originated (Bianchi *et al.*, 1998; Cherubini *et al.*, 2000; Masi *et al.*, 2005). In this study hERG expression in HEK293 and NIH-3T3 cells has shown transforming effects similar to those also reported with the closely related EAG K^+ channel. Expression of EAG and hERG channels each gives rise to adhesion-independent growth in soft agar assays. A loss of contact inhibited growth was also noted with both channels, although EAG expression formed discrete foci (Pardo *et al.*, 1999), whereas in this project hERG expression caused a much more diffuse pattern of overgrowth in the stable cell-lines used. hERG channel expression was also shown to cause a confluency-dependent change in cell morphology that resulted in a more spindle-like appearance. This morphology change seemed to be the result of a reduction in focal adhesion and stress fiber formation. A possible direct consequence of this was an observed increase in motility. However, there are important differences between the effects of EAG and hERG channel expression. EAG induces a dramatic increase in proliferation, whilst hERG channel expression showed no signs of increasing proliferation. This agrees with primary tissue studies where hERG expression has been found to correlate with the more aggressive types of cancers rather than hyper-proliferative lesions (Arcangeli, 2005).

It would seem that hERG channel expression in normal cells acts as a pro-survival tool rather than affecting the rate of cell proliferation. hERG expression increases growth in harsh environments, such as soft agar (adhesion-independent growth), confluent cultures, and gives rise to a reduced dependence on growth factors, especially if hERG is expressed at high levels (seen in the HEK293 clones). The observation that hERG channel expression showed reduced cell death in the presence of arsenic trioxide (relative to vector control cells) is also in support of the idea that hERG channel expression increases survival.

Growth in soft agar is an important finding, as these assays are known to correlate well with *in vivo* tumourigenicity assays. Other transformation phenotypes such as loss of contact inhibition and serum independence are dissociable from tumourorigenicity (Shin *et al.*, 1975). Growth of transplanted cells in immune-deficient animals, such as nude mice (which exhibit defective thymus development, and are functionally devoid of T cell-dependent immunity) or SCID (severe combined immune deficiency) mice, is acknowledged to be the gold standard for assessing oncogenic growth. The finding that hERG expression allows growth in soft agar and evidence that the EAG channel has shown growth in SCID mice (Pardo *et al.*, 1999) predicts that hERG expression should also allow growth *in vivo*. Indeed the stable cells used in this project have subsequently been used in nude mice assays. Preliminary results suggest that NIH-16 and NIH-50 clones do show the ability to cause tumour growth *in vivo*. However, it was found that the growth of the hERG-expressing tumours is much slower than that where v-Ras- or EAG-expressing cells have been introduced to "seed" tumour growth. This correlates well with the results from the soft agar assays, where the NIH-Ras clone forms many more viable colonies than the hERG-expressing clones. Thus, stable hERG expression is able to transform healthy cells (at least in the case of the NIH-3T3 and HEK293 cell-types), however its transformative activity is low compared to that observed for potent oncogenes, such as v-Ras.

Ion flux through the hERG channel is not important for the protein's transforming effects

An interesting and important finding in this project was that the effect of hERG on cell proliferation and motility appeared to be independent of ion flux through the channel. hERG channel-specific blockers were used in a variety of assays and no effects were observed at drug concentrations that should fully block channel conductance. Co-expression of dominant-negative

(G628S) hERG channel subunits also had no effect on hERG-induced cell transformation. These results may initially seem contradictory to those obtained in previous studies (LeppleWienhues *et al.*, 1996; Macfarlane & Sontheimer, 2000; Pillozzi *et al.*, 2002; Crociani *et al.*, 2003). However, it is important to note that in these previous studies far higher concentrations of compound have been applied, which may potentially lead to non-specific effects. Indeed, in the present study I found that exposure to high concentrations of terfenadine, dofetilide or fluoxetine might be toxic to the cells. These results could have been construed as being significant in the absence of the appropriate negative controls. The EAG channel has also been shown to induce its transforming effects upon the cell independently of ion flux (Hegle *et al.*, 2006). Hegle *et al.* have reported that expression of either Wild-type or a non-conducting EAG mutant channel (F456A) in NIH-3T3 cells was sufficient to increase proliferation, and reduce the serum dependence of growth. This provides further support for the idea that the hERG channel does not transform cells via ion flux or associated changes in membrane potential, even though (as shown in chapter 4) these are a consequence of hERG channel expression.

An important caveat to this conclusion is the absence of data showing that the transforming effects seen on expression of the hERG channel can be ablated by removal of the channel. hERG trafficking inhibitors used in an attempt to remove hERG channels from the plasma membrane, had very little impact on the transformed phenotype. This may be due to an ineffective inhibition of trafficking due to limitations of the compounds. Unfortunately attempts to generate an adenovirus expressing a dominant negative trafficking deficient (A561V) hERG channel mutant were unsuccessful. It is hoped that future work will be able to exploit the initial constructs generated in my project for further investigations. Whilst hERG expression correlates well with a transformed phenotype in HEK293 and NIH-3T3 clones there is not yet conclusive evidence to suggest that hERG is directly responsible for this effect.

It would seem very unlikely that a non-specific side effect of stable cell line generation could produce the transforming effects seen in the hERG expressing clones. This is especially true as similar effects were seen in multiple clones from different cell types, helping to rule out clonal variation and spontaneous transformation. The fact that vector control clones behave similarly to wild-type cells also argues that the process of generating the stable cell-line was not a cause of the changes observed in the behaviours of hERG-expressing cells. Vector control clones also

demonstrate that the expression of the pcDNA3 vector and subsequent growth in selection medium has little effect upon the cells. However, although all the evidence points to cell transformation being a direct effect of hERG channel expression, this theory still needs to be confirmed. A possible method for future investigations could be the use of RNAi to reduce hERG channel expression. This method was used to great effect in studies of the EAG channel (Pardo *et al.*, 1999; Weber *et al.*, 2006).

hERG is dependent on cell signalling pathways to generate a transformed phenotype

In recent studies researchers have begun to show that many different ion channels can have effects upon cell phenotype that cannot be explained just on the basis of ion flux (Kaczmarek, 2006). A recent key study in this field was performed by Hegle *et al.* (2006) who demonstrated a conformation dependent, and ion flux independent, p38 MAPK signalling property for EAG channels that is proposed to be responsible for the observed increase in cell proliferation rate (Hegle *et al.*, 2006). In the present study I have shown that ERK1/2 activation and expression levels are not affected by hERG expression, and that MEK inhibition does not have a substantial effect in hERG-expressing clones. In contrast, p38 MAPK signalling proved to be essential for the loss of contact inhibition seen with hERG-expressing NIH-3T3 clones. Kinase inhibitors used in this project also showed that PI3K and Src activation are required for loss of contact inhibition in hERG-expressing cells.

It was interesting that although hERG channel expression seemed to give no proliferative advantage to NIH-3T3 cells under normal culture conditions, hERG expression allowed unaltered growth in the presence of the Src kinase inhibitor PP2 (which significantly reduced growth in all other clones). Similarly hERG expression reduced cell death in the presence of arsenic trioxide. These results are again suggestive of a pro-survival role for hERG channels that warrants further study. Taken together the experimental results from this project suggest that hERG expression acts on the cell through PI3K and p38 MAPK signalling pathways. This occurs independently of hERG conductance, ERK1/2 or Src activation.

Clinical relevance of ion channels as therapeutic targets

The findings in this study provide evidence that expression of hERG in non-excitable cells is sufficient to give rise to a transformed phenotype. Indeed ongoing experiments appear to show

that hERG expression is able to cause tumorigenesis in mouse models. Together this indicates that the hERG expression seen in many primary tumours may be the cause of that cancer rather than simply an up-regulation of channel expression consequent to cancer development. This may have relevance to the future treatment of cancers, as abnormal hERG expression could be used as an indicator of early stage cancerous growth and those tumours most likely to metastasise.

It is becoming clear that many ion channels are potentially involved in the development of a cancerous phenotype. The expression of specific ion channels may be differentially regulated throughout the progression of a tumour. This has lead to the idea that the ion channels are necessary for the progression of the tumour and that blockade of ion channel function, or reduction in expression, may be of therapeutic benefit. Many studies have shown that block or reduction of expression of specific ion channels reduces the proliferation of the host cells. However, as mentioned in a recent review (Schönherr, 2005), there is presently insufficient evidence that these ion channels are active in the cancer tissues *in vivo*. So far, most studies have concentrated on investigating the effects of altering expression of these ion channels in cultured cells. *In vivo* the activity of ion channels may differ substantially from that seen in cultured cells. It is routine to record channel activity using patch clamp procedures in serum free recording conditions. The validity of these experiments is challenged by Kunzelmann who argues that the presence of serum is known to depolarise cells, thus changing the open probability of ion channels within the cell (Kunzelmann, 2005). This author goes further and points out that in many studies unsynchronized cells are used despite good evidence to suggest that ion channel expression changes, often dramatically, through the cell cycle. For these reasons it will need to be determined whether ion channels such as hERG are indeed active in primary tumours *in vivo* before commitment to drug design can begin. The data produced in this Thesis also demonstrate that attempts to reduce the hERG-transforming effect with channel blockers are likely to be futile, even if tissue-specific drugs could be developed, and other approaches to interfering with hERG function will need to be devised.

A major point of concern with drug block of ion channels as a therapeutic approach for treatment of cancer is the non-specific block of channels in normal healthy tissue. For instance block of the hERG channel may very well have beneficial effects upon tumour growth, but if the drugs cannot be made tissue specific then the patient will suffer from potentially lethal LQTs.

Ion channel expression in cancerous tissue may have a role to play in the prognosis of cancer. Tumour ion channel expression profiles can be referenced against a database to see how likely metastasis is, which drugs are likely to have a beneficial effect, and how advanced the tumour is. For instance, an increase in hERG expression in colon cancer may help to diagnose a metastatic phenotype. GIRK1 is also a good marker for prostate cancer (Schönherr, 2005). The ion channel expression profile may also help to indicate how heterogeneous the population of cancer cells are and thus which combinations of drugs should be used therapeutically. Infrared fluorophore-conjugated antibodies can now be viewed *in vivo* and so antibodies to ion channels may allow the detection of tumours that previously would remain undetected (Pardo *et al.*, 2005). The use of specific extracellular markers for cancer may allow the targeting of cytotoxic, anti-cancer drugs directly to that cancer. Antibodies can be used for directed drug action in the body. Antibodies specific to the hERG channel could be used to target therapeutically the hERG-expressing cancerous cells. This might be by facilitating the delivery of an enzyme that would locally convert a pro-drug into a cytotoxic chemical, or the antibody could be used to direct the hosts own immune system to attack the tumour, or perhaps the antibody could deliver radiation directly to the tumour (Pardo *et al.*, 2005). All of these methods would need to ensure that the cancerous tissue is preferentially targeted over natively hERG-expressing cells, such as cardiomyocytes and nervous tissue.

Experimental evidence provided in this Thesis suggests that hERG channel expression in non-excitable cells increases pro-survival signalling within the cell. This may be important in treatment of hERG-expressing cancers, and suggests that these cancers may have increased resistance to cytotoxic treatments used in chemotherapy. Instead a better course of action may be to combine these cytotoxic approaches with drugs designed to inhibit hERG-induced survival signalling.

Future work

In this study I have provided the foundations for further investigations into the mechanism by which hERG channel expression can transform non-excitable cells. Future studies are now needed to characterize more fully the changes in cell signalling pathways that occur with hERG

expression. Also, it will be important to investigate potential methods for reversing the transformed phenotype seen in this project, either using hERG protein trafficking inhibitors or RNAi techniques. There are also many further questions that need to be answered about the role of hERG in cancer, some of which are summarized below.

Are the results obtained in cultured cells consistent with those from primary cancers?

In this project stably transfected immortalised cell lines have been used to investigate the effects of hERG channel expression. The results of this study have shown that hERG is capable of transforming a cultured cell-line, however, the oncogenic potential of hERG needs now to be investigated in primary cancer cells. One of the main reasons for this is the difference in extracellular environment. Cancer cells will be surrounded by other similar cells all competing for nutrients that are in short supply. While hypoxic conditions can be created *in vitro* there are also many signalling molecules that may also be present in a developing tumour. For instance TNF-α is found at high concentrations in developing tumours and may have an effect upon the hERG mediated transformation seen in this study (see below). While cell-lines can be cultured on a variety of substrates, it is not possible to mimic precisely the extracellular environment of a tumour in the "test-tube". This may mean that potentially important cell-cell and cell-ECM interactions are absent. Therefore, studies in primary cancer tissue expressing hERG may provide more clinically relevance information than can be obtained using a cultured cell-line.

How does the hERG channel interact with signalling molecules?

As has been mentioned many times in this report, there is abundant data to suggest that the hERG channel may interact directly with cell signalling pathways, independently of ion flux. So far there is no definitive evidence that this is indeed the case and it is important that future studies address this issue, by asking the following questions: (1) how does hERG couple to intracellular signalling pathways? (2) Does hERG directly interact with membrane-bound signalling molecules? (3) Is the conformation of the hERG channel important for its interactions with intracellular signalling components?

This area of study may also provide answers as to the functions of the PAS domain of the hERG channel. With respect to this it is interesting that Heinemann and colleagues have recently

announced that their (as yet unpublished) results show an interaction between VHL and the hERG channel; if correct, these data will further confirm the regulation of hERG by hypoxia-activated mechanisms.

There is evidence linking hERG with a number of focal adhesion signalling proteins including FAK and integrins (Hofmann *et al.*, 2001; Cherubini *et al.*, 2002; Arcangeli *et al.*, 2004; Cherubini *et al.*, 2005). However, all of the data so far relies on co-immunoprecipitation and FRET-based techniques. These methods often fail to distinguish between direct protein-protein interactions, and non-direct interactions involving scaffolding molecules. Hence it is not yet possible to tell from these data which, if any, focal adhesion proteins directly interact with hERG. Data on direct hERG protein interactions may also be helped by investigations with hERG1b *N*-termini truncated transcript. hERG1b channels have no PAS domain and are unable to co-immunoprecipitate with β1-integrins (Cherubini *et al.*, 2005). This suggests that it is the *N*-terminal that is likely involved in the hERG channels interactions with the focal adhesion complex. This raises the issue of whether the hERG1b protein possesses the same oncogenic potential as the hERG1 channel if it cannot fully participate in a full spectrum of protein-protein interactions? There is already evidence to suggest that hERG1b is expressed in tumour cell-lines and primary tumours, and that its expression is cell cycle-dependent (Crociani *et al.*, 2003). Further work is also needed to ascertain the transforming ability of the hERG splice variant $hERG_{(USO)}$.

Are hERGs transforming effects dependent upon confluency or cell-cell contact?

In this project the transforming effects of hERG channel expression have appeared confluency dependent. It is not known whether the effects of the hERG channel upon transformation are potentiated by confluency or whether cell-cell contacts are essential for these effects. It is known that the continuous culture of NIH-3T3 cells at high density can lead to spontaneous transformation (Rubin, 2005). It is unlikely that spontaneous transforming events are responsible for the effects seen in clones NIH-16 and NIH-50 for a number of reasons: 1) both NIH-16 and NIH-50 clones exhibit nearly identical phenotypes, and 2) NIH-VC showed no evidence of spontaneous transformation in the assays used in this project. Even though spontaneous transformation may not be the cause of the observed transformation, similar processes within the NIH-3T3 cell line may potentiate hERG mediated transformation at high cell density. Hence it

will be important to investigate this effect more fully and whether this is a cell type specific phenomenon.

Is tumour necrosis factor important for hERG-mediated transformation?

An important area for future investigations is that of the hERG channel, and the TNF-α receptor (TNFR). NF-κB is a downstream target of TNFR activation and has been shown to be important in the development of a transformed phenotype. As discussed above, constitutive activation of NF-κB has been documented in many tumours, such as non-small-cell lung cancer, breast, prostrate, pancreatic, thyroid and melanoma (Richmond, 2002). The activation of NF-κB correlates with increased tumour growth, angiogenesis and metastasis in melanoma cells (Richmond, 2002). The block of NF-κB activation in tumour cells causes reduction of tumour formation, a reduction in VEGF production, and apoptosis (Sunwoo *et al.*, 2001; Richmond, 2002). Conversely, antisense treatment to decrease cellular levels of IκB results in oncogenic transformation (Royds *et al.*, 1998). hERG expression has been demonstrated to increase TNFR production and its localisation to the plasma membrane (Wang *et al.*, 2002). The hERG channel has also been shown to associate with TNFR in co-immunoprecipitation assays (Wang *et al.*, 2002). This interaction may be important for hERGs pro-survival signalling and also it's transforming effects because TNFR activation is important in the activation of the transcription factor NF-κB. Further, the increased amount and activity of TNFR in hERG expressing cancers leads to increased activity of NF-κB relative to non-hERG expressing cancer lines (Wang *et al.*, 2002).

How is the hERG channel involved in angiogenesis and hypoxia?

hERG expression may be important for cancer development in hypoxic conditions. hERG channels are modulated by hypoxic conditions such that they spend more time in the activated state (Fontana *et al.*). This could potentially alter the ability of the channel protein to interact with signalling cascades, analogous to the EAG channel (Hegle *et al.*, 2006). As already discussed, the regulation of the channel is thought to be via its HIF-1-like PAS domain (Morais Cabral *et al.*, 1998). hERG channel protein levels may also be regulated by hypoxic conditions, and it has been proposed by Heinemann et al. that the hERG channel may directed for degradation by a mechanism analogous to the regulation of HIF-1 by VHL.

Vascular endothelial growth factor (VEGF) is found in many hypoxic tumours and is highly important for angiogenesis – the development of new vasculature into developing tumours (Royds *et al.*, 1998; Ferrara *et al.*, 2003). VEGF promotes the proliferation and migration of epithelial cells into the tumour mass. This property of cancer cells has also been linked with hERG channel expression. Block of hERG channels decreased VEGF secretion in glioblastoma multiforme (GBM) cell-lines, but did not affect VEFG secretion in GBM cell lines not expressing hERG (Masi *et al.*, 2005). hERG channel-mediated expression of VEGF also correlates with the observation that hERG channel expression is increased in more developed, metastatic cancers (Lastraioli *et al.*, 2004; Masi *et al.*, 2005). While VEGF secretion correlates with hERG channel block Masi *et al.* propose that hERG current (or consequent biophysical effects) does not regulate VEGF secretion (Masi *et al.*, 2005). Their reasoning is that the hELK channel (which has similar voltage dependence of activation) cannot substitute for hERG expression, even though it should produce similar K^+ currents (Becchetti *et al.*, 2002). Instead the authors propose that hERG expression could increase VEGF secretion through PAS domain interactions.

Future studies should address the modulation of the hERG channel by hypoxia and the mechanism by which this happens. Further to this, studies should also look at the potential effects of hypoxia upon the transforming ability of the hERG channel. The results of these studies would potentially allow a more detailed understanding of hERG channel function in cancer.

Concluding statement

In this project I have found that the hERG channel can exert a transforming effect when stably expressed in immortalised, mammalian cell-lines. The expression of the hERG channel is responsible for changes in focal adhesions and cytoskeleton interactions that lead to increased cell migration and morphology changes. Interestingly these changes seem to be confluency-dependent. Adhesion-independent growth and loss of contact inhibition were also demonstrated in hERG expressing cells. Continuing *in vivo* assays in nude mice also promise to show tumorigenic properties of hERG channel expression in non-excitable cells. A variety of hERG channel blockers and a pore blocked dominant negative mutant were used to demonstrate for the first time that reduction/block of functional hERG current does not affect the transforming effects of hERG.

Whilst it was found that hERG channel expression gave effects upon cellular phenotype that are commonly associated with metastasis, there was no evidence for a proliferative advantage. While this may seem to disagree with other studies, this is the first investigation into cell proliferation upon hERG expression (with appropriate negative controls), rather than relying upon the effects of hERG channel blockers. Preliminary pharmacological investigations suggest that the hERG channel causes its transforming effects via signalling through PI3K, Src and p38 MAPK. Further investigations into this area should help to elucidate the protein-protein interactions of the hERG channel. This will lead to a better understanding of hERG channel signalling and may also provide new directions for therapeutic intervention in cancer.

Bibliography

ABDUL, M. & HOOSEIN, N. (2002). Voltage-gated potassium ion channels in colon cancer. *Oncology Report*, **9,** 961-4.

ABDUL, M. & HOOSEIN, N. (2002b). Expression and activity of potassium ion channels in human prostate cancer. *Cancer Letters*, **186,** 99-105.

ABRAMS, C.S. & ZHAO, W. (1995). SH3 domains specifically regulate kinase activity of expressed Src family proteins. *Journal of Biological Chemistry*, **270,** 333-9.

AGOCHIYA, M., BRUNTON, V.G., OWENS, D.W., PARKINSON, E.K., PARASKEVA, C., KEITH, W.N. & FRAME, M.C. (1999). Increased dosage and amplification of the focal adhesion kinase gene in human cancer cells. *Oncogene*, **18,** 5646-53.

AKBARALI, H.I., THATTE, H., HE, X.D., GILES, W.R. & GOYAL, R.K. (1999). Role of hERG-like K^+ currents in opossum esophageal circular smooth muscle. *American Journal of Physiology - Cell Physiology*, **277,** C1284-90.

ALLEN, M.J., OLIVER, S.D., NEWGREEN, M.W. & NICHOLS, D.J. (2002). Pharmacodynamic effect of continuous vs intermittent dosing of dofetilide on QT interval. *British Journal of Clinical Pharmacolology*, **53,** 59-65.

ANDERSON, C.L., DELISLE, B.P., ANSON, B.D., KILBY, J.A., WILL, M.L., TESTER, D.J., GONG, Q., ZHOU, Z., ACKERMAN, M.J. & JANUARY, C.T. (2006). Most LQT2 mutations reduce Kv11.1 (hERG) current by a class 2 (trafficking-deficient) mechanism. *Circulation*, **113,** 365-73.

APLIN, A.E., HOWE, A., ALAHARI, S.K. & JULIANO, R.L. (1998). Signal transduction and signal modulation by cell adhesion receptors: the role of integrins, cadherins, immunoglobulin-cell adhesion molecules, and selectins. *Pharmacol Review*, **50,** 197-263.

ARCANGELI, A. (2005). Expression and role of hERG channels in cancer cells. *Novartis Foundoundation Symposium*, **266,** 225-32; discussion 232-4.

ARCANGELI, A., BECCHETTI, A., CHERUBINI, A., CROCIANI, O., DEFILIPPI, P., GUASTI, L., HOFMANN, G., PILLOZZI, S., OLIVOTTO, M. & WANKE, E. (2004). Physical and functional interaction between integrins and hERG potassium channels. *Biochemical Society Transactions*, **32,** 826-827.

ARCANGELI, A., BIANCHI, L., BECCHETTI, A., FARAVELLI, L., CORONNELLO, M., MINI, E., OLIVOTTO, M. & WANKE, E. (1995). A novel inward-rectifying K^+ current with a cell-cycle dependence governs the resting potential of mammalian neuroblastoma cells. *Journal of Physiology-London*, **489,** 455-471.

ARCANGELI, A., ROSATI, B., CHERUBINI, A., CROCIANI, O., FONTANA, L., ZILLER, C., WANKE, E. & OLIVOTTO, M. (1997). hERG- and IRK-like inward rectifier currents are

sequentially expressed during neuronal development of neural crest cells and their derivatives. *European Journal of Neuroscience*, **9,** 2596-2604.

ARTYM, V.V. & PETTY, H.R. (2002). Molecular proximity of Kv1.3 voltage-gated potassium channels and beta(1)-integrins on the plasma membrane of melanoma cells: Effects of cell adherence and channel blockers. *Journal of General Physiology*, **120,** 29-37.

BAKIN, A.V., RINEHART, C., TOMLINSON, A.K. & ARTEAGA, C.L. (2002). p38 mitogen-activated protein kinase is required for TGFbeta-mediated fibroblastic transdifferentiation and cell migration. *Journal of Cell Science*, **115,** 3193-206.

BAR-SAGI, D. & HALL, A. (2000). Ras and Rho GTPases: a family reunion. *Cell*, **103,** 227-38.

BARBACID, M. (1987). ras genes. *Annual Review of Biochemistry*, **56,** 779-827.

BARON, W., DECKER, L., COLOGNATO, H. & FFRENCH-CONSTANT, C. (2003). Regulation of integrin growth factor interactions in oligodendrocytes by lipid raft microdomains. *Current Biology*, **13,** 151-155.

BAUER, C.K. (1998). The erg inwardly rectifying K^+ current and its modulation by thyrotrophin-releasing hormone in giant clonal rat anterior pituitary cells. *Journal of Physiology-London*, **510,** 63-70.

BAUER, C.K., SCHAFER, R., SCHIEMANN, D., REID, G., HANGANU, I. & SCHWARZ, J.R. (1999). A functional role of the erg-like inward-rectifying K+ current in prolactin secretion from rat lactotrophs. *Molecular and Cellular Endocrinology*, **148,** 37-45.

BECCHETTI, A., DE FUSCO, M., CROCIANI, O., CHERUBINI, A., RESTANO-CASSULINI, R., LECCHI, M., MASI, A., ARCANGELI, A., CASARI, G. & WANKE, E. (2002). The functional properties of the human ether-a-go-go-like (HELK2) K^+ channel. *European Journal of Neuroscience*, **16,** 415-28.

BENDER, K., WELLNER-KIENITZ, M.C. & POTT, L. (2002). Transfection of a phosphatidyl-4-phosphate 5-kinase gene into rat atrial myocytes removes inhibition of GIRK current by endothelin and alpha-adrenergic agonists. *FEBS Letters*, **529,** 356-60.

BENNETT, E.S., SMITH, B.A. & HARPER, J.M. (2004). Voltage-gated Na^+ channels confer invasive properties on human prostate cancer cells. *Pflugers Archiv-European Journal of Physiology*, **447,** 908-14.

BEZANILLA, F. (2005). Voltage-gated ion channels. *IEEE Trans Nanobioscience*, **4,** 34-48.

BHOWMICK, N.A., GHIASSI, M., BAKIN, A., AAKRE, M., LUNDQUIST, C.A., ENGEL, M.E., ARTEAGA, C.L. & MOSES, H.L. (2001a). Transforming growth factor-beta1 mediates epithelial to mesenchymal transdifferentiation through a RhoA-dependent mechanism. *Molecular Biology of the Cell*, **12,** 27-36.

BHOWMICK, N.A., ZENT, R., GHIASSI, M., MCDONNELL, M. & MOSES, H.L. (2001b). Integrin beta 1 signaling is necessary for transforming growth factor-beta activation of p38MAPK and epithelial plasticity. *Journal of Biological Chemistry*, **276,** 46707-13.

BIANCHI, L., WIBLE, B., ARCANGELI, A., TAGLIALATELA, M., MORRA, F., CASTALDO, P., CROCIANI, O., ROSATI, B., FARAVELLI, L., OLIVOTTO, M. & WANKE, E. (1998). hERG encodes a K^+ current highly conserved in tumors of different histogenesis: A selective advantage for cancer cells? *Cancer Research*, **58,** 815-822.

BILL, H.M., KNUDSEN, B., MOORES, S.L., MUTHUSWAMY, S.K., RAO, V.R., BRUGGE, J.S. & MIRANTI, C.K. (2004). Epidermal growth factor receptor-dependent regulation of integrin-mediated signaling and cell cycle entry in epithelial cells. *Molecular and Cellular Biology*, **24,** 8586-99.

BJORGE, J.D., JAKYMIW, A. & FUJITA, D.J. (2000). Selected glimpses into the activation and function of Src kinase. *Oncogene*, **19,** 5620-35.

BLOCH, M., OUSINGSAWAT, J., SIMON, R., SCHRAML, P., GASSER, T.C., MIHATSCH, M.J., KUNZELMANN, K. & BUBENDORF, L. (In press). KCNMA1 gene amplification promotes tumor cell proliferation in human prostate cancer. *Oncogene*, **In press,** 1-10.

BORTNER, C.D., HUGHES, F.M. & CIDLOWSKI, J.A. (1997). A primary role for K^+ and Na^+ efflux in the activation of apoptosis. *Journal of Biological Chemistry*, **272,** 32436-32442.

BRIDGLAND-TAYLOR, M.H., HARGREAVES, A.C., EASTER, A., ORME, A., HENTHORN, D.C., DING, M., DAVIS, A.M., SMALL, B.G., HEAPY, C.G., ABI-GERGES, N., PERSSON, F., JACOBSON, I., SULLIVAN, M., ALBERTSON, N., HAMMOND, T.G., SULLIVAN, E., VALENTIN, J.P. & POLLARD, C.E. (2006). Optimisation and validation of a medium-throughput electrophysiology-based hERG assay using IonWorkstrade mark HT. *Journal of Pharmacological and Toxicological Methods*, **58,** 189.

BROWN, L.F., BERSE, B., JACKMAN, R.W., TOGNAZZI, K., GUIDI, A.J., DVORAK, H.F., SENGER, D.R., CONNOLLY, J.L. & SCHNITT, S.J. (1995). Expression of vascular permeability factor (vascular endothelial growth factor) and its receptors in breast cancer. *Human Pathology*, **26,** 86-91.

BRUENING, W., GIASSON, B., MUSHYNSKI, W. & DURHAM, H.D. (1998). Activation of stress-activated MAP protein kinases up-regulates expression of transgenes driven by the cytomegalovirus immediate/early promoter. *Nucleic Acids Research*, **26,** 486-9.

BRUGGEMANN, A., STUHMER, W. & PARDO, L.A. (1997). Mitosis-promoting factor-mediated suppression of a cloned delayed rectifier potassium channel expressed in Xenopus oocytes. *Proceedings of the National Academy of Sciences of the United States of America*, **94,** 537-42.

BRUNTON, V.G., AVIZIENYTE, E., FINCHAM, V.J., SERRELS, B., METCALF, C.A., SAWYER, T.K. & FRAME, M.C. (2005). Identification of Src-specific phosphorylation site on focal adhesion kinase: Dissection of the role of Src SH2 and catalytic functions and their consequences for tumor cell behavior. *Cancer Research*, **65,** 1335-1342.

CAMACHO, J. (2006). Ether a go-go potassium channels and cancer. *Cancer Letters*, **233,** 1-9.

CAMACHO, J., SANCHEZ, A., STUHMER, W. & PARDO, L.A. (2000). Cytoskeletal interactions determine the electrophysiological properties of human EAG potassium channels. *Pflugers Archiv-European Journal of Physiology*, **441,** 167-174.

CARMELIET, P., DOR, Y., HERBERT, J.M., FUKUMURA, D., BRUSSELMANS, K., DEWERCHIN, M., NEEMAN, M., BONO, F., ABRAMOVITCH, R., MAXWELL, P., KOCH, C.J., RATCLIFFE, P., MOONS, L., JAIN, R.K., COLLEN, D. & KESHERT, E. (1998). Role of HIF-1alpha in hypoxia-mediated apoptosis, cell proliferation and tumour angiogenesis. *Nature*, **394,** 485-90.

CAYABYAB, F.S. & SCHLICHTER, L.C. (2002). Regulation of an ERG K^+ current by Src tyrosine kinase. *Journal of Biological Chemistry*, **277,** 13673-13681.

CHANG, J.H., GILL, S., SETTLEMAN, J. & PARSONS, S.J. (1995). c-Src regulates the simultaneous rearrangement of actin cytoskeleton, p190RhoGAP, and p120RasGAP following epidermal growth factor stimulation. *Journal of Cell Biology*, **130,** 355-68.

CHEN, L., WANG, L., ZHU, L., NIE, S., ZHANG, J., ZHONG, P., CAI, B., LUO, H. & JACOB, T.J. (2002). Cell cycle-dependent expression of volume-activated chloride currents in nasopharyngeal carcinoma cells. *American Journal of Physiology - Cell Physiology*, **283,** C1313-23.

CHERUBINI, A., HOFMANN, G., PILLOZZI, S., GUASTI, L., CROCIANI, O., CILIA, E., DI STEFANO, P., DEGANI, S., BALZI, M., OLIVOTTO, M., WANKE, E., BECCHETTI, A., DEFILIPPI, P., WYMORE, R. & ARCANGELI, A. (2005). Human ether-a-go-go-related gene 1 channels are physically linked to beta(1) integrins and modulate adhesion-dependent signaling. *Molecular Biology of the Cell*, **16,** 2972-2983.

CHERUBINI, A., PILLOZZI, S., HOFMANN, G., CROCIANI, O., GUASTI, L., LASTRAIOLI, E., POLVANI, S., MASI, A., BECCHETTI, A., WANKE, E., OLIVOTTO, M. & ARCANGELI, A. (2002). HERG K+ channels and beta 1 integrins interact through the assembly of a macromolecular complex. In *Cell Signaling, Transcription, and Translation as Therapeutic Targets*. pp. 559-561.

CHERUBINI, A., TADDEI, G.L., CROCIANI, O., PAGLIERANI, M., BUCCOLIERO, A.M., FONTANA, L., NOCI, I., BORRI, P., BORRANI, E., GIACHI, M., BECCHETTI, A., ROSATI, B., WANKE, E., OLIVOTTO, M. & ARCANGELI, A. (2000). hERG potassium channels are more frequently expressed in human endometrial cancer as compared to non-cancerous endometrium. *British Journal of Cancer*, **83,** 1722-1729.

CHIESA, N., ROSATI, B., ARCANGELI, A., OLIVOTTO, M. & WANKE, E. (1997). A novel role for hERG K^+ channels: spike-frequency adaptation. *Journal of Physiology-London*, **501 (Pt 2),** 313-8.

CHITTAJALLU, R., CHEN, Y., WANG, H., YUAN, X., GHIANI, C.A., HECKMAN, T., MCBAIN, C.J. & GALLO, V. (2002). Regulation of Kv1 subunit expression in oligodendrocyte

progenitor cells and their role in G1/S phase progression of the cell cycle. *Proceedings of the National Academy of Sciences of the United States of America*, **99,** 2350-5.

CLAPHAM, D.E., JULIUS, D., MONTELL, C. & SCHULTZ, G. (2005). International Union of Pharmacology. XLIX. Nomenclature and structure-function relationships of transient receptor potential channels. *Pharmacol Review*, **57,** 427-50.

COCKERILL, S., TOBIN, A., WILLARS, G., STANDEN, N. & MITCHESON, J. (2006). Modulation of hERG potassium currents by protein kinase C. Evidence for the direct phosphorylation of channel protein. *In press*.

CONLON, I. & RAFF, M. (2003). Differences in the way a mammalian cell and yeast cells coordinate cell growth and cell-cycle progression. *Journal of Biology*, **2,** 7.

CORDES, J.S., SUN, Z., LLOYD, D.B., BRADLEY, J.A., OPSAHL, A.C., TENGOWSKI, M.W., CHEN, X. & ZHOU, J. (2005). Pentamidine reduces hERG expression to prolong the QT interval. *British Journal of Pharmacology*, **145,** 15-23.

CROCIANI, O., CHERUBINI, A., PICCINI, E., POLVANI, S., COSTA, L., FONTANA, L., HOFMANN, G., ROSATI, B., WANKE, E., OLIVOTTO, M. & ARCANGELI, A. (2000). erg gene(s) expression during development of the nervous and muscular system of quail embryos. *Mechanisms of Development*, **95,** 239-243.

CROCIANI, O., GUASTI, L., BALZI, M., BECCHETTI, A., WANKE, E., OLIVOTTO, M., WYMORE, R.S. & ARCANGELI, A. (2003). Cell cycle-dependent expression of hERG1 and hERG1B isoforms in tumor cells. *Journal of Biological Chemistry*, **278,** 2947-2955.

CRUMB, W.J., JR. (2000). Loratadine blockade of K(+) channels in human heart: comparison with terfenadine under physiological conditions. *Journal of Pharmacology and Experimental Therapeutics*, **292,** 261-4.

CZARNECKI, A., DUFY-BARBE, L., HUET, S., ODESSA, M.F. & BRESSON-BEPOLDIN, L. (2003). Potassium channel expression level is dependent on the proliferation state in the GH3 pituitary cell line. *American Journal of Physiology - Cell Physiology*, **284,** C1054-C1064.

CZARNECKI, A., VAUR, S., DUFY-BARBE, L., DUFY, B. & BRESSON-BEPOLDIN, L. (2000). Cell cycle-related changes in transient K^+ current density in the GH3 pituitary cell line. *American Journal of Physiology - Cell Physiology*, **279,** C1819-28.

DARTSCH, P.C., RITTER, M., HAUSSINGER, D. & LANG, F. (1994). Cytoskeletal reorganization in NIH 3T3 fibroblasts expressing the ras oncogene. *European Journal of Cell Biology*, **63,** 316-25.

DATTA, S.R., BRUNET, A. & GREENBERG, M.E. (1999). Cellular survival: a play in three Akts. *Genes & Development*, **13,** 2905-27.

DAVIES, S.P., REDDY, H. & COHEN, P. (2000). Specificity and mechanism of action of some commonly used protein kinase inhibitors. *Biochemical Journal*, **351,** 95-105.

DAY, M.L., JOHNSON, M.H. & COOK, D.I. (1998). A cytoplasmic cell cycle controls the activity of a K^+ channel in pre-implantation mouse embryos. *Embo Journal*, **17,** 1952-60.

DAY, M.L., WINSTON, N., MCCONNELL, J.L., COOK, D. & JOHNSON, M.H. (2001). tiK^+ toK^+: an embryonic clock? *Reproduction, fertility and Development*, **13,** 69-79.

DE MIGUEL, M.P., ROYUELA, M., BETHENCOURT, F.R., SANTAMARIA, L., FRAILE, B. & PANIAGUA, R. (2000). Immunoexpression of tumour necrosis factor-alpha and its receptors 1 and 2 correlates with proliferation/apoptosis equilibrium in normal, hyperplasic and carcinomatous human prostate. *Cytokine*, **12,** 535-8.

DEEKEN, R., IVASHIKINA, N., CZIRJAK, T., PHILIPPAR, K., BECKER, D., ACHE, P. & HEDRICH, R. (2003). Tumour development in Arabidopsis thaliana involves the Shaker-like K^+ channels AKT1 and AKT2/3. *Plant Journal*, **34,** 778-87.

DIAZ, G.J., DANIELL, K., LEITZA, S.T., MARTIN, R.L., SU, Z., MCDERMOTT, J.S., COX, B.F. & GINTANT, G.A. (2004). The [3H]dofetilide binding assay is a predictive screening tool for hERG blockade and proarrhythmia: Comparison of intact cell and membrane preparations and effects of altering [K+]o. *Journal of Pharmacological and Toxicological Methods*, **50,** 187.

DISS, J.K., STEWART, D., FRASER, S.P., BLACK, J.A., DIB-HAJJ, S., WAXMAN, S.G., ARCHER, S.N. & DJAMGOZ, M.B. (1998). Expression of skeletal muscle-type voltage-gated Na^+ channel in rat and human prostate cancer cell lines. *FEBS Letters*, **427,** 5-10.

DOYLE, D.A., MORAIS CABRAL, J., PFUETZNER, R.A., KUO, A., GULBIS, J.M., COHEN, S.L., CHAIT, B.T. & MACKINNON, R. (1998). The structure of the potassium channel: molecular basis of K+ conduction and selectivity. *Science*, **280,** 69-77.

DUBOIS, J.M. & ROUZAIRE-DUBOIS, B. (2004). The influence of cell volume changes on tumour cell proliferation. *European Biophysical Journal*, **33,** 227-32. .

ECKHARDT, L.L., RAJAMANI, S. & JANUARY, C.T. (2005). Protein trafficking abnormalities: a new mechanism in drug-induced long QT syndrome. *British Journal of Pharmacology*, **145,** 3-4.

ELLISON, B.J. & RUBIN, H. (1992). Individual transforming events in long-term cell culture of NIH 3T3 cells as products of epigenetic induction. *Cancer Research*, **52,** 667-73.

FARIAS, L.M.B., OCANA, D.B., DIAZ, L., LARREA, F., AVILA-CHAVEZ, E., CADENA, A., HINOJOSA, L.M., LARA, G., VILLANUEVA, L.A., VARGAS, C., HERNANDEZ-GALLEGOS, E., CAMACHO-ARROYO, I., DUENAS-GONZALEZ, A., PEREZ-CARDENAS, E., PARDO, L.A., MORALES, A., TAJA-CHAYEB, L., ESCAMILLA, J., SANCHEZ-PENA, C. & CAMACHO, J. (2004). Ether a go-go potassium channels as human cervical cancer markers. *Cancer Research*, **64,** 6996-7001.

FAUST, D., DOLADO, I., CUADRADO, A., OESCH, F., WEISS, C., NEBREDA, A.R. & DIETRICH, C. (2005). p38alpha MAPK is required for contact inhibition. *Oncogene*, **29,** 7941.

FERRARA, N. & ALITALO, K. (1999). Clinical applications of angiogenic growth factors and their inhibitors. *Nature Medicine*, **5,** 1359-64.

FERRARA, N., GERBER, H.P. & LECOUTER, J. (2003). The biology of VEGF and its receptors. *Nature Medicine*, **9,** 669-76.

FICKER, E., DENNIS, A.T., OBEJERO-PAZ, C.A., CASTALDO, P., TAGLIALATELA, M. & BROWN, A.M. (2000). Retention in the endoplasmic reticulum as a mechanism of dominant-negative current suppression in human long QT syndrome. *Journal of Molecular and Cellular Cardiology*, **32,** 2327-2337.

FICKER, E., DENNIS, A.T., WANG, L. & BROWN, A.M. (2003). Role of the cytosolic chaperones Hsp70 and Hsp90 in maturation of the cardiac potassium channel hERG. *Circulation Research*, **92,** E87-E100.

FICKER, E., KURYSHEV, Y.A., DENNIS, A.T., OBEJERO-PAZ, C., LU, W., HAWRYLUK, P., WIBLE, B.A. & BROWN, A.M. (2004). Mechanisms of arsenic-induced prolongation of cardiac repolarization. *Molecular Pharmacology*, **66,** 33-44.

FONTANA, L., D'AMICO, M., CROCIANI, O., BIAGIOTTI, T., SOLAZZO, M., ROSATI, B., ARCANGELI, A., WANKE, E. & OLIVOTTO, M. (2001). Long-Term Modulation of hERG Channel Gating in Hypoxia. *Biochemical and Biophysical Research Communications*, **286,** 857-862.

FRASER, S.P., DISS, J.K., CHIONI, A.M., MYCIELSKA, M.E., PAN, H., YAMACI, R.F., PANI, F., SIWY, Z., KRASOWSKA, M., GRZYWNA, Z., BRACKENBURY, W.J., THEODOROU, D., KOYUTURK, M., KAYA, H., BATTALOGLU, E., DE BELLA, M.T., SLADE, M.J., TOLHURST, R., PALMIERI, C., JIANG, J., LATCHMAN, D.S., COOMBES, R.C. & DJAMGOZ, M.B. (2005). Voltage-gated sodium channel expression and potentiation of human breast cancer metastasis. *Clinical Cancer Research*, **11,** 5381-9.

FRASER, S.P., DISS, J.K., LLOYD, L.J., PANI, F., CHIONI, A.M., GEORGE, A.J. & DJAMGOZ, M.B. (2004). T-lymphocyte invasiveness: control by voltage-gated Na^+ channel activity. *FEBS Letters*, **569,** 191-4.

FRASER, S.P., SALVADOR, V., MANNING, E.A., MIZAL, J., ALTUN, S., RAZA, M., BERRIDGE, R.J. & DJAMGOZ, M.B. (2003). Contribution of functional voltage-gated Na+ channel expression to cell behaviors involved in the metastatic cascade in rat prostate cancer: I. Lateral motility. *Journal of Cellular Physiology.*, **195,** 479-87.

FRESNO VARA, J.A., CASADO, E., DE CASTRO, J., CEJAS, P., BELDA-INIESTA, C. & GONZALEZ-BARON, M. (2004). PI3K/Akt signalling pathway and cancer. *Cancer Treatment Review*, **30,** 193-204.

FRIEDL, P. (2004). Prespecification and plasticity: shifting mechanisms of cell migration. *Current Opinion in Cell Biology*, **16,** 14-23.

FRIEDL, P., HEGERFELDT, Y. & TUSCH, M. (2004). Collective cell migration in morphogenesis and cancer. *International Journal of developmental biology*, **48,** 441-9.

FRISCH, S.M. & FRANCIS, H. (1994). Disruption of epithelial cell-matrix interactions induces apoptosis. *Journal of Cell Biology*, **124,** 619-26.

FRISCH, S.M. & SCREATON, R.A. (2001). Anoikis mechanisms. *Current Opinion in Cell Biology*, **13,** 555-62.

FRISCH, S.M., VUORI, K., RUOSLAHTI, E. & CHAN-HUI, P.Y. (1996). Control of adhesion-dependent cell survival by focal adhesion kinase. *Journal of Cell Biology*, **134,** 793-9.

GAVRILOVA-RUCH, O., SCHONHERR, K., GESSNER, G., SCHÖNHERR, R., KLAPPERSTUCK, T., WOHLRAB, W. & HEINEMANN, S.H. (2002). Effects of imipramine on ion channels and proliferation of IGR1 melanoma cells. *Journal of Membrane Biology*, **188,** 137-149.

GHIANI, C.A., YUAN, X., EISEN, A.M., KNUTSON, P.L., DEPINHO, R.A., MCBAIN, C.J. & GALLO, V. (1999). Voltage-activated K+ channels and membrane depolarization regulate accumulation of the cyclin-dependent kinase inhibitors p27(Kip1) and p21(CIP1) in glial progenitor cells. *Journal of Neuroscience*, **19,** 5380-92.

GILLE, H. & DOWNWARD, J. (1999). Multiple ras effector pathways contribute to G(1) cell cycle progression. *Journal of Biological Chemistry*, **274,** 22033-40.

GONG, Q., ANDERSON, C.L., JANUARY, C.T. & ZHOU, Z. (2002). Role of glycosylation in cell surface expression and stability of HERG potassium channels. *American Journal of Physiology-Heart And Circulation Physiology*, **283,** H77-84.

GRADL, G., FAUST, D., OESCH, F. & WIESER, R.J. (1995). Density-dependent regulation of cell growth by contactinhibin and the contactinhibin receptor. *Current Biology*, **5,** 526-35.

GREIG, R.G., KOESTLER, T.P., TRAINER, D.L., CORWIN, S.P., MILES, L., KLINE, T., SWEET, R., YOKOYAMA, S. & POSTE, G. (1985). Tumorigenic and metastatic properties of "normal" and ras-transfected NIH/3T3 cells. *Proceedings of the National Academy of Sciences of the United States of America*, **82,** 3698-701.

GREWAL, S.S. & EDGAR, B.A. (2003). Controlling cell division in yeast and animals: does size matter? *Journal of Biology*, **2,** 5.

GRUNDEL, R. & RUBIN, H. (1992). Adaptation and Selection as Factors in the Spontaneous Transformation of Nih-3t3 Cells. *Carcinogenesis*, **13,** 1873-1877.

GUO, T.B., LU, J., LI, T., LU, Z., XU, G., XU, M., LU, L. & DAI, W. (2005). Insulin-activated, K+-channel-sensitive Akt pathway is primary mediator of ML-1 cell proliferation. *American Journal of Physiology - Cell Physiology*, **289,** C257-63.

HAHN, S.J., CHOI, J.S., RHIE, D.J., OH, C.S., JO, Y.H. & KIM, M.S. (1999). Inhibition by fluoxetine of voltage-activated ion channels in rat PC12 cells. *European Journal of Pharmacology*, **367,** 113-8.

HANAHAN, D. & WEINBERG, R.A. (2000). The hallmarks of cancer. *Cell*, **100,** 57-70.

HANCOX, J.C., LEVI, A.J. & WITCHEL, H.J. (1998). Time course and voltage dependence of expressed HERG current compared with native "rapid" delayed rectifier K current during the cardiac ventricular action potential. *Pflugers Archiv-European Journal of Physiology*, **436,** 843-853.

HARDY, M.E., LAWRENCE, C.L., STANDEN, N.B. & RODRIGO, G.C. (2006). Can optical recordings of membrane potential be used to screen for drug-induced action potential prolongation in single cardiac myocytes? *Journal of Pharmacological and Toxicological Methods*, **54,** 173-82.

HEGLE, A.P., MARBLE, D.D. & WILSON, G.F. (2006). A voltage-driven switch for ion-independent signaling by ether-a-go-go K+ channels. *Proceedings of the National Academy of Sciences of the United States of America*, **103,** 2886-2891.

HEIT, I., WIESER, R.J., HERGET, T., FAUST, D., BORCHERT-STUHLTRAGER, M., OESCH, F. & DIETRICH, C. (2001). Involvement of protein kinase Cdelta in contact-dependent inhibition of growth in human and murine fibroblasts. *Oncogene*, **20,** 5143-54.

HILLE, B. (2001). *Ion channels of excitable membranes*. Massachusetts: Sinauer Associates.

HISCOX, S., MORGAN, L., GREEN, T.P., BARROW, D., GEE, J. & NICHOLSON, R.I. (2006). Elevated Src activity promotes cellular invasion and motility in tamoxifen resistant breast cancer cells. *Breast Cancer Research and Treatment*, **97,** 263-74.

HOFMANN, G., BERNABEI, P.A., CROCIANI, O., CHERUBINI, A., GUASTI, L., PILLOZZI, S., LASTRAIOLI, E., POLVANI, S., BARTOLOZZI, B., SOLAZZO, V., GRAGNANI, L., DEFILIPPI, P., ROSATI, B., WANKE, E., OLIVOTTO, R. & ARCANGELI, A. (2001). hERG K+ channels activation during beta(1) integrin-mediated adhesion to fibronectin induces an up-regulation of alpha(v)beta(3) integrin in the preosteoclastic leukemia cell line FLG 29.1. *Journal of Biological Chemistry*, **276,** 4923-4931.

HOOD, J.D. & CHERESH, D.A. (2002). Role of integrins in cell invasion and migration. *Nature Reviews Cancer*, **2,** 91-100.

HUANG, S., CHEN, C.S. & INGBER, D.E. (1998). Control of cyclin D1, p27(Kip1), and cell cycle progression in human capillary endothelial cells by cell shape and cytoskeletal tension. *Molecular Biology of the Cell*, **9,** 3179-93.

HUGHES, P.E. & PFAFF, M. (1998). Integrin affinity modulation. *Trends in Cell Biology*, **8,** 359-64.

HUTTER, D.E., TILL, B.G. & GREENE, J.J. (1997). Redox state changes in density-dependent regulation of proliferation. *Experimental cell research*, **232,** 435-8.

IRBY, R.B. & YEATMAN, T.J. (2000). Role of Src expression and activation in human cancer. *Oncogene*, **19,** 5636-42.

JAAKKOLA, P., MOLE, D.R., TIAN, Y.M., WILSON, M.I., GIELBERT, J., GASKELL, S.J., KRIEGSHEIM, A., HEBESTREIT, H.F., MUKHERJI, M., SCHOFIELD, C.J., MAXWELL, P.H.,

PUGH, C.W. & RATCLIFFE, P.J. (2001). Targeting of HIF-alpha to the von Hippel-Lindau ubiquitylation complex by O2-regulated prolyl hydroxylation. *Science*, **292,** 468-72.

JAGER, H., DREKER, T., BUCK, A., GIEHL, K., GRESS, T. & GRISSMER, S. (2004). Blockage of intermediate-conductance Ca^{2+}-activated K^+ channels inhibit human pancreatic cancer cell growth in vitro. *Molecular Pharmacology*, **65,** 630-8.

JAINCHILL, J.L., AARONSON, S.A. & TODARO, G.J. (1969). Murine sarcoma and leukemia viruses: assay using clonal lines of contact-inhibited mouse cells. *Journal of Virology*, **4,** 549-53.

JIANG, B., HATTORI, N., LIU, B., NAKAYAMA, Y., KITAGAWA, K., SUMITA, K. & INAGAKI, C. (2004). Expression and roles of Cl- channel ClC-5 in cell cycles of myeloid cells. *Biochemical and Biophysical Research Communications*, **317,** 192-7.

JOUANNEAU, J., LONGUET, M. & BERTRAND, S. (1989). Transformed NIH 3T3 cells expressing human melanoma N-ras oncogene metastasize to lymph node in nude mice. *Clinical and Experimental Metastasis*, **7,** 391-403.

JULIANO, R.L. (2002). Signal transduction by cell adhesion receptors and the cytoskeleton: Functions of integrins, cadherins, selectins, and immunoglobulin-superfamily members. *Annual Review of Pharmacology and Toxicology*, **42,** 283-323.

KACZMAREK, L.K. (2006). Non-conducting functions of voltage-gated ion channels. *Nature Reviews Neuroscience*, **7,** 761-71.

KAGAN, A., YU, Z., FISHMAN, G.I. & MCDONALD, T.V. (2000). The dominant negative LQT2 mutation A561V reduces wild-type HERG expression. *Journal of Biological Chemistry*, **275,** 11241-8.

KALLURI, R. & NEILSON, E.G. (2003). Epithelial-mesenchymal transition and its implications for fibrosis. *Journal of Clinical Investigations*, **112,** 1776-84.

KATZ, B.Z., ROMER, L., MIYAMOTO, S., VOLBERG, T., MATSUMOTO, K., CUKIERMAN, E., GEIGER, B. & YAMADA, K.M. (2003). Targeting membrane-localized focal adhesion kinase to focal adhesions: roles of tyrosine phosphorylation and SRC family kinases. *Journal of Biological Chemistry*, **278,** 29115-20.

KAWAKAMI, T., KAWAKAMI, Y., AARONSON, S.A. & ROBBINS, K.C. (1988). Acquisition of Transforming Properties by FYN, a Normal SRC-Related Human Gene *Proceedings of the National Academy of Sciences of the United States of America*, **85,** 3870.

KAZANSKY, A.V. & ROSEN, J.M. (2001). Signal transducers and activators of transcription 5B potentiates v-Src-mediated transformation of NIH-3T3 cells. *Cell Growth & Differentiation*, **12,** 1-7.

KEATING, M.T. & SANGUINETTI, M.C. (2001). Molecular and cellular mechanisms of cardiac arrhythmias. *Cell*, **104,** 569-80.

KEELY, P., PARISE, L. & JULIANO, R. (1998). Integrins and GTPases in tumour cell growth, motility and invasion. *Trends in Cell Biology*, **8,** 101-106.

KIEMER, A.K., TAKEUCHI, K. & QUINLAN, M.P. (2001). Identification of genes involved in epithelial-mesenchymal transition and tumor progression. *Oncogene*, **20,** 6679-88.

KIM, J.H., KANG, M.J., PARK, C.U., KWAK, H.J., HWANG, Y. & KOH, G.Y. (1999). Amplified CDK2 and cdc2 activities in primary colorectal carcinoma. *Cancer*, **85,** 546-53.

KNAUF, J.A., OUYANG, B., KNUDSEN, E.S., FUKASAWA, K., BABCOCK, G. & FAGIN, J.A. (2006). Oncogenic RAS induces accelerated transition through G2/M and promotes defects in the G2 DNA damage and mitotic spindle checkpoints. *Journal of Biological Chemistry*, **281,** 3800-9.

KOONG, A.C., CHEN, E.Y. & GIACCIA, A.J. (1994). Hypoxia causes the activation of nuclear factor kappa B through the phosphorylation of I kappa B alpha on tyrosine residues. *Cancer Research*, **54,** 1425-30.

KRAUSS, G. (2003). *Biochemistry of Signal Transduction and Regulation*: WILEY-VCH Verlag GmbH & Co.

KUGA, T., KOBAYASHI, S., HIRAKAWA, Y., KANAIDE, H. & TAKESHITA, A. (1996). Cell cycle--dependent expression of L- and T-type Ca2+ currents in rat aortic smooth muscle cells in primary culture. *Circulation Research*, **79,** 14-9.

KUNZELMANN, K. (2005). Ion channels and cancer. *Journal of Membrane Biology*, **205,** 159-73.

KUO, W.Y., LIN, J.Y. & TANG, T.K. (2000). Human glucose-6-phosphate dehydrogenase (G6PD) gene transforms NIH 3T3 cells and induces tumors in nude mice. *International Journal of Cancer*, **85,** 857-864.

KUPERSHMIDT, S., SNYDERS, D.J., RAES, A. & RODEN, D.M. (1998). A K^+ channel splice variant common in human heart lacks a C- terminal domain required for expression of rapidly activating delayed rectifier current. *Journal of Biological Chemistry*, **273,** 27231-27235.

KUROKAWA, H., LEE, D.S., WATANABE, M., SAGAMI, I., MIKAMI, B., RAMAN, C.S. & SHIMIZU, T. (2004). A redox-controlled molecular switch revealed by the crystal structure of a bacterial heme PAS sensor. *Journal of Biological Chemistry*, **279,** 20186-93.

KURYSHEV, Y.A., FICKER, E., WANG, L., HAWRYLUK, P., DENNIS, A.T., WIBLE, B.A., BROWN, A.M., KANG, J.S., CHEN, X.L., SAWAMURA, K., REYNOLDS, W. & RAMPE, D. (2005). Pentamidine-induced long QT syndrome and block of hERG trafficking. *Journal of Pharmacology and Experimental Therapeutics*, **312,** 316-323.

LASTRAIOLI, E., GUASTI, L., CROCIANI, O., POLVANI, S., HOFMANN, G., WITCHEL, H., BENCINI, L., CALISTRI, M., MESSERINI, L., SCATIZZI, M., MORETTI, R., WANKE, E., OLIVOTTO, M., MUGNAI, G. & ARCANGELI, A. (2004). herg1 gene and hERG1 protein are overexpressed in colorectal cancers and regulate cell invasion of tumor cells. *Cancer Research*, **64,** 606-611.

LAURITZEN, I., ZANZOURI, M., HONORE, E., DUPRAT, F., EHRENGRUBER, M.U., LAZDUNSKI, M. & PATEL, A.J. (2003). K+-dependent cerebellar granule neuron apoptosis. Role of task leak K+ channels. *Journal of Biological Chemistry*, **278,** 32068-76.

LEPPLEWIENHUES, A., BERWECK, S., BOHMIG, M., LEO, C.P., MEYLING, B., GARBE, C. & WIEDERHOLT, M. (1996). K^+ channels and the intracellular calcium signal in human melanoma cell proliferation. *Journal of Membrane Biology*, **151,** 149-157.

LODISH, H., BERK, A., MATSUDARIA, P., KAISER, C.A., KREIGER, M., SCOTT, M.P., ZIPURSKY, S.L. & DARNELL, J. (2003). *Molecular Cell Biology*. New York: Tenny, S.

LOWRY, O.H., ROSEBROUGH, N.J., LEWIS FARR, A. & RANDALL, R.J. (1951). Protein Measurement with the Folin Phenol Reagent. *Journal of Biological Chemistry*, **193,** 265.

MACFARLANE, S.N. & SONTHEIMER, H. (2000). Changes in ion channel expression accompany cell cycle progression of spinal cord astrocytes. *Glia*, **30,** 39-48.

MAENO, E., SHIMIZU, T. & OKADA, Y. (2006). Normotonic cell shrinkage induces apoptosis under extracellular low Cl conditions in human lymphoid and epithelial cells. *Acta Physiol (Oxf)*, **187,** 217-22.

MAERTENS, C., WEI, L., VOETS, T., DROOGMANS, G. & NILIUS, B. (1999). Block by fluoxetine of volume-regulated anion channels. *British Journal of Pharmacology*, **126,** 508-14.

MASI, A., BECCHETTI, A., RESTANO-CASSULINI, R., POLVANI, S., HOFMANN, G., BUCCOLIERO, A.M., PAGLIERANI, M., POLLO, B., TADDEI, G.L., GALLINA, P., DI LORENZO, N., FRANCESCHETTI, S., WANKE, E. & ARCANGELI, A. (2005). hERG1 channels are overexpressed in glioblastoma multiforme and modulate VEGF secretion in glioblastoma cell lines. *British Journal of Cancer*, **93,** 781-92.

MASSZI, A., DI CIANO, C., SIROKMANY, G., ARTHUR, W.T., ROTSTEIN, O.D., WANG, J., MCCULLOCH, C.A., ROSIVALL, L., MUCSI, I. & KAPUS, A. (2003). Central role for Rho in TGF-beta1-induced alpha-smooth muscle actin expression during epithelial-mesenchymal transition. *American Journal of physiology-Renal Physiology*, **284,** F911-24.

MEANS, A.R. (1994). Calcium, Calmodulin and Cell-Cycle Regulation. *FEBS Letters*, **347,** 1-4.

MERCER, K., CHILOECHES, A., HUSER, M., KIERNAN, M., MARAIS, R. & PRITCHARD, C. (2002). ERK signalling and oncogene transformation are not impaired in cells lacking A-Raf. *Oncogene*, **21,** 347-355.

MEYER, R. & HEINEMANN, S.H. (1998). Characterization of an eag-like potassium channel in human neuroblastoma cells. *Journal of Physiology-London*, **508,** 49-56.

MILNES, J.T., DEMPSEY, C.E., RIDLEY, J.M., CROCIANI, O., ARCANGELI, A., HANCOX, J.C. & WITCHEL, H.J. (2003). Preferential closed channel blockade of HERG potassium currents by chemically synthesised BeKm-1 scorpion toxin. *FEBS Letters*, **547,** 20-6.

MISCHAK, H., GOODNIGHT, J.A., KOLCH, W., MARTINY-BARON, G., SCHAECHTLE, C., KAZANIETZ, M.G., BLUMBERG, P.M., PIERCE, J.H. & MUSHINSKI, J.F. (1993a). Overexpression of protein kinase C-delta and -epsilon in NIH 3T3 cells induces opposite effects on growth, morphology, anchorage dependence, and tumorigenicity. *Journal of Biological Chemistry*, **268,** 6090-6.

MISCHAK, H., PIERCE, J.H., GOODNIGHT, J., KAZANIETZ, M.G., BLUMBERG, P.M. & MUSHINSKI, J.F. (1993b). Phorbol ester-induced myeloid differentiation is mediated by protein kinase C-alpha and -delta and not by protein kinase C-beta II, -epsilon, -zeta, and -eta. *Journal of Biological Chemistry*, **268,** 20110-5.

MITCHESON, J.S., CHEN, J. & SANGUINETTI, M.C. (2000). Trapping of a methanesulfonanilide by closure of the hERG potassium channel activation gate. *Journal of General Physiology*, **115,** 229-239.

MITCHESON, J.S. & SANGUINETTI, M.C. (1999). Biophysical properties and molecular basis of cardiac rapid and slow delayed rectifier potassium channels. *Cellular Physiology and Biochemistry*, **9,** 201-16.

MIZEJEWSKI, G.J. (1999). Role of integrins in cancer: survey of expression patterns. *Proc Soc Exp Biol Med*, **222,** 124-38.

MORAIS CABRAL, J.H., LEE, A., COHEN, S.L., CHAIT, B.T., LI, M. & MACKINNON, R. (1998). Crystal structure and functional analysis of the HERG potassium channel N terminus: a eukaryotic PAS domain. *Cell*, **95,** 649-55.

MU, D., CHEN, L., ZHANG, X., SEE, L.H., KOCH, C.M., YEN, C., TONG, J.J., SPIEGEL, L., NGUYEN, K.C., SERVOSS, A., PENG, Y., PEI, L., MARKS, J.R., LOWE, S., HOEY, T., JAN, L.Y., MCCOMBIE, W.R., WIGLER, M.H. & POWERS, S. (2003). Genomic amplification and oncogenic properties of the KCNK9 potassium channel gene. *Cancer Cell*, **3,** 297-302.

MUTHUSWAMY, S.K., SIEGEL, P.M., DANKORT, D.L., WEBSTER, M.A. & MULLER, W.J. (1994). Mammary tumors expressing the neu proto-oncogene possess elevated c-Src tyrosine kinase activity. *Molecular and Cellular Biology*, **14,** 735-43.

NAPP, J., MONJE, F., STUHMER, W. & PARDO, L.A. (2005). Glycosylation of Eag1 (Kv10.1) potassium channels: intracellular trafficking and functional consequences. *Journal of Biological Chemistry*, **280,** 29506-12.

NELSON, C.M. & CHEN, C.S. (2002). Cell-cell signaling by direct contact increases cell proliferation via a PI3K-dependent signal. *FEBS Letters*, **514,** 238-42.

NEWELL, M.K. & DESBARATS, J. (1999). Fas ligand: receptor or ligand? *Apoptosis*, **4,** 311-315.

NICHOLS, C.G. & LOPATIN, A.N. (1997). Inward rectifier potassium channels. *Annual Review of Physiology*, **59,** 171-191.

OHYA, S., ASAKURA, K., MURAKI, K., WATANABE, M. & IMAIZUMI, Y. (2002). Molecular and functional characterization of ERG, KCNQ, and KCNE subtypes in rat stomach smooth muscle. *American Journal of Physiology - Gastrointestinal Liver Physiology*, **282,** G277-87.

ONO, K. & HAN, J. (2000). The p38 signal transduction pathway: activation and function. *Cellular Signalling*, **12,** 1-13.

ORR, A.W., PALLERO, M.A. & MURPHY-ULLRICH, J.E. (2002). Thrombospondin stimulates focal adhesion disassembly through Gi- and phosphoinositide 3-kinase-dependent ERK activation. *Journal of Biological Chemistry*, **277,** 20453-60.

OUADID-AHIDOUCH, H., LE BOURHIS, X., ROUDBARAKI, M., TOILLON, R.A., DELCOURT, P. & PREVARSKAYA, N. (2001). Changes in the K^+ current-density of MCF-7 cells during progression through the cell cycle: Possible involvement of a h-ether.a-gogo K^+ channel. *Receptors Channels*, **7,** 345-356.

OVERHOLT, J.L., FICKER, E., YANG, T., SHAMS, H., BRIGHT, G.R. & PRABHAKAR, N.R. (2000). HERG-Like potassium current regulates the resting membrane potential in glomus cells of the rabbit carotid body. *Journal of Neurophysiology*, **83,** 1150-7.

PALECEK, S.P., HORWITZ, A.F. & LAUFFENBURGER, D.A. (1999). Kinetic model for integrin-mediated adhesion release during cell migration. *Ann Biomed Eng*, **27,** 219-35.

PALECEK, S.P., SCHMIDT, C.E., LAUFFENBURGER, D.A. & HORWITZ, A.F. (1996). Integrin dynamics on the tail region of migrating fibroblasts. *Journal of Cell Science*, **109,** 941-52.

PANI, G., COLAVITTI, R., BEDOGNI, B., ANZEVINO, R., BORRELLO, S. & GALEOTTI, T. (2000). A redox signaling mechanism for density-dependent inhibition of cell growth. *Journal of Biological Chemistry*, **275,** 38891-9.

PANNER, A., CRIBBS, L.L., ZAINELLI, G.M., ORIGITANO, T.C., SINGH, S. & WURSTER, R.D. (2005). Variation of T-type calcium channel protein expression affects cell division of cultured tumor cells. *Cell Calcium*, **37,** 105-19.

PARDO-LOPEZ, L., ZHANG, M., LIU, J., JIANG, M., POSSANI, L.D. & TSENG, G.N. (2002). Mapping the binding site of a human ether-a-go-go-related gene-specific peptide toxin (ErgTx) to the channel's outer vestibule. *Journal of Biological Chemistry*, **277,** 16403-11.

PARDO, L.A., BRUGGEMANN, A., CAMACHO, J. & STUHMER, W. (1998). Cell cycle-related changes in the conducting properties of r-eag K^+ channels. *Journal of Cell Biology*, **143,** 767-775.

PARDO, L.A., CONTRERAS-JURADO, C., ZIENTKOWSKA, M., ALVES, F. & STUHMER, W. (2005). Role of voltage-gated potassium channels in cancer. *Journal of Membrane Biology*, **205,** 115-24.

PARDO, L.A., DEL CAMINO, D., SANCHEZ, A., ALVES, F., BRUGGEMANN, A., BECKH, S. & STUHMER, W. (1999). Oncogenic potential of EAG K+ channels. *Embo Journal*, **18,** 5540-5547.

PARK, C.C., ZHANG, H., PALLAVICINI, M., GRAY, J.W., BAEHNER, F., PARK, C.J. & BISSELL, M.J. (2006). Beta1 integrin inhibitory antibody induces apoptosis of breast cancer cells, inhibits growth, and distinguishes malignant from normal phenotype in three dimensional cultures and in vivo. *Cancer Research*, **66,** 1526-35.

PARR, E., POZO, M.J., HOROWITZ, B., NELSON, M.T. & MAWE, G.M. (2003). ERG K+ channels modulate the electrical and contractile activities of gallbladder smooth muscle. *American Journal of Physiology - Gastrointestinal Liver Physiology*, **284,** G392-8.

PATEL, A.J. & LAZDUNSKI, M. (2004). The 2P-domain K^+ channels: role in apoptosis and tumorigenesis. *Pflugers Archiv-European Journal of Physiology*, **448,** 261-73.

PAWLAK, G. & HELFMAN, D.M. (2001). Cytoskeletal changes in cell transformation and tumorigenesis. *Current Opinion in Genetics & Development*, **11,** 41-47.

PEI, L., WISER, O., SLAVIN, A., MU, D., POWERS, S., JAN, L.Y. & HOEY, T. (2003). Oncogenic potential of TASK3 (Kcnk9) depends on K^+ channel function. *Proceedings of the National Academy of Sciences of the United States of America*, **100,** 7803-7807.

PENG, B.L., FLEMING, J.B., BRESLIN, T., GRAU, A.M., FOJIOKA, S., ABBRUZZESE, J.L., EVANS, D.B., AYERS, D., WATHEN, K., WU, T.N., ROBERTSON, K.D. & CHIAO, P.J. (2002). Suppression of tumorigenesis and induction of p15(ink4b) by Smad4/DPC4 in human pancreatic cancer cells. *Clinical Cancer Research*, **8,** 3628-3638.

PENG, J.B., ZHUANG, L., BERGER, U.V., ADAM, R.M., WILLIAMS, B.J., BROWN, E.M., HEDIGER, M.A. & FREEMAN, M.R. (2001). CaT1 expression correlates with tumor grade in prostate cancer. *Biochemical and Biophysical Research Communications*, **282,** 729-34.

PETIT, V. & THIERY, J.P. (2000). Focal adhesions: structure and dynamics. *Biology of the Cell*, **92,** 477-94.

PETRECCA, K., ATANASIU, R., AKHAVAN, A. & SHRIER, A. (1999). N-linked glycosylation sites determine hERG channel surface membrane expression. *Journal of Physiology-London*, **515 (Pt 1),** 41-8.

PILLOZZI, S., BRIZZI, M.F., BALZI, M., CROCIANI, O., CHERUBINI, A., GUASTI, L., BARTOLOZZI, B., BECCHETTI, A., WANKE, E., BERNABEI, P.A., OLIVOTTO, M., PEGORARO, L. & ARCANGELI, A. (2002). HERG potassium channels are constitutively expressed in primary human acute myeloid leukemias and regulate cell proliferation of normal and leukemic hemopoietic progenitors. *Leukemia*, **16,** 1791-1798.

POSTMA, F.R., JALINK, K., HENGEVELD, T., BOT, A.G., ALBLAS, J., DE JONGE, H.R. & MOOLENAAR, W.H. (1996). Serum-induced membrane depolarization in quiescent

fibroblasts: activation of a chloride conductance through the G protein-coupled LPA receptor. *Embo Journal*, **15,** 63-72.

PREUSSAT, K., BEETZ, C., SCHREY, M., KRAFT, R., WOLFL, S., KALFF, R. & PATT, S. (2003). Expression of voltage-gated potassium channels Kv1.3 and Kv1.5 in human gliomas. *Neuroscience Letters*, **346,** 33-6.

PRITCHARD, C.A., HAYES, L., WOJNOWSKI, L., ZIMMER, A., MARAIS, R.M. & NORMAN, J.C. (2004). B-raf acts via the ROCKII/LIMK/cofilin pathway to maintain actin stress fibers in fibroblasts. *Molecular and Cellular Biology*, **24,** 5937-5952.

RASMUSSON, R.L., MORALES, M.J., WANG, S., LIU, S., CAMPBELL, D.L., BRAHMAJOTHI, M.V. & STRAUSS, H.C. (1998). Inactivation of voltage-gated cardiac K+ channels. *Circulation Research*, **82,** 739-50.

RAUCHER, D. & SHEETZ, M.P. (2000). Cell spreading and lamellipodial extension rate is regulated by membrane tension. *Journal of Cell Biology*, **148,** 127-36.

REDDIG, P.J. & JULIANO, R.L. (2005). Clinging to life: cell to matrix adhesion and cell survival. *Cancer Metastasis Review*, **24,** 425-39.

RESCH, G.P., GOLDIE, K.N., KREBS, A., HOENGER, A. & SMALL, J.V. (2002). Visualisation of the actin cytoskeleton by cryo-electron microscopy. *Journal of Cell Science*, **115,** 1877-82.

RICHMOND, A. (2002). Nf-kappa B, chemokine gene transcription and tumour growth. *Nature Reviews Immunology*, **2,** 664-74.

RODERICK, C., REINACH, P.S., WANG, L. & LU, L. (2003). Modulation of rabbit corneal epithelial cell proliferation by growth factor-regulated K(+) channel activity. *Journal of Membrane Biology*, **196,** 41-50.

RODRIGUEZ-VICIANA, P., WARNE, P.H., KHWAJA, A., MARTE, B.M., PAPPIN, D., DAS, P., WATERFIELD, M.D., RIDLEY, A. & DOWNWARD, J. (1997). Role of phosphoinositide 3-OH kinase in cell transformation and control of the actin cytoskeleton by Ras. *Cell*, **89,** 457-67.

RODRIGUEZ FERNANDEZ, J.L., GEIGER, B., SALOMON, D. & BEN-ZE'EV, A. (1993). Suppression of vinculin expression by antisense transfection confers changes in cell morphology, motility, and anchorage-dependent growth of 3T3 cells. *Journal of Cell Biology*, **122,** 1285-94.

ROOVERS, K. & ASSOIAN, R.K. (2000). Integrating the MAP kinase signal into the G1 phase cell cycle machinery. *Bioessays*, **22,** 818-26.

ROTI, E.C., MYERS, C.D., AYERS, R.A., BOATMAN, D.E., DELFOSSE, S.A., CHAN, E.K., ACKERMAN, M.J., JANUARY, C.T. & ROBERTSON, G.A. (2002). Interaction with GM130 during hERG ion channel trafficking. Disruption by type 2 congenital long QT syndrome mutations. Human Ether-a-go-go-Related Gene. *Journal of Biological Chemistry*, **277,** 47779-85.

ROUZAIRE-DUBOIS, B. & DUBOIS, J.M. (1998). K+ channel block-induced mammalian neuroblastoma cell swelling: a possible mechanism to influence proliferation. *Journal of Physiology-London*, **510,** 93-102.

ROUZAIRE-DUBOIS, B., MILANDRI, J.B., BOSTEL, S. & DUBOIS, J.M. (2000). Control of cell proliferation by cell volume alterations in rat C6 glioma cells. *Pflugers Archiv-European Journal of Physiology*, **440,** 881-8.

ROYDS, J.A., DOWER, S.K., QWARNSTROM, E.E. & LEWIS, C.E. (1998). Response of tumour cells to hypoxia: role of p53 and NF-kappaB. *Journal of Clinical Pathology- Molecular Pathology*, **51,** 55-61.

RUBIN, H. (2005). Degrees and kinds of selection in spontaneous neoplastic transformation: an operational analysis. *Proceedings of the National Academy of Sciences of the United States of America*, **102,** 9276-81.

RUSSELL, D.H. (1973). *Polyamines in normal and neoplastic growth*: Raven Press.

SAKAI, T., LI, S., DOCHEVA, D., GRASHOFF, C., SAKAI, K., KOSTKA, G., BRAUN, A., PFEIFER, A., YURCHENCO, P.D. & FASSLER, R. (2003). Integrin-linked kinase (ILK) is required for polarizing the epiblast, cell adhesion, and controlling actin accumulation. *Genes & Development*, **17,** 926-40.

SANGUINETTI, M.C., CURRAN, M.E., SPECTOR, P.S. & KEATING, M.T. (1996). Spectrum of hERG K^+-channel dysfunction in an inherited cardiac arrhythmia. *Proceedings of the National Academy of Sciences of the United States of America*, **93,** 2208-12.

SANGUINETTI, M.C., JIANG, C., CURRAN, M.E. & KEATING, M.T. (1995). A mechanistic link between an inherited and an acquired cardiac arrhythmia: HERG encodes the IKr potassium channel. *Cell*, **81,** 299-307.

SANGUINETTI, M.C. & MITCHESON, J.S. (2005). Predicting drug-hERG channel interactions that cause acquired long QT syndrome. *Trends in Pharmacological Sciences*, **26,** 119-24.

SANGUINETTI, M.C. & TRISTANI-FIROUZI, M. (2006). hERG potassium channels and cardiac arrhythmia. *Nature*, **440,** 463-9.

SCHAFER, R., WULFSEN, I., BEHRENS, S., WEINSBERG, F., BAUER, C.K. & SCHWARZ, J.R. (1999). The erg-like potassium current in rat lactotrophs. *Journal of Physiology-London*, **518,** 401-16.

SCHÖNHERR, R. (2005). Clinical relevance of ion channels for diagnosis and therapy of cancer. *Journal of Membrane Biology*, **205,** 175-84.

SCHÖNHERR, R. & HEINEMANN, S.H. (1996). Molecular determinants for activation and inactivation of hERG, a human inward rectifier potassium channel. *Journal of Physiology-London*, **493,** 635-42.

SCHOOTS, O., YUE, K.T., MACDONALD, J.F., HAMPSON, D.R., NOBREGA, J.N., DIXON, L.M. & VAN TOL, H.H. (1996). Cloning of a G protein-activated inwardly rectifying potassium channel from human cerebellum. *Molecular Brain Research*, **39,** 23-30.

SCHROEDER, K., NEAGLE, B., TREZISE, D.J. & WORLEY, J. (2003). Ionworks HT: a new high-throughput electrophysiology measurement platform. *Journal of Biomolecular Screening*, **8,** 50-64.

SCHWAB, A. (2001). Function and spatial distribution of ion channels and transporters in cell migration. *American Journal of Physiology-Renal Physiology*, **280,** F739-F747.

SHAH, N., THOMAS, T., SHIRAHATA, A., SIGAL, L.H. & THOMAS, T.J. (1999). Activation of nuclear factor kappa B by polyamines in breast cancer cells. *Biochemistry*, **38,** 14763-14774.

SHALLOWAY, D., JOHNSON, P.J., FREED, E.O., COULTER, D. & FLOOD, W.A., JR. (1987). Transformation of NIH 3T3 cells by cotransfection with c-src and nuclear oncogenes. *Molecular and Cellular Biology* **7,** 3582-90.

SHEN, M.R., YANG, T.P. & TANG, M.J. (2002). A novel function of BCL-2 overexpression in regulatory volume decrease. Enhancing swelling-activated Ca(2+) entry and Cl(-) channel activity. *Journal of Biological Chemistry*, **277,** 15592-9.

SHIN, S.I., FREEDMAN, V.H., RISSER, R. & POLLACK, R. (1975). Tumorigenicity of virus-transformed cells in nude mice is correlated specifically with anchorage independent growth in vitro. *Proceedings of the National Academy of Sciences of the United States of America*, **72,** 4435-9.

SHOEB, F., MALYKHINA, A.P. & AKBARALI, H.I. (2003). Cloning and functional characterization of the smooth muscle ether-a-go-go-related gene K+ channel. Potential role of a conserved amino acid substitution in the S4 region. *Journal of Biological Chemistry*, **278,** 2503-14.

SILBERMAN, S., JANULIS, M. & SCHULTZ, R.M. (1997). Characterization of downstream Ras signals that induce alternative protease-dependent invasive phenotypes. *Journal of Biological Chemistry*, **272,** 5927-35.

SLACK, J.K., ADAMS, R.B., ROVIN, J.D., BISSONETTE, E.A., STOKER, C.E. & PARSONS, J.T. (2001). Alterations in the focal adhesion kinase/Src signal transduction pathway correlate with increased migratory capacity of prostate carcinoma cells. *Oncogene*, **20,** 1152-63.

SMITH, G.A.M., TSUI, H.W., NEWELL, E.W., JIANG, X.P., ZHU, X.P., TSUI, F.W.L. & SCHLICHTER, L.C. (2002). Functional up-regulation of hERG K^+ channels in neoplastic hematopoietic cells. *Journal of Biological Chemistry*, **277,** 18528-18534.

SOLTOFF, S.P. (2001). Rottlerin Is a Mitochondrial Uncoupler That Decreases Cellular ATP Levels and Indirectly Blocks Protein Kinase C delta Tyrosine Phosphorylation. *Journal of Biological Chemistry*, **276,** 37986.

SPECTOR, P.S., CURRAN, M.E., ZOU, A.R. & SANGUINETTI, M.C. (1996). Fast inactivation causes rectification of the I-Kr channel. *Journal of General Physiology*, **107,** 611-619.

STEWART, Z.A., WESTFALL, M.D. & PIETENPOL, J.A. (2003). Cell-cycle dysregulation and anticancer therapy. *Trends in Pharmacological Sciences*, **24,** 139-145.

STRINGER, B.K., COOPER, A.G. & SHEPARD, S.B. (2001). Overexpression of the G-protein inwardly rectifying potassium channel 1 (GIRK1) in primary breast carcinomas correlates with axillary lymph node metastasis. *Cancer Research*, **61,** 582-8.

SUNWOO, J.B., CHEN, Z., DONG, G., YEH, N., CROWL BANCROFT, C., SAUSVILLE, E., ADAMS, J., ELLIOTT, P. & VAN WAES, C. (2001). Novel proteasome inhibitor PS-341 inhibits activation of nuclear factor-kappa B, cell survival, tumor growth, and angiogenesis in squamous cell carcinoma. *Clinical Cancer Research*, **7,** 1419-28.

TAGLIALATELA, M., PANNACCIONE, A., CASTALDO, P., GIORGIO, G., ZHOU, Z., JANUARY, C.T., GENOVESE, A., MARONE, G. & ANNUNZIATO, L. (1998). Molecular basis for the lack of HERG K+ channel block-related cardiotoxicity by the H1 receptor blocker cetirizine compared with other second-generation antihistamines. *Molecular Pharmacology*, **54,** 113-21.

TAJIMA, N., SCHÖNHERR, K., NIEDLING, S., KAATZ, M., KANNO, H., SCHONHERR, R. & HEINEMANN, S.H. (2006). Ca^{2+}-activated K^+ channels in human melanoma cells are up-regulated by hypoxia involving hypoxia-inducible factor-1alpha and the von Hippel-Lindau protein. *Journal of Physiology-London*, **571,** 349-59.

TAKANAMI, I., INOUE, Y. & GIKA, M. (2004). G-protein inwardly rectifying potassium channel 1 (GIRK 1) gene expression correlates with tumor progression in non-small cell lung cancer. *BMC Cancer*, **4,** 79.

TAYLOR, B.L. & ZHULIN, I.B. (1999). PAS domains: internal sensors of oxygen, redox potential, and light. *Microbiol and Molecular Biology Review*, **63,** 479-506.

TROUSSARD, A.A., MAWJI, N.M., ONG, C., MUI, A., ST -ARNAUD, R. & DEDHAR, S. (2003). Conditional knock-out of integrin-linked kinase demonstrates an essential role in protein kinase B/Akt activation. *Journal of Biological Chemistry*, **278,** 22374-8.

TSAVALER, L., SHAPERO, M.H., MORKOWSKI, S. & LAUS, R. (2001). Trp-p8, a novel prostate-specific gene, is up-regulated in prostate cancer and other malignancies and shares high homology with transient receptor potential calcium channel proteins. *Cancer Research*, **61,** 3760-9.

ULLRICH, N. & SONTHEIMER, H. (1997). Cell cycle-dependent expression of a glioma-specific chloride current: proposed link to cytoskeletal changes. *American Journal of Physiology - Cell Physiology*, **273,** C1290-7.

VAN COPPENOLLE, F., SKRYMA, R., OUADID-AHIDOUCH, H., SLOMIANNY, C., ROUDBARAKI, M., DELCOURT, P., DEWAILLY, E., HUMEZ, S., CREPIN, A., GOURDOU, I., DJIANE, J.,

BONNAL, J.L., MAUROY, B. & PREVARSKAYA, N. (2004). Prolactin stimulates cell proliferation through a long form of prolactin receptor and K+ channel activation. *Biochemical Journal*, **377,** 569-578.

VAN NIMWEGEN, M.J., VERKOEIJEN, S., VAN BUREN, L., BURG, D. & VAN DE WATER, B. (2005). Requirement for focal adhesion kinase in the early phase of mammary adenocarcinoma lung metastasis formation. *Cancer Research*, **65,** 4698-706.

VANDENBERG, J.I., TORRES, A.M., CAMPBELL, T.J. & KUCHEL, P.W. (2004). The hERG K^+ channel: progress in understanding the molecular basis of its unusual gating kinetics. *European Biophysical Journal*, **33,** 89-97.

VIVANCO, I. & SAWYERS, C.L. (2002). The phosphatidylinositol 3-Kinase AKT pathway in human cancer. *Nature Reviews Cancer*, **2,** 489-501.

VREEDE, J., VAN DER HORST, M.A., HELLINGWERF, K.J., CRIELAARD, W. & VAN AALTEN, D.M.F. (2003). PAS domains - Common structure and common flexibility. *Journal of Biological Chemistry*, **278,** 18434-18439.

WALKER, J.L. & ASSOIAN, R.K. (2005). Integrin-dependent signal transduction regulating cyclin D1 expression and G1 phase cell cycle progression. *Cancer Metastasis Review*, **24,** 383-93.

WANG, H.Z., ZHANG, Y.Q., CAO, L.W., HAN, H., WANG, J.X., YANG, B.F., NATTEL, S. & WANG, Z.G. (2002). hERG K^+ channel, a regulator of tumor cell apoptosis and proliferation. *Cancer Research*, **62,** 4843-4848.

WANG, J., TRUDEAU, M.C., ZAPPIA, A.M. & ROBERTSON, G.A. (1998a). Regulation of deactivation by an amino terminal domain in human ether-a-go-go-related gene potassium channels. *Journal of General Physiology*, **112,** 637-47.

WANG, L., FENG, Z.P., KONDO, C.S., SHELDON, R.S. & DUFF, H.J. (1996). Developmental changes in the delayed rectifier K+ channels in mouse heart. *Circulation Research*, **79,** 79-85.

WANG, L.H. (2004). Molecular signaling regulating anchorage-independent growth of cancer cells. *Mt Sinai Journal of Medicine*, **71,** 361-7.

WANG, S., LIU, S., MORALES, M.J., STRAUSS, H.C. & RASMUSSON, R.L. (1997). A quantitative analysis of the activation and inactivation kinetics of hERG expressed in Xenopus oocytes. *Journal of Physiology-London*, **502,** 45-60.

WANG, S., MELKOUMIAN, Z., WOODFORK, K.A., CATHER, C., DAVIDSON, A.G., WONDERLIN, W.F. & STROBL, J.S. (1998b). Evidence for an early G1 ionic event necessary for cell cycle progression and survival in the MCF-7 human breast carcinoma cell line. *Journal of Cellular Physiology.*, **176,** 456-64.

WANG, X.T., NAGABA, Y., CROSS, H.S., WRBA, F., ZHANG, L. & GUGGINO, S.E. (2000). The mRNA of L-type calcium channel elevated in colon cancer: protein distribution in normal and cancerous colon. *American Journal of Pathology*, **157,** 1549-62.

WAYNE, J., SIELSKI, J., RIZVI, A., GEORGES, K. & HUTTER, D. (2006). ERK regulation upon contact inhibition in fibroblasts. *Molecular and Cellular Biochemistry*, 1-9.

WEBER, C., MELLO DE QUEIROZ, F., DOWNIE, B.R., SUCKOW, A., STUHMER, W. & PARDO, L.A. (2006). Silencing the activity and proliferative properties of the human Eag1 potassium channel by RNAi. *Journal of Biological Chemistry*, **281,** 13030-13037.

WEERAPURA, M., NATTEL, S., CHARTIER, D., CABALLERO, R. & HEBERT, T.E. (2002). A Comparison of currents carried by hERG, with and without coexpression of MiRP1, and the native rapid delayed rectifier current. Is MiRP1 the missing link? . *Journal of Physiology-London*, **540.1,** 15-27.

WEINER, T.M., LIU, E.T., CRAVEN, R.J. & CANCE, W.G. (1993). Expression of focal adhesion kinase gene and invasive cancer. *Lancet*, **342,** 1024-5.

WESTERMARCK, J., LI, S.P., KALLUNKI, T., HAN, J. & KAHARI, V.M. (2001). p38 mitogen-activated protein kinase-dependent activation of protein phosphatases 1 and 2A inhibits MEK1 and MEK2 activity and collagenase 1 (MMP-1) gene expression. *Molecular and Cellular Biology*, **21,** 2373-83.

WIESER, R.J., BAUMANN, C.E. & OESCH, F. (1995). Cell-contact mediated modulation of the sialylation of contactinhibin. *Glycoconjugate journal*, **12,** 672-9.

WIESER, R.J., HECK, R. & OESCH, F. (1985). Involvement of plasma membrane glycoproteins in the contact-dependent inhibition of growth of human fibroblasts. *Experimental cell research*, **158,** 493-9.

WIESER, R.J., SCHUTZ, S., TSCHANK, G., THOMAS, H., DIENES, H.P. & OESCH, F. (1990). Isolation and characterization of a 60-70-kD plasma membrane glycoprotein involved in the contact-dependent inhibition of growth. *Journal of Cell Biology*, **111,** 2681-92.

WITCHEL, H.J., DEMPSEY, C.E., SESSIONS, R.B., PERRY, M., MILNES, J.T., HANCOX, J.C. & MITCHESON, J.S. (2004). The low-potency, voltage-dependent HERG blocker propafenone--molecular determinants and drug trapping. *Molecular Pharmacology*, **66,** 1201-12.

WONDERLIN, W.F. & STROBL, J.S. (1996). Potassium channels, proliferation and G1 progression. *Journal of Membrane Biology*, **154,** 91-107.

WOO, S.Y., LEE, M.Y., JUNG, Y.J., YOO, E.S., SEOH, J.Y., SHIN, H.Y., AHN, H.S. & RYU, K.H. (2006). Arsenic trioxide inhibits cell growth in SH-SY5Y and SK-N-AS neuroblastoma cell lines by a different mechanism. *Pediatr Hematol Oncol*, **23,** 231-43.

WOZNIAK, M.A., MODZELEWSKA, K., KWONG, L. & KEELY, P.J. (2004). Focal adhesion regulation of cell behavior. *Biochimica Et Biophysica Acta*, **1692,** 103-19.

XU, L.H., YANG, X., BRADHAM, C.A., BRENNER, D.A., BALDWIN, A.S., JR., CRAVEN, R.J. & CANCE, W.G. (2000). The focal adhesion kinase suppresses transformation-associated, anchorage-independent apoptosis in human breast cancer cells. Involvement of death receptor-related signaling pathways. *Journal of Biological Chemistry*, **275,** 30597-604.

XU, X.P. & BEST, P.M. (1990). Increase in T-type calcium current in atrial myocytes from adult rats with growth hormone-secreting tumors. *Proceedings of the National Academy of Sciences of the United States of America*, **87,** 4655-9.

YANCOPOULOS, G.D., DAVIS, S., GALE, N.W., RUDGE, J.S., WIEGAND, S.J. & HOLASH, J. (2000). Vascular-specific growth factors and blood vessel formation. *Nature*, **407,** 242-8.

YU, S.P., CANZONIERO, L.M.T. & CHOI, D.W. (2001). Ion homeostasis and apoptosis. *Current Opinion in Cell Biology*, **13,** 405-411.

ZHANG, L. & BARRITT, G.J. (2004). Evidence that TRPM8 is an androgen-dependent Ca2+ channel required for the survival of prostate cancer cells. *Cancer Research*, **64,** 8365-73.

ZHANG, Y.Q., WANG, H.Z., WANG, J.X., HAN, H., NATTEL, S. & WANG, Z.G. (2003). Normal function of hERG K^+ channels expressed in HEK293 cells requires basal protein kinase B activity. *FEBS Letters*, **534,** 125-132.

ZHOU, Z., GONG, Q., EPSTEIN, M.L. & JANUARY, C.T. (1998a). hERG channel dysfunction in human long QT syndrome. Intracellular transport and functional defects. *Journal of Biological Chemistry*, **273,** 21061-6.

ZHOU, Z., GONG, Q., YE, B., FAN, Z., MAKIELSKI, J.C., ROBERTSON, G.A. & JANUARY, C.T. (1998b). Properties of HERG channels stably expressed in HEK 293 cells studied at physiological temperature. *Biophysical Journal.*, **74,** 230-41.

Proliferation						
		NIH-WT	NIH-VC	NIH-Ras	NIH-16	NIH-50
Control (% change in confluency / hr)		1.9 ± 0.1	1.9 ± 0.1	1.7 ± 0.1	1.6 ± 0.1	1.5 ± 0.1
hERG Blockers	Terfenidine 1 μM	-3.6 ± 19.1	-29.9 ± 4.8	-14.7 ± 8.2	-11.6 ± 0	-38.4 ± 20.5
	Terfenidine 10 μM	-119.8 ± 9.5 ***	-127.4 ± 6.3 ***	-103.7 ± 0.3 ***	-103.8 ± 1.8 ***	-109.1 ± 1.3 ***
hERG trafficking inhibitors	Arsenic Trioxide 1 μM	19 ± 15.8	-25.3 ± 9.2	-27.3 ± 7.7	-15.8 ± 16.5	-9.3 ± 17.6
	Arsenic Trioxide 10 μM	-42.1 ± 20 *	-63.6 ± 12.5 *	-79.6 ± 12.1 ***	-23.9 ± 7.1	-30.1 ± 5.5
Src inhibitor	PP2 10 μM	-53.4 ± 6.5 ***	-56.4 ± 9.0 ***	-23.9 ± 2.9	-10.1 ± 13.5	0 ± 9.1
	PP3 (control) 10 μM	13.6 ± 7.1	-6.0 ± 8.4	-5.6 ± 4.5	11.9 ± 14.8	13.5 ± 9.8
p38 inhibitor	SB202190 10 μM	19.3 ± 9.4	-18.7 ± 9.9	-16.2 ± 5.1	-2.8 ± 9.4	-15.8 ± 12.4
	SB202474 (control) 10 μM	9.9 ± 13.6	-16.5 ± 9.2	-18.3 ± 5.7	3.7 ± 19.3	-13.9 ± 9.9
PI3K inhibitor	LY294002 10 μM	-24.2 ± 12.1	-38.3 ± 7.5	-44.7 ± 7.7 **	-23.1 ± 18.5	-38.8 ± 9.7
	LY303511 (control) 10 μM	-2.6 ± 13.7	-19.1 ± 4.1	-10.9 ± 7.0	3.7 ± 18.2	-19.5 ± 6.1
Adenovirus	G628Sa	-17.6 ± 11.3	8.6 ± 14.2	-41.7 ± 16.8	-26.9 ± 14.1	-14.9 ± 15.7
	G628S	-1.7 ± 5.2	-1.1 ± 14.7	-20.1 ± 6.8	-29.3 ± 11.7	-6.9 ± 3.1
	Empty	-51.9 ± 0.9 *	-27.8 ± 12.2	-84.2 ± 19.6 *	-22.2 ± 8.8	-21.4 ± 2.6

Appendix 1: Effects of compounds upon proliferation rates. Values are mean percentage change (± SEM) relative to control values from the same cell line. Data analysed using a Two-way ANOVA (* $p < 0.05$) (** $p < 0.01$) (*** $p < 0.001$)

Saturation density						
		NIH-WT	NIH-VC	NIH-Ras	NIH-16	NIH-50
Control (microns hr-1)		1781000 ± 134408	1078000 ± 39565	2961000 ± 140680	2754000 ± 83352	2310000 ± 91919
Serum concentration	5%	7.1 ± 9.3	-5.0 ± 1.9	-12.1 ± 2.4	-24.4 ± 1.6 **	-22.2 ± 4.1
	1%	-33.2 ± 4.9 *	-26.5 ± 3.9	-23.1 ± 1.8	-50.7 ± 3.0 ***	-51.1 ± 5.6 ***
External [K+]	10 mM	43 ± 4.0	15.5 ± 5.4	1.9 ± 6.5	1.3 ± 3.5	11.5 ± 5.4
	40 mM	17.4 ± 4.1	-5.4 ± 6.7	-19.7 ± 4.3 **	-31.9 ± 2.1 ***	-28.3 ± 3.3 ***
	100 mM	-71.9 ± 9.9 ***	-74.8 ± 4.7 ***	-90.8 ± 2.9 ***	-80.2 ± 5.1 ***	-83.5 ± 5.0 ***
	140 mM	-89.5 ± 0.1 ***	-83.2 ± 0.4 ***	-98.6 ± 0.1 ***	-94.0 ± 0.6 ***	-93.7 ± 0.3 ***
hERG Blockers	Terfenidine 1µM	36 ± 2.0	7.9 ± 5.5	-16.5 ± 0.8	22.1 ± 5.2	2.4 ± 9.6
	Fluoxitine 3 µM	31.2 ± 6.5	18.6 ± 3.6	-2.7 ± 1.0	7.2 ± 4.9	-6.4 ± 1.6
hERG trafficking inhibitors	Fluoxitine 10 µM	-20.8 ± 32.8	15.4 ± 10.5	-44.8 ± 19.4 ***	-22.5 ±4.7	-1.4 ± 7.4
	Fluoxitine 30 µM	-86.9 ± 0.4 ***	-79.3 ± 1.1	-91.9 ± 1.1 ***	-87.6 ± 0.1 ***	-86.5 ± 2.2 ***
	Arsenic Trioxide 1 µM	18.4 ± 2.1	-3.8 ± 3.5	-10.7 ± 2.8	-0.5 ± 11.1	-5.7 ± 12.6
	Arsenic Trioxide 10 µM	0.5 ± 5.4	-64.5 ± 12.7	-51.7 ± 9.4 ***	-23.7 ± 7.6 *	-29.4 ± 11.7 *
Src inhibitor	PP2 10 µM	0.1 ± 7.4	-20.9 ± 6.3	-19.3 ± 11.7	-36.6 ± 3.8 ***	-48.0 ± 2.2 ***
	PP3 (control) 10 µM	64.2 ± 8.2 ***	31.1 ± 9.0	-7.0 ± 5.7	0.9 ± 3.7	6.5 ± 9.7
p38 inhibitor	SB202190 10 µM	-24.3 ± 7.8 ***	12.9 ±8.2	-38.8 ± 2.8 ***	-67.5 ± 2.4 ***	-48.9 ± 1.9 ***
	SB202474 (control) 10 µM	-5.1 ± 4.1	2.8 ± 12.8	-29.6 ± 2.8 ***	-23.3 ± 2.9 ***	-3.9 ± 3.7
PI3K inhibitor	LY294002 10 µM	-17.5 ± 4.2	-24.8 ± 2.3	-40.1 ± 2.7 ***	-52.1 ±1.9 ***	-40.8 ± 4.5 **
	LY303511 (control) 10 µM	30.6 ± 6.6	25 ± 7.3	-11.8 ± 1.3	6.9 ± 3.9	15.8 ± 6.7
PKC inhibitor	BIS I 1 µM	-7.4 ± 17.7	5.7 ± 4.4	22.5 ± 17.4	1.3 ± 1.5	3 ± 3.2
	BIS V (control) 1 µM	-27.7 ± 19.9	1.1 ± 1.3	5.1 ± 11.1	-6.9 ± 2.9	-3.1 ± 2.5
Adenovirus	Empty	-	1.9 ± 9.8	-	-8.4 ± 5.5	-31.6 ± 0
	G628S	-	1.1 ± 0.6	-	-13.5 ± 10.1	-30.8 ± 3.2
	G628Sa	-	-34.3 ± 10.6	-	-45.1 ± 12.9	-59.9 ± 8.5

Appendix 2: Effects of compounds upon saturation density. Values are percentage change relative to control values from the same cell line (± SEM).
Data analysed using a Two-way ANOVA (* $p < 0.05$) (** $p < 0.01$) (*** $p < 0.001$)

Migration						
		NIH-WT	NIH-VC	NIH-Ras	NIH-16	NIH-50
Control (microns / hr)		30.8 ± 0.9	32.8 ± 1.1	53.9 ± 1.4	47.6 ± 0.8	44.4 ± 1.3
Serum concentration	5%	-19.9 ± 5.9	-33.4 ± 6.8 **	-4.4 ± 3.1	-19.8 ± 5.5 *	-38.2 ± 5.0 ***
	1%	-37.7 ± 6.9 **	-52.3 ± 4.5 ***	-24.3 ± 7.2 ***	-28.4 ± 6.6 ***	-50.5 ± 3.5 ***
External [K+]	10 mM	9.7 ± 6.1	-4.3 ± 8.6	-9.6 ± 3.3	-3.3 ± 2.2	-2.4 ± 4.3
	20 mM	5.4 ± 3.7	-2.2 ± 3.1	-12.0 ± 3.0	-1.0 ± 3.0	-1.7 ± 6.8
	40 mM	15.2 ± 4.1	8.2 ± 4.6	-13.2 ± 4.8	-2.6 ± 6.4	-3.5 ± 4.0
	100 mM	-5.9 ± 3.0	-0.5 ± 5.0	-37.6 ± 4.2 **	-51.2 ± 2.4 **	-28.4 ± 2.8 **
	140 mM	-84.3 ± 1.0 ***	-78.9 ± 1.7 ***	-91.5 ± 2.8 ***	-96.6 ± 0.5 ***	-88.2 ± 0.8 ***
hERG Blockers	Dofetilide 10 µM	5.8 ± 4.6	-8.6 ± 5.6	3.4 ± 9.3	8.9 ± 5.8	4.1 ± 4.3
	Terfenidine 1 µM	-4.2 ± 4.2	4.9 ± 2.9	-14.3 ± 5.3 **	-5.5 ± 4.1	-29.1 ± 2.2 **
	Terfenidine 10 µM	-7.4 ± 1.9	-9.1 ± 2.8	-1.4 ± 1.1	-18.2 ± 3.9	-24.8 ± 1.2 **
	Fluoxitine 3 µM	16.2 ± 8.1	37.6 ± 5.6	32.6 ± 5.7 ***	5.4 ± 9.3	4.4 ± 6.9
hERG trafficking inhibitors	Fluoxitine 10 µM	9.3 ± 5.4	43.1 ± 2.6	8.9 ± 5.6	26.4 ± 8.8	20.9 ± 5.1
	Fluoxitine 30 µM	-116.2 ± 3.9 ***	-100.7 ± 0.6 ***	-109.2 ± 4.2 ***	-109.7 ± 6.9 ***	-103.0 ± 3.0 ***
	Pentamidine 10 µM	11.2 ± 3.8	7.3 ± 2.7	5.5 ± 4.9	6 ± 2.3	-7.7 ± 1.3
	Arsenic Trioxide 1 µM	-15.4 ± 2.6	24.4 ± 6.3 **	1.2 ± 5.6	-13.6 ± 6.0	-19.2 ± 5.1 *
	Arsenic Trioxide 10 µM	-21.8 ± 2.5	-25.1 ± 3.1 **	-53.9 ± 2.3 ***	-18.9 ± 2.0 *	-18.1 ± 5.6 **
Src inhibitor	PP2 10 µM	-79.2 ± 1.2 ***	-55.1 ± 8.7 ***	-45.8 ± 8.7 ***	-62.4 ± 3.7 ***	-63.4 ± 1.7 ***
	PP3 (control) 10 µM	-14.5 ± 9.3	-11.6 ± 11.7	-7.8 ± 13.3	-2.8 ± 4.1	-8.3 ± 4.1
p38 inhibitor	SB203580 2 µM	-31.8 ± 4.2	-17.1 ± 0.2	-28 ± 9.6	5.1 ± 6.3	-1.6 ± 9.0
	SB203580 20 µM	-24.3 ± 3.1	-1.4 ± 31.8	-29.7 ± 1.9	-25.3 ± 2.2	-33.9 ± 7.7
	SB202190 10 µM	-22.9 ± 2.8	-34.2 ± 6.0 ***	-14.5 ± 3.3 **	-13.7 ± 3.5 *	-8.3 ± 5.3
	SB202474 (control) 10 µM	-2.1 ± 2.0	-21.7 ± 5.7 *	4.7 ± 2.7	0.5 ± 3.1	-4.1 ± 5.4
PI3K inhibitor	LY294002 10 µM	-61.6 ± 5.4 ***	-31.0 ± 8.4 **	-53.4 ± 5.6 ***	-26.2 ± 5.5 ***	-34.2 ± 3.9 ***
	LY303511 (control) 10 µM	-13.5 ± 2.6	-4.8 ± 3.3	-10.7 ± 3.6	3.3 ± 2.9	8.7 ± 4.2
MEK inhibitor	U0126 10 µM	-5.2 ± 19.4	-7.3 ± 2.9	-25.1 ± 7.1 ***	-12.3 ± 3.7	-15.2 ± 3.4
	UO124 (control) 10 µM	-12.8 ± 13.9	11.4 ± 5.5	15.2 ± 2.8 *	8 ± 2.4	11.6 ± 6.6
PKC inhibitor	Rottlerin 3 µM	22.9 ± 27.3	23.6 ± 4.1	18.3 ± 4.6 **	-6.5 ± 6.0	-1.9 ± 7.0
	BIS I 1 µM	25.5 ± 4.8	31.2 ± 4.5 *	17.4 ± 4.3 **	28.9 ± 3.6 ***	18.6 ± 3.8
	BIS V (control) 1 µM	18.7 ± 6.8	21.4 ± 2.9	22.6 ± 7.2 ***	26.7 ± 4.6 **	23.6 ± 7.2 **
Adenovirus	G628Sa	-11.9 ± 5.1	-19.8 ± 4.8 *	-22.4 ± 11.1 *	-29.2 ± 8.0 ***	-2.5 ± 5.7
	G628S	-5.4 ± 4.3	-21.7 ± 3.9	-16.5 ± 9.8	-5.1 ± 5.2	12.9 ± 5.0
	Empty	43.8 ± 5.3 **	18.1 ± 7.3	3.9 ± 12.9	13 ± 6.4	50.7 ± 4.5 ***

Appendix 3: Effects of compounds upon migration rates. Values are percentage change relative to control values from the same cell line (± SEM).
Data analysed using a Two-way ANOVA (* $p < 0.05$) (** $p < 0.01$) (*** $p < 0.001$)

Appendix 4 Calculating the number of hERG channels per cell from [^{3}H]-dofetilide ligand binding data.

The specific activity of the [^{3}H]-dofetilide sample is 75 Ci/mmol. This is equivalent to 13.3 pmol/μCi.

For the NIH-16 clone the specific binding of [^{3}H]-dofetilide was 1103 d.p.m. per assay.

We know that there are 2.22 x 10^6 d.p.m. per μCi. Therefore the binding of the NIH-16 clone is equivalent to:

$$(1103/2.22 \times 10^6) \times 13.3 \times 1000 = 6.61 \text{ fmol/assay}$$

Each assay was performed with a total of 75 μg protein. Therefore we can calculate the amount of ligand binding per unit protein:

$$6.61 \times 1000/75 = 88.1 \text{ fmol/mg protein}$$

Due to limited availability of [^{3}H]-dofetilide the concentration used in the assay was 10 nM. The best estimate of K_d of [^{3}H]-dofetilide for binding to hERG is 35 nM (Diaz *et al.*, 2004). Therefore, at 10 nM [^{3}H]-dofetilide the occupancy of hERG channels is approx. 15%

$$88.1 \times 100/15 = 587 \text{ fmol/mg protein at 100\% occupancy}$$

Assuming that 1 mg of protein is equivalent to ~1 x 10^6 cells (see figure 5.4) and that [^{3}H]-dofetilide-hERG channel binding stoichiometry is 1:1 then,

$$587 \times 10^{-15}/1 \times 10^6 = 5.87 \times 10^{-19} \text{ M hERG channel per cell}$$

Avogadro's number = 6.022 x 10^{23} molecules per M thus,

$$5.87 \times 10^{-19} \times 6.022 \times 10^{23} = \underline{\mathbf{353,500}} \text{ hERG channels per NIH-16 cell}$$

Publications

D. Pier, R. A. J. Challiss, J. S. Mitcheson (2005). Oncogenic Potential of Recombinant hERG: Effects on Growth and Role of Functional Current. American Society for Cell Biology, Meeting abstract.

D. Pier, R. A. J. Challiss, J. S. Mitcheson. Oncogenis Potential of Human Ether a-go-go Related Gene(hERG). Manuscript in preparation.